



**ABSORPTION SPECTROSCOPY
OF CARBON AND SULFUR CHAINS
IN 6 K NEON MATRICES**

INAUGURALDISSERTATION

zur

Erlangung der Würde eines

Doktors der Philosophie

vorgelegt der

Philosophisch-Naturwissenschaftlichen Fakultät

der Universität Basel

von

Ivan G. Shnitko

aus Magadan, Russland

Basel, 2008

Genehmigt von der Philosophisch-Naturwissenschaftlichen Fakultät

auf Antrag von

Prof. Dr. John P. Maier und Prof. Dr. Markus Meuwly

Basel, den 19. Februar 2008

Prof. Dr. Hans-Peter Hauri

Dekan

TO MY PARENTS AND BROTHER

ACKNOWLEDGEMENT

During the course of my PhD studies I had the opportunity to meet and work with many excellent and intelligent people, some of whom deserve a great deal of credit for the work presented in this thesis.

I would first like to thank Prof. John P. Maier for giving me the opportunity to work in his group. His professional advice, as well as his readiness to help and guide, are greatly acknowledged. I would also like to thank Prof. Markus Meuwly for his courteous agreement to act as a co-referee of my thesis.

My immeasurable thanks are addressed to Doctor Jan Fulara. This guru of matrix isolation, with his perfect knowledge of the experimental set-up, taught me all the basics of the technique. His continuing help during his visits in Basel, as well as any time given through e-mail are cordially appreciated. Professor Pavel Rosmus is thanked for theoretical support.

I am grateful to my colleague and friend Anton Batalov with whom I worked shoulder to shoulder for several years, and he is thanked for creating an excellent working environment. My new colleagues, Iryna Garkusha and Adam Nagy, are also thanked for their assistance with the experiment and for being patient with me.

I kindly thank Dr. Evan Jochnowitz and Dr. Corey Rice for sharing their knowledge, continuous willingness to help, and especially for the new stream of energy they brought to our group. My appreciations are addressed to all former and present group fellows: Elena Achkasova, Evgueni Riaplov, Pawel Cias, Alexey Denisov, Andrey Boguslavskiy, Tatiana Dorosheva, Petre Bîrză, Cristina Apetrei, Dr. Andrey Chirokolava, Dr. Jennifer van Wijngaarden, Dr. Mitsunori Araki, Dr. Przemyslaw Kolek, Dmitry Khoroshev, Egor Chasovskikh, Vitaly Rudnev, Anatoly Johnson, Hongbin Ding, Richa Chauhan, Dr. Fabio Mazzotti, Ranjini Raghunandan, Lukasz Chacaga, Dr. Zohra Guennoun (we were waiting for you so much!), Dr. Ramya Nagarajan, all of whom are thanked for providing a friendly working environment and good team spirit.

I am also grateful to the people who were technically involved in the experiment for their help and assistance. Dieter Wild, Grischa Martin, and Karl Mutchler from the mechanical workshop are thanked for their wonderful skills in constructing technical devices; Georg Holderied is thanked for his outstanding knowledge of the electronics; Ester Stalder and Daniela Tischhauser are thanked for taking care of bureaucratic matters and making my life easier; Jacques Lecoultre is thanked for synthesizing the necessary chemicals. The Swiss National Science Foundation and the City of Basel are thanked for their financial support.

Special thanks and appreciation to Dr. L.A. Belchenko and Prof. N.M. Bazhin, without whom I would have never obtained this position.

All my friends: Jürgen Wintner, Markus Schneider, Dmitry Nazarov, Yavor Kamdzhilov, Pavel Müller, Mariusz Grzelakowski, Pavel Kuban, Stanislav Ivan, Lukasz Lesinski, Marco Haase, Florian Troester, Beau Ballard, Ian Hamriding, Sergei Zhulin, Alexander Pugaseev, Oleg Sadovskiy, Amir Bobrovskih, Nikolay Ohalin, Eldar Zaripov, Alexander Neverov, Anton Baluev, Eduard Duban, Denis Kim, Alexey Fedorov, Sergiu Turcanu, Eduard Turcanu, Vladimir Reznik, Alex Kudryavtsev, Igor Likholat, Vsevolod Xenofontov, Victor Grosu, Max Surdu, Alexey Karpov, Alessandro Napoli, Pavel Vinogradov, Sergei Drjamov, Brendan Kerins, Nelson Guerreiro, and many others are thanked not only for being close friends but also for moral support and all the good times we spent together.

Finally, I would like to thank cordially my parents, my brother and his wife, my nephews and all my relatives and people who were close to me throughout all this time, for their affection and constant encouragement, THANK YOU EVER SO MUCH.

I declare that I wrote this thesis “Absorption spectroscopy of carbon and sulfur chains in 6 K neon matrices” with help indicated and only handed it in to the faculty of science of the University of Basel and no other faculty and no other university.

Basel, 19.02.2008

Ivan G. Shnitko

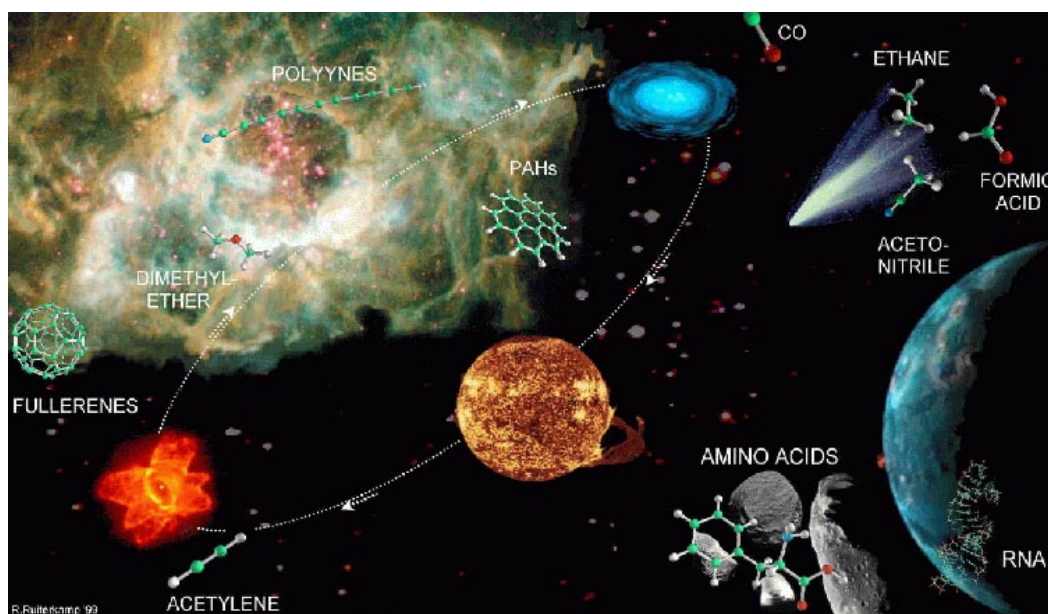
The work presented here was initiated and supervised by Prof. Dr. John Paul Maier at the Chemistry Department of the University of Basel.

TABLE OF CONTENTS

TABLE OF CONTENTS	9
CHAPTER 1. INTRODUCTION	11
PREFACE	12
INTERSTELLAR MEDIUM	15
<i>How did it all start?</i>	15
<i>Up there</i>	17
Molecular clouds	19
Ionized hydrogen regions	21
DIFFUSE INTERSTELLAR BANDS	22
<i>Characteristics of the diffuse interstellar bands</i>	24
<i>Proposals for the origin of the diffuse bands</i>	25
Polycyclic Aromatic Hydrocarbons	26
Carbon chains	27
BIBLIOGRAPHY	29
CHAPTER 2. EXPERIMENTAL	37
MATRIX ISOLATION TECHNIQUE	38
<i>Matrix features</i>	40
Advantages	45
Disadvantages	45
APPARATUS	46
<i>From a breath down to 10^{-7} mbar</i>	47
<i>A deposition</i>	49
<i>Some helpful features</i>	52
Photoneutralization	53
A scavenger	54
Annealing	54
<i>Ions sources</i>	55
Electron impact ion sources	55
Cesium sputter source	57
<i>Measurements</i>	59
UV-Vis	59
IR region	61
BIBLIOGRAPHY	63
CHAPTER 3. CARBON CHAIN CATIONS	67
LINEAR AND CYCLIC C_6^+	68
<i>Introduction</i>	68
<i>Experimental</i>	68
<i>Results and Discussion</i>	69
<i>Conclusions</i>	80
LINEAR AND CYCLIC C_N^+ ($N=7-9$)	82
<i>Introduction</i>	82
<i>Experimental</i>	82
<i>Results and discussions</i>	83
Electronic absorption spectra of C_7^+	83
Electronic absorption spectrum of C_9^+	88

Electronic absorption spectra of C_8^+ -----	90
BIBLIOGRAPHY -----	99
CHAPTER 4. CARBON CHAINS TERMINATED WITH A HYDROGEN ATOM -----	105
LINEAR C_6H^+ AND C_8H^+ -----	106
<i>Introduction</i> -----	106
<i>Theory</i> -----	107
<i>Results and Discussion</i> -----	109
Electronic spectrum of C_6H^+ -----	109
Theoretical prediction for C_6H^+ -----	113
Electronic spectrum of C_8H^+ -----	115
<i>Conclusions</i> -----	120
BIBLIOGRAPHY -----	121
CHAPTER 5. SULFUR SPECIES -----	125
ELECTRONIC TRANSITIONS OF S_2^- AND S_3^- -----	126
<i>Introduction</i> -----	126
<i>Experimental</i> -----	127
<i>Results and discussion</i> -----	127
Linear S_2^- -----	127
Linear S_3^- -----	132
BIBLIOGRAPHY -----	138
CHAPTER 6. APPENDIX -----	143
C_6H_4 -----	144
B_3 -----	149
C_nCl ($n=5,6$) -----	152
C_3Cl and C_4Cl -----	157
$H_2C_nH^+$ ($n=4,6,8$) -----	164
OUTLOOK -----	169
CURRICULUM VITAE -----	172
LIST OF PUBLICATIONS -----	173

CHAPTER 1. INTRODUCTION



PREFACE

Spectroscopy is one of the most powerful tools for gaining insight into molecules and ions. Absorption and emission spectra can be used for molecular identification and structure determination, while information concerning intramolecular dynamics can be inferred to understand and predict the behavior of chemical reactions. Today, rotational, vibrational and electronic spectra of chemical intermediates and radicals (energetically unstable and therefore nonexistent under normal laboratory conditions) can be measured. This information is not only of fundamental interest but is valuable in many branches of chemistry, particularly in astrochemistry where molecules exist under harsh interstellar conditions.

Spectroscopic data allowed the detection of diatomic radicals, such as CN, CH and CH^+ ion in the interstellar medium more than a century ago [1, 2]. Since then many unknown molecular species have become relevant in the field of interstellar chemistry, including various diatomic and polyatomic species, such as CO, HNO, bare carbon chains, carbon chain molecules containing an oxygen (C_2O) or sulfur atom (C_3S), carbon chains containing one or more hydrogen atoms, and cyanopolyynes. To date, the largest molecule detected in space is HC_{11}N [3-8], observed in molecular clouds using microwave spectroscopy. In total, more than 140 molecules have been detected in the interstellar medium (ISM) or circumstellar shells (Table 1.1), most of them unsaturated carbon containing molecules [9]. Long carbon chains, fullerenes, carbon nanoparticles and polycyclic aromatic hydrocarbons (PAHs) are also predicted to be interstellar. Current theory assumes that the latter and carbon chains are the most probable carriers of the diffuse interstellar bands (DIBs).

Carbon and hydrocarbon clusters are of interest not only due to their detection in space, but also from a fundamental point of view. Carbon clusters are also found in hydrocarbon flames and other soot-forming systems [10-13], and the study of these species is necessary for acquiring a thorough understanding of these complex chemical environments. Carbon clusters are proposed intermediates in the gas-phase chemistry taking place in chemical vapor deposition systems for production of thin diamond and

silicon carbide films [14-16]. Clearly, a detailed knowledge of the physical and chemical properties of carbon clusters is important for understanding a large variety of chemical systems. In addition, carbon clusters are fascinating examples of the richness and variety of carbon chemistry in itself. Due to carbon's enormous bonding flexibility, namely its unique ability to form stable single, double, or triple bonds, carbon clusters appear in a wide range of structural forms that are synthesized spontaneously in hot carbon plasmas. While great progress has been made, many unanswered questions still remain [17]. The fairly incomplete knowledge of the neutral and ionic analogues of carbon chain molecules is a strong impulse for the laboratory investigation of their spectral fingerprints.

The goal of this work was to contribute new experimental data concerning astrophysically relevant molecules using an approach that combines mass-selection with matrix isolation spectroscopy. The bare carbon chain cations C_n^+ ($n=6-9$) and singly protonated carbon chains C_nH^+ ($n=6,8$) were spectroscopically characterized for the first time. The identification of the electronic spectra of these astrophysically important species in neon matrices allows a good starting point for undertaking gas-phase studies, from which a direct comparison with astronomical data can be made.

Sulfur S_n^- ($n=2-3$) anions were also investigated within this work. Of the 140 different varieties of molecules detected in interstellar medium, 15 contain sulfur (Table 1.1) [18]. S and S_2 have also been observed by the Hubble Space Telescope in the volcanically driven atmosphere of Jupiter's moon Io [19, 20]. Sulfur is also expected to be contained in many molecules, which still remain undetected. It has more allotropes than any other element. All this makes sulfur containing compounds to be fascinating targets for further investigations.

TABLE 1.1 The 150 reported interstellar and circumstellar molecules. All molecules have been detected (also) by rotational spectroscopy in the radiofrequency to far-infrared regions unless indicated otherwise. * indicates molecules that have been detected by their rotation-vibration spectrum, ** those detected by electronic spectroscopy only.

Two Atoms	Three Atoms	Four Atoms	Five Atoms	Six Atoms	Seven Atoms	Eight Atoms	Nine Atoms
H ₂	C ₃ *	c-C ₃ H	C ₅ *	C ₅ H	C ₆ H	CH ₃ C ₃ N	CH ₃ C ₄ H
AlF	C ₂ H	l-C ₃ H	C ₄ H	l-H ₂ C ₄	CH ₂ CHCN	CH ₃ COOH	CH ₃ CH ₂ CN 2007
AlCl	C ₂ O	C ₃ N	C ₄ Si	C ₂ H ₄ *	CH ₃ C ₂ H	HC(O)OCH ₃	(CH ₃) ₂ O
C ₂ **	C ₂ S	C ₃ O	l-C ₃ H ₂	CH ₃ CN	HC ₅ N	C ₇ H	CH ₃ CH ₂ OH
CH	CH ₂	C ₃ S	c-C ₃ H ₂	CH ₃ NC	CH ₃ CHO	H ₂ C ₆	HC ₇ N
CH ⁺	HCN 2006	C ₂ H ₂ *	H ₂ CCN	CH ₃ OH	CH ₃ NH ₂	CH ₂ OHCHO 2006	CH ₃ C(O)NH ₂ 2006
CN	HCO	CH ₃ *	CH ₄ *	CH ₃ SH	c-C ₂ H ₄ O	CH ₂ CHCHO	C ₈ H
CO	HCO ⁺	HCCN	HC ₃ N	HC ₃ NH ⁺	H ₂ CCHOH	l-HC ₆ H *	C ₃ H ₆ 2007
CO ⁺	HCS ⁺	HCNH ⁺	HC ₂ NC	H ₂ CNNH? 2006	C ₆ H ⁻ 2006	CH ₂ CCHCN 2006	C ₈ H ⁻ 2007
CP	HOC ⁺	HNCO	HCOOH	NH ₂ CHO			
SiC	HNC	HNCS	H ₂ CHN	C ₅ N			
HCl	H ₂ S	HOCO ⁺	H ₂ C ₂ O	HC ₄ N			
KCl	H ₂ O 2007	H ₂ CO	C ₄ H ⁻ 2007	c-H ₂ C ₃ O 2006			
NH	HNO	H ₂ CN	HNC ₃	HC ₂ CHO			
NO	MgCN	H ₂ CS	SiH ₄ *	l-HC ₄ H? *			
NS	MgNC	H ₃ O ⁺	H ₂ COH ⁺				
NaCl	N ₂ H ⁺	NH ₃	H ₂ NCN				
OH	N ₂ O	c-SiC ₃					
PN	NaCN						
SO	OCS						
SO ⁺	SO ₂						
SiN	c-SiC ₂						
SiO	CO ₂ *						
SiS	NH ₂						
CS	H ₃ ⁺ *						
HF	SiCN						
SH *	AiNC		Ten Atoms		Eleven Atoms	Twelve Atoms	Thirteen Atoms
FeO?	SiNC		CH ₃ CH ₂ CHO		HC ₉ N	C ₂ H ₅ OCH ₃ ?	HC ₁₁ N
O ₂ 2007	HCP 2007		CH ₃ C ₅ N 2006		CH ₃ C ₆ H 2006	C ₆ H ₆ ? *	
SiH?	H ₂ D ⁺		(CH ₂ OH) ₂				
HD	HD ₂ ⁺		(CH ₃) ₂ CO				
CF ⁺ 2006							
PO 2007							

INTERSTELLAR MEDIUM

HOW DID IT ALL START?

By the end of 18th century scientists were investigating the composition of the interstellar medium. Astronomers and scientists believed that the space between stars and planets was not empty, but rather filled with matter which absorbs star light. The advent of deep photographic imaging allowed Edward Barnard to produce the first images of dark nebulae silhouetted against the background star field of the galaxy, while the first actual detection of cold diffuse matter in interstellar space was made by Johannes Hartmann in 1904 through the use of absorption line spectroscopy [21, 22]. In this historic study of the spectrum and orbit of δ -Orionis, Hartmann observed the light coming from this star and realized that some of this light was being absorbed before it reached the Earth. Hartmann reported that absorption from the K line of calcium appeared “extraordinarily weak, but almost perfectly sharp” and also reported a “quite surprising result that the calcium line at 393.4 nm does not share in the periodic displacements of the lines caused by the orbital motion of the spectroscopic binary star.” The stationary nature of the line led Hartmann to conclude that the gas responsible for the absorption was not present in the atmosphere of δ -Orionis but was instead located within an isolated cloud of matter residing somewhere along the line-of-sight¹ to this star. This discovery launched the study of the ISM.

Following the identification of interstellar calcium absorption by Hartmann, observations of the H and K lines of calcium by Beals revealed double and asymmetric profiles in the spectra of ϵ - and ζ -Orionis [23]. These were the first steps in the study of the very complex interstellar sightline toward Orion. Asymmetric absorption line profiles are the result of the superposition of multiple absorption lines, each corresponding to the same atomic transition (for example the K line of calcium) but

¹ line-of-sight: an imaginary straight line between the Earth and a star. The light emitted by this star is studied after it has been absorbed by the interstellar matter.

occurring in interstellar clouds with different radial velocities. Each cloud has a different velocity, either toward or away from the observer/Earth, the absorption lines occurring within each cloud is either blueshifted or redshifted, respectively, from the lines rest wavelength through the Doppler Effect [24]. These observations highlight that matter is not distributed homogeneously and were the first evidence for the presence of multiple discrete clouds within the ISM.

The growing evidence for interstellar material led William Henry Pickering to comment in 1912 that

while the interstellar absorbing medium may be simply the ether, yet the character of its selective absorption, as indicated by Kapteyn, is characteristic of a gas, and free gaseous molecules are certainly there, since they are probably constantly being expelled by the Sun and stars, and certainly in a smaller way by the planets and comets. This is further indicated by the fact that the younger stars seem to be more massive than the older ones [25].

The same year Victor Hess's discovery of cosmic rays, highly energetic charged particles that rain down on the Earth from space, led others to speculate whether they also pervaded interstellar space. The following year the Norwegian explorer and physicist Kristian Birkeland wrote:

It seems to be a natural consequence of our points of view to assume that the whole of space is filled with electrons and flying electric ions of all kinds. We have assumed that each stellar system in evolutions throws off electric corpuscles into space. It does not seem unreasonable therefore to think that the greater part of the material masses in the universe is found, not in the solar systems or nebulae, but in "empty" space [26].

In 1930 Samuel L. Thorndike notes that

it could scarcely have been believed that the enormous gaps between the stars are completely void. Terrestrial aurorae are not improbably excited by charged particles emitted by the Sun. If the millions of other stars are also ejecting ions, as is undoubtedly true, no absolute vacuum can exist within the galaxy [27].

Today, the interstellar medium is one of the most interesting and fascinating topics. Scientists and astronomers all over the world attempt to understand those subjects which still remain unclear.

There are many reasons why people are interested in the interstellar medium:

- The neighboring interstellar gas is the only sample of space not from our solar system that we can study directly;
- The interstellar gas is what our sun, the planets and all the stars are made of;
- The interstellar gas is an important component of the Milky Way² and other galaxies;
- The composition of the interstellar gas contains information about the evolution of the universe and our galaxy.

UP THERE

Many of us might think that the outer space is a complete vacuum, void of any material. The stars, being the heaviest bodies of our universe, occupy only 10^{-27} of its volume. The vast space between them, called among astronomers as interstellar medium, is not entirely empty and contains interstellar gas (99%) and dust (1%) [28]. The interstellar gas consists partly of neutral atoms and molecules, as well as charged particles, such as ions and electrons [29]. This gas, with an average density of about 1 particle/cm³, is extremely dilute compare with the air we breathe, which contains about 3×10^{19} molecules/cm³. The total mass of the gas and dust in the ISM is about 15% of the total mass of the visible matter in the Milky Way [30]. In spite of the fact that ISM is a better vacuum, by several orders of magnitude, than any physicists can create in the laboratory there is still about of 5–10 billion M_{\odot} (mass of the Sun) of gas and dust. The primordial matter produced in the Big Bang³ was almost entirely hydrogen and helium

² Milky Way: The band of light that encircles the sky, caused by the bending of light from many stars lying near the plane of the galaxy; also sometimes used to refer to the galaxy in which the sun belongs.

³ Big Bang model: A theory of the evolution of the universe that postulates its origin, in an event called Big Bang, from a hot, dense state that rapidly expanded to cooler, less-dense states.

with trace amount of lithium, beryllium and boron. Most of the interstellar medium today is still made up of these elements but there are also other heavy elements as it is shown in Figure 1.1.

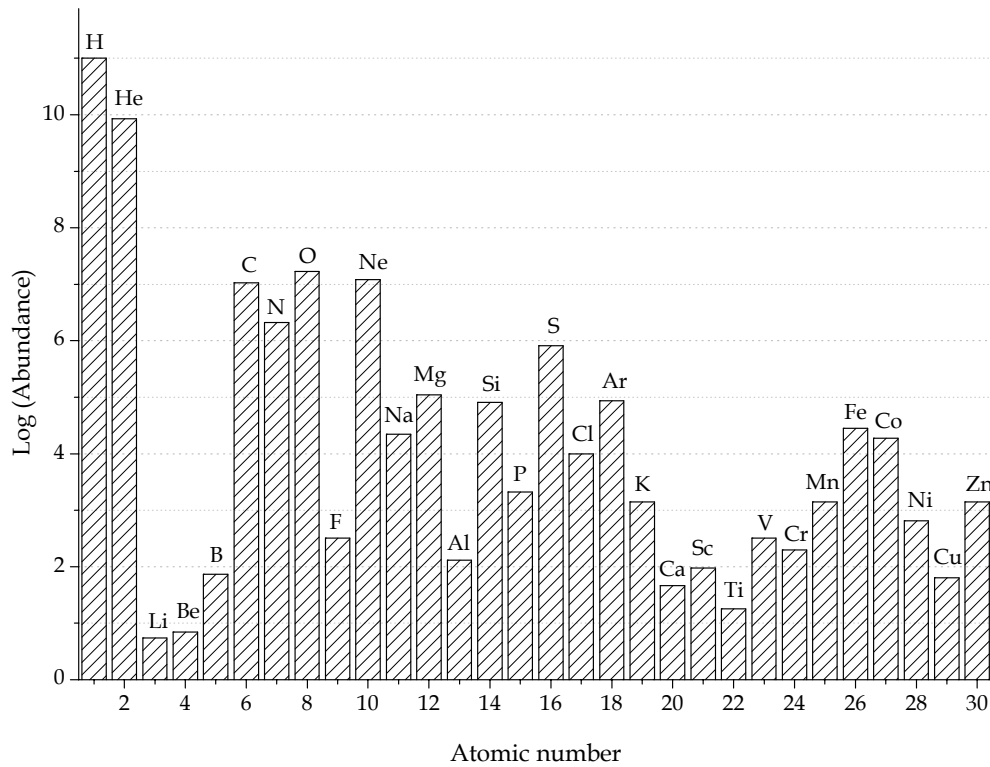


FIGURE 1.1 Relative abundance of elements in the interstellar medium. An interesting point is that lithium, beryllium and boron are 10^6 times less abundant than that of carbon.

The interstellar gas is typically found in two forms:

- Cold clouds of atomic or molecular hydrogen;
- Hot ionized hydrogen near hot young stars.

MOLECULAR CLOUDS

The interstellar clouds, referred to as nebulae (nebula=singular), can be divided into three types:

- a) dark clouds, which are essentially made of very cold ($T \sim 10\text{--}20$ K) molecular gas and block of light from background stars,
- b) diffuse clouds, which consist of cold ($T \sim 100$ K) atomic gas and are almost transparent to the background starlight, and
- c) translucent clouds, which contain molecular and atomic gases and have intermediate visual extinction.⁴

The rest of the interstellar matter, spread out between the clouds, exists in three different forms: warm (mostly neutral) atomic, warm ionized, and hot ionized, where warm refers to a temperature of $\sim 10^4$ K and hot to a temperature of $\sim 10^6$ K (Table 1.2) [29]. The dense cold clouds, also known as dark clouds, are the birthplaces of stars. They are built of large amounts (1000 molecules/cm³) of hydrogen having a temperature of around $10\text{--}20$ K. Molecular hydrogen is difficult to detect through infrared and radio observations because it possess no permanent electric dipole moment of inertia, so all its permitted transitions lie outside the radio domain [31]. In this connection, the molecule most often used to determine the presence of H₂ is CO (carbon monoxide), which has a $J=1 \rightarrow 0$ rotational transition at a radio wavelength of 2.6 mm; the corresponding emission line has become the primary tracer of molecular interstellar gas [32].

There are several types of nebulae, three of them (emission, absorption and reflection nebulae) are shown in Figure 1.2, all of which differ in their temperature and concentration of hydrogen. One of most famous and photographed nebulae is emission nebula, which contains mostly atoms and atomic ions. Its characteristic red color being due to light released by hydrogen atoms around $10\ 000$ K. Absorption nebulae, a

⁴ Extinction: the dimming of light when it passes through some medium, such as the earth's atmosphere or interstellar material, by both absorption & scattering processes. Assume light from a star passes through a dusty cloud. If the cloud removes a fraction k per meter of the light, then $I = I_0 e^{-kl} = I_0 e^{-t}$; where t is the so-called optical depth of the cloud, I_0 is the light intensity entering the cloud and I is the remaining fraction of light continuing along the line of travel.



FIGURE 1.2 Three types of nebulae: emission (Orion), absorption (Horsehead), and reflection (Pleiades).

different type of gas-dust cloud, are also found in the interstellar medium. They appear dark, indicating their low temperatures, sometimes as low as 10 K. At such temperatures, atoms can bond together to form molecules like water (H_2O), CO and methane (CH_4). In turn, these molecules can absorb to the cold dust grains in an absorption nebula and be altered by high-energy light to form still other, different molecules. The third type, reflection nebulae, normally display a blue color due to light scattered by their dust grains, the light originating in nearby stars. Sometimes all these types of nebulae can be found on a single photograph as is shown in the case of Horsehead Nebula (Fig. 1.2) A comprehensive review of the interstellar environment of our galaxy can be found elsewhere [29].

The clouds are surrounded by warm neutral intercloud gas and hot ionized coronal gases that fill most of the space (Table 1.2).

TABLE 1.2 Interstellar medium phases [33].

<i>Component</i>	<i>Fractional Volume</i>	<i>Temperature K</i>	<i>Density (atoms/cm³)</i>	<i>State</i>
Molecular clouds	< 1%	20–50	10^3 – 10^6	hydrogen molecules
Cold Neutral Medium	1–5%	50–100	1 – 10^3	neutral hydrogen atoms
Warm Neutral Medium	10–20%	1000–5000	10^{-1} – 10	neutral hydrogen atoms
Warm Ionized Medium	20–50%	10^3 – 10^4	10^{-2}	ionized hydrogen
H II regions	~10%	10^4	10^2 – 10^4	ionized hydrogen
Coronal gas Hot Ionized Medium (HIM)	30–70%	10^6 – 10^7	10^{-4} – 10^{-2}	highly ionized (both hydrogen and trace metals)

IONIZED HYDROGEN REGIONS

Normally, atoms and molecules are electronically neutral. Most of the matter that surrounds us is in this form; however, when there are energy sources available electrons can be gained or lost. The loss of electrons (ionization), which is the more common process in astrophysical environments, converts an atom into a positively charged ion. Conversely, gaining electrons creates negatively charged ions.

Photoionization of hydrogen occurs when UV photons from massive stars emit radiation greater than 13.6 eV or in wavelengths less than 91.2 nm [34, 35]. Such regions of ionized hydrogen are called H II regions, while cold unionized hydrogen clouds are termed H I regions [36]. All H II regions differ noticeably in their physical properties. They vary in size from ultra-compact regions [37] which are around a light-year⁵ across to giant H II regions several hundred light-years across [38]. Their size depends on the intensity of the source of ionizing photons and the density of the region. The latter range from ~ a million particles/cm³ to only a few particles/cm³ in the largest and most extended regions [39-41]. This implies total masses between perhaps 10^2 and

⁵ light-year: the distance light travels in one year, about 30.9×10^{12} kilometers.

10^5 solar masses.⁶ Depending on the size of an H II region there may be up to several thousand of hot ($\sim 10^4$ K) bright stars within it. These stars are many times more massive than the sun and are the shortest-lived stars, with total lifetimes of only a few million years (for comparison the sun lives for several billion years). Therefore, it was presumed that H II regions must be regions in which new stars are forming. The H II regions are mostly ionized [36], and the ionized gas (plasma) can contain magnetic fields which are produced by moving electric charges in the plasma [42, 43]; moreover, some observations have suggested that H II regions also contain electric fields [44]. These regions consist of about 90% hydrogen. The strongest hydrogen emission line is produced by visible light emitted at 656.3 nm when electrons recombine with the ionized hydrogen in these regions [45, 46]. This emission line gives H II regions their characteristic red color. The Orion Nebula is one of the best known among H II regions (Fig. 1.2). Most of the rest of an H II region consists of helium, with trace amounts of heavier elements. The complete details of massive star formation within H II regions are not yet well known. Two major problems complicate research in this area:

- Considerable distances from the Earth to large H II regions with the nearest H II region being over 1000 light-years away; other H II regions are several times that distance away from Earth;
- The formation of these stars is deeply obscured by dust and visible light observations are impossible. Radio and infrared light can penetrate the dust but the youngest stars may not emit much light at these wavelengths.

DIFFUSE INTERSTELLAR BANDS

One of the longest unsolved problem in astrophysical spectroscopy is that of diffuse interstellar bands. Diffuse interstellar bands are absorption features seen in the spectra of astronomical objects in our galaxy. They have been detected in different

⁶ Solar mass: The solar mass is a standard way to express mass in astronomy, used to describe the masses of other stars and galaxies. It is equal to the mass of the sun, about two nonillion kilograms or about 332 950 times the mass of the Earth. Its conventional symbol and value are: $M_{\odot}=1.9891\times 10^{30}$ kg.

regions of the interstellar medium indicating an ubiquitous presence of their carrier in space.

Diffuse interstellar bands were first recorded on photographic plates in spectra of distance stars by astronomer Mary Lea Heger during her doctorate research in 1922 [47]. Their interstellar nature was shown by the fact that the strength of the observed absorption was roughly proportional to the extinction, and in objects with widely differing radial velocities, the absorption bands were not affected by Doppler shifting [24], implying that the absorption was not occurring in or around the object concerned. The name diffuse interstellar band was coined to reflect the fact that the absorption features are much broader than the normal absorption lines seen in stellar spectra. The spectra are confined to the range between ~ 400 and ~ 1300 nm with the highest density of bands found in the visible (540–690 nm) [48, 49], which is roughly equivalent to photon energies in the 1–3 eV range (Fig. 1.3).

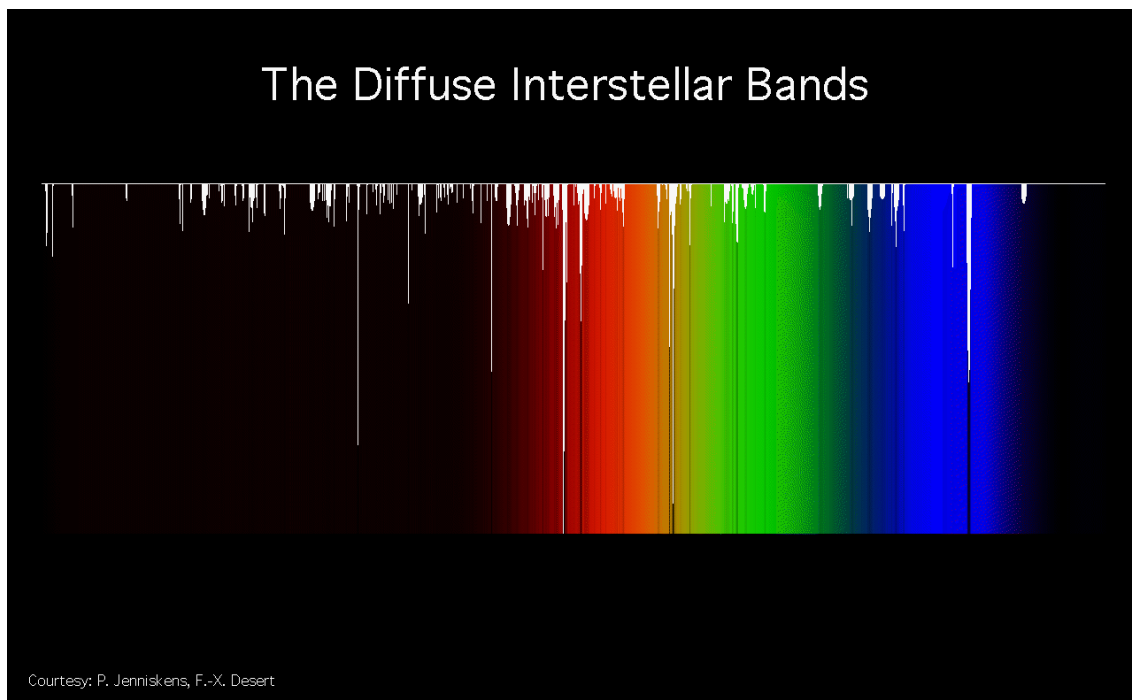


FIGURE 1.3 *The diffuse interstellar bands. The picture is taken from an article written by P. Jenniskens and F.-X. Désert [50].*

Despite decades of intensive investigation, since Merrill (1934) [51, 52] first established their origin in the ISM, the identity of the carrier or carriers of the DIBs has not been established.

CHARACTERISTICS OF THE DIFFUSE INTERSTELLAR BANDS

Diffuse interstellar bands have their origin in the diffuse ISM, one of the various phases present (Table 1.2). The diffuse ISM is characterized by low density (25–30 particles/cm³), low temperature (<100 K) clouds of dust, composed primarily of carbonaceous and/or silicate materials and gas separated by vast regions of vacuum [53]. The gaseous fraction of the diffuse clouds is made up of atoms, as well as molecules. The most abundant elements in the diffuse interstellar space, as well as in the whole universe, are H, C, O and N. To date, over 300 diffuse interstellar bands have been documented, almost a hundred times more than in 1975 [54].

The most remarkable characteristic of the diffuse interstellar bands is that their positions are closely reproducible when measured from various molecular clouds [55], their widths, which range between ~ 2 and ~ 100 cm⁻¹, is broad compared to atomic bands [48]. The diffuseness is most commonly attributed to short lifetimes of the excited states of the transitions [56]. These characteristics of DIBs make no doubts that they have a molecular origin as was first suggested by Herzberg in 1967. The existence of sub-structure in DIBs supports this idea [57]. In a molecule containing, say, three carbon atoms, some of the carbon will be in the form of the carbon-13 (¹³C) isotope, so that while most molecules will contain three carbon-12 (¹²C) atoms, some will contain two ¹²C atoms and one ¹³C atom, even fewer will contain one ¹²C and two ¹³Cs, and a very small fraction will contain three ¹³C molecules. Each of these isotopomers will result in slightly shifted absorption lines. Higher resolution spectra of some DIBs have been measured and reproducible profiles have been obtained [58-60]. Such spectra could provide more insight into understanding the nature of the carriers.

Although the positions of the DIBs remain the same, the relative intensities of them vary from cloud to cloud. That proves that their origin comes from not only one

carrier but from many. As soon as the exact correspondence between several lines is found irrespective of the cloud they were observed in, one can separate them into “families of bands” [61], which can be helpful in assignment.

PROPOSALS FOR THE ORIGIN OF THE DIFFUSE BANDS

Plenty of the candidates were considered as DIB carriers, including: the electronic transitions between excited states of H₂ [62], porphyrins [63], dust grains [64], fullerenes [65], carbon chains [66] and PAHs [67]. The full history of these considerations in the time period from 1975 till 2006 is reviewed in a number of papers [48, 54, 68-70]. Despite a wide variety of suggested species, they all tend to include carbon. The abundance of carbon in the universe [71-74], the readiness of carbon atoms to form stable compounds with themselves and with atoms of other elements (H, N, O) and the radioastronomical observation of many interstellar molecules with a carbon skeleton point to carbon as the basic building material of the DIB carriers.

Dust grains resemble the ions embedded in neon matrices. In the experimental section of this work gas-matrix shifts in Ne environments and band broadenings are discussed. With this thought in mind, one can conclude with some confidence that dust grains can not be responsible for the DIB bands.

The discovery of C₆₀ was made in experiments partly motivated by the search for DIBs. These experiments have shown that this system composed of 60 carbon atoms is exceptionally stable. The hypothesis that C₆₀ is a carrier was disproved when the strongest absorption of C₆₀ appeared to fall within the UV region [75, 76] that says that it would barely survive the harsh interstellar conditions. In the case of C₆₀⁺, the spectrum of this ion in a neon matrix (Fig. 1.4) measured by Fulara *et al.* [77] is in a good correlation with the DIBs observed by Foing and Ehrenfreund in 1994 [78]. The definite answer as to whether fullerene cations are responsible for some DIBs will be

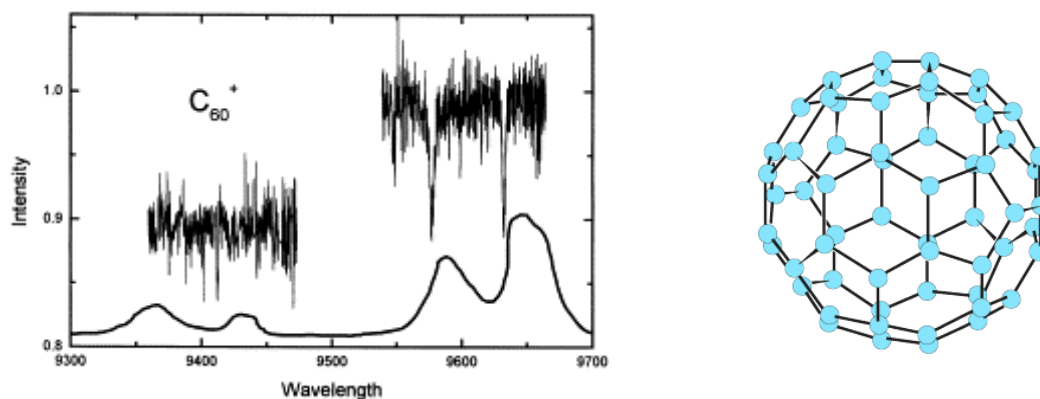


FIGURE 1.4 Comparison of the electronic absorption spectrum of C_{60}^+ isolated in a neon matrix (the lower trace; Fulara et al. [77]) with the DIB spectrum recorded on the background of BD +40° 4220 star.

conclusive once the absorption spectrum of gas-phase C_{60}^+ is known. The current situation concerning C_{60} and its cation is discussed in recent comprehensive work by Herbig [79].

Among the remaining possible carriers, polycyclic aromatic hydrocarbons and carbon chains including their derivatives seem to be the most promising candidates [80].

POLYCYCLIC AROMATIC HYDROCARBONS

Polycyclic aromatic hydrocarbons have been proposed as potential DIB carriers based on their expected abundance in the ISM and their stability against ultraviolet photodissociation [81-83]. While neutral PAHs of medium size have their strongest absorptions in the UV (DIBs are present in 440 nm – NIR region) their cation derivatives are more promising candidates [82, 84]. These are open-shell systems with electronic absorptions in the visible and NIR, exactly where DIBs are located. Moreover, large size PAH cations are believed to be more abundant in ISM and resistant to its conditions.

CARBON CHAINS

The suggestion that carbon chains should be considered as possible carriers of the DIBs was postulated by Douglas in 1977 [66]. Their presence in the diffuse clouds is suspected due to the fact that carbon chains absorb in the DIB wavelength range and, furthermore, they have been previously identified by radio astronomy in the dense clouds [85]. Several overviews on carbon chains and their relevance to astrophysics were recently reported [86]. Carbon chains are characterized by several interesting peculiarities. For a homologous series carbon-chain species (i.e. C_{2n} is a constant fragment where $n=1,2,\dots$) the strongest absorption bands shift from the blue toward the red with increasing chain length as it is shown in Figure 1.5. Oscillator strength of a given electronic transitions increases with the wavelength of carbon atoms [87].

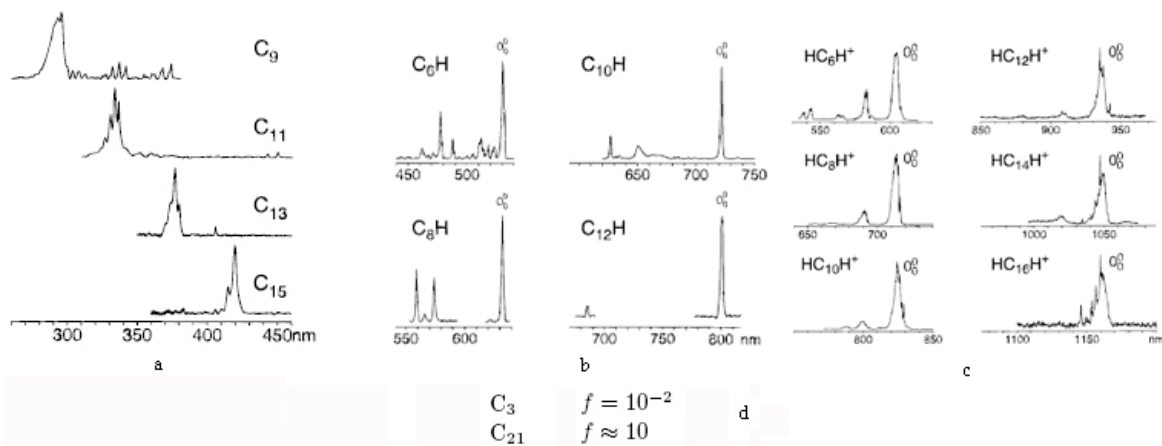


FIGURE 1.5 The shift of the strongest absorption bands from the blue toward the red with increasing chain length is shown by the example of three different homologues series of carbon species. Spectra are taken from the studies on carbon chain species embedded in Ne matrices [88-90]. Trace d shows that the oscillator strength (f) increases with the wavelength of carbon atoms.

The neon matrices experiments on mass-selected highly unsaturated hydrocarbon anions ($C_nH_m^-$, where $n=6-16$, $m\leq 3$), revealed a possible correspondence in band positions with 17 DIBs lying at wavelengths of 600 nm and higher [91, 92].

In contrast to the Douglas's hypothesis, recent studies of Boguslavskiy *et al.* show that carbon chains comprising of up to 15 carbon atoms can not be the carriers, while larger carbon chains still remain viable candidates. Moreover, this statement applies not only to the bare carbon chains but also to their derivatives such as those containing hydrogen, C_nH , comprising up to around a dozen atoms [93]. It was shown that the abundance of open-shell (HC_nH , C_{2n} , C_nH) carbon-chain systems (up to 10 atoms) are too small to account for DIBs. It was also shown that the lowest energy electronic transitions of these molecules do not possess a large enough oscillator strength, whereas higher energy ones in the UV do; therefore, chains would have to be longer than 20 atoms for these absorptions to shift into the DIB's 400–900 nm wavelength region. The exceptions are the odd-numbered bare carbon chains with their closed-shell systems (C_{2n+1} , $C_{2n+1}H^+$): these chains (15–31 carbon atoms) have very strong electronic transitions in the proper region.

At the present time, none of the laboratory gas-phase bands of carbon-chain radicals can be assigned with confidence to any interstellar feature. At the current time, the largest carbon molecule identified optically in diffuse clouds is C_3 [94, 95]. However, identifying the molecules responsible for each DIB is still very much a work in progress, and as Theodore Snow concluded in a recent paper: "...we should keep in mind the rich diversity of chemistry, and consider the likelihood that we have simply not yet thought of the best candidates for the DIB carriers" [96].

BIBLIOGRAPHY

- [1] A.E. DOUGLAS and G. HERZBERG. CH⁺ in interstellar space and in the laboratory. *The Astrophysical Journal*, 94: 381, 1941
- [2] P. SWINGS and L. ROSENFELD Considerations regarding interstellar molecules. *The Astrophysical Journal*, 86: 483-486, 1937
- [3] P. THADDEUS, C.A. GOTTLIEB, R. MOLLAAGHABABA, and J.M. VRTILEK. Free carbenes in the interstellar gas. *Journal of the Chemical Society, Faraday Transactions*, 89: 2125-2129, 1993
- [4] H.W. KROTO. The spectra of interstellar molecules. *International Reviews in Physical Chemistry*, 1: 309-376, 1981
- [5] K.N. RAO and A. WEBER, *Spectroscopy of the Earth's atmosphere and interstellar medium*. 1992, New York: Academic Press Inc.
- [6] W.W. DULLEY and D.A. WILLIAMS. *Interstellar Chemistry*. Academic Press Inc., London, 1984
- [7] M.C. MCCARTHY, M.J. TRAVERS, A. KOVÁCS, C.A. GOTTLIEB, and P. THADDEUS. Eight new carbon chain molecules. *The Astrophysical Journal Supplement Series*, 113: 105-120, 1997
- [8] M.B. BELL, P.A. FELDMAN, S. KWOK, and H.E. MATTEWS. Detection of HC₁₁N in IRC+10°216. *Nature*, 295: 389-391, 1982
- [9] THE COLOGNE DATABASE FOR MOLECULAR SPECTROSCOPY, CDMS. *The 140 reported interstellar and circumstellar molecules*. cited 08.2007; Available from: <http://www.ph1.uni-koeln.de/vorhersagen/>.
- [10] H.W. KROTO and K. MCKAY. The formation of quasi-icosahedral spiral shell carbon particles. *Nature*, 331: 328-331, 1988
- [11] P. GERHARDT, S. LÖFFLER, and K.H. HOMANN. Polyhedral carbon ions in hydrocarbon flames. *Chemical Physics Letters*, 137: 306-310, 1987
- [12] K.H. HOMANN. Fullerenes and soot formation-new pathways to large particles in flames. *Angewandte Chemie International Edition*, 37: 2434-2451, 1998
- [13] Q.L. ZHANG, S.C. O'BRIEN, J.R. HEATH, Y. LIU, R.F. CURL, H.W. KROTO, and R.E. SMALLEY. Reactivity of large carbon clusters: spheroidal carbon shells and their possible relevance to the formation and morphology of soot. *Journal of Physical Chemistry*, 90: 525-528, 1986

- [14] T. FUJII and M. KAREEV. Mass spectrometric studies of a CH₄/H₂ microwave plasma under diamond deposition conditions. *Journal of Applied Physics*, 89: 2543-2546, 2001
- [15] H. KOINUMA, T. HORIUCHI, K. INOMATA, H.-K. HA, K. NAKAJIMA, and K.A. CHAUDHARY. Synthesis of carbon clusters and thin films by low temperature plasma chemical vapor deposition under atmospheric pressure. *Pure and Applied Chemistry*, 68: 1151-1154, 1996
- [16] M.D. ALLENDORF. Equilibrium prediction of the role of organosilicon compounds in the chemical vapor deposition of silicon carbide. *Journal of The Electrochemical Society*, 140: 747-753, 1993
- [17] A. VAN ORDEN and R. SAYKALLY. Small carbon clusters: spectroscopy, structure, and energetics. *Chemical Reviews*, 98: 2313-2357, 1998
- [18] E.L.O. BAKES, *The astronomical evolution of the interstellar medium*. 1997, Vledder Twin Press.
- [19] L.M. FEAGA, M.A. MCGRATH, and P.D. FELDMAN. The abundance of atomic sulfur in the atmosphere of Io. *The Astrophysical Journal*, 570: 439-446, 2002
- [20] J.R. SPENCER, K.L. JESSUP, M.A. MCGRATH, G.E. BALLESTER, and R. YELLE. Discovery of gaseous S₂ in Io's Pele plume. *Science*, 288: 1208-1210, 2000
- [21] T. DUNHAM. Interstellar neutral potassium and neutral calcium. *Publications of the Astronomical Society of the Pacific*, 49: 26-28, 1937
- [22] P.W. MERILL. Identification of lines in the spectrum of η Catinae. *Publications of the Astronomical Society of the Pacific*, 48: 79-81, 1936
- [23] C.S. BEALS. On the interpretation of interstellar lines. *Monthly notices of Royal Astronomical Society*, 96: 661-678, 1936
- [24] C. DOPPLER. Concerning the coloured light of double stars and some other heavenly bodies. *Royal Bohemian Scientific Society*, 1842
- [25] W.H. PICKERING. The motion of the Solar system relatively to the interstellar absorption medium. *Monthly notices of Royal Astronomical Society*, 72: 740-756, 1912
- [26] K. BIRKELAND. Interstellar matter. *Publications of the Astronomical Society of the Pacific*: 720, 1913
- [27] S.L. THORNDIKE. Interstellar matter. *Publications of the Astronomical Society of the Pacific*, 42: 99-104, 1930

- [28] G. WYNN-WILLIAMS, *The Fullness of Space*. 1992: Cambridge University Press.
- [29] K.M. FERRIÈRE. The interstellar environment of our galaxy. *Reviews of Modern Physics*, 73: 1031-1066, 2001
- [30] D. T.M., D. HARTMANN, and P. THADDEUS. The Milky Way in molecular clouds: a new complete CO survey. *The Astrophysical Journal*, 547: 792-813, 2001
- [31] G.B. FIELD, W.B. SOMERVILLE, and K. DRESSLER. Hydrogen molecules in astronomy. *Annual Review of Astronomy and Astrophysics*, 4: 207-244, 1966
- [32] N.Z. SCOVILLE and D.B. SANDERS, *Interstellar processes*, D.J. Hollenbach and H.A. Thronson Jr., Editors. 1987, Reidel: Dordrecht. p. 21.
- [33] C.F. MCKEE and J.P. OSTRIKER. A theory of the interstellar medium: three components regulated by supernova explosions in an inhomogeneous substrate. *The Astrophysical Journal*, 218: 148-169, 1977
- [34] B. STRÖMGREN. The physical state of interstellar hydrogen. *The Astrophysical Journal*, 89: 526-547, 1939
- [35] F.D. KAHN. The acceleration of interstellar clouds. *Bulletin of the Astronomical Institutes of the Netherlands*, 12: 187-200, 1954
- [36] J. FRANCO, G. TENORIO-TAGLE, and P. BODENHEIMER. On the formation and expansion of H II regions. *The Astrophysical Journal*, 349: 126-140, 1990
- [37] D.O.S. WOOD and E. CHURCHWELL. The morphologies and physical properties of ultracompact H II regions. *The Astrophysical Journal Supplement Series*, 69: 831-895, 1989
- [38] G. GARCÍA-SEGURA and J. FRANCO. From ultracompact to extended H II regions. *The Astrophysical Journal*, 469: 171-188, 1996
- [39] P. BODENHEIMER, G. TENORIO-TAGLE, and H.W. YORKE. The gas dynamics of H II regions. *The Astrophysical Journal*, 233: 85-96, 1979
- [40] G. TENORIO-TAGLE. The gas dynamics of H II regions. *Astronomy and Astrophysics*, 71: 59-65, 1979
- [41] P. HOFNER, F. WYROWSKI, C.M. WALMSLEY, and E. CHURCHWELL. A C¹⁷O survey toward ultra-compact H II regions. *The Astrophysical Journal*, 536: 393-405, 2000
- [42] C. HEILES, Y.-H. CHU, and T.H. TROLAND. Magnetic fields strengths in the H II regions. *The Astrophysical Journal*, 247: L77-L80, 1981

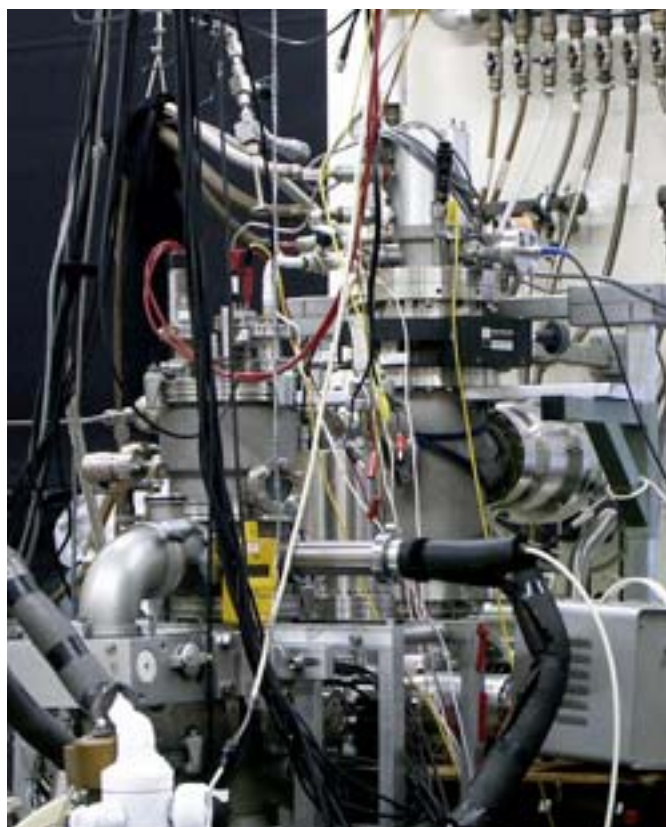
- [43] R.M. CRUTCHER. Magnetic fields in molecular clouds: observations confront theory. *The Astrophysical Journal*, 520: 706-713, 1999
- [44] T. OOSTERLOO, R. MORGANTI, E.M. SADLER, A. FERGUSON, T. VAN DER HULST, and H. JERJEN. Tidal remnants and intergalactic H II regions. *Astronomical Society of the Pacific*: 486, 2004
- [45] D. PAN. A study of H II region emission lines. *Quantum Physics II*: 1-8,
- [46] *The hydrogen 21-cm emission line*, in *Demystifying Scientific Data*. 2006. p. 167-176.
- [47] M.L. HEGER. The spectra of certain class B stars in the regions 563-668 and 328-338 nm. *Lick Observatory bulletin*, 337: 141-147, 1922
- [48] G.H. HERBIG. The diffuse interstellar bands. *Annual Review of Astronomy and Astrophysics*, 33: 19-73, 1995
- [49] P. JENNISKENS and F.-X. DÉSSERT. A survey of diffuse interstellar bands (380-868 nm). *Astronomy and Astrophysics Supplement Series*, 106: 39-78, 1994
- [50] P. JENNISKENS and F.-X. DÉSSERT, *The Diffuse Interstellar Bands*, in: *The Diffuse Interstellar Bands*, A.G.G.M. Tielens and T.P. Snow, Editors. 1995, Kluwer Academic Publishers: Dordrecht. p. 39 (cover).
- [51] P.W. MERRILL. Stationary lines in the spectrum of the binary star boss 6142. *The Astrophysical Journal*, 83: 126-128, 1936
- [52] P.W. MERRILL. Unidentified interstellar lines. *Publications of the Astronomical Society of the Pacific*, 46: 206-207, 1934
- [53] E.L. FITZPATRICK. The composition of the diffuse interstellar medium. *The Astrophysical Journal*, 473: L55-L-58, 1996
- [54] G.H. HERBIG. The diffuse interstellar bands. IV. The region 440-685 nm. *The Astrophysical Journal*, 196: 129-160, 1975
- [55] S.J. FOSSEY and W.B. SOMMERVILLE, *The diffuse interstellar bands and interstellar dust*, in: *The Diffuse Interstellar Bands*, A.G.G.M. Tielens and T.P. Snow, Editors. 1995, Kluwer Academic Publishers: Dordrecht. p. 241.
- [56] W.H. SMITH, T.P. SNOW, JR., and D.G. YORK. Comments on the origins of the diffuse interstellar bands. *The Astrophysical Journal*, 218: 124-132, 1977
- [57] P.J. SARRE, J.R. MILES, T.H. KERR, R.E. HIBBINS, S.J. FOSSEY, and W.B. SOMMERVILLE. Resolution of intrinsic fine structure in spectra of narrow diffuse

- interstellar bands. *Monthly Notices of the Royal Astronomical Society*, 277: L41-L43, 1995
- [58] G.H. HERBIG and D.R. SODERBLOM. The diffuse interstellar bands. V. High-resolution observations. *The Astrophysical Journal*, 252: 610-615, 1982
- [59] T.H. KERR, R.E. HIBBINS, S.J. FOSSEY, J.R. MILES, and P.J. SARRE. Ultrafine structure in the 579.7 diffuse interstellar absorption band. *The Astrophysical Journal*, 495: 941-945, 1998
- [60] G.A.H. WALKER, A.S. WEBSTER, D.A. BOHLENDER, and J. KRĘŁOWSKI. Profiles of the $\lambda 619.6$ and $\lambda 637.9$ diffuse interstellar bands. *The Astrophysical Journal*, 561: 272-281, 2001
- [61] J. KRĘŁOWSKI. Diffuse interstellar bands. Some observational aspects. *Astronomische Nachrichten*, 310: 255, 1989
- [62] P.P. SOROKIN and J.H. GLOWNIA. A theory attributing optical diffuse interstellar absorption bands, "Unidentified Infrared" emission bands, and cloud reddening to H₂ nonlinear absorption. *The Astrophysical Journal*, 473: 900-920, 1996
- [63] F.M. JOHNSON. Interstellar matter II: diffuse interstellar lines and porphyrins. *Annals of the New York Academy of Sciences*, 187: 186-206, 1972
- [64] J.R. BURKE and D.J. HOLLENBACH. The gas-grain interaction in the interstellar medium: thermal accommodation and trapping *The Astrophysical Journal*, 265: 223-234, 1983
- [65] H.W. KROTO, J.R. HEATH, S.C. O'BRIEN, R.F. CURL, and R.E. SMALLEY. C₆₀ Buckminsterfullerene. *Nature*, 318: 162-163, 1985
- [66] A.E. DOUGLAS. Origin of diffuse interstellar lines. *Nature*, 269: 130-132, 1977
- [67] A. LÉGER and J.L. PUGET. Identification of the 'unidentified' IR emission features of interstellar dust. *Astronomy and Astrophysics*, 137: L5-L8, 1984
- [68] T.P. SNOW, *edited by A.G.G.M. Tielens, and T.P. Snow.*, in: *The Diffuse Interstellar Bands*, A.G.G.M. Tielens and T.P. Snow, Editors. 1995, Kluwer Academic Publishers: Dordrecht. p. 325-340.
- [69] T.P. SNOW. The unidentified diffuse interstellar bands as evidence for large organic molecules in the interstellar medium. *Spectrochimica Acta Part A*, 57: 615-626, 2001
- [70] P.J. SARRE. The diffuse interstellar bands: a major problem in astronomical spectroscopy. *Journal of Molecular spectroscopy*, 238: 1-10, 2006

- [71] J.A. CARDELLI, D.M. MEYER, M. JURA, and B.D. SAVAGE. The abundance of interstellar carbon. *The Astrophysical Journal*, 467: 334-340, 1996
- [72] U.J. SOFIA, J.A. CARDELLI, and K. GUERIN. Carbon in the diffuse interstellar medium. *The Astrophysical Journal*, 482: L105-L108, 1997
- [73] T. HENNING and F. SALAMA. Carbon in the Universe. *Science*, 282: 2204-2210, 1998
- [74] T.P. SNOW and A.N. WITT. The interstellar carbon budget and the role of carbon in dust and large molecules. *Science*, 270: 1455-1460, 1995
- [75] R.E. HAUFLER, Y. CHAI, L.P.F. CHIBANTE, M.R. FRAELICH, R.B. WEISMAN, R.F. CURL, and R.E. SMALLEY. Cold molecular beam electronic spectrum of C₆₀ and C₇₀. *The Journal of Chemical Physics*, 95: 2197-2199, 1991
- [76] W. KRÄTSCHMER. Laboratory study of carbon particles and clusters. *Journal of the Chemical Society, Faraday Transactions*, 89: 2285-2287, 1993
- [77] J. FULARA, M. JAKOBI, and J.P. MAIER. Electronic and infrared spectra of C₆₀⁺ and C₆₀⁻ in neon and argon matrices. *Chemical Physics Letters*, 211: 227-234, 1993
- [78] B.H. FOING and P. EHRENFREUND. Detection of two interstellar absorption bands coincident with spectral features of C₆₀⁺. *Nature*, 369: 296-298, 1994
- [79] G.H. HERBIG. The Search for Interstellar C₆₀. *The Astrophysical Journal*, 542: 334-343, 2000
- [80] J. FULARA and J. KREŁOWSKI. Origin of diffuse interstellar bands: spectroscopic studies of their possible carriers. *New Astronomy Reviews*, 44: 581-597, 2000
- [81] A. LEGER and L. D'HENDECOURT. Are polycyclic aromatic hydrocarbons the carriers of the diffuse interstellar bands in the visible? *Astronomy and Astrophysics*, 146: 81-85, 1985
- [82] G.P. VAN DER ZWET and L.J. ALLAMANDOLA. Polycyclic aromatic hydrocarbons and the diffuse interstellar bands. *Astronomy and Astrophysics*, 146: 76-80, 1985
- [83] F. SALAMA, G.A. GALAZUTDINOV, J. KREŁOWSKI, L.J. ALLAMANDOLA, and F.A. MUSAIEV. Polycyclic aromatic hydrocarbons and the diffuse interstellar bands: a survey. *The Astrophysical Journal*, 526: 265-273, 1999
- [84] M.K. CRAWFORD, A.G.G.M. TIELENS, and L.J. ALLAMANDOLA. Ionized polycyclic aromatic hydrocarbons and the diffuse interstellar bands. *The Astrophysical Journal*, 293: L45-L48, 1985

- [85] M.B. BELL, P.A. FELDMAN, J.K.G. WATSON, M.C. MCCARTHY, M.J. TRAVERS, C.A. GOTTLIEB, and P. THADDEUS. Observations of long C_nH molecules in the dust cloud TMC-1. *The Astrophysical Journal*, 518: 740-747, 1999
- [86] J.P. MAIER, G.A.H. WALKER, and D.A. BOHLENDER. On the possible role of carbon chains as carriers of diffuse interstellar bands. *The Astrophysical Journal*, 602: 286-290, 2004
- [87] J.P. MAIER. *Electronic spectra of carbon chains - relevance to Astrophysics*. in: *The Physics and Chemistry of Clusters*. 2001. London: World Scientific.
- [88] D. FORNEY, P. FREIVOGEL, M. GRUTTER, and J.P. MAIER. Electronic absorption spectra of linear carbon chains in neon matrices. IV. C_{2n+1} $n=2-7$. *The Journal of Chemical Physics*, 104: 4954-4960, 1996
- [89] P. FREIVOGEL, J. FULARA, D. LESSEN, D. FORNEY, and J.P. MAIER. Absorption spectra of conjugated hydrocarbon cation chains in neon matrices. *Chemical Physics*, 189: 335-341, 1994
- [90] P. FREIVOGEL, J. FULARA, M. JAKOBI, D. FORNEY, and J.P. MAIER. Electronic absorption spectra of linear carbon chains in neon matrices. II. C, C_{2n} , and $C_{2n}H$. *The Journal of Chemical Physics*, 103: 54-59, 1995
- [91] J. FULARA, D. LESSEN, P. FREIVOGEL, and J.P. MAIER. Laboratory evidence for highly unsaturated hydrocarbons as carriers of some of the diffuse interstellar bands. *Nature*, 366: 439-441, 1993
- [92] P. FREIVOGEL, J. FULARA, and J.P. MAIER. *The Astrophysical Journal*, 431: L51, 1994
- [93] A.E. BOGUSLAVSKIY, A. DGHZONSON, and J.P. MAIER, *The electronic spectra of carbon chains, rings, and Ions of astrophysical interest*, in *Astrochemistry, From Laboratory Studies to Astronomical Observations*, R.I. Kaiser, P. Bernath, Y. Osamura, S. Petrie, and A.M. Mebel, Editors. 2005. p. 201-208.
- [94] L.M. HAFFNER and D.M. MEYER. A search for interstellar C_3 in the translucent cloud toward HD 147889. *The Astrophysical Journal*, 453: 450-453, 1995
- [95] J.P. MAIER, N.M. LAKIN, G.A.H. WALKER, and D.A. BOHLENDER. Detection of C_3 in diffuse interstellar clouds. *The Astrophysical Journal*, 553: 267-273, 2001
- [96] T.P. SNOW and B.J. MCCALL. Diffuse atomic and molecular clouds. *Annual Review of Astronomy and Astrophysics*, 44: 367-414, 2006

CHAPTER 2. EXPERIMENTAL



MATRIX ISOLATION TECHNIQUE

The technique of matrix isolation was originally invented as a means of trapping reactive species and studying them spectroscopically. These species would readily react in the gas-phase, whereas in frozen solvent mixtures they could be stabilized for several hours. This makes matrix isolation a very interesting and fascinating tool for investigation intermediates and other short-lived molecules. A mixture of ether, isopentane and alcohol turned out to be the best host material in the 1930s [1] due to its limited reactivity, however, it displayed poor transparency over large regions of the IR.

It was Eric Whittle, David Dows and George Pimentel who first used noble gases as host material in 1954 [2]. The experimental advances reported in their single-page paper were modest. The lowest temperature initially available in Pimentel's laboratory was just 66 K – cold enough to form xenon matrices, but too warm for neon, argon or krypton. Furthermore, at this temperature even xenon formed rather “soft” matrices, which failed to isolate some of the species. Nevertheless, the great idea to use noble gases as a host material has been put in action and its potential was already appreciated; therefore, 1954 is always regarded as the “*Anno Domini*” of matrix isolation [3].

Solid rare gases are all optically transparent across the spectrum, from vacuum ultraviolet (VUV) to the far infrared (FIR). High ionization energies and low polarizability (Table 2.1) cause limited interactions between embedded molecules. After comparing the physical properties of noble gases one can conclude that He would be the best host material. It gathers around guest species in a more compact manner, hence better preventing interactions. It also has the lowest polarizability and the highest ionization energy, making its matrix lattice more stable. However, helium's low melting point (0.95 K) makes it less attractive. It is not a problem to reach such a temperature, but to run an experiment on a daily basis would be an expensive pleasure. All this makes Ne as an ideal host material for matrix isolation.

TABLE 2.1 Thermal and physical properties of noble matrix hosts [3-5].

Host	T_d / K^a	T_m / K	T_b / K	$\alpha / 10^3 \text{ nm}^3$	IE / eV	E / nm
He	<0.95	0.95	4.2	0.14 [6]	24.58	58.43
Ne	10	24.5	27.1	0.39	21.56	73.59
Ar	35	83.9	87.4	1.63	15.8	104.82
Kr	50	116.6	120.8	2.46	14.0	116.49
Xe	65	161.2	166	4.02	12.1	129.56

^a The temperature at which diffusion of trapped guests first become appreciable. In the last column are shown the lowest allowed electronic transitions for solid noble gases.

Today, matrix isolation is challenged by a variety of laser-based techniques which have demonstrated their ability to obtain high-resolution vibrational and electronic spectra of transient molecules in the gas phase, free of possible perturbation by the matrix environment. Despite this challenge, there are important reasons why matrix studies of transient molecules are, in fact, complementary to lasers studies and should continue to yield valuable contributions to the study of chemical reaction intermediates. While lasers are tuneable over limited spectral ranges, observations in rare-gas matrices provide a broad spectral survey, extending from the FIR to the VUV.⁷ Thus, all of the products can be detected. A shift of matrix bands from the gas-phase band center are typically small enough to provide a guide for the choice and tuning of lasers for more detailed gas-phase studies. While isotopic substitution is crucial to positively identify a particular system, these studies are more readily conducted in matrices. Matrix absorption observations may also be helpful in spectral assignments, because spectral contributions from hot bands⁸ are eliminated; at cryogenic

⁷ vacuum ultraviolet (10 nm – 200 nm): is named because it is absorbed strongly by air and is used in vacuums.

⁸ hot band: a transition between two states of a single normal mode of vibration, neither of which is the ground state.

temperatures all absorptions originate from the molecular ground state [7].

MATRIX FEATURES

The interpretation of spectroscopic data for reactive species in a frozen matrix requires care. In spite of the fact that host-guest interactions in solidified noble gases are weak, the host does exert a substantial influence on the rotational and diffusion motion of the guest species; even the most inert host will interact electronically with trapped species if they are sufficiently reactive. The most obvious effect of the matrix host is to

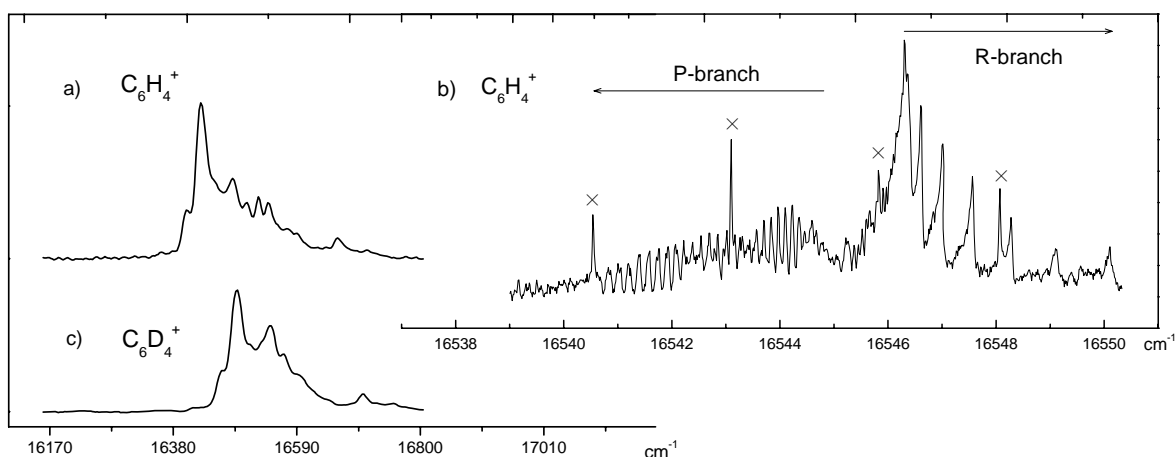


FIGURE 2.1 Electronic absorption spectra of $C_6H_4^+$ (traces (a) and (b)) and $C_6D_4^+$ (trace (c)). Trace (a) and (c) were measured in 6 K matrices after co-deposition of mass-selected cations with an excess of neon. The band at 16420 cm^{-1} (trace (a)) corresponds to the gas-phase band at 16545 cm^{-1} (trace (b)). The latter was observed using CRD spectroscopy through a planar supersonic plasma expansion [8]; lines marked with \times are due to another molecule.

prevent rotation of the guest [9], which can be easily seen in the figure above.

Figure 2.1 shows electronic absorption spectra measured using two different techniques. Trace (a) and (c) represent matrix isolation experiments on $C_6H_4^+$ and $C_6D_4^+$ respectively, whereas trace (b) was measured using CRD spectroscopy through a planar supersonic plasma [8]. While the gas-phase absorption (trace (b)) has *P* and *R* branches with rotationally resolved structure, the matrix absorption is a broad band with all rotational fine structure eliminated. By comparing traces (a) and (b) one sees that the positions of the origin bands are not the same. This is a common feature for matrix spectra to have so-called *matrix shifts*. These shifts are due to interactions between the excited and ground states of the guest molecules with the host.

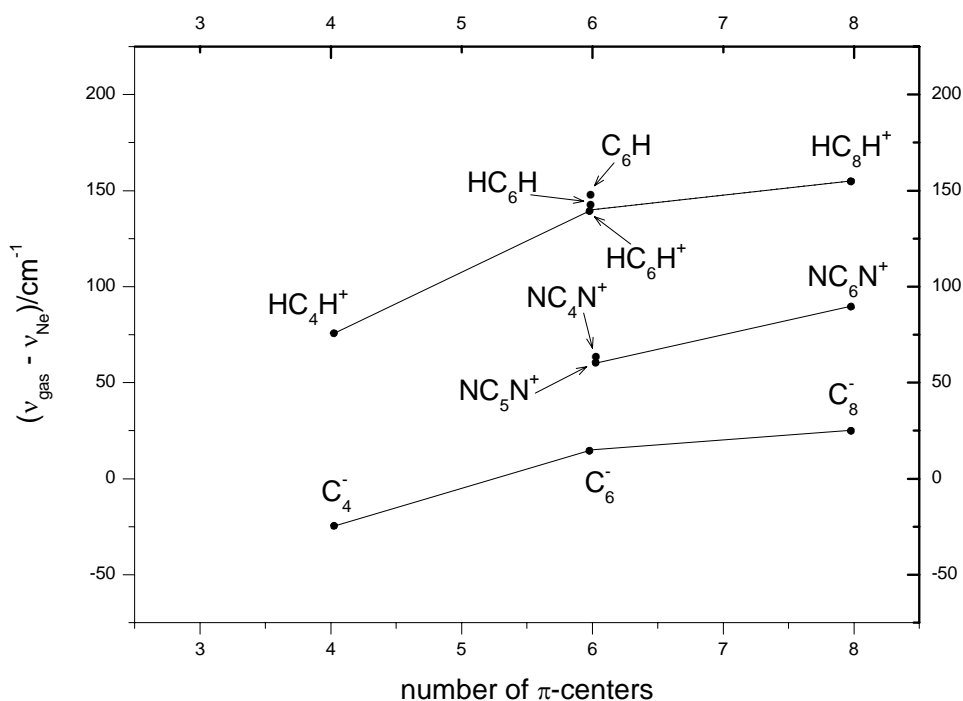


FIGURE 2.2 Variation of the gas-neon matrix shift of the π - π electronic transitions of carbon chains. The positive values imply that the gas-phase frequencies are at higher energies [10].

Comparisons between observed values in rare-gas matrices and in the gas phase have been made in the case of electronic and vibrational transitions of diatomic molecules [11-13]. Commonly, the shifts are to lower energies on passing from the gas-phase to neon; moreover, the shift increases with the size of the species (Fig. 2.2). The exceptions are the smaller carbon anions where the shift is to the blue (*e.g.*, C_4^-), but it goes over to a redshift for the longer ones (*e.g.*, C_6^-), similarly to the other chains. Cations and neutrals with the same number of carbon atoms demonstrate comparable displacements, *e.g.*, $HC_6H^+ \approx 135 \text{ cm}^{-1}$, $C_6H \approx 131 \text{ cm}^{-1}$. The isoelectronic cyanopolyacetylene cations have smaller shifts (Fig. 2.2). The significant trend is that the shift increases with longer species, and becomes larger on going from neon to xenon matrices. In view of this data, gas-phase energies can be predicted to within 50 cm^{-1} on the basis of the values observed in a neon matrix. This is sufficient for searches in the laboratory to be undertaken, but on the other hand, the uncertainty is still too large for direct comparisons to be made with astronomical data [10].

Going back to Figure 2.1, the sub-bands in traces (a) and (c) are due to matrix splittings or so-called *site effects*, which are very common for matrix isolation experiments [14]. The main cause of the band splitting is a host-guest interactions, which arise when the guest can occupy more than one type of vacancy in the host lattice. Host-guest interactions can usually be identified by obtaining spectra of the species of interest in more than one matrix host. The cavity sizes in Ne, Ar, Kr and Xe matrixes, for example, vary considerably, and band splittings due to host-guest interactions will also vary as consequence. Aggregation of the guest molecules in lattice vacancies can result in various forms of guest-guest interactions and band splittings caused by these interactions can usually be identified by varying the host to guest ratio. At sufficiently high dilution, the trapped molecules will be well isolated and guest-guest interactions minimized [3].

A small gas-phase molecule excited into a bound electronic state cannot relax nonradiatively, and will, in the absence of collisions, emit from the originally populated rotational and vibrational level. The situation is different in a solid matrix. One of the important strengths of matrix-isolation technique is that one can take advantage of the

relaxation phenomena and nonradiative cascade processes to access electronic states which, due to spectroscopic selection rules, can not be directly excited from the ground state in a gas-phase experiment. Moreover, the lattice may also carry away some or all of the excess vibrational energy. In many instances this simplifies the spectra and facilitates the assignment [15].

The rotational structure of spectra embedded in a solid matrix usually consists of a single sharp line, the so-called zero-phonon line, and a side-band [16]. When the host matrix contains many molecules, each will contribute a zero-phonon line and a phonon

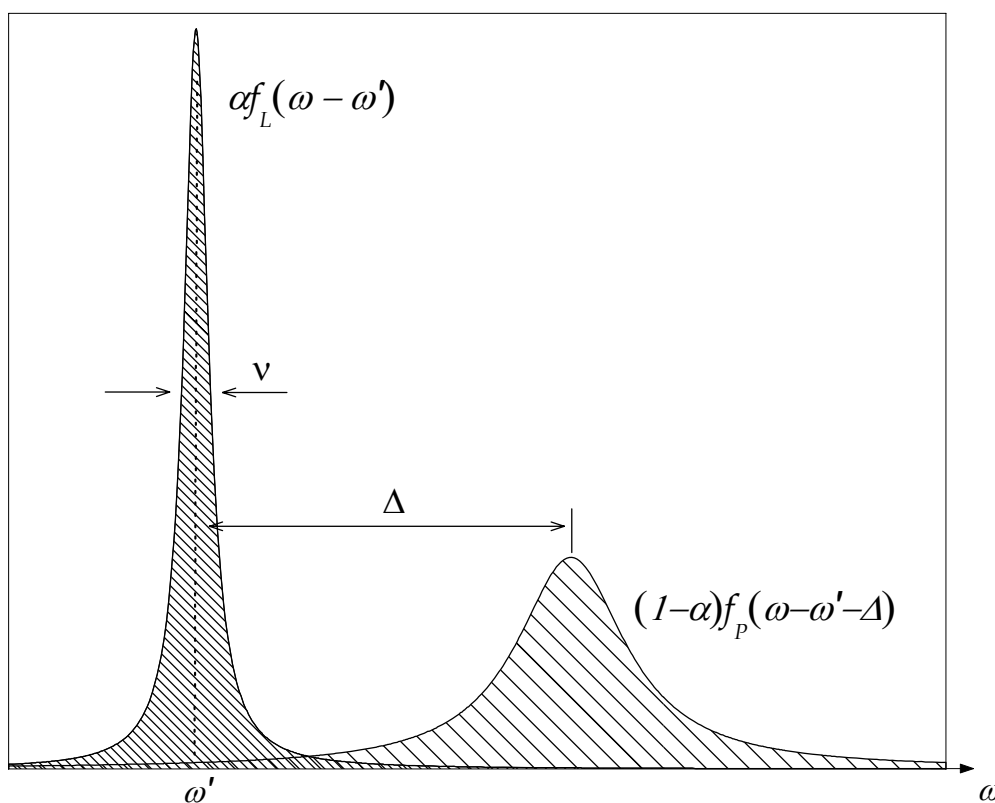


FIGURE 2.3 Schematic representation of the line shape of an electronic excitation. The narrow component at the frequency ω' is the zero-phonon line and the broader feature is the phonon side-band.

side-band to the absorption spectra. Figure 2.3 shows the typical line shape for electronic transitions of individual molecules in a solid matrix. The zero-phonon line is located at a frequency ω' determined by the intrinsic difference in energy levels between ground and excited state, as well as by the local environment. The phonon side-band is shifted to higher frequency. The frequency gap Δ between the zero-phonon line and the peak of the phonon side-band is determined by Franck-Condon principles. The distribution of intensity between the zero-phonon line and the phonon side-band is strongly dependent on temperature. At room temperature there is enough thermal energy to excite many phonons and the probability of a zero-phonon transition is close to zero.

Sometimes during matrix deposition experiment, several species (for instance cation, anion and neutral) may have been deposited at the same time rather than just one. To distinguish which bands belong to a single molecular species, one can use a basic rule of matrix isolation: bands which grow together at the same rate and diminish together at the same rate belong to the same species. Ideally, species of interest are generated by as many different methods as possible. One tries to find several ways of destroying it in the matrix, for example, by annealing, bimolecular reaction, or photolysis. With careful work, one can have reasonable confidence that a set of bands belongs to a single species [3]. Another trick in matrix isolation spectroscopy is the isotopic substitution of the species of interest [17]. The resulting isotope shift can be of decisive help in identifying reactive species and assigning bands to particular vibrations. It is seen that the absorption spectrum of $C_6H_4^+$ in Figure 2.1 (trace (a)) is redshifted in comparison to the spectrum of its deuterated analogue, $C_6D_4^+$, (trace (c)) recorded in an experiment with the same conditions.

In concluding, there are several advantages and disadvantages of matrix isolation spectroscopy some of which are listed below:

ADVANTAGES

- The possibility to work with free radicals and other unstable or transient species.
- The species of interest can be accumulated and stored over long periods of time, and in this way the detection sensitivity can be enhanced.
- For optical detection, large spectral areas can be explored in a relatively short time, which makes the initial search for unknown transitions much less tedious than in the gas phase.
- Low temperature of matrix deposition experiments implies that the absorption bands will always originate from the ground electronic and vibrational states, simplifying the spectral assignments because contributions of hot bands to the spectrum are eliminated.
- The ability to study electronic transitions which may be forbidden under normal selection rules.

DISADVANTAGES

- The interaction between the embedded species and the host lattice results in some matrix effects, such as broadening of the bands (*site structure*) and shifts of the observed transition in comparison with the gas-phase values.
- The host lattice prevents rotational motion of the guest, eliminating many spectral features essential for structural identification.

The survey of the literature shows that in spite of the fact that more than 50 years have elapsed since Pimentel has coined its name, matrix isolation remains a very viable and useful technique [18].

APPARATUS

The general experimental arrangement is shown in Figure 2.4. Mass-selected beams of interest are embedded in frozen noble gas environments and spectroscopically investigated. Thanks to the continuous labor of former graduate students [19-21] and invaluable help of various research collaborators this machine is a well-functioning and fascinating tool. The experimental setup consists of five main sections: ion source, with its system of electrostatic lenses for ion guidance; quadrupole bender with following

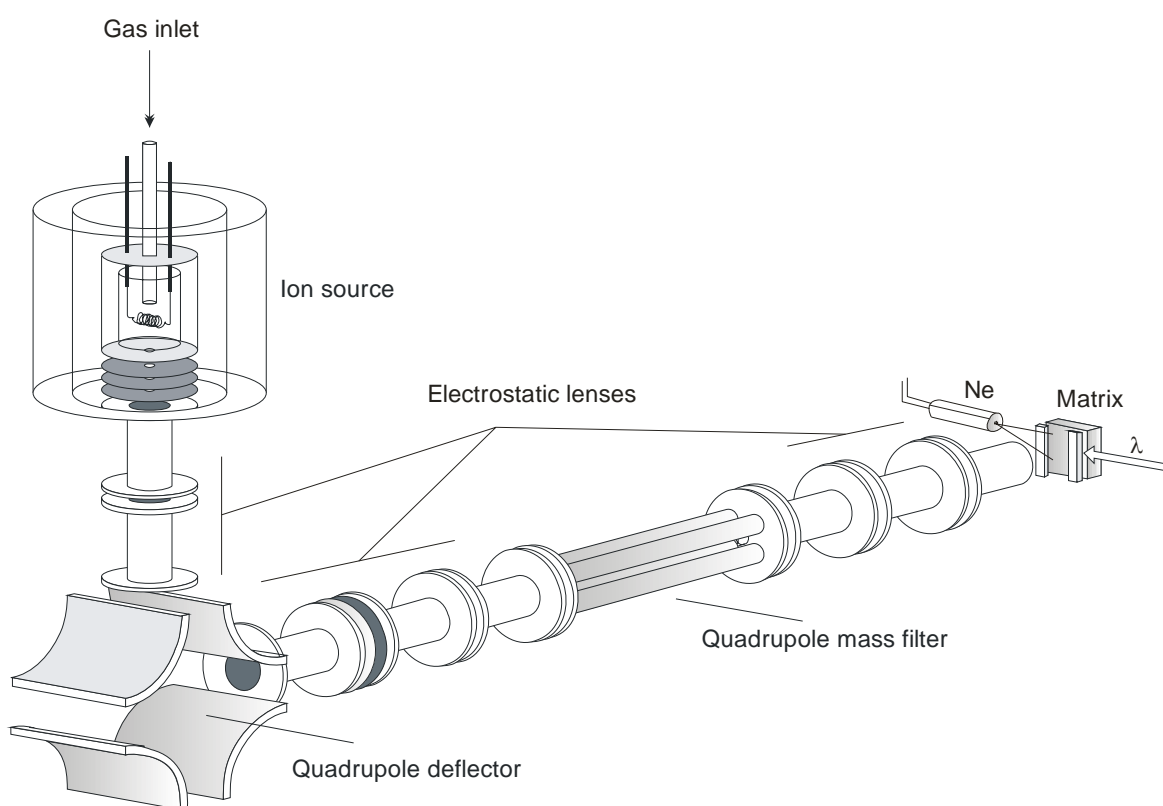


FIGURE 2.4 Scheme of the experimental setup. One can distinguish five main sections: ion source, quadrupole bender, quadrupole mass filter, matrix and cryostat system (shown in Fig. 2.5).

electrostatic lenses; quadrupole mass selector; matrix section and the cryo-system, which keeps the matrix cold. The whole apparatus is kept under vacuum through the use of several types of vacuum pumps.

FROM A BREATH DOWN TO 10^{-7} MBAR

To start generating the species of interest, optimal conditions for production must first be found. Because it is impossible to work with free radicals and other unstable species under atmospheric pressure, the system is kept under as deep of a vacuum as possible. In the present setup, it is achieved by means of a set of vacuum pumps. All parts of the machine are kept under different vacuum stages. The pressure in the source chamber (10^{-5} mbar) is supported by two oil diffusion pumps with the pumping speed (for air) of 280 and 650 $l s^{-1}$. The quadrupole chamber is pumped by a turbo molecular pump with a 56 $l s^{-1}$ pumping speed, whereas two additional pumps (170 and 300 $l s^{-1}$) are responsible for the matrix chamber, normally kept at $\sim 1 \times 10^{-7}$ mbar. All three turbo pumps, as well as the diffusion pumps, are backed by rotary fore-pumps (Fig. 2.5). One diffusion and rotary pump are responsible for the vacuum in the precursor chamber. The vacuum in the Fourier-Transform (FT) spectrometer section is supported by a rotary pump. For monitoring the pressure two kinds of gauges are used. Perani gauges measure the pressure starting from atmospheric to 10^{-3} mbar, whereas Penning gauges are used at $< 10^{-3}$ mbar.

A differential pumping scheme, employed in the apparatus, is necessary due to the need in suppressing possible penetration of a precursor into the matrix chamber. To reach a desirable vacuum, firstly open the rotary pumps and then, after a vacuum of 10^{-2} – 10^{-3} is reached, open the diffusion pumps. The turbo pumps can be switched on directly after the rotary pumps. It takes ~ 2 hours to reach a workable vacuum. A valve which is introduced between the quadrupole and diffusion pump separates the latter from the rest of the system, that makes it possible to reach the fore-vacuum using the rotary pumps. A valve introduced between the source and deflector chambers helps keeping a hot source separate from the system after a deposition is finished,

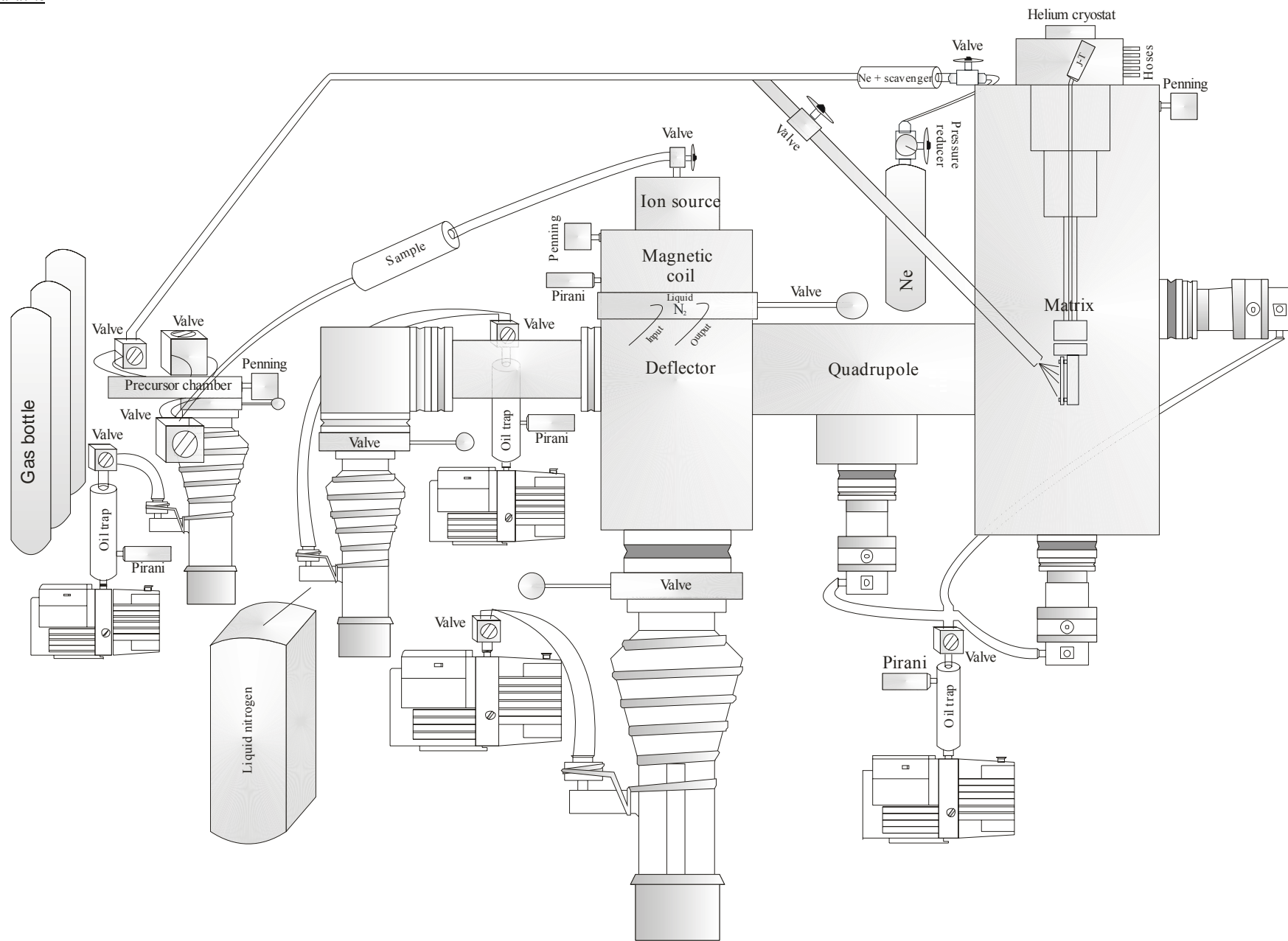


FIGURE 2.5 Vacuum scheme of the apparatus.

eliminating the possibility of influencing the latter on the grown matrix. An electromagnetic coil, which is used in the experiments with positive ions, is helpful in guiding ions. Its variable magnetic field, which surrounds the source, controls the ionization efficiency by varying the mean free path of free electrons inside the source; it allows one to increase the ion current sufficiently. A cylindrical liquid nitrogen trap, located directly after the source around the first electrostatic system, is used to collect all dust particles. Liquid nitrogen is used through an experiment keeping the trap and collected impurities cold. By introducing a valve (Fig. 2.5) between the source and deflector, it became possible to isolate the hot source and trap from the rest of the system, thus eliminating the need for liquid nitrogen after a deposition. By closing the valve, system is secured from a pressure increase which can cause matrix melting.

A DEPOSITION

The temperature of the matrix substrate is provided by a closed-cycle three-stage helium cryostat (HS-4 UHV), which can attain 3.6 K. To reach the deposition temperature (6 K for neon) starting from the room temperature (~300 K) usually takes 3.5–4 hours; therefore, the compressor is programmed the evening before. The temperature is measured and controlled with a silicon diode sensor and a 25 W heater. To begin an experiment one chooses a precursor, which is specific for each ion of interest. Depending on the nature of the latter, there are two different ways to proceed further. The present apparatus allows the use of gaseous, liquid and solid precursors. In the case of gaseous and liquid samples, mixtures with He (in different ratios) are prepared in the precursor chamber (Fig. 2.5). Using a pure precursor is possible but shortens the source stability time because the source becomes squalid faster and the filament gets thinner. All these cause less stable work conditions for the source and, as a consequence, the current drops. As soon as a mixture is ready, it is placed to a sample tank (Fig. 2.5) and then introduced into the source. Solid samples, on the other hand, are heated first to obtain sufficient sample vapor, and only afterwards it can be introduced into the source. A resistively heatable oven is used to sustain adequate vapor in- and outside the source. The latter one is the best solution because the temperature of the

heating can be easily controlled. When an oven is located inside the source, an additional heat comes from a filament and a temperature (~ 700 K) is higher than it needs for being evaporated, which causes the source to become squalid and wastes the sample.

In Figure 2.6 a resistively heatable oven is depicted. It is made of stainless steel and has two teflon tubes inside. Helium comes from one of the tubes, and after mixing with evaporated sample, exits the oven through the second tube. A generated gaseous mixture of He and precursor is further introduced into the source by means of a fine dose valve. The generated ions of interest are extracted by a set of electrostatic lenses and guided further to the deflector where the ion beam is bent by 90° . The purpose of bending the ions is to extract all neutrals from the ion beam thus, presumably, experiments can take place with charged particles which are then guided by electrostatic lenses into the quadrupole mass selector. Mass selection is used to filter the ions of

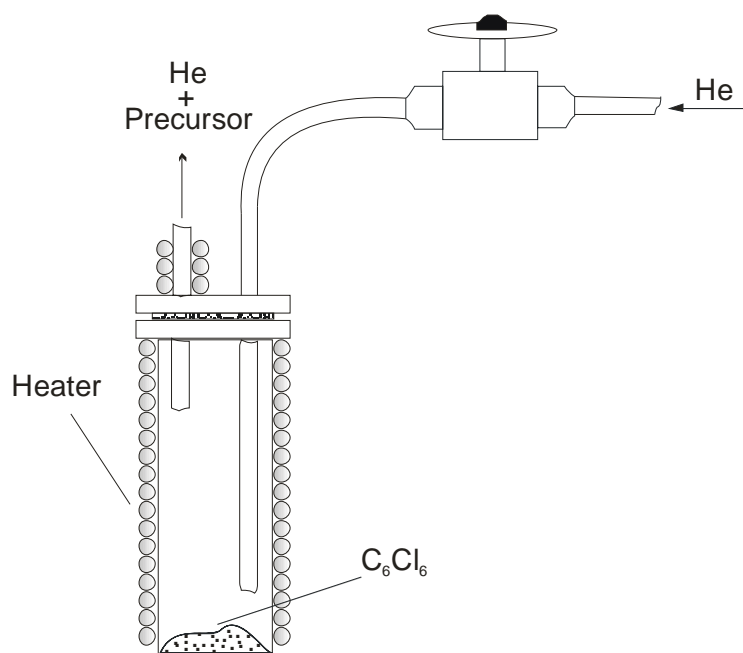


FIGURE 2.6 A typical oven used in experiments with solid samples.

interest. It consists of four 211 mm long 18.8 mm in diameter metal cylindrical rods and has a working range of 10–200 m/z . At high resolution it is possible to separate each mass. The rods are electrically connected in pairs with the following electrical potentials:

$$\Phi = B \pm (U + V \cos(2\pi f t)),$$

where $f = 1.5$ MHz, B the reference potential, V radio frequency amplitude, U DC voltage, t time. At the given U/V ratio the ions of certain mass have stable oscillating trajectories along the quadrupole axis, while the other ones have unstable trajectories, and therefore can not pass the quadrupole dissipating inside its chamber. Subsequently, the beam, consisting only of ions of a certain mass, is directed onto the surface of the matrix substrate where it is quenched with matrix gas (Ne or Ar), introduced via a special inlet (Fig. 2.5), which allows depositing the ions uniformly on the matrix surface. There are at least three major problems. First, in order to be able to detect the isolated species, one needs either an extremely sensitive detection technique, or a very intense ion beam. The generation of sufficiently intense mass-selected beams is one serious obstacle. The second problem involves decelerating the beam and “soft landing” the species of interest in the matrix. To accomplish effective mass selection, one typically has to accelerate the ions to appreciable energies exceeding 50 eV. On the other hand, the binding energy of two rare gas atoms is of the order of 10 meV. Unless the ions impinging on the matrix are sufficiently slowed down, they can fragment on impact at the surface. Even if strongly bound ions fragmentation can be avoided, the ion kinetic energy can result in surface melting and vaporization of a number of matrix atoms. The guest ion can then penetrate deep into the matrix and recombine or react with some of the other guests or impurity molecules already present, and the selectivity can thus be lost. A third elusive problem is maintaining the overall neutrality of the matrix, opposing the goal of accumulating a high number density of a specific ion. The neutrality of the matrix is achieved by impurity molecules which are always present in the apparatus. Since traces of water or other atmospheric components are difficult to

eliminate completely, undesired products (C_2^\pm , N_2^+ etc.) due to reactions with these impurities can appear deposited together with the ions of interest. If the absorption spectra of these products are known, they can be even of help in the following assignment.

The temperature of the matrix substrate (*ca.* 6 K) is achieved by the last stage of the closed cycle helium cryostat when the Joule-Thomson (shown in Fig. 2.5) valve is opened. The matrix substrate (Fig. 2.7) is made of sapphire coated with rhodium and has a dimension of 3×3 cm. The typical amount of deposited ions varies from 10^{12} to 10^{15} molecules [22] and depends on the achieved current which is measured by a picoamperemeter. All deposited molecules are separated from each other by a huge amount of guest molecules, that excludes a possibility of their interaction.

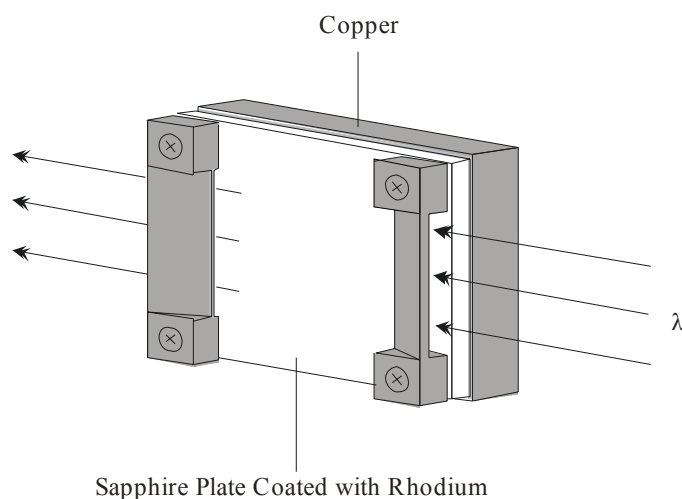


FIGURE 2.7 Matrix substrate.

SOME HELPFUL FEATURES

One might think that the deposition process is a simple procedure, but it is far from the case. It has to be mentioned that the matrix substrate remains neutral during deposition contrary to the fact that one deposits ions. After several minutes of deposition, the positive charge (while depositing cations) is built on the matrix and further arriving cations are repelled from its surface to the surrounding chamber walls.

The free electrons released on hitting the metal walls are attracted by the matrix and penetrate into it neutralizing some of the cations. If the electron affinity of the formed neutrals is sufficient, they can even accept one more electron, thereby forming anions. This explains why sometimes it is possible to see all three types of particles in one matrix: positive, neutral and negative. In the third and fourth parts of this thesis, it is shown that during the depositions of C_n^+ ($n=6-9$) [23, 24] and C_6H^+ [25] cations the neutrals species (C_n , C_6H) are also seen; moreover, in the experiments on C_6^+ and C_7^+ one can even see their negative analogues. If the kinetic energy of the deposited ions upon reaching the matrix is high (*ca.* 50 eV), fragmentation may take place leading to the appearance of smaller fragments in the matrix. Several procedures are used in the matrix experiments to help with spectral assignments, including: photoneutralization, the use of an electronic scavenger and annealing the matrix.

PHOTONEUTRALIZATION

One of the most instrumented procedures to distinguish between ions and neutrals is irradiating the matrix. Two kinds of lamps are used to irradiate the matrix: medium pressure mercury lamp with its UV band at 4.9 eV and a more powerful xenon arc lamp with UV band around 5.6 eV. If necessary, cut-off filters can be applied to restrict the energy range. To prevent heating the matrix, a quartz cuvette filled with bi-distilled water is placed between the matrix window and the lamp. The UV photons emitted by the lamp release free electrons from the metal walls which then recombine with the deposited cations neutralizing them. In the case of anions, the neutralization goes directly through electron photodetachment. Firstly, all spectra are measured after deposition and only after this the matrix is irradiated (30–40 minutes) and the whole spectral range measured again. After irradiation all peaks due to charged species decrease in intensities while those from neutrals grow. Ions and neutrals can be easily distinguished comparing the spectra measured before and after irradiation. If irradiation is not sufficient to neutralize the ions, the matrix is irradiated again. Sometimes the procedure may need several steps or a more energetic light source. The reason for this is that, for example, neutral analogues of anions might have a high electron affinity and

after gaining an electron they convert to the anions resulting in the increasing of their intensities.

A SCAVENGER

Molecules which can easily accept electrons, so-called electron scavengers, can be very helpful during matrix deposition. Instead of using pure Ne, a scavenger can be mixed in and used as a host material for deposition. Deposition in such mixtures makes it possible to collect more cations of interest. The scavengers prevent the cations from neutralizing. Two types of scavengers, N₂O and CCl₄, were used during the present work. They were mixed with neon and introduced during deposition through the same inlet as in the case of Ne (Fig. 2.5). An optimal ratio of Ne to scavenger was calculated to be 300:1 but if necessary it could be increased. The electron affinity of N₂O (0.22 eV) [26] is much less than for CCl₄ (2.0 eV) [27], resulting in inefficiency of the irradiation in experiments with CCl₄.

ANNEALING

Another procedure which is used to help assign spectra is increasing the temperature of the matrix. The procedure is called annealing; one increases the temperature up to 8–9 K and keeps it there for *ca.* 30 minutes. At these temperatures species start to diffuse due to their enhanced mobility, and if the concentration of species is sufficient, they might even interact with each other producing larger species. Another effect of the annealing process is a redistribution of the *site structure*. The lower energy orientation of the molecules becomes more favorable.

In an ideal situation, as was already mentioned, species of interest are generated by as many different techniques as possible to study all possible fragments. By performing a careful analysis, a reasonable assignment of the band systems can be made with a degree of confidence.

IONS SOURCES

ELECTRON IMPACT ION SOURCES

Two kinds of electron impact ion sources are used to produce positive and negative ions. An advantage of an electron impact source is that it produces a continuous ion beam. The one depicted in Figure 2.8 is aimed for production of positive ions. All kinds of samples: gaseous, liquid and solid can be used as a precursor. Normally, the gaseous (vapor in the case of solids and liquids) precursor is mixed with He (Ar) in a 1:3 ratio. As was previously mentioned, a pure sample can be used but it shortens the lifetime of the filament. The mixture is held in a special reservoir from which it is then introduced into the source by means of a needle valve. The source consists of two hollow cylinders of 6 and 5 cm in diameter. The first cylinder represents

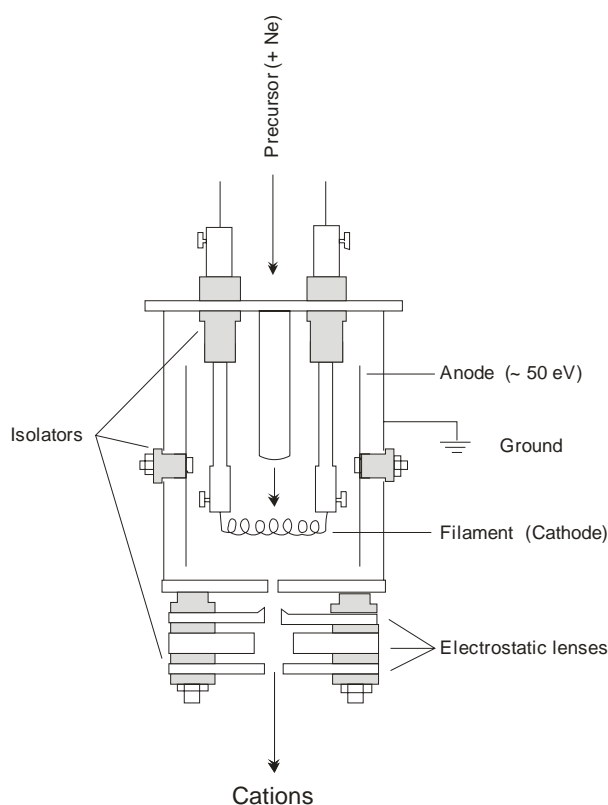


FIGURE 2.8 *Electron impact ion source for production of positive species of interest.*

a frame of the source and a second, connected by two isolators to the first, which works as an anode with ~ 50 eV potential on it. A cathode, represented by a filament, is made of tungsten and located inside the anode. The filament is 0.35 mm in diameter and has a length of ~ 4 – 5 cm; it is normally heated by 9–10 A current which is enough to emit electrons. The precursor gas is first introduced into the source and then ionized by an electrical discharge between the ground and anode, stimulated by the emitted electrons. Electron bombardment destroys the sample, forming ions and radicals which react with each other, leaving the source by extraction with the first electrostatic lens. The molecular free path was estimated to be ~ 3 mm for nitrogen and hence much smaller for larger ions [22]. As experience shows, the production of species longer than the precursor is possible. A good example of this is an experiment of C_6H^+ using diacetylene as a precursor (discussed in the fourth chapter).

Another electron impact ion source which is used for the production of negative ions is shown in Figure 2.9. This source is a modified version of a Branscomb-type ion source [28]. It consists of the same type of filament which is mounted on a cathode floated at a negative potential of about 300–500 V. As in the case of the previous source, the filament emits free electrons by heating it up to 9–10 A current. By monitoring the discharge between the cathode and the extraction plate, which is under about -100 V, one regulates the degree of ionization inside the source. A sample (graphite, aluminium *etc.*) together with the ceramic cylinder (or metal) and the extraction plate build a small volume where the collision processes with ions formation happen. Created in this volume species are extracted through a small orifice by the field of the first electrostatic lens. This field penetrates inside the source at the distance of the orifice diameter.

With both sources it is possible to obtain unity mass resolution, but after several hours of deposition, the source becomes too hot and dirty due to the coating of soot and the fact that the filament becomes thinner. All this reduce the resolution abilities, as well as to malfunctions in the source.

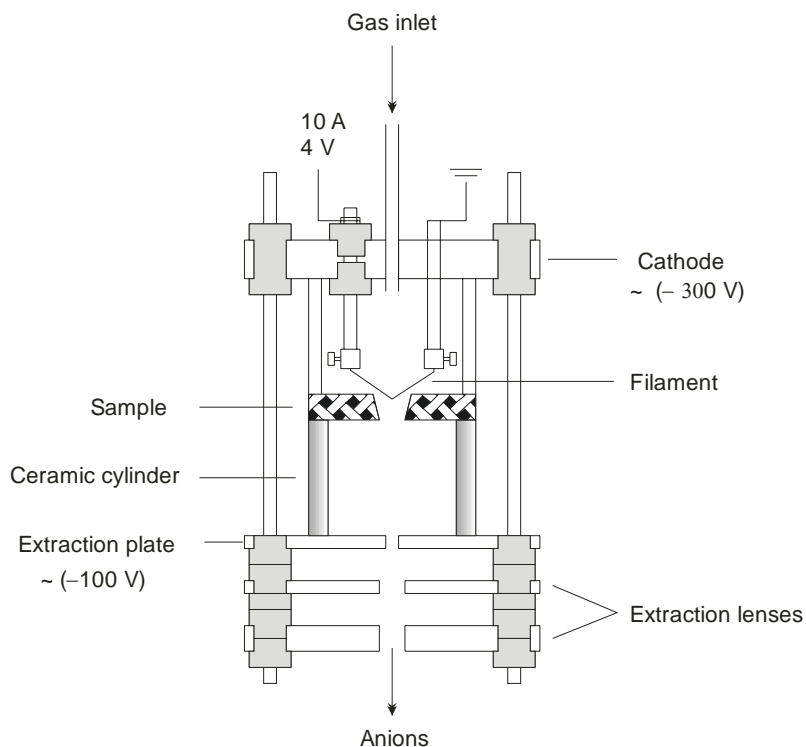


FIGURE 2.9 *Electron impact ion source for production of negative species of interest.*

As experience shows, some samples are not pure enough (especially the solid ones) and the first mass spectra consist of many other species apart from the precursor. For example, while working with sulfur powder and using the impact source for positive ion production, preliminary mass spectra display many additional non-sulfur species, however, after heating the sample for a couple of minutes, an elegant and cleaner mass spectrum is obtained, consisting only of sulfur species (Fig. 2.10).

CESIUM SPUTTER SOURCE

A cesium sputter source is used for producing negative ions. It is built based on models designed to produce intense atomic molecular beams in tandem accelerators [29]. It is shown in Figure 2.11 and consists of an ionizer, a sample, an extractor and a cesium tube. The tube is heated up to $\sim 300^\circ\text{C}$ which is enough to evaporate the cesium,

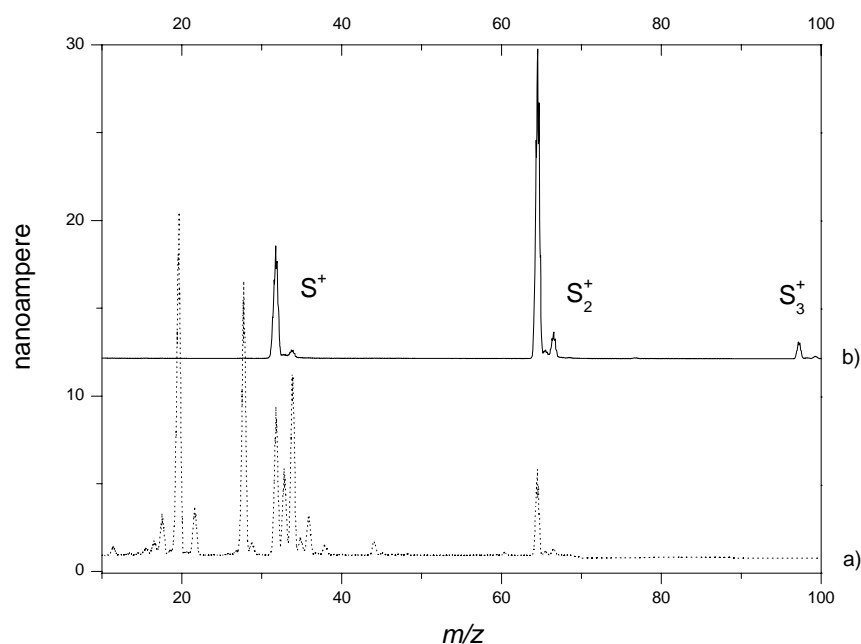


FIGURE 2.10 Mass spectrum of sulfur species produced from sulfur powder using the electron impact ion source. Impurities which are present in trace (a) disappear after several minutes of heating the sample (trace (b)).

introducing small portions into the source. The vapor of cesium is ionized on the surface of a coaxial tantalum wire resistively heated to 1000°C . Cs^+ ions are repelled from the ionizer by its 1000 V potential and bombard the sample rod (carbon, boron *etc.*) ejecting different species in the so-called sputter manner. The sample target, located above the ionizer, has a negative potential of $\sim 50\text{ V}$. The produced ions are extracted from the source in the same way as in the case of two previous sources. After several experiments, the cesium is covered with an oxide layer that decreases its sputtering efficiency. To produce different forms of sample species, gas mixtures can be introduced through a hole drilled in the sample rod. Firstly, the idea of the present source was to produce negatively charged carbon chains from graphite as well as

carbon-boron derivatives. Using this source plenty of anions have been investigated, including:

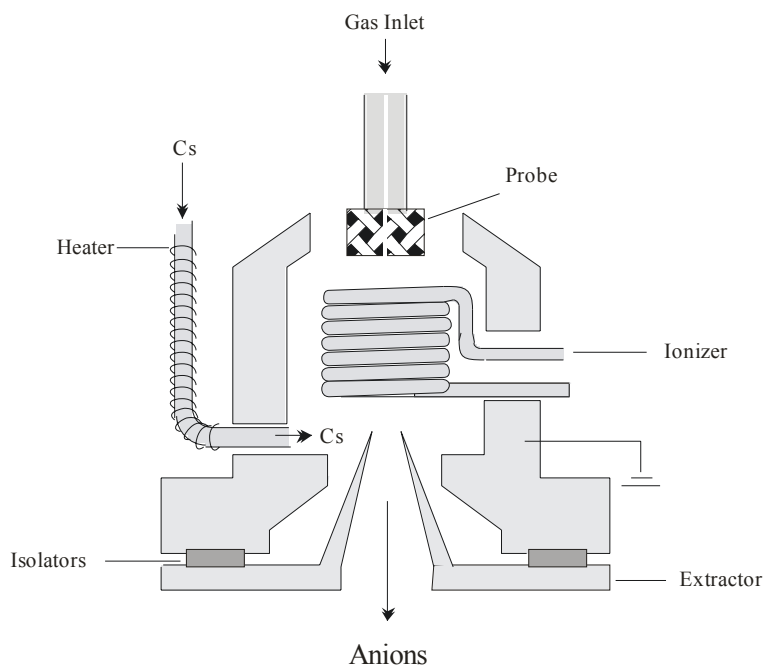


FIGURE 2.11 *Cesium sputter source.*

C_n^- (n – even and odd) [30, 31], Si_n^- [32], SiC^- [33], BC_n^- [34] as well as their neutral analogues.

MEASUREMENTS

UV-VIS

After the deposition procedure is completed, absorption spectra can be measured. Normally, a measurement starts from the visible region because it is easier to calibrate the system for a better signal from a detector due to the opportunity to observe the light coming from a light source. Two different lamps are used in the UV and visible regions: a halogen lamp for 350–1100 nm, and a xenon arc lamp for UV light. The latter has a line emission spectrum in the region higher than 360 nm that excludes its

possibility to be used in this region in spite of the fact that it produces more light than the halogen lamp. From the light source, light goes through a SPEX monochromator (Fig. 2.12) and then it is focused by two adjustable quartz lenses and enters the matrix

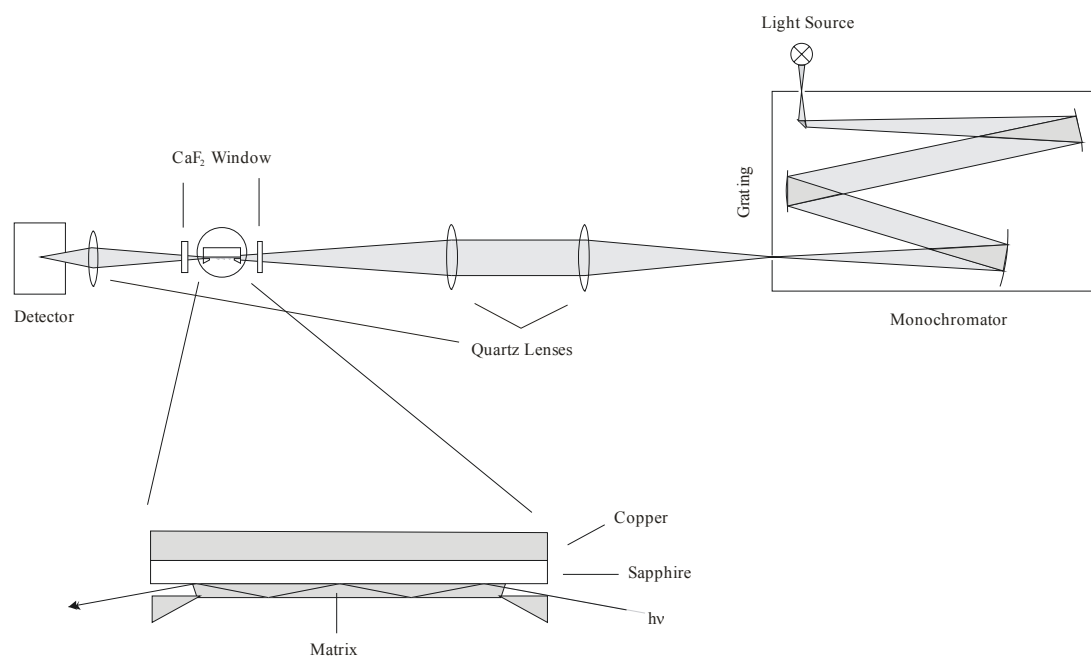


FIGURE 2.12 Optical scheme of the set-up for measuring UV/Vis spectra in a waveguide manner.

chamber via the first CaF_2 window. Due to the ability to adjust the lenses one can point the light directly to the first matrix slit. On travelling through the grown matrix in so-called waveguide manner [35], the light via another slit leaves the matrix chamber through the second CaF_2 window and gets detected by a detector. A photomultiplier is used in the 220–650 nm spectral region, whereas going up to NIR (640–1100 nm) it is a silicon diode. Due to the high sensitivity of the detectors, one has to isolate them from the external stimulus (light *etc.*). For calibration of the monochromator, the emission spectrum of a medium pressure mercury pencil lamp is used [36]. After the calibration by a mercury lamp, as well as by the positions of already known species (impurities, fragments), an accuracy of ± 0.2 nm can be obtained.

IR REGION

When the measurements in the UV/Vis region are finished, the matrix substrate is rotated by $\sim 135^\circ$ and the infrared region is scanned. An FT spectrometer (Bruker IFS 66v/S) is employed to measure spectra in the $12000\text{--}1100\text{ cm}^{-1}$ ($834\text{--}9090\text{ nm}$) region. The Bruker instrument is evacuated to $\sim 1\text{ mbar}$ by a rotary pump to obtain a semi- H_2O and CO_2 -free environment. In Figure 2.13, a general scheme for IR measurements is shown. The IR radiation coming from the light source is focused by a set of parabolic

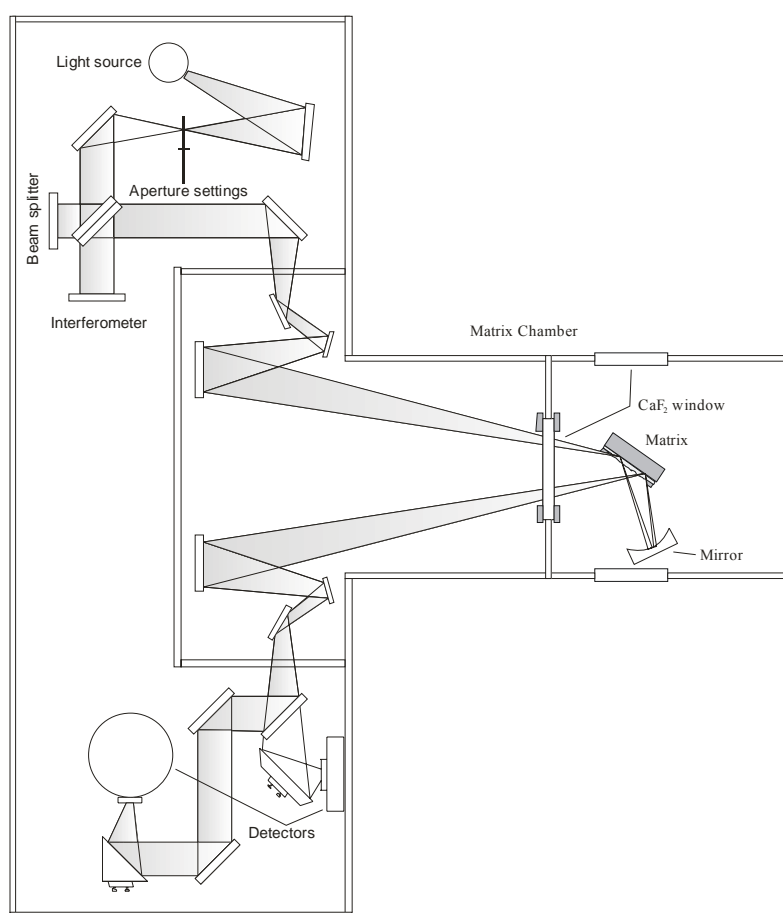


FIGURE 2.13 *Double reflection method for measuring IR spectra using FT spectrometer.*

mirrors onto the matrix surface, enters the matrix chamber via a CaF₂ window, and then reflects from the matrix surface to a concave mirror and goes back to the former. After reflecting off of the matrix surface, the light beam is guided to the detector by a set of parabolic mirrors. In this way the sensitivity is several times better than in a single reflection scheme is obtained. Two kinds of detectors are used: mercury cadmium telluride (MCT) (1100–4000 cm⁻¹) and indium antimonide (InSb) (4000–12000 cm⁻¹). Both of them are cooled by liquid nitrogen before the measurements. An accuracy of ±0.2 cm⁻¹ is reached by internal calibration of the Bruker FT spectrometer with a HeNe laser line at 632.8 nm.

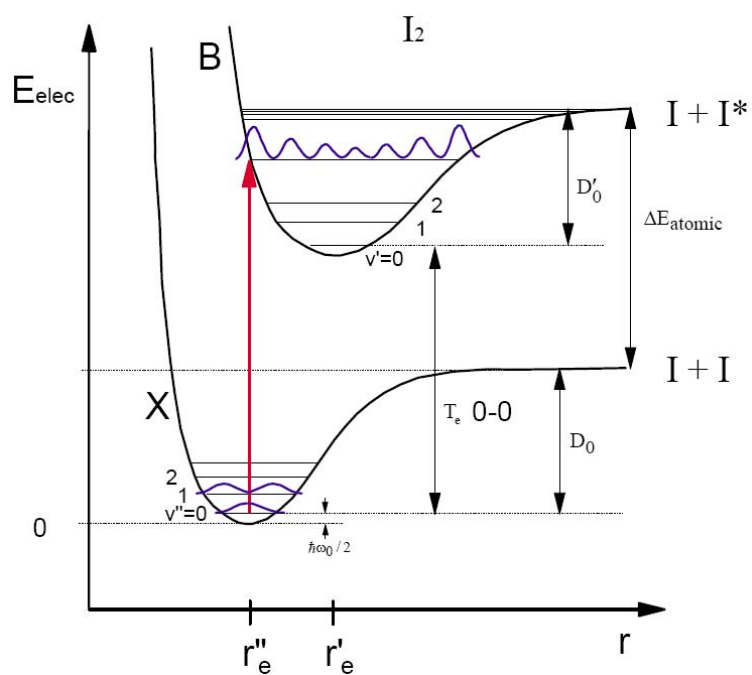
BIBLIOGRAPHY

- [1] G.N. LEWIS and D. LIPKIN. Reversible photochemical processes in rigid media: the dissociation of organic molecules into radicals and ions. *Journal of the American Chemical Society*, 64: 2801-2808, 1942
- [2] E. WHITTLE, D.A. DOWS, and G.C. PIMENTEL. Matrix isolation method for the experimental study of unstable species. *The Journal of Chemical Physics*, 22: 1943-1943, 1954
- [3] I.R. DUNKIN, *Matrix-isolation techniques*, ed. L.M. Harwood and C.J. Moody. 1998, Glasgow: Oxford University Press.
- [4] B. MEYER, *Low temperature spectroscopy*. 1971, New York: Elsevier.
- [5] H.J. JODL, *Solid-state aspects of matrices*, in: *Chemistry and Physics of Matrix-Isolated Species*, L. Andrews and M. Moskovits, Editors. 1989, Elsevier Science Publishers: Amsterdam. p. 343-415.
- [6] M. MASILI. Static and dynamic dipole polarizability of the helium atom using wave functions involving logarithmic terms. *Physical Review A*, 68: 012508(1-11), 2003
- [7] M.E. JACOX, *The stabilization and spectroscopy of free radicals and reactive molecules in inert matrices*, in: *Chemistry and Physics of Matrix-Isolated Species*, L. Andrews and M. Moskovits, Editors. 1989, Elsevier Science Publishers. p. 75-105.
- [8] M. ARAKI, H. LINNARTZ, P. CIAS, A. DENISOV, J. FULARA, A. BATALOV, I. SHNITKO, and J.P. MAIER. High-resolution electronic spectroscopy of a nonlinear carbon chain radical $C_6H_4^+$. *The Journal of Chemical Physics*, 118: 10561-10565, 2003
- [9] H.E. HALLAM, *Vibrational Spectroscopy of Trapped Species*, ed. H.E. Hallam. 1973, London: Wiley.
- [10] J.P. MAIER. Electronic spectroscopy of carbon chains. *Journal of Physical Chemistry A*, 102: 3462-3469, 1998
- [11] M.E. JACOX. Ground-state vibrational energy levels of polyatomic transient molecules. *Journal of Physical and Chemical Reference Data*, 13: 945-1068, 1984
- [12] M.E. JACOX. Comparison of the ground state vibrational fundamentals of diatomic molecules in the gas-phase and in inert solid matrices. *Journal of Molecular Spectroscopy*, 113: 286-301, 1985

- [13] M.E. JACOX. Comparison of the electronic energy levels of diatomic molecules in the gas phase and in inert solid matrices. *Journal of Molecular Spectroscopy*, 157: 43-59, 1987
- [14] S. JAGANNATHAN, J.R. COOPER, and C.L. WILKINS. Matrix effects in matrix isolation infrared spectroscopy. *Applied Spectroscopy*, 43: 781-786, 1989
- [15] V.E. BONDYBEY, *Time-resolved laser-induced fluorescence studies of the spectroscopy and dynamics of matrix isolated molecules*, in: *Chemistry and Physics of Matrix-Isolated Species*, L. Andrews and M. Moskovits, Editors. 1989, Elsevier Science Publishers: Amsterdam. p. 107-137.
- [16] K. REBANE, *Elementary theory of vibrational structure*, in: *Impurity Spectra of Solids*. 1970, Plenum Press: New York. p. 253.
- [17] P. KLAEBOE AND C.J. NIELSEN. Recent advances in infrared matrix isolation spectroscopy. *The Analyst*, 117: 335-341, 1992
- [18] V.E. BONDYBEY, A.M. SMITH, and J. AGREITER. New developments in matrix isolation spectroscopy. *Chemical Reviews*, 96: 2113-2134, 1996
- [19] P. FREIVOGEL, *Spektroskopie an Massenselektierten Kohlenstoffketten in Neonmatrizen*, in *Institute of Physical Chemistry*. 1997, University of Basel.
- [20] M. GRUTTER, *Spectroscopy of mass selected carbon chains in neon matrices*, in *Institute of Physical Chemistry*. 1999, University of Basel.
- [21] E. RIAPLOV, *Spectroscopy of mass selected carbon and boron species in solid neon*, in *Institute of Physical Chemistry*. 2002, University of Basel.
- [22] A. BATALOV, *Absorption spectroscopy of mass-selected hydrocarbon and boron species in 6 K neon matrices*, in *Institute of Physical Chemistry*. 2006, University of Basel.
- [23] J. FULARA, E. RIAPLOV, A. BATALOV, I. SHNITKO, and J.P. MAIER. Electronic and infrared absorption spectra of linear and cyclic C_6^+ in a neon matrix. *The Journal of Chemical Physics*, 120: 7520-7525, 2004
- [24] J. FULARA, I. SHNITKO, A. BATALOV, and J.P. MAIER. Electronic absorption spectra of linear and cyclic C_n^+ $n=7-9$ in a neon matrix. *The Journal of Chemical Physics*, 123: 044305-044311, 2005
- [25] I. SHNITKO, J. FULARA, A. BATALOV, C. GILLERY, H. MASSO, P. ROSMUS, and J.P. MAIER. $^3\Sigma^- - X^3\Sigma^-$ Electronic transition of linear C_6H^+ and C_8H^+ in neon matrices. *Journal of Physical Chemistry A*, 110: 2885-2889, 2006
- [26] T.O. TIERNAN and R.L. WU. *Journal of Mass spectrometry*, 7A: 136, 1978

- [27] K. LACMANN, M.J.P. MANEIRA, A.M.C. MOUTINHO, and U. WEIGMANN. Total and double differential cross sections of ion-pair formation in collisions of K atoms with S_nCl_4 and CCl_4 . *The Journal of Chemical Physics*, 78: 1767-1776, 1983
- [28] H.B. ELLIS JR. and G.B. ELLISON. Photoelectron spectroscopy of HNO^- and DNO^- . *The Journal of Chemical Physics*, 78: 6541-6558, 1983
- [29] R. MIDDLETON. Versatile high intensity negative ion source. *Nuclear instruments and methods in physics research*, 214: 139-150, 1983
- [30] D. FORNEY, M. GRUTTER, P. FREIVOGEL, and J.P. MAIER. Electronic absorption spectra of carbon chain anions C_{2n+1}^- ($n=2-5$) in neon matrices. *Journal of Physical Chemistry A*, 101: 5292-5295, 1997
- [31] P. FREIVOGEL, M. GRUTTER, D. FORNEY, and J.P. MAIER. Infrared bands of mass-selected carbon chains C_n ($n=8-12$) and C_n^- ($n=5-10,12$) in neon matrices. *Chemical Physics*, 216: 401-406, 1997
- [32] J. FULARA, P. FREIVOGEL, M. GRUTTER, and J.P. MAIER. Electronic absorption spectra of Si_n and Si_n^- ($n=2-4$) in neon matrices. *Journal of Physical Chemistry*, 100: 18042-18047, 1996
- [33] M. GRUTTER, P. FREIVOGEL, and J.P. MAIER. Electronic absorption spectra of SiC^- and SiC in neon matrices. *Journal of Physical Chemistry A*, 101: 275-277, 1997
- [34] M. WYSS, M. GRUTTER, and J.P. MAIER. Electronic absorption spectra of BC , BC^- , BC_2 and BC_2^- in neon matrices. *Journal of Physical Chemistry A*, 102: 9106-9108, 1998
- [35] R. ROSSETTI and L.E. BRUS. Waveguide propagation in frozen gas matrices. *Review of Scientific Instruments*, 51: 467-470, 1980
- [36] C.J. SANSONETTI, M.L. SALIT, and J. READER. Wavelengths of spectral lines in mercury pencil lamps. *Applied Optics*, 35: 74-77, 1996

CHAPTER 3. CARBON CHAIN CATIONS



This chapter is a slightly modified form of the articles published in:
Fulara et. al., The Journal of Chemical Physics, 120: 7520–7525, 2004 and
Fulara et. al., The Journal of Chemical Physics, 123: 044305–6, 2005

LINEAR AND CYCLIC C_6^+

INTRODUCTION

The bare carbon cations C_n^+ are of interest in terrestrial and space environments as well as from a fundamental point of view. They are reactive intermediates in flames and discharges through organic vapors and also play a role in astrochemical processes in circumstellar shells around carbon stars and interstellar clouds [1, 2].

Experimentally they have been mainly generated by laser ablation of graphite and studied by mass spectrometry [3-6] regarding their structure, energetics, stability [7-12], and reactivity with simple molecules [13-19]. These have revealed that the small C_n^+ cations ($n \leq 6$) have a linear structure, larger ($n > 10$) a cyclic one, and those of the intermediate size ($7 \leq n \leq 10$) adopt both forms. Such cations have been also extensively studied by theoretical methods [20-24], the results lead to the same conclusion as the experiments concerning the structures. The small linear and cyclic C_n^+ isomers have similar energies but their relative stability changes depending on the theoretical method used.

However, the carbon cations remain exotic objects in term of spectroscopy in contrast to their neutral and anionic counterparts [1, 2]. The reports are limited to the simplest (C_2^+) [25] and large fullerene cations (C_{60}^+ , C_{70}^+) [26-28]. The present contribution enlarges this very short list and reports the observation of the electronic and infrared transitions of mass-selected C_6^+ ions isolated in 6 K neon matrices.

EXPERIMENTAL

The experimental setup has been described previously [29]. The C_6^+ cations were generated in a hot cathode-discharge ion source (Fig. 2.8) from perchloro- or perbromobenzene. C_6^+ was selected from a mixture of ions formed in the source by means of a quadrupole mass filter. In order to get a sufficient ion current for the matrix

production, the resolution of the mass filter was reduced, whereby ions differing by ± 2 amu from C_6^+ were not separated.

Beams of C_6^+ with 10–30 nA current and kinetic energy of about 50 eV were codeposited with an excess of neon onto a rhodium coated sapphire substrate held at 6 K. Absorption spectra were subsequently measured in the 230–1100 nm range. The effective optical path of the light through the matrix using a waveguide technique was about 2 cm. The infrared spectra were measured by doubly reflecting light from a Fourier-Transform infrared spectrometer through the matrix achieving a path length of ~ 1 mm.

RESULTS AND DISCUSSION

Figure 3.1 shows various recordings of electronic absorption spectra of mass-selected species (72 ± 2 amu) in neon matrices. Trace (a) is from a previous study using a cesium sputter source (Fig. 2.11) and the absorption bands marked are due to the $(1)^2\Pi_g \leftarrow X^2\Pi_u$ electronic transition of linear C_6^- [30]. Traces (b) and (d) are the present measurements. Using hexachlorobenzene as precursor and C_6^+ selection trace (b) is observed. Trace (c) is the $^3\Sigma_u^- \leftarrow X^3\Sigma_g^-$ absorption system of linear C_6 identified in a previous study [30]. C_6 is already present in trace (b) as a result of neutralization of the cations with electrons. The matrix remains electrically neutral during the deposition because the positive charge is compensated by anions formed in electron attachment processes with impurity molecules (*e.g.*, H_2O , CO_2). After the first few seconds of deposition, positive charge builds up which repels further cations arriving. Those with about 50 eV kinetic energy hit metal surfaces and release free electrons. These are attracted to the matrix and lead to a partial neutralization of the cations. Some electrons are captured by neutral molecules and form anions, the reason that C_6^- is also present in the matrix (trace (b)). Such processes take place continuously during the whole matrix growth. In addition to the $l-C_6^-$ bands and the neutral $l-C_6$ system several new absorption peaks at 646, 632, 570, and 520 nm are seen. Because these absorptions are absent in traces (a) and (c), and due to the mass-selection of C_6^+ , they are attributed to ions.

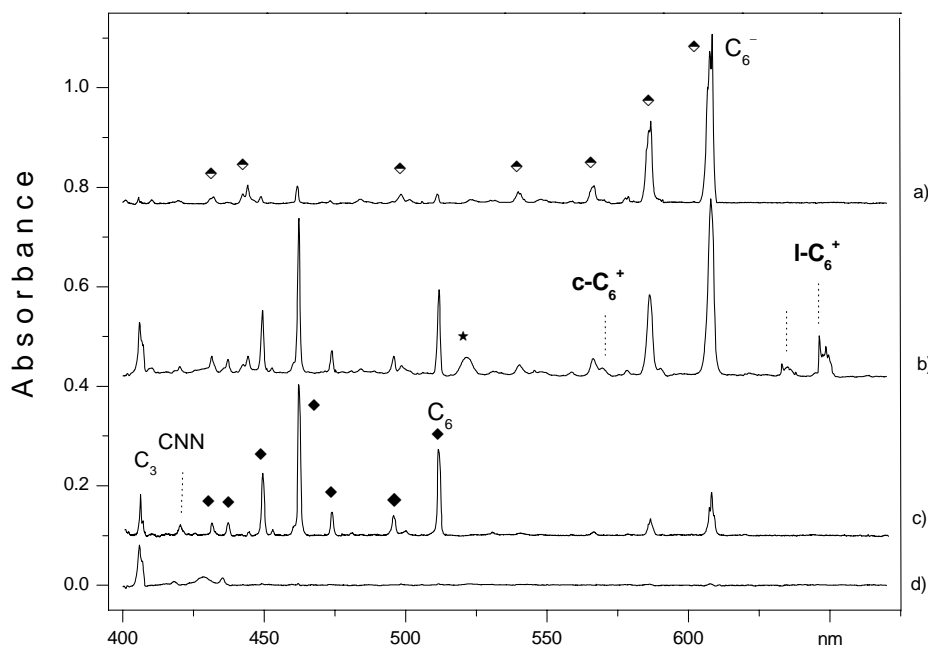


FIGURE 3.1 Electronic absorption spectra of mass-selected species (72 ± 2 a.m.u.) in 6 K neon matrices. Trace (a) is the ${}^2\Pi_g \leftarrow X^2\Pi_u$ transition of linear C_6^- obtained previously using a cesium sputter ion source [30]. Trace (b) is observed after deposition of C_6^+ generated from C_6Cl_6 in the hot cathode ion source. Trace (c) shows the ${}^3\Sigma_u^- \leftarrow X^3\Sigma_g^-$ system of linear C_6 obtained after UV irradiation of the matrix containing C_6^- . Trace (d) is the absorption of C_3Cl^+ produced from C_3Cl_6 . The bands of C_6^- , marked with ◆ in trace (a) and those of linear neutral C_6 , marked with ◆ in trace (c) were normalized in such a way that their intensities are the same as in trace (b); ★ is the band of cyclic C_6^- .

In order to exclude the possibility that the selected ions with 72 ± 2 a.m.u. are not C_6^+ but C_3Cl^+ , trace (d) was recorded. For this C_3Cl_6 was introduced into the ion source and C_3Cl^+ mass selected. No absorptions are seen at the positions of the four new peaks of trace (b). In order to exclude the possibility that the bands seen in Figure 3.1(b)

originate from fragments of C_6^+ (C_n^p $n=4, 5, p=\pm 1$), C_4^+ and C_5^+ generated from C_4Cl_6 and C_5Cl_6 as precursors were mass selected and deposited. None of the bands seen in Figure 3.1(b) (except C_3) were observed in the spectra. The results of these experiments indicate that the bands at 646, 570, and 520 nm originate from a species with six carbon atoms. The disappearance of these bands under ultraviolet (UV) irradiation ($\lambda < 305$ nm) and the simultaneous growth in intensity of the C_6 bands (Fig. 3.2(b)) indicates that these three absorption peaks are due to C_6^+ or C_6^- ions.

C_6^+ was also generated from C_6Br_6 . Figure 3.2 compares the spectra obtained from C_6Cl_6 (traces (a) and (b)) and C_6Br_6 (traces (c) and (d)) as precursors. The bands of C_6^- , linear C_6 , and the origin band of C_3 dominate. In addition, a moderately intense band at 570 nm is present, whereas the 646 and 520 nm ones are absent. No other bands were detected in the 650–1100 nm range, and only the absorption peaks of $l-C_6$ and C_3 between 230 and 400 nm were observed [31] as when using the C_6Cl_6 precursor. The peak at 570 nm vanishes and the bands of $l-C_6^-$ diminish substantially after irradiation of the matrix with UV photons, whereas those of $l-C_6$ grow in intensity (Fig. 3.2(d)). From this it is concluded that the bands seen at 520, 570, and 646 nm in Figure 3.1(b) originate from at least two different C_6^p ($p=\pm 1$) ions.

The sign of the charge of carbon ions responsible for these three absorption bands was determined by deposition of mass-selected C_6^+ in a neon matrix in the presence of CCl_4 (CCl_4 -Ne ratio of 1:2000), which acts as an electron scavenger. The absorption spectrum observed is shown in Figure 3.3(a). In spite of 50% larger C_6^+ current in comparison with the experimental conditions without the electron scavenger (Fig. 3.2(a)), the bands of C_6^- are two times weaker, the band at 520 nm is absent and the ones at 646 and 570 nm are much stronger than expected. After irradiation of the matrix with UV photons the bands of $l-C_6^-$ and the systems with the onsets at 646 and 570 nm decrease drastically (Fig. 3.3(b)). Due to the absence of the band at 520 nm in the experiment with CCl_4 it is concluded that this absorption is most likely due to a non-linear isomer of C_6^- . CCl_4 competes with other molecules present in a matrix in the

capture of free electrons. As a result the bands of $l-C_6^-$ become weaker in the presence of a scavenger, whereas the 520 nm absorption of the other isomer of C_6^- is absent due to its low electron affinity.

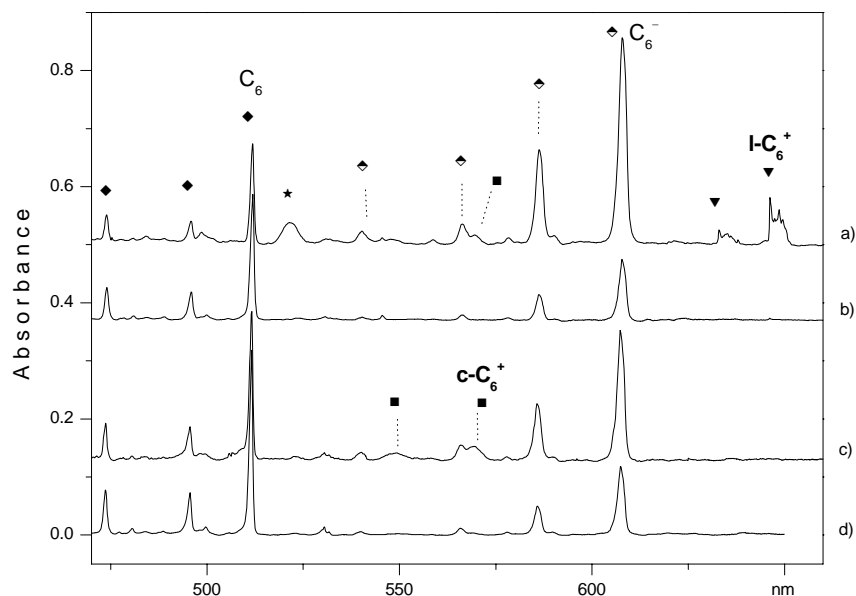


FIGURE 3.2 Absorption bands observed after deposition of mass-selected C_6^+ produced from C_6Cl_6 (trace (a)) and C_6Br_6 (trace (c)). Traces (b) and (d) are the spectra of the same matrices obtained after irradiation with UV photons ($\lambda > 305$ nm). The bands of cyclic C_6^+ are identified with \blacksquare , those of linear C_6^+ with \blacktriangledown , the ones of C_6 by \blacklozenge and \blacklozenge for C_6^- ; \star is the band of cyclic C_6^- .

The band systems with the onsets at 570 and 646 nm originate from two different isomers of C_6^+ (cyclic and a linear one). This conclusion is based on the behavior of these bands under UV irradiation and the presence of the electron scavenger (compare traces (a) and (c) in Fig. 3.2). The bands at 570 and 646 nm have a similar

bleaching behavior with respect to UV photons as is typical for cations. The bands of C_6^+ are stronger in the matrix doped with CCl_4 because it captures electrons and thus reduces their recombination with C_6^+ . The 570 and 646 nm bands are present in the

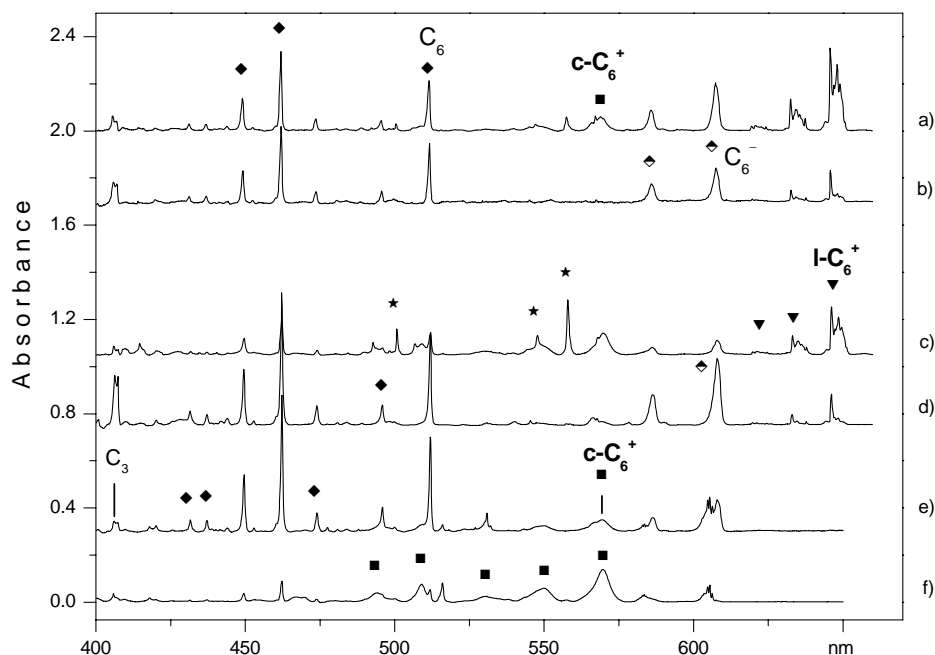


FIGURE 3.3 Influence of doping neon matrices with electron scavengers (CCl_4 , N_2O) on the intensity of C_6^+ and C_6^- electronic absorption bands. Trace (a) is observed after deposition of mass-selected C_6^+ produced from C_6Cl_6 in a neon matrix containing 0.05% CCl_4 . Trace (b) is observed after subsequent irradiation of the same matrix with UV photons ($\lambda > 305$ nm). Traces (c) and (f) show the spectra recorded after deposition of mass-selected C_6^+ in neon matrices including 1% of N_2O . Traces (d) and (e) were obtained after irradiation. The cations were generated from C_6Cl_6 (traces (c) and (d)) and from C_6Br_6 (traces (e) and (f)). \blacktriangledown indicates the bands of linear C_6^+ , \blacksquare the ones of cyclic C_6^+ , whereas \star shows the bands of the reaction product of linear C_6^+ with N_2O . The other symbols have the same meaning as in Figure 3.2.

spectrum recorded after deposition of C_6^+ with C_6Cl_6 as a precursor (Fig. 3.2(a)), but with C_6Br_6 only the 570 nm band is observed (Fig. 3.2(c)).

Though the intensity of the band at 570 nm in the spectrum of C_6^+ (Fig. 3.2(a)) is much weaker than at 646 nm, the isomer that is responsible predominates in the matrix. The UV light-induced decay of the 570 nm absorption gives rise to the concurrent intensity increase of the bands of $l-C_6$. The absorbance of the origin band of $l-C_6$ increases by a factor of 3 relative to the initial absorbance of the peak at 570 nm. Linear C_6 is also produced in the matrix as a result of photodetachment of electrons from C_6^- anions. However, the decay of the bands of $l-C_6^-$ can only account for a very small fraction of the increase in the absorbance of $l-C_6$ because the oscillator strength for the origin band of $l-C_6^-$ is an order of magnitude larger than for $l-C_6$ [32, 33].

It is difficult to conclude exclusively from the spectroscopic data which isomer of C_6^+ absorbs at which wavelength. However, an indication comes from the ion mobility and bimolecular reactivity studies on C_n^+ ions [11, 13, 14, 19]. These show that the predominant form of C_6^+ is the linear one irrespective how C_6^+ is produced. Thus, the reaction of C_6^+ with N_2O in a neon matrix was studied.

Mass-selected C_6^+ cations generated from C_6Cl_6 or C_6Br_6 were deposited in a neon matrix containing 1 % of N_2O . The resulting electronic absorption spectra are shown in Figures 3.3(c) and 3.3(f) with C_6Cl_6 as precursor. Apart from the C_6^+ bands at 570 and 646 nm a strong system (marked with ★ in Fig. 3.3(c)) with the onset at 558 nm is clearly discernible. This band system vanishes upon UV irradiation, which suggests that it originates from the C_6O^+ , or C_6N^+ , cation according to the gas-phase reaction $C_6^+ + N_2O$ [18]. The bands of C_6^+ also diminish substantially (Fig. 3.3(d)) whereas the ones of neutral linear C_6 and C_3 grow in intensity. The appearance of the new bands in the spectrum of C_6^+ in the presence of N_2O (Fig. 3.3(c)) as well as the comparison of the intensity ratio of the 570 and 646 nm peaks shown in Figure 3.3(a), leads to the conclusion that the isomer of C_6^+ which absorbs at 646 nm reacts with N_2O in a 6 K matrix.

In contrast to the situation with C_6Cl_6 as precursor, the C_6^+ isomer generated from C_6Br_6 does not react with N_2O in a neon matrix (Fig. 3.3(f)). This is composed of the strong band system of C_6^+ with the origin at 570 nm. The bands of neutral linear C_6 are barely seen. Thus, N_2O acts as an electron scavenger and the trapping efficiency of C_6^+ in the matrix is close to unity (the recombination of cations with electrons is negligible in this case). No other bands were observed in this spectrum except those at 604 and 516 nm, which are due to hydrogenated C_6^+ cations (e.g., HC_6H^+), and are present in the matrix as a result of contamination of the C_6Br_6 sample used for generation of C_6^+ with $C_6H_2Br_4$ because the mass selection was ± 2 amu. Irradiation with UV photons leads to a significant decrease of the C_6^+ bands relative to those of the linear C_6 (Fig. 3.3(e)).

The reaction of C_6^+ with N_2O reveals that the 646 nm isomer of C_6^+ is reactive, whereas the 570 nm one is not. Gas-phase reactivity studies indicate that the linear isomer of C_6^+ is reactive. Therefore, the band system with the onset at 646 nm originates from linear C_6^+ , whereas that at 570 nm belongs to cyclic C_6^+ . In our hot-cathode ion source (Fig. 2.8), contrary to the experiments reported in the literature [19], the *c*- C_6^+ is produced in a major quantity from C_6Cl_6 as well as C_6Br_6 precursors.

Harmonic frequencies have been calculated at the B3LYP/cc-pVDZ level for linear C_6^+ and cyclic (C_{2v}) C_6^+ in their ground electronic states [34]. By comparison with these values (given in the footnote to Table 3.1) vibrational assignments in the excited electronic states have been made using the same numbering of modes. For the *l*- C_6^+ there are 3 totally symmetric modes (σ_g^+) which can be excited in transitions from the lowest vibrational level of the ground electronic state where the total population is concentrated at 6 K. The electronic spectrum of *l*- C_6^+ shows the single excitation of the ν_1 and ν_3 modes, as well as $\nu_7(\pi_g)$ in double quanta. In case of cyclic C_6^+ (C_{2v}) there are five totally symmetric modes (a_1) and the spectrum shows the excitation of three of these fundamentals. The highest frequency is presumably the $\nu_1(a_1)$ mode and the other two are $\nu_2(a_1)$ or $\nu_3(a_1)$ and $\nu_4(a_1)$ or $\nu_5(a_1)$. The calculations predict these pairs to have similar frequencies.

TABLE 3.1 Observed vibronic transitions of linear, ${}^2\Pi_g-X{}^2\Pi_u$, and cyclic $(2) {}^2B_2-X{}^2A_1$ C_6^+ in 6 K neon matrices with suggested assignment. The wavelengths correspond to the most prominent site in the absorption spectrum: $\lambda=\pm 0.2$ nm, $\tilde{\nu} \pm 5$ cm^{-1} .

λ (nm)	$\tilde{\nu}$ (cm^{-1})	$\Delta\tilde{\nu}$ (cm^{-1})	Assignment*
645.8	15484	0	0_0^0 ${}^2\Pi_g-X{}^2\Pi_u$ $l-C_6^+$
632.5	15811	327	7_0^2
619.5	16143	659	$3_0^1, 7_0^4$
567.2	17630	2146	1_0^1
547.1	18277	2793	$1_0^1 7_0^2$
569.6	17558	0	0_0^0 $(2) {}^2B_2-X{}^2A_1$ $c-C_6^+$
549.8	18188	630	4_0^1 or 5_0^1
530.4	18855	1297	2_0^1 or 3_0^1
508.9	19650	2092	1_0^1
493.9	20248	2690	$1_0^1 4_0^1$ or $1_0^1 5_0^1, 2_0^2$
467.0	21414	3856	$1_0^1 2_0^1 3_0^1, 1_0^2$

* Using numbering of the calculated frequencies (cm^{-1}) for the ground state from Ref. [34].

$l-C_6^+$: $\nu_1(\sigma_g)=2200$, $\nu_2(\sigma_g)=1584$, $\nu_3(\sigma_g)=662$, $\nu_4(\sigma_u)=2068$, $\nu_5(\sigma_u)=1171$, $\nu_6(\pi_g)=689/607$, $\nu_7(\pi_g)=205/172$, $\nu_8(\pi_u)=397/362$, $\nu_9(\pi_u)=99/91$; $c-C_6^+$: $\nu_1(a_1)=1778$, $\nu_2(a_1)=1236$, $\nu_3(a_1)=1195$, $\nu_4(a_1)=661$, $\nu_5(a_1)=563$, $\nu_6(a_2)=459$, $\nu_7(b_1)=476$, $\nu_8(b_1)=364$, $\nu_9(b_2)=2076$, $\nu_{10}(b_2)=1561$, $\nu_{11}(b_2)=1307$, $\nu_{12}(b_2)=641$.

Irradiation of $c-C_6^+$ with UV photons leads to the appearance of $l-C_6$ in the matrix. Apart from the bands of $l-C_6$ no new absorptions grew in intensity upon UV irradiation and which could be assigned to $c-C_6$. The electronic absorption spectrum of $c-C_6$ is unknown, but theory predicts an electronic transition at 2.96 eV [35]. The absence of the $c-C_6$ bands in our experiments can be due to a small oscillator strength of this transition and/or its photo-instability leading to ring opening and formation of $l-C_6$. The formation of $l-C_6$ can also proceed during recombination of $c-C_6^+$ with electrons. The close to unity conversion yield of $c-C_6^+$ to $l-C_6$ allows an estimation of the

oscillator strength of the electronic transition of $c-C_6^+$ with reference to that of $l-C_6$; the former is comparable or almost two times weaker.

In the case of $l-C_6^+$ we cannot separate the contribution of the cyclic form to the increase of the intensity of the band system of $l-C_6$ upon UV irradiation, because $l-C_6^+$ coexists in a large excess of $c-C_6$. Apart from the direct UV photodissociation, $l-C_6^+$ also undergoes dissociative recombination with free electrons, leading to the C_3 fragment. This latter reaction supports the proposed assignment because the fragmentation of $l-C_6^+$ to C_3 is energetically more favorable than from $c-C_6^+$ where two C-C bonds must be broken.

Ab initio multireference configuration interaction (MRCI) calculations predict that the lowest excited state of linear C_6^+ has $^2\Pi_u$ symmetry and two electronic transitions at 2.57 and 2.94 eV are expected, whereas the strongest vertical electronic transition ($2^2B_2 \leftarrow X^2A_1$) for the $c-C_6^+$ is calculated at 3.08 eV [23]. These theoretical results support the assignment of the 646 nm band to the $^2\Pi_g \leftarrow X^2\Pi_u$ electronic transition of $l-C_6^+$. The calculations overestimate the excitation energy to the $^2\Pi_g$ electronic state by 0.65 eV; the discrepancy is larger than the likely error quoted [23]. However, the results of extensive MRCI *ab initio* calculations agree better, predicting the energy of the allowed electronic transition at 1.88 eV [36] close to the experimental value of 2.18 eV.

The band system originating at 570 nm is assigned to the ($2^2B_2 \leftarrow X^2A_1$) electronic transition of $c-C_6^+$. The difference between calculated vertical and the experimental transition energy is much larger (0.9 eV) in this case [23]. The reason for this large difference appears to lie with geometry change in the two electronic states and the new multiconfigurational complete active space self-consistent (CASSCF) method leads to a value of 2.39 eV for this transition [36].

In order to corroborate the above assignment of the electronic absorption bands to a specific form of C_6^+ , infrared spectra were also recorded. The section of the infrared spectrum around 2000 cm^{-1} of mass-selected C_6^+ generated from C_6Br_6 is shown in Figure 3.4(a) (solid line). The dotted line represents the IR spectrum observed after UV irradiation of the matrix. Three bands at 1972 , 1962 , and 1959 cm^{-1} are clearly seen

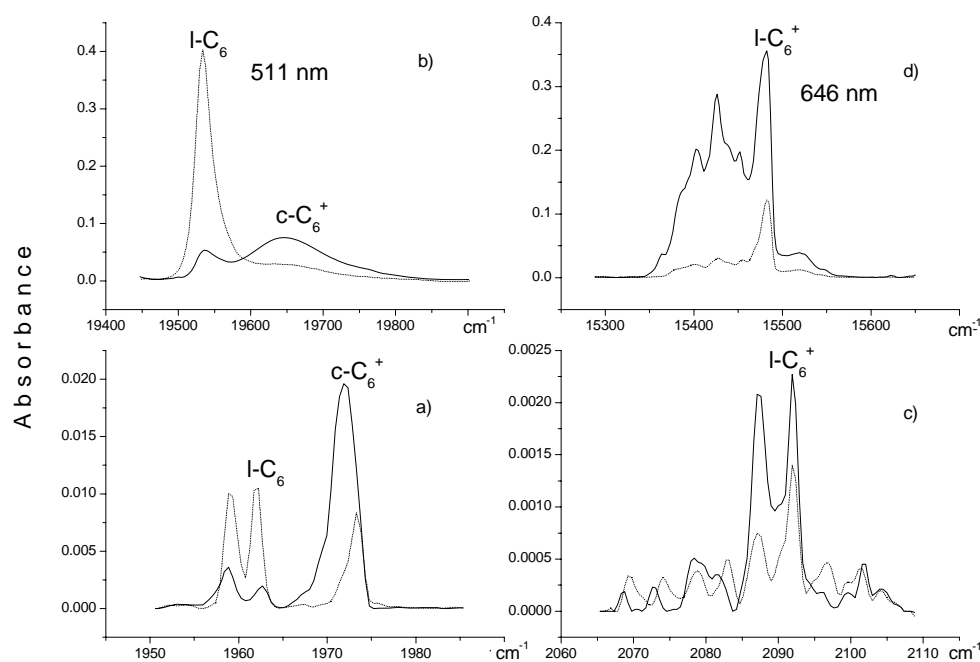


FIGURE 3.4 IR bands of cyclic C_6^+ (solid line in (a)), linear C_6 and linear C_6^+ (solid line (c)) observed after deposition of mass-selected C_6^+ produced from C_6Br_6 and C_6Cl_6 , respectively. Dotted lines show the same bands recorded after subsequent irradiation with UV photons ($\lambda < 305\text{ nm}$). The photochemical behavior of the electronic absorption bands of linear C_6 , cyclic C_6^+ , and linear C_6^+ is shown in traces (b) and (d). They were measured with the same matrices as the IR bands. Solid lines show the spectra recorded after deposition of mass-selected C_6^+ , dotted ones after UV irradiation.

(Fig. 3.4(a)). The band at 1972 cm^{-1} decreases upon UV irradiation whereas the ones at 1959 and 1962 cm^{-1} grow in intensity. The behavior of these bands closely mimics the electronic absorption of the $c\text{-}C_6^+$ cation (at 570 nm) and of $l\text{-}C_6$ (at 511 nm) upon UV radiation (Fig. 3.4(b)).

The band at 1959 cm^{-1} was observed previously in a neon matrix [37] and assigned to the ν_4 antisymmetric mode of $l\text{-}C_6$. The band at 1962 cm^{-1} most likely originates from the occupation of another site in the matrix. The earlier results indicate that the 570 nm electronic system and the IR band at 1972 cm^{-1} originate from the same molecule, namely $c\text{-}C_6^+$. Photoconversion of $c\text{-}C_6^+$ in the matrix leads to $l\text{-}C_6$. We did not observe the IR band at 1700 cm^{-1} which was assigned [38] to a neutral cyclic C_6 . This is consistent with the failure to detect the visible spectrum, as discussed earlier.

Another part of the IR spectrum of C_6^+ trapped in a neon matrix containing CCl_4 as electron scavenger is seen in Figure 3.4(c) (solid line), and after UV irradiation (dotted line). The spectra were recorded with the same matrix as for the electronic spectra of Figures 3.3(a), 3.3(b). Apart from the bands at 1972 , 1962 , and 1959 cm^{-1} observed with C_6Br_6 as the precursor, an additional band with a doublet structure (at 2087.3 and 2092.1 cm^{-1}) is apparent. One component of this doublet (2087.3 cm^{-1}) vanishes entirely, whereas the second diminishes substantially upon irradiation with UV photons. In addition, after irradiation the 2043 cm^{-1} band of C_3 appears in the IR spectrum (not shown in Fig. 3.4(c)). From comparison of the traces in Figures 3.4(c), 3.4(d) we can see that the origin band of the electronic transition of $l\text{-}C_6^+$ at 646 nm behaves exactly as the 2087.3 and 2092.1 cm^{-1} IR doublet. This indicates that the electronic system with the onset at 646 nm and this IR transition originate from $l\text{-}C_6^+$. Moreover, $l\text{-}C_6^+$ recombines dissociatively with an electron and forms neutral C_3 in the matrix upon absorption of an UV photon.

The fundamental modes in the ground and excited electronic states of $l\text{-}C_6^+$ and $c\text{-}C_6^+$ inferred from the IR and electronic absorption spectra are given in Table 3.2. The experimental and theoretical electronic transition energies of these cations are also

TABLE 3.2 Experimental and calculated electronic transition energies and vibrational frequencies of linear and cyclic C_6^+ .

Cation	Electronic state	T_e/eV		$\tilde{\nu}/cm^{-1}$		Mode	
		Exp.	Calc.	Exp.	Calc.		
$l-C_6^+$	$X^2\Pi_u$		0	2092	2068 ^{c)}	$\nu_4(\sigma_u)$	
	$(2)^2\Pi_g$	1.92	2.57 ^{a)}	164		$\nu_7(\pi_g)$	
			1.88 ^{b)}		659		$\nu_3(\sigma_g)$
					2146		$\nu_1(\sigma_g)$
$c-C_6^+$	X^2A_1		0	1972	2076 ^{c)}	$\nu_9(b_2)$	
	$(2)^2B_2$	2.18	3.08 ^{a)}		630	$\nu_4(a_1)$ or $\nu_5(a_1)$	
			2.39 ^{b)}		1297	$\nu_2(a_1)$ or $\nu_3(a_1)$	
					2092	$\nu_1(a_1)$	

^{a)}Reference [23], ^{b)}Reference [36], ^{c)}Reference [22].

collected there. The normal modes of linear and cyclic C_6^+ have been calculated by a discrete Fourier transform [22]. These calculations predict the antisymmetric $\nu_4(\sigma_u)$ mode of $l-C_6^+$ and $\nu_9(b_2)$ vibrations of $c-C_6^+$ at 2068 and 2076 cm^{-1} , respectively. The calculated vibrational frequencies of the C_6^+ isomers are similar and associated with a large error.

CONCLUSIONS

Cyclic C_6^+ is solely formed in the hot cathode ion source with C_6Br_6 as the precursor, whereas from C_6Cl_6 the cyclic and linear C_6^+ isomers are produced. The

linear isomer of C₆⁺ has the ${}^2\Pi_g \leftarrow X {}^2\Pi_u$ electronic transition with origin band at 646 nm. Cyclic C₆⁺ also absorbs in the visible with origin band at 570 nm for the (2) ${}^2B_2 \leftarrow X {}^2A_1$ transition.

Irradiation of *c*-C₆⁺ with UV photons leads to the appearance of *l*-C₆ in a matrix, whereas *l*-C₆⁺ fragments to C₃ as a result of dissociative recombination with electrons liberated from weakly bonded anions. Linear C₆⁺ reacts with N₂O in the neon matrix whereas the cyclic one is unreactive. The observation and identification of the electronic transition of *l*-C₆⁺ and *c*-C₆⁺ in 6 K matrices opens the way for spectroscopic studies of these astrophysically important ions in the gas phase.

LINEAR AND CYCLIC C_N⁺ (N=7-9)

INTRODUCTION

Bare carbon molecules and ions have been the focus of numerous experimental and theoretical studies [1, 2]. They have not only attracted attention as intermediates in combustion, as building units for fullerenes and nanotubes, but also in astrophysics. Spectroscopic laboratory data are a requisite for the detection of these molecules in such environments. C₃ and C₅ have been detected in the envelopes of carbon-rich stars in the infrared [39, 40] and C₃ has also been observed in diffuse interstellar clouds by its electronic transition at 405 nm [41].

Carbon chains of the size C_n 5<n<15 were proposed as carriers of diffuse interstellar bands long ago [42]. However, as the unsuccessful attempt to detect C₄ and C₅ [43] shows, the smaller chains cannot be responsible [44]. Because the diffuse interstellar medium is permeated by a strong radiation field capable of ionizing any polyatomic species, carbon cations should also be investigated.

Carbon cations have been extensively studied by mass spectrometry with respect to their structure [11, 45, 46], stability [5-7, 9], and reactivity with small molecules [13, 15-19]. These results led to the conclusion that medium size C_n⁺ 5<n<10 species coexist in the linear and cyclic forms. Theoretical calculations on the structure and energetics of C_n⁺ corroborate the experimental results [20-23, 47]. On the other hand, spectroscopic data are scarce and limited to C₂⁺ in the gas phase [25, 48] and C₆₀⁺ and C₇₀⁺ in neon matrices [26-28]. Recently the electronic absorption spectra of linear and cyclic C₆⁺ in a 6 K neon matrix have been identified [49] (discussed above). The study of the corresponding spectra of C_n⁺ n=7-9 is the purpose of the present work.

EXPERIMENTAL

The experimental approach combines mass selection with matrix isolation spectroscopy [29]. Bare carbon cations were generated in a hot cathode discharge ion source (Fig. 2.8) from perchloronaphthalene in a helium buffer gas. The cations were extracted from the source and guided through a quadrupole mass filter to the matrix.

The mass resolution was degraded to ± 2 amu to yield a larger current. The mass-selected ions were codeposited with an excess of neon onto a rhodium-coated sapphire substrate held at 6 K. Typical integrated ion charge of C_n^+ deposited was 48, 30, and 17 μC for $n=7, 8$, and 9, respectively. A matrix of ~ 150 μm thickness was grown over a period of 3 hours. The 220–1100 nm region was then scanned using a waveguide technique resulting in a 2 cm light path through the matrix. After irradiation with a medium-pressure mercury lamp ($\lambda > 305$ nm), a common procedure used to eliminate cations, the spectra were recorded anew.

RESULTS AND DISCUSSIONS

ELECTRONIC ABSORPTION SPECTRA OF C_7^+

C_7^+ was produced from the $C_{10}Cl_8$ precursor in the ion source. The electronic absorption spectrum measured in a neon matrix after deposition of mass-selected C_7^+ is shown in trace (a) in Figures 3.5–3.7. The 480–530 and 340–400 nm ranges do not show absorptions relevant to C_7^+ . In the red part of the spectrum (Fig. 3.5) several new bands are present. In the visible (Fig. 3.6), apart from the known bands of HC_4Cl^+ and recently identified ones of C_4Cl^+ , a new intense peak at 448.5 nm is discernible. The strongest absorptions, which likely form four band systems, are observed in the UV range (Fig. 3.7(a)). There one can recognize two band systems of neutral linear C_7 . The two remaining band systems are unique for the C_7^+ experiment. Neutral C_7 is present in the matrix as a result of the charge neutralization of deposited cations. The bands of C_4Cl^+ and HC_4Cl^+ appear due to the low mass resolution used and because $C_{10}Cl_8$ is contaminated with not fully chlorinated naphthalene.

To distinguish the bands of cations from those of neutrals photobleaching was carried out. The matrix was irradiated with a medium-pressure mercury lamp with $\lambda > 305$ nm causing electron detachment from weakly bound anions. The electrons migrate in the matrix and on meeting cations form neutrals. The spectrum recorded after UV irradiation is shown in trace (b) in Figures 3.5–3.7, and the systems show different

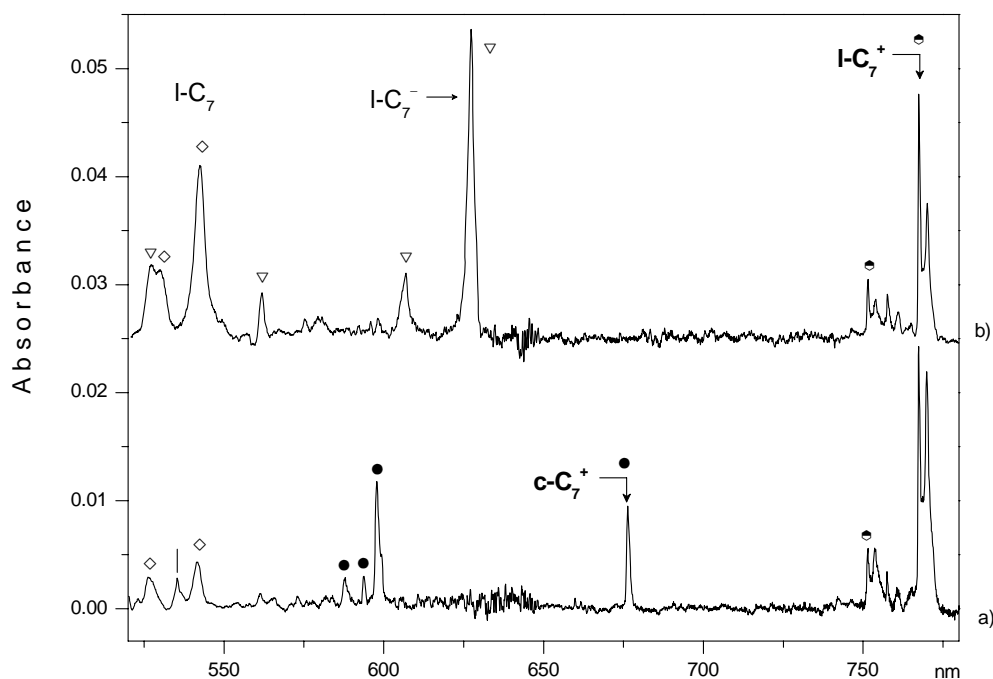


FIGURE 3.5 The electronic transitions of $l\text{-C}_7^+$ (\odot) and $c\text{-C}_7^+$ (\bullet) observed in a 6 K neon matrix after codeposition of C_7^+ (produced from $C_{10}Cl_8$) with an excess of neon (trace (a)) and subsequent UV irradiation (trace (b)). The electronic absorption bands of $l\text{-C}_7$ (\diamond) and $l\text{-C}_7^-$ (∇) are also present as a result of the neutralization and capture of electrons by C_7 .

behavior: some appear or grow in intensity and others which diminish or vanish.

The bands of linear neutral C_7 (marked with \diamond in Fig. 3.5) grow in intensity after photobleaching. The UV section of the electronic absorption spectrum of $l\text{-C}_7$ measured previously [50] is shown in trace (c) in Figure 3.7 for reference. The bands which appear in the matrix upon UV irradiation belong to $l\text{-C}_7^-$ (marked with ∇ in Figs. 3.5 and 3.6). This occurs because $l\text{-C}_7$ captures electrons detached from weakly bound anions and forms $l\text{-C}_7^-$. The same effect was also observed for C_6^- [49]. For a better comparison the spectrum of $l\text{-C}_7^-$ obtained when anions were generated from graphite and deposited in a neon matrix [50], is shown in trace (c) of Figure 3.6.

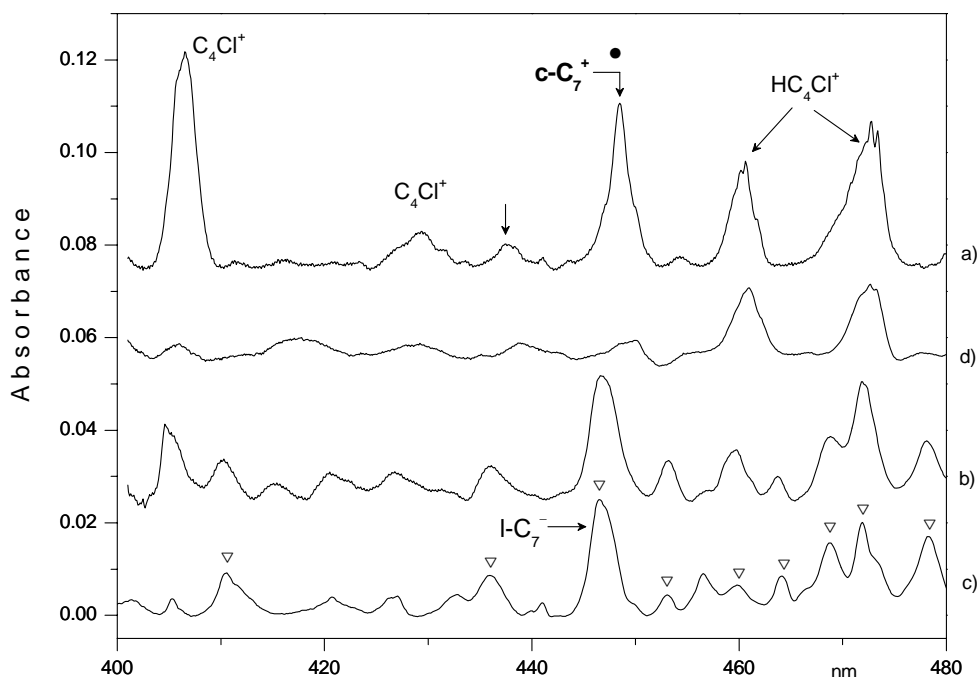


FIGURE 3.6 The electronic transition of $c-C_7^+$ (●) observed in the visible region after deposition of mass-selected C_7^+ in a 6 K neon matrix (trace (a)). Trace (b) shows the spectrum recorded after UV irradiation; the bands which grow in intensity originate from $l-C_7^-$. To facilitate the identification of these bands in trace (b), the spectrum of C_7^- (▽) obtained previously [50], where anions were produced from graphite in a Cs^+ sputter source (Fig. 2.11) is shown in trace (c). Apart from $c-C_7^+$ the electronic absorption bands of C_4Cl^+ , HC_4Cl^+ are also present in trace (a) due to the low mass resolution (± 2 amu) used. The spectrum of HC_4Cl^+ generated from C_6HCl_5 is shown in trace (d) for comparison.

The bands that decrease or disappear upon UV irradiation originate from cations. The section of the electronic absorption spectrum of HC_4Cl^+ in a neon matrix, produced from C_6Cl_5H , is shown in trace (d) of Figure 3.6 for comparison with trace (a). The

electronic spectrum of C_4Cl^+ has recently been studied in a neon matrix and the band at 405 nm in trace (a) (Fig. 3.6) originates from it [51]. Neither C_4Cl^+ nor HC_4Cl^+ have absorptions in the 530–800 nm range and therefore the bands in this spectral region which diminish or vanish upon UV irradiation originate from C_7^+ .

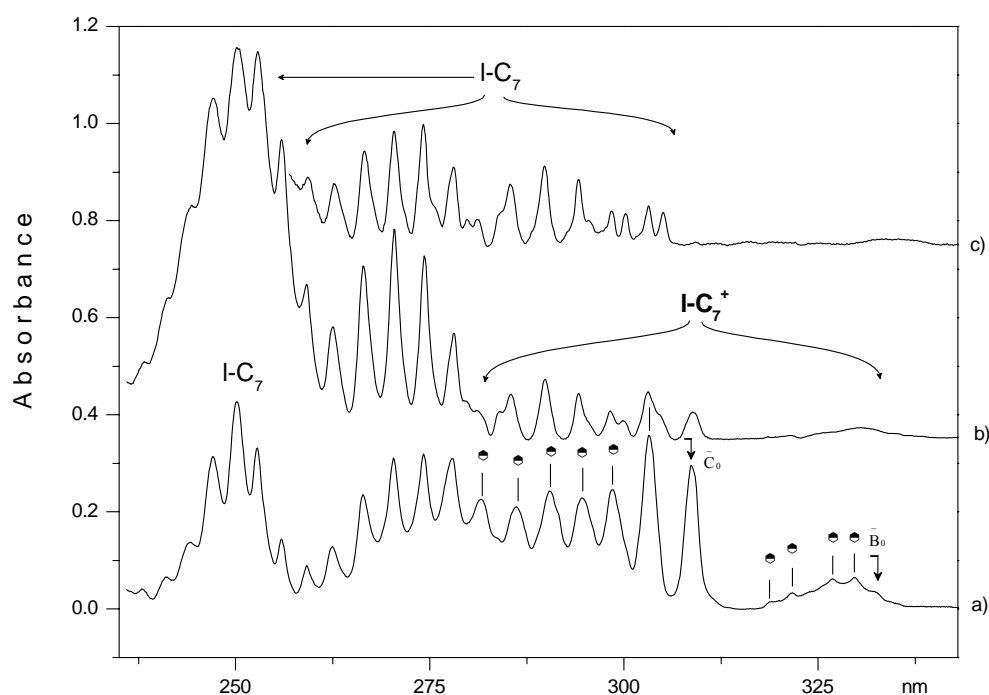


FIGURE 3.7 The UV electronic transitions of $l-C_7^+$ (●) observed after deposition of mass-selected C_7^+ in a neon matrix (trace (a)). The bands of neutral $l-C_7$ are also present. The bands of $l-C_7$ grow in intensity after UV irradiation (trace (b)). Trace (c) shows the bands of $l-C_7$ obtained earlier [50].

The system with the origin band at 770.1 nm decreases in intensity after photobleaching. Two other band systems in the spectrum of C_7^+ which lie in the UV

range (trace (a) in Fig. 3.7) behave in a similar way, while the systems with the onset at 676.3 and 448.5 nm vanish. One can conclude that the bands which differ in the photobleaching behavior originate from two structural isomers of C_7^+ : the linear and cyclic one. Such two isomers of C_6^+ were spectroscopically identified in a neon matrix [49] (discussed earlier).

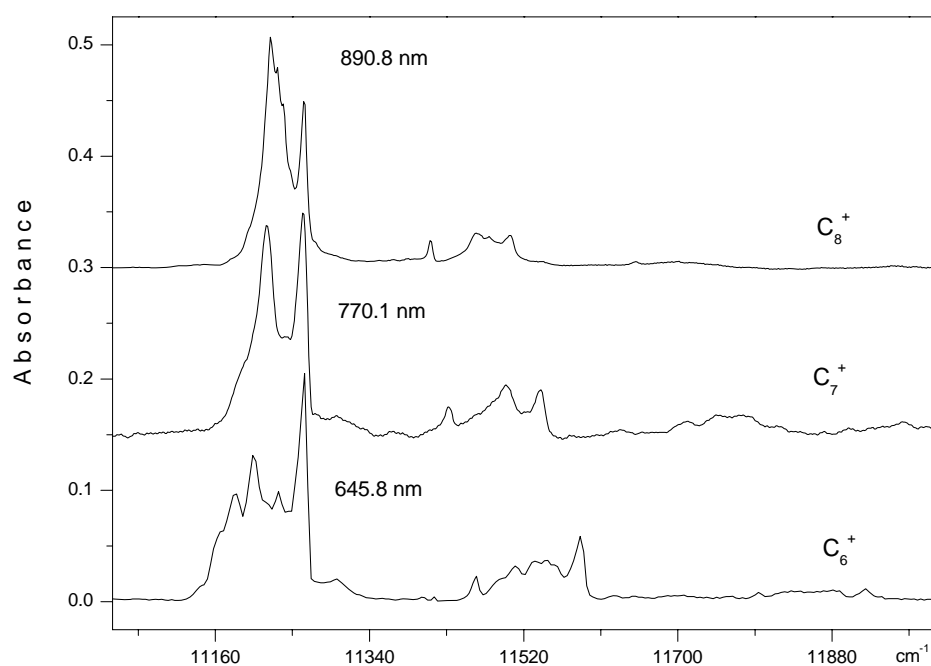


FIGURE 3.8 The lowest-energy electronic transitions of $l\text{-}C_n^+$ ($n=6-8$) observed in a 6 K neon matrix. The spectra are plotted with the origin bands shifted to the same wavenumber for a better comparison of the shape and vibrational spacing.

The attribution of the observed absorption systems to $l\text{-}C_7^+$ or $c\text{-}C_7^+$ is made on the following grounds. In the case of the C_6^+ theoretical calculations as well as the reactivity of the two isomers in neon matrices enabled the $l\text{-}C_6^+$ and $c\text{-}C_6^+$ systems to be

identified [28] (discussed above). The bands of these two isomers show differing site structure and shape, as do the 770 and 676 nm bands of C_7^+ . Specifically the 770 nm band has a more complex pattern, similar to the one of $l-C_6^+$. This is shown in Figure 3.8, where the corresponding origin band for $l-C_8^+$ is included. Furthermore, when the wavelengths of these three origin bands are plotted versus the number of carbon atoms, a linear dependence is obtained. This is not the case if the $c-C_7^+$ origin band at 676 nm, with a different band shape, is used instead.

Such a linear dependence on the length of the chain is reasonable in view of the π -electron excitations involved in these transitions. These are dominated by the configurations $\dots\pi^3\pi^2 \leftarrow \dots\pi^4\pi^1 \tilde{X}^2\Pi$ for C_6^+ and C_8^+ and $\dots\pi^3\pi^4 \leftarrow \dots\pi^4\pi^3 \tilde{X}^2\Pi$ for C_7^+ . In both cases the excitation is between the penultimate-filled π molecular orbital (MO) and the partly filled highest occupied molecular orbital (HOMO). It is not surprising that the usual particle in a box-type arguments lead to a quasilinear dependence between λ and the number of carbon atoms.

The strongest absorption of $l-C_7^+$ has an onset at 308.7 nm (Fig. 3.7(a)). Two other weaker electronic transitions lie at 770.1 and 332.3 nm (1.61 and 3.73 eV). The two systems with onset at 676.3 and 448.5 nm (1.83 and 2.78 eV) are of the cyclic C_7^+ isomer.

The assignment to specific electronic transitions will require theoretical predictions. These are underway [52] but preliminary results show that both for the linear isomer with $\tilde{X}^2\Pi_u$ ground state, and the cyclic one (\tilde{X}^2B_2 in C_{2v} symmetry) mixing of the excited states is significant and will require considerable computational effort. The suggested vibrational assignment of the $l-C_7^+$ and $c-C_7^+$ systems in Table 3.3 is made by reference to the *ab initio* calculations of the normal-mode frequencies in the ground electronic state of C_7^+ and/or C_7 [22, 47, 53].

ELECTRONIC ABSORPTION SPECTRUM OF C_9^+

The C_9^+ cations were also generated from the $C_{10}Cl_8$ precursor. The absorption spectrum corresponding to this mass selection is shown in trace (a) of Figure 3.9, and

trace (b) is observed after photobleaching. Only the strongest electronic transition of C_9^+ lying in the 350–380 nm region was detected. In the visible range the bands of known carbon chlorinated species (C_6Cl , C_6Cl^+ and HC_6Cl^+) [54] are present and in the UV those of C_6Cl and C_6Cl^+ [54] interfere. For this reason the absorption spectra of these species generated from C_6Cl_6 are also included in traces (c) and (d) of Figure 3.9 recorded after deposition and after photobleaching, respectively.

A new band system with onset at 371.5 nm, unique for C_9^+ deposition, is

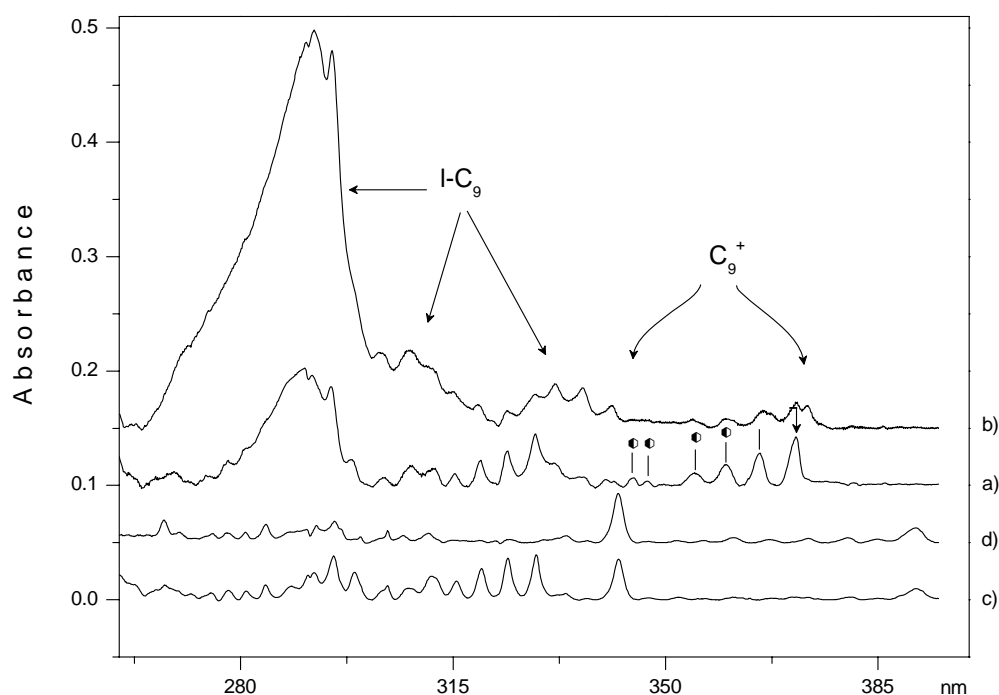


FIGURE 3.9 The UV electronic transition of $l-C_9^+$ (●) observed in a 6 K neon matrix after deposition of C_9^+ generated from $C_{10}Cl_8$ (trace (a)). The known absorption bands of neutral $l-C_9$ are also seen in the spectrum and these become stronger after UV irradiation (trace (b)). The spectra of C_6Cl^+ and C_6Cl (which may also be present) are shown in trace (c) and (d), respectively; C_6Cl^+ was generated from C_6Cl_6 in this case.

apparent in the spectrum shown in trace (a) of Figure 3.9. This diminishes after UV irradiation, and simultaneously the systems of *l*-C₉ in the 275–340 nm range grow in intensity. Therefore, the new band system is assigned to an electronic transition of C₉⁺ (Table 3.3). No theoretical calculations exist on the excited electronic states of this cation. It is assigned to an allowed transition from the $\tilde{X}^2\Pi_g^+$ state ground state of *l*-C₉⁺ based on the behavior of this system with photobleaching, resembling *l*-C₇⁺ more than *c*-C₇⁺. The bands of *c*-C₇⁺ vanish under such conditions. Moreover, *l*-C₇⁺ has the strongest absorption bands in the UV range.

ELECTRONIC ABSORPTION SPECTRA OF C₈⁺

C₈⁺ was also produced by dissociative electron-impact ionization of C₁₀Cl₈. The absorption spectrum in neon shows a more complicated band structure than for C₇⁺ and extends from 900 nm to the UV (Figs. 3.10–3.12 trace (a)). Two strong bands at 890.8 and 308.1 nm dominate, and numerous weaker bands are apparent.

The spectrum recorded after irradiation with UV photons is shown in trace (b) of Figures 3.10–3.12. Three band sets can be distinguished. The strongest at 890.8, 308.1 nm, and several weaker ones in the visible and red spectral range diminish. The weak bands at 639.8 and 564.8 nm and the strong one at 277.2 nm increase in intensity. They were previously assigned to neutral linear C₈ [31, 55]. The well-pronounced band at 791.7 nm, the strong system in the 330–380 nm, and several weaker peaks in the visible to red region vanish.

Two band systems, which decrease or disappear after photobleaching, are due to two structural isomers of C₈⁺. The results of theoretical calculations [22, 56] indicate that linear and cyclic C₈⁺ have comparable thermodynamic stability. It was presumed that the band systems which vanish upon UV irradiation originate from a cyclic C₈⁺ while the ones which diminish from linear C₈⁺. To confirm this mass-selected C₈⁺ ions were trapped in a neon matrix containing 0.25% of N₂O. It is known from gas-phase [18] and matrix experiments [49] that N₂O is less reactive with the cyclic isomer of C_n⁺ than its linear one.

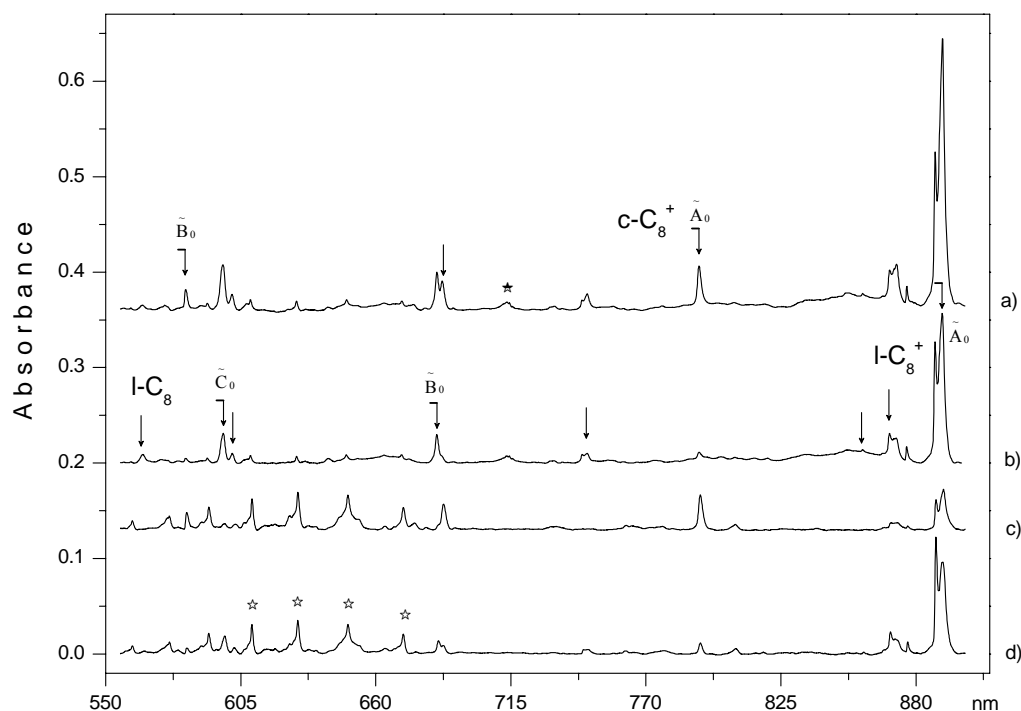


FIGURE 3.10 The electronic absorption spectra recorded in a 6 K neon matrix: (a) after deposition of mass-selected C_8^+ cations produced from $C_{10}Cl_8$; (b) after subsequent UV irradiation; (c) after deposition of C_8^+ in a matrix containing 0.25% of N_2O ; (d) after subsequent UV irradiation. Peaks assigned to $c-C_8^+$ and $l-C_8^+$ are labelled with \downarrow in traces (a) and (b). Letters \tilde{A}_0 , \tilde{B}_0 , \tilde{C}_0 , indicate the positions of the origin band of the respective electronic transition of C_8^+ . The origin band of HC_8H^+ (present as a result of contamination of $C_{10}Cl_8$ with not fully chlorinated naphthalene) is marked with \star in trace (a) and \star in trace (d) indicates the bands of the reaction product of C_8^+ with N_2O .

The electronic absorption spectrum of C_8^+ in the presence of N_2O is shown in trace (c) in Figures 3.10–3.12, and after photobleaching in (d). The matrix was not transparent below 320 nm due to scattering of the UV light. A large difference is apparent in the relative intensity of the band systems exhibiting varied photobleaching

behavior (traces (a) and (c)). This is illustrated in Figure 3.10 for the bands at 890.8 and 791.7 nm being members of two different systems. The intensity of the band at 791.7 nm remains nearly the same as in the experiment without N₂O, while the peak at 890.8 nm (and the others that belong to the same system) becomes much weaker. C₈⁺ ions were generated from the same precursor (C₁₀Cl₈) and the ion current in both experiments was similar.

The results of this indicate that the system with the onset at 791.7 nm originates from the less reactive isomer of C₈⁺, the cyclic one. The transition with the origin at 890.8 nm belongs to linear C₈⁺ (*l*-C₈⁺). The results of the photobleaching experiment (trace (d) in Figs. 3.10–3.12) substantiate this conclusion. The absorption system with the onset at 791.7 nm vanishes and simultaneously the second one with origin at 890.8 nm increases in intensity after irradiation with UV photons.

N₂O plays a dual role in the matrix: as a reactant with C₈⁺ and as an electron scavenger. In the presence of N₂O the neutralization of the cations is suppressed because the electrons liberated from weakly bound anions are captured by other N₂O molecules and the process repeats after absorption of the next UV photon. Therefore cyclic C₈⁺ (*c*-C₈⁺) decays in a different way after UV irradiation. The growth in intensity of the *l*-C₈⁺ bands suggests that this cation is formed as a result of photoinduced ring opening reaction of *c*-C₈⁺ in the matrix doped with N₂O. This reaction is also responsible for a more efficient decay of *c*-C₈⁺ than *l*-C₈⁺ in the photobleaching experiment in a pure neon matrix (trace (b) in Figs. 3.10–3.12).

Apart from the bands which can be assigned to *c*-C₈⁺ or *l*-C₈⁺ in the 550–670 nm region a medium intensity system with a well-resolved vibronic structure is also seen in traces (c) and (d) in Figures 3.10 and 3.11. These absorptions are due to the reaction product of C₈⁺ with O and/or N because it is barely seen in the spectra of C₈⁺ isolated in a pure neon matrix (traces (a) and (b) in Figs. 3.10 and 3.11).

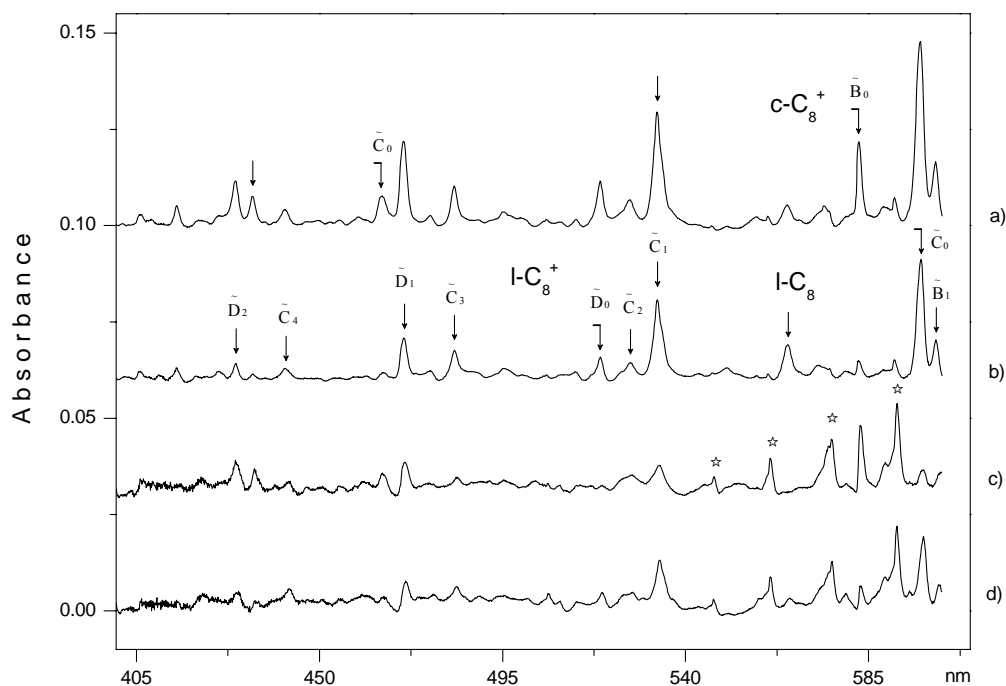


FIGURE 3.11 The visible section of the electronic absorption spectra recorded in a 6 K neon matrix: (a) after deposition of mass-selected C_8^+ ; (b) after subsequent UV irradiation; (c) in a neon matrix containing also 0.25% of N_2O ; (d) after subsequent UV irradiation. The bands assigned to $c-C_8^+$ and $l-C_8^+$ are labeled with arrows in traces (a) and (b). The origin bands of the electronic transitions of C_8^+ are identified by the letters $\tilde{C}_0, \tilde{D}_0, \dots$. The bands of the reaction product of C_8^+ with N_2O are marked with \star .

To exclude the possibility that the band systems assigned to C_8^+ originate from C_5Cl^+ , cations of mass 96 were produced from C_6Cl_6 and codeposited with neon. The UV section of the spectrum relevant to the C_8^+ absorption is seen in trace (e) and after irradiation of the matrix in trace (f) in Figure 3.12. Several bands originate from chlorinated species (C_5Cl, C_5Cl^+), whose electronic spectra have been identified in neon matrices [54].

The results of the above experiments permit an assignment of the bands in Figures 3.10–3.12 to the two isomers of C_8^+ . A more difficult task is to designate the observed bands to specific transitions. Distinct ones of l - C_8^+ with origin bands at 890.8 and 308.1 nm and three of c - C_8^+ 791.7, 382.2 and 336.5 nm can be located. In the visible range the absorptions of C_8^+ are particularly complicated (Fig. 3.11). Three band systems of l - C_8^+ and two of c - C_8^+ are found by taking into account the vibrational spacing and the intensity distribution. The assignment in this spectral region is tentative due to overlap of the electronic transitions and apparent strong vibronic coupling. The capital letters with the subscripts mark the bands that belong to the same electronic transition (e.g. \tilde{C}_0 being the origin to the \tilde{C} state). Five band systems of l - C_8^+ and five of c - C_8^+ have thus been identified (Table 3.3). The numbering and symmetry of the modes are made by reference to the calculated frequencies of C_8^+ and/or C_8 in the ground electronic state [22, 53].

l - C_8^+ and c - C_8^+ (C_{4h} the optimized geometry) have been studied by the MRD-CI method [56]. The two isomers have comparable energies with c - C_8^+ being marginally more stable. The ground electronic states are $\tilde{X}^2\Pi_g$ for l - C_8^+ and \tilde{X}^2B_u for c - C_8^+ . The theory shows that considerable state mixing takes place, leading to many electronic transitions with nonzero oscillator strength. This situation has already been encountered in the analysis of the electronic absorption spectra of C_6^+ and there even the highest-level calculations could not lead to an unambiguous interpretation [36]. It appears that the situation for C_8^+ is just as complex.

The lowest energy dipole-allowed transition of l - C_8^+ (${}^2\Delta_u \leftarrow \tilde{X}^2\Pi_g$) is predicted at 1.69 eV with oscillator strength $f \sim 10^{-3}$, with two further systems to the ${}^2\Pi_u$ and ${}^2\Sigma_u^-$ states with comparable excitation energies. The experiment shows the origin of the first system at 1.39 eV and four other ones are observed between 1.8 and 4.0 eV. There the theory predicts 18 electronic transitions of non-zero intensity. Thus there is no point in trying to make specific symmetry assignment to the identified band systems in the experiment. The most intense transition, ${}^2\Pi_u \leftarrow \tilde{X}^2\Pi_g$, with oscillator strength ($f \sim 0.3$)

predicted at 5.45 eV is two orders of magnitude larger than for the systems observed. Because such a strong band system is not apparent in the measured spectra, it must be located at wavelengths below 250 nm (i.e., >5 eV), a region not accessible in our measurements.

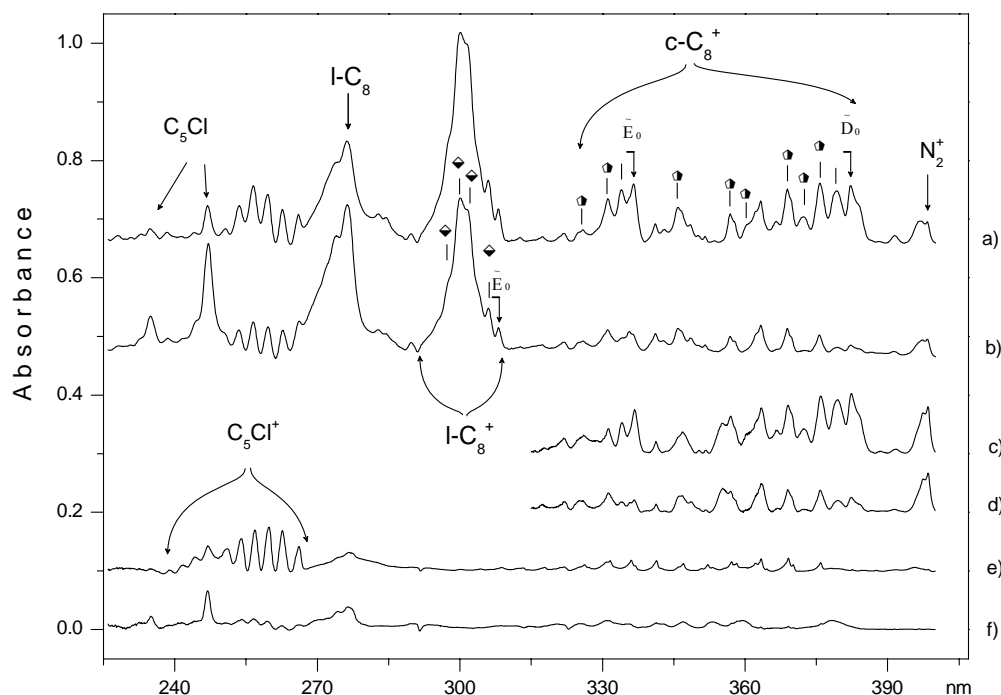


FIGURE 3.12 The UV section of the absorption spectra recorded in a 6 K neon matrix: (a) after deposition of mass-selected C_8^+ ; (b) after subsequent UV irradiation; (c) in a neon matrix containing also 0.25% of N_2O ; (d) after subsequent UV irradiation. The matrix was not transparent below 320 nm due to enhanced UV light scattering. The bands assigned to $c-C_8^+$ and $l-C_8^+$ are labeled with \blacklozenge and \blacklozenge in traces (a) and (b). Absorptions of C_5Cl and C_5Cl^+ are also present due to the low mass resolution (± 2 amu) used. In trace (e) was measured C_5Cl^+ produced from C_6Cl_6 and in (f) after UV irradiation.

In the case of $c\text{-}C_8^+$, the lowest energy transition ($f \sim 10^{-3}$) is expected at 0.77 eV, in the NIR where the waveguide method could not be used. In the region where observations were made, theory predicts two stronger transitions, $2 \ ^2B_g \leftarrow \tilde{X} \ ^2B_u$ at 1.8 eV and $^2E_g \leftarrow \tilde{X} \ ^2B_u$ at 4.2 eV both with $f \sim 10^{-2}$. The first corresponds to the absorption band system with origin at 1.57 eV and the second presumably the one at 3.69 eV. However three further transitions are observed experimentally between these.

TABLE 3.3 Observed bands (± 0.2 nm, λ in air, ν in vacuum) in the electronic absorption spectra of linear and cyclic C_n^+ ($n=7-9$) in a 6 K neon matrix and the suggested assignments. The letters given in the last column, refer to the excited electronic states as shown in Figures 3.5–312.

λ [nm]	ν [cm^{-1}]	Δ [cm^{-1}]	Assignment
770.1	12985	0	$l\text{-}C_7^+$ $\tilde{A} - \tilde{X} \ ^2\Pi_u$ 0_0^0
754.0	13263	278	$2\nu_8(\pi_g)$
332.3	30093	0	$\tilde{B} - \tilde{X}$ 0_0^0 (\tilde{B}_0)
329.7	30331	238	$2\nu_8(\pi_g)$
326.9	30590	497	$\nu_3(\sigma_g)$
321.6	31095	1002	$2\nu_3$
318.8	31368	1275	$2\nu_3 + 2\nu_8$
308.7	32395	0	$\tilde{C} - \tilde{X}$ 0_0^0 (\tilde{C}_0)
303.3	32971	576	$\nu_3(\sigma_g)$
298.5	33503	1108	$2\nu_3$
294.6	33944	1549	$\nu_2(\sigma_g)$
290.4	34431	2036	$\nu_1(\sigma_g)$
286.1	34952	2557	$\nu_1 + \nu_3$
281.6	35509	3114	$\nu_1 + 2\nu_3$
676.3	14786	0	$c\text{-}C_7^+$ $\tilde{A} - \tilde{X} \ ^2B_2$ 0_0^0
597.5	16736	1950	$\nu_1(a')$
593.7	16844	2058	
587.5	17020	2234	
535.1	18687	3901	$2\nu_1(a')$
448.5	22297	0	$\tilde{B} - \tilde{X}$ 0_0^0
429.3	23292	995	$\nu_4(a_1)$

371.5	26918	0	$l-C_9^+$	$\tilde{A}-\tilde{X}$	${}^2\Pi_g$	0_0^0	
365.5	27360	442		$v_4(\sigma_g)$			
360.0	27778	860		$2v_4$			
354.7	28193	1275		$v_3(\sigma_g)$			
347.0	28818	1900		$v_2(\sigma_g)$			
344.6	29019	2101		$v_1(\sigma_g)$			
890.8	11226	0	$l-C_8^+$	$\tilde{A}-\tilde{X}$	${}^2\Pi_g$	0_0^0	(\tilde{A}_0)
872.1	11467	241		$2v_{10}(\pi_g)$			
852.2	11735	509		$v_4(\sigma_g)$			
746.0	13405	2179		$v_1(\sigma_g)$			
684.8	14603	0		$\tilde{B}-\tilde{X}$	${}^2\Pi_g$	0_0^0	(\tilde{B}_0)
601.5	16624	2021		$v_2(\sigma_g)$			(\tilde{B}_1)
597.8	16729	0		$\tilde{C}-\tilde{X}$	${}^2\Pi_g$	0_0^0	(\tilde{C}_0)
532.9	18764	2035		$v_2(\sigma_g)$			(\tilde{C}_1)
526.3	19000	2271					(\tilde{C}_2)
483.1	20699	3970		$2v_2$			(\tilde{C}_3)
441.5	22651	5922		$3v_2$			(\tilde{C}_4)
519.0	19268	0		$\tilde{D}-\tilde{X}$	${}^2\Pi_g$	0_0^0	(\tilde{D}_0)
470.6	21248	1980		$v_2(\sigma_g)$			(\tilde{D}_1)
429.3	23295	4027		$2v_2$			(\tilde{D}_2)
308.1	32453	0		$\tilde{E}-\tilde{X}$	${}^2\Pi_g$	0_0^0	(\tilde{E}_0)
306.0	32675	222		$2v_{10}(\pi_g)$			
301.9	33127	674		$v_4(\sigma_g)$			
299.9	33350	897		v_4+2v_{10}			
297.2	33647	1194		$2v_4$			
791.7	12630	0	$c-C_8^+$	$\tilde{A}-\tilde{X}$	2B_u	0_0^0	(\tilde{A}_0)
687.1	14554	1924		$v_1(a_g)$			
582.6	17164	0		$\tilde{B}-\tilde{X}$	2B_u	0_0^0	(\tilde{B}_0)
530.0	18763	1599		v_1			
465.3	21490	0		$\tilde{C}-\tilde{X}$	2B_u	0_0^0	(\tilde{C}_0)
433.5	23068	1578		v_1			
382.2	26163	0		$\tilde{D}-\tilde{X}$	2B_u	0_0^0	(\tilde{D}_0)
379.3	26367	204		$2v_7(b_g)$			
375.7	26617	454		$2v_{11}(b_u)$			
372.3	26863	700		$v_3(a_g)$			
368.9	27111	948		$v_2(a_g)$			
360.3	27752	1589		v_2+v_3			

356.8	28023	1860	$\nu_1(a_g)$		
345.9	28912	2749	$\nu_1+\nu_2$		
336.5	29718	0	$\tilde{E}-\tilde{X} \ ^2B_u$	0_0^0	(\tilde{E}_0)
333.9	29945	227	$2\nu_7(b_g)$		
331.1	30202	484	$2\nu_{11}(b_u)$		
325.8	30691	973	$\nu_2(a_g)$		

The results of the spectroscopic studies on C_n⁺ n=7-9 reported here and for n=6 in a section before [49] locate the wavelength range and the relative intensities of their electronic absorptions. Additionally the photobleaching experiments permit a comparison with the transition intensities of their neutral counterparts. Thus gas phase spectra of these neutral and cation carbon chains are now required.

BIBLIOGRAPHY

- [1] W. WELTNER JR. and R.J. VAN ZEE. Carbon molecules, ions, and clusters. *Chemical Review*, 89: 1713-1747, 1989
- [2] A. VAN ORDEN and R.J. SAYKALLY. Small carbon clusters: spectroscopy, structure, and energetics. *Chemical Review*, 98: 2313-2357, 1998
- [3] E.A. ROHLFING, D.M. COX, and A. KALDOR. Production and characterization of supersonic carbon cluster beams. *The Journal of Chemical Physics*, 83: 3322-3330, 1984
- [4] J.J. GAUMET, A. WAKISAKA, Y. SHIMIZU, and Y. TAMORI. Energetics for carbon clusters produced directly by laser vaporization of graphite : dependence on laser power and wavelength. *Journal of the Chemical Society, Faraday Transactions*, 89: 1667-1670, 1993
- [5] B.P. POZNIAK and R.C. DUNBAR. Photodissociation studies of C_n^+ at 193 nm ($n=5-19$). *International Journal of Mass Spectrometry and Ion Processes*, 165/166: 299-313, 1997
- [6] C.H. BAE and S.M. PARK. A time-of-flight quadrupole mass spectrometric study of C_n^+ ($n=1-24$) ions produced by laser ablation of a graphite target. *The Journal of Chemical Physics*, 177: 5347-5353, 2002
- [7] M.E. GEUSIC, M.F. JARROLD, T.J. MCLLRATH, R.R. FREEMAN, and W.L. BROWN. Photodissociation of carbon cluster cations. *The Journal of Chemical Physics*, 86: 3862-3869, 1987
- [8] P.P. RADI, M.E. RINCON, M.T. HSU, J. BRODBELT-LUSTIG, P.R. KEMPER, and M.T. BOWERS. Structure, reactivity, and energetics of covalently bound carbon cluster ions, C_5^+ to C_{11}^+ : experiment and theory. *Journal of Physical Chemistry*, 93: 6187-6197, 1989
- [9] M.B. SOWA, P.A. HINTZ, and S.L. ANDERSON. Dissociation energies for carbon cluster ions (C_{2-15}^+): a system where photodissociation is misleading. *The Journal of Chemical Physics*, 95: 4719-4720, 1991
- [10] K.B. SHELIMOV, J.M. HUNTER, and M.F. JARROLD. Small carbon rings: dissociation, isomerization, and a simple model based on strain. *International Journal of Mass Spectrometry and Ion Processes*, 138: 17-31, 1994
- [11] G. VON HELDEN, N.G. GOTTS, W.E. PALKE, and M.T. BOWERS. Structures and energies of small carbon clusters: what experiment and theory have to say about C_8^+ , C_9^+ and C_{10}^+ . *International Journal of Mass Spectrometry and Ion Processes*, 138: 33-47, 1994

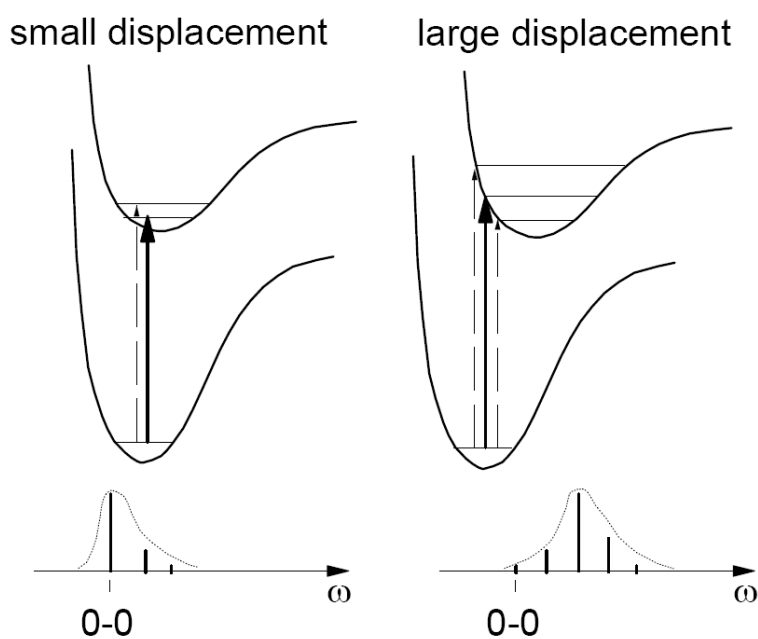
- [12] M.B. SOWA-RESAT, P.A. HINTZ, and S.L. ANDERSON. Dissociation energies for small carbon cluster ions (C_{2-19}^+) measured by collision-induced dissociation. *Journal of Physical Chemistry*, 99: 10736-10741, 1995
- [13] S.W. MCELVANY, B.I. DUNLAP, and A. O'KEEFE. Ion molecule reactions of carbon cluster ions with D_2 and O_2 . *The Journal of Chemical Physics*, 86: 715-725, 1987
- [14] C. LIFSHITZ, T. PERES, and I. AGRANAT. Properties of carbon cluster ions C_n^+ , formed by dissociative ionization. *International Journal of Mass Spectrometry and Ion Processes*, 93: 149-163, 1989
- [15] D.K. BOHME and S. WLODEK. Hydrogenation of carbon-cluster cations with molecular hydrogen: implications for the growth of carbon-cluster molecules. *International Journal of Mass Spectrometry and Ion Processes*, 102: 133-149, 1990
- [16] C. LIFSHITZ and P. SANDLER. Application of thermal kinetics to small carbon ion clusters. *Journal of Physical Chemistry*, 97: 6592-6597, 1993
- [17] B.P. POZNIAK and R.C. DUNBAR. Reactivity of carbon cluster ions with benzene: 4-fold periodicity and possible aromaticity effects. *Journal of the American Chemical Society*, 116: 4113-4114, 1994
- [18] M.B. SOWA-RESAT, J.N. SMOLANOFF, and I.B. GOLDMAN. N-O versus N-N bond activation in reaction of N_2O with carbon cluster ions: experimental and ab initio studies of the effects of geometric and electronic structure. *The Journal of Chemical Physics*, 100: 8784-8794, 1994
- [19] A. FURA, F. TUREČEK, and F.W. MCLAFFERTY. Small carbon clusters (C_n^0 , C_n^+ , C_n^-) from acyclic and cyclic precursors: Neutralization-reionization and theory. *International Journal of Mass Spectrometry*, 217: 81-96, 2002
- [20] K.S. PITZER and E. CLEMENTI. Large molecules in carbon vapor. *Journal of the American Chemical Society*, 81: 4477-4485, 1959
- [21] K. RAGHAVACHARI and J.S. BINKLEY. Structure, stability, and fragmentation of small carbon clusters. *The Journal of Chemical Physics*, 87: 2191-2197, 1987
- [22] M.G. GIUFFREDA, M.S. DELEUZE, and J.-P. FRANÇOIS. Structural, rotational, vibrational, and electronic properties of ionized carbon clusters C_n^+ ($n=4-19$). *Journal of Physical Chemistry A*, 103: 5137-5151, 1999
- [23] J. HAUBRICH, M. MÜHLHÄUSER, and S.D. PEYERIMHOFF. The electronic spectrum of linear and cyclic C_6^+ . A theoretical study. *Physical Chemistry Chemical Physics*, 4: 2891-2896, 2002

- [24] G. ORLOVA and J.D. GODDARD. Is density functional theory free of spatial symmetry breaking? The case of the linear carbon radical cations: C_3^+ , C_5^+ , C_7^+ , and C_9^+ . *Chemical Physics Letters*, 363: 486-491, 2002
- [25] J.P. MAIER and M. RÖSSLEIN. The $B^4\Sigma_v^- - X^4\Sigma_g^-$ electronic transition of C_2^+ . *The Journal of Chemical Physics*, 88: 4614-4620, 1988
- [26] Z. GASZYNA, L. ANDREWS, and P.N. SCHATZ. Near-infrared absorption spectra of C_{60} radical cations and anions prepared simultaneously in solid argon. *Journal of Physical Chemistry*, 96: 1525-1527, 1992
- [27] J. FULARA, M. JAKOBI, and J.P. MAIER. Electronic and infrared spectra of C_{60}^+ and C_{60}^- in neon and argon matrices. *Chemical Physics Letters*, 211: 227-234, 1993
- [28] J. FULARA, M. JAKOBI, and J.P. MAIER. Electronic spectra of the C_{70} molecule and C_{70}^+ , C_{70}^- ions in neon matrices. *Chemical Physics Letters*, 206: 203-209, 1993
- [29] P. FREIVOGEL, J. FULARA, D. LESSEN, D. FORNEY, and J.P. MAIER. Absorption spectra of conjugated hydrocarbon cation chains in neon matrices. *Chemical Physics*, 189: 335-341, 1994
- [30] D. FORNEY, J. FULARA, P. FREIVOGEL, M. JAKOBI, D. LESSEN, and J.P. MAIER. Electronic absorption spectra of linear carbon chains in neon matrices. I. C_6^- , C_6 , and C_6H . *The Journal of Chemical Physics*, 103: 48-53, 1995
- [31] M. GRUTTER, M. WYSS, E. RIAPLOV, and J.P. MAIER. Electronic absorption spectra of linear C_6 , C_8 and cyclic C_{10} , C_{12} in neon matrices. *The Journal of Chemical Physics*, 111: 7397-7401, 1999
- [32] Z. CAO and S.D. PEYERIMHOFF. MRD-CI characterization of electronic spectra of isoelectronic species C_6^- , NC_4N^+ , and CNC_3N^+ . *Journal of Physical Chemistry*, 105: 627-631, 2001
- [33] M. HANRATH, S.D. PEYERIMHOFF, and F. GREIN. Theoretical studies on the electronic spectrum of linear C_6 . *Chemical Physics*, 249: 121-128, 1999
- [34] M.G. GIUFFREDA, *PhD thesis*. 2001, University of Limburg: Belgium.
- [35] F. GREIN, J. FRANZ, M. HANRATH, and S.D. PEYERIMHOFF. Theoretical studies on the electronic spectra of cyclic C_6 , in D_{3h} and D_{6h} symmetries. *Chemical Physics*, 263: 55-60, 2001
- [36] C. GILLERY, P. ROSMUS, H.-J. WERNER, H. STOLL, and J.P. MAIER. A theoretical study of the electronically excited states in linear and cyclic C_6^+ . *Molecular Physics*, 102: 2227-2236, 2004

- [37] A.M. SMITH, J. AGREITER, M. HÄRTLE, C. ENGEL, and V.E. BONDYBEY. Rare gas matrix studies of absorption and fluorescence of reactive intermediates formed in discharges through acetylene. *Chemical Physics*, 189: 315-334, 1994
- [38] J.D. PRESILLA-MÁRQUEZ, J.A. SHEEHY, J.D. MILLS, P.G. CARRICK, and C.W. LARSON. Vibrational spectra of cyclic C_6 in solid argon. *Chemical Physics Letters*, 274: 439-444, 1997
- [39] K.W. HINKLE, J.J. KEADY, and P.F. BERNATH. Detection of C_3 in the circumstellar shell of IRC+10216. *Science*, 241: 1319-1322, 1988
- [40] P.F. BERNATH, K.W. HINKLE, and J.J. KEADY. Detection of C_5 in the circumstellar shell of IRC+10216. *Science*, 244: 562-564, 1989
- [41] J.P. MAIER, N.M. LAKIN, G.A.H. WALKER, and D.A. BOHLENDER. Detection of C_3 in Diffuse Interstellar Clouds. *The Astrophysical Journal*, 553: 267-273, 2001
- [42] A.E. DOUGLAS. Origin of diffuse interstellar lines. *Nature*, 269: 130-132, 1977
- [43] J.P. MAIER, G.A.H. WALKER, and D.A. BOHLENDER. Limits to Interstellar C_4 and C_5 toward ζ Ophiuchi. *The Astrophysical Journal*, 566: 332-335, 2002
- [44] J.P. MAIER, G.A.H. WALKER, and D.A. BOHLENDER. On the possible role of carbon chains as carriers of diffuse interstellar bands. *The Astrophysical Journal*, 602: 286-290, 2004
- [45] G. VON HELDEN, M.-T. HSU, P.R. KEMPER, and M.T. BOWERS. Structures of carbon cluster ions from 3 to 60 atoms: Linears to rings to fullerenes. *The Journal of Chemical Physics*, 95: 3835-3837, 1991
- [46] G. VON HELDEN, N.G. GOTTS, and M.T. BOWERS. C_7^+ is cyclic: experimental evidence. *Chemical Physics Letters*, 212: 241-246, 1993
- [47] G. VON HELDEN, W.E. PALKE, and M.T. BOWERS. The lowest energy structures of C_7^+ , C_7 and C_7^- . An ab initio study. *Chemical Physics Letters*, 212: 247-252, 1993
- [48] C.G. TARSITANO, C.F. NEESE, and T. OKA. High-resolution spectroscopy of the $2^2\Pi_u \leftarrow X^4\Sigma_g^-$ -forbidden transitions of C_2^+ . *The Journal of Chemical Physics*, 121: 6290-6297, 2004
- [49] J. FULARA, E. RIAPLOV, A. BATALOV, I. SHNITKO, and J.P. MAIER. Electronic and infrared absorption spectra of linear and cyclic C_6^+ in a neon matrix. *The Journal of Chemical Physics*, 120: 7520-7525, 2004

- [50] D. FORNEY, M. GRUTTER, P. FREIVOGEL, and J.P. MAIER. Electronic absorption spectra of carbon chain anions C_{2n+1}^- ($n=2-5$) in neon matrices. *Journal of Physical Chemistry A*, 101: 5292-5295, 1997
- [51] J. VAN WIJNGAARDEN, I. SHNITKO, A. BATALOV, P. KOLEK, J. FULARA, and J.P. MAIER. Electronic absorption spectra of C_3Cl , C_4Cl , and their ions in neon matrices. *Journal of Physical Chemistry A*, 109: 5553-5559,
- [52] C. GILLERY, *PhD Thesis*. 2005, University of Marne la Vallée: France.
- [53] J.M.L. MARTIN, J. EL-YAZAL, and J.-P. FRANÇOIS. Structure and vibrational spectra of carbon clusters C_n ($n=2-10, 12, 14, 16, 18$) using density functional theory including exact exchange contributions. *Chemical Physics Letters*, 242: 570-579, 1995
- [54] J. VAN WIJNGAARDEN, A. BATALOV, I. SHNITKO, J. FULARA, and J.P. MAIER. Electronic absorption spectra of C_nCl radicals ($n=5, 6$) and their cations in neon matrices. *Journal of Physical Chemistry A*, 108: 4219-4223, 2004
- [55] P. FREIVOGEL, J. FULARA, M. JAKOBI, D. FORNEY, and J.P. MAIER. Electronic absorption spectra of linear carbon chains in neon matrices. II. C_{2n}^+ , C_{2n} , and $C_{2n}H$. *The Journal of Chemical Physics*, 103: 54-59, 1995
- [56] J. HAUBRICH, M. MÜHLHÄUSER, and S.D. PEYERIMHOFF. A comparative MRD-CI study of the electronic spectrum of linear and cyclic C_8^+ clusters. *Journal of Molecular Spectroscopy*, 228: 31-37, 2004
- [57] M. MÜHLHÄUSER, G.E. FROUDAKIS, and S.D. PEYERIMHOFF. MRD-CI study of the electronic spectrum of linear C_9 . *Chemical Physics Letters*, 336: 171-176, 2001

CHAPTER 4. CARBON CHAINS TERMINATED WITH A HYDROGEN ATOM



This chapter is a slightly modified form of the article published in:
Shnitko et. al., Journal of Physical Chemistry A, 110: 2885–2889, 2006

LINEAR C_6H^+ AND C_8H^+

INTRODUCTION

C_nH are the second longest carbon chains after cyanopolyynes detected in the interstellar medium [1]. These radicals were observed both in dark molecular clouds [2] and in the envelopes of carbon rich stars [3]. Despite the higher reactivity of the open shell C_nH species, their abundance in these environments is only slightly lower than the same sized closed shell $H(CC)_nCN$ molecules.

The C_nH radicals have been extensively studied in the microwave and visible spectral ranges. Chains up to $n \leq 14$ were generated in an electrical discharge through a mixture of diacetylene with neon and identified using rotational spectroscopy [4, 5]. Electronic absorption spectra of $C_{2n}H$, $3 \leq n \leq 8$, have been measured in neon matrices [6] and in the gas phase up to $n=6$ using cavity ring down methods [7-9]. The medium size chains $n=2-4$ have also been studied using theoretical methods [10-13]. These reveal two close lying $^2\Sigma$ and $^2\Pi$ electronic states, the latter being the lowest for $n \geq 3$.

In contrast to the C_nH neutral radicals, little is known about their molecular ions. The reaction of medium size C_nH^+ ($n=2-6$) with CO was studied using mass spectrometry [14]. However, only the smallest member of this group CH^+ has been characterized spectroscopically [15], which was also detected long ago in diffuse interstellar clouds by its A $^1\Pi-X^1\Sigma^+$ electronic transition [16]. In view of the significant abundance of the neutral counterparts in the interstellar medium one would also expect that C_nH^+ should be present. Therefore their spectroscopic characterization is a prerequisite. This thesis is the first experimental report on the electronic spectra of linear C_6H^+ and C_8H^+ that have been observed in 6 K neon matrices. No theoretical study on the electronically excited states for these two cations has been reported.

EXPERIMENTAL

The measurements were carried out using mass selection combined with matrix absorption spectroscopy [17]. The ions were produced in a hot cathode discharge source (Fig. 2.8) and accelerated to about 50 eV. The C_nH^+ ions were mass selected with a

quadrupole and deposited with an excess of neon on a rhodium-coated sapphire plate at 6 K. The resolution of the mass filter was ± 1 amu to obtain a sufficient current. The matrix was grown for 2 hours, after which the absorption spectrum was measured in the 220–1100 nm region using a waveguide technique [18] with a xenon arc or halogen lamp light source, a monochromator, and a photomultiplier or silicon diode detector. To neutralize charged molecules, the surface of the matrix was irradiated with a medium pressure-mercury lamp after deposition.

THEORY

The influence of atomic orbital basis sets, active orbitals in CASSCF approach, and reference wave functions for internally contracted MRCI calculations on the precision for electronic excitation energy and transition moment was previously investigated in an extensive theoretical study on C_6^+ [19] (discussed in the previous chapter). Because most of the excited states have strongly multiconfigurational character, accurate calculations of these properties in cumulenyl carbon chains remain a difficult problem.

On the basis of the experience with C_6^+ , the following computational scheme was adapted for C_6H^+ . The geometry optimizations of several states were performed with the aug-cc-pVTZ basis set of Dunning [20, 21] and the CASSCF [22] method. The $5-8\sigma$, $1-4\pi$ orbitals were active for the linear structure and $5-11a_1$, $2-4b_1$, $4-7b_2$, $1-2a_2$ for the cyclic one. Excitations from lower orbitals were not considered. The following equilibrium geometries were calculated for the linear structure of C_6H^+ (all distances in Å for R_i $i=1,6$, Figure 4.1): $X^3\Sigma^-$ 1.299, 1.280, 1.263, 1.297, 1.212, and 1.082; $2^3\Sigma^-$ 1.309, 1.290, 1.267, 1.259, 1.283, and 1.083; $1^3\Pi$ 1.234, 1.314, 1.223, 1.339, 1.192, and 1.079. In the case of the C_{2v} cyclic structure (R_i $i=1,4$ and angles in degree for α_i $i=1,3$, cf. Figure 4.1): X^1A_1 1.067, 1.371, 1.287, 1.313, 131.8, 142.7, and 94.4; 1^1B_1 1.071, 1.446, 1.292, 1.307, 123.2, 122.4, and 115.0; 1^1B_2 1.068, 1.358, 1.301, 1.358, 135.5, 142.2, and 118.8. The ground-state geometries of the linear and cyclic ground state of C_6H^+ from an earlier study [22] are in overall agreement with the present results, though some bond distances differ by up to 0.048 Å.

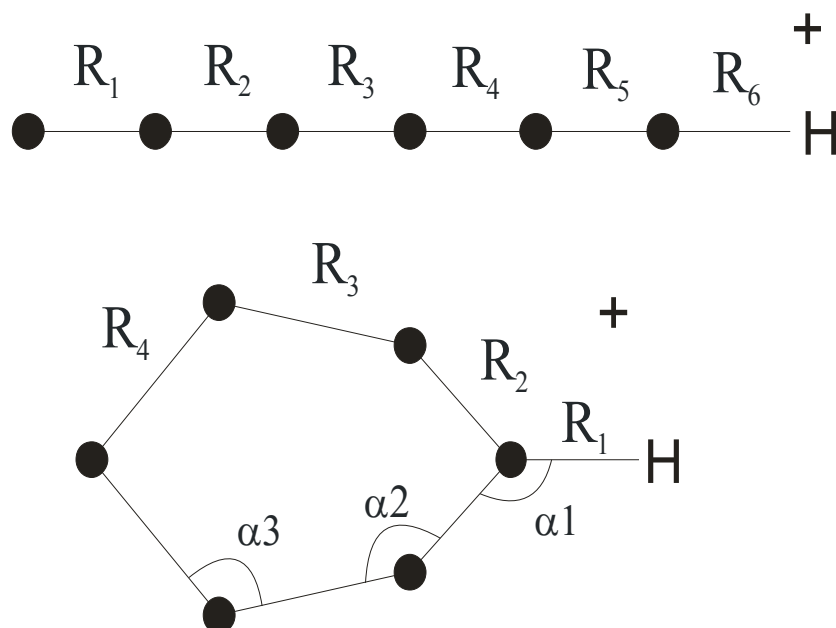


FIGURE 4.1 Definition of the coordinates for linear and cyclic C_6H^+ . The calculated distances and angles for the ground and excited states are given in the text.

The vertical and adiabatic excitation energies were all calculated in the C_{2v} point group. Four states in each irreducible representation were averaged together in the CASSCF calculations comprising about 4.3×10^6 CSF's (triplets) or 2.3×10^6 CSF's (singlets) with an active space $5-9\sigma$, $1-5\pi$ molecular orbitals for the linear structure. An active space consisting of $5-11a_1$, $1-4b_1$, $4-7b_2$ and $1-2a_2$ molecular orbitals was used in the case of the cyclic structure. In the calculations of the adiabatic excitation energies for $l-C_6H^+$, the lowest σ orbital from the space defined above was closed; for $c-C_6H^+$ the active space remained unchanged. All calculations were performed with the MOLPRO code [23]. More comprehensive information can be found in ref [24].

RESULTS AND DISCUSSION

ELECTRONIC SPECTRUM OF C_6H^+

The electronic absorption spectrum recorded after deposition of mass-selected C_6H^+ in a 6 K neon matrix is shown in trace (a) of Figure 4.2. The cations were generated in the source from pentachlorobenzene, C_6Cl_5H , as the precursor. A photobleaching procedure was used to distinguish the absorption bands of cations from those of neutral species. In this the matrix was irradiated with UV photons ($\lambda \geq 305$ nm) and the spectrum was recorded anew, leading to trace (b). Most of the bands seen in trace (a) increase in intensity after irradiation except for the peaks at 515.8 nm and that of HC_6H^+ at 604 nm which both diminish. The bands which increase originate from known species, namely, linear C_6 , C_6H and C_6^- [25]. To facilitate the identification of these bands, the previously obtained electronic spectra of $l-C_6$ and $l-C_6^-$ are shown in traces (c) and (d).

The origin band of the $A^2\Pi_g-X^2\Pi_u$ band system of triacetylene cation, HC_6H^+ , is seen weakly in trace (a) as a result of the limited mass resolution (± 1 amu) and the contamination of the C_6Cl_5H sample with chlorobenzenes containing more than one hydrogen atom. $l-C_6$ and C_3 (at 405 nm) are present in the matrix as a result of collisionally induced fragmentation of the C_6H^+ cations during deposition. Another reason for the presence of $l-C_6$ can be the charge neutralization of C_6^+ , which is co-deposited with C_6H^+ due to the restricted mass resolution. However, the known absorption [26] of C_6^+ was not detected.

After irradiation of the matrix, the origin band of HC_6H^+ and the new distinct band at 515.8 nm diminish while the $l-C_6H$ bands grow in intensity (trace (b) of Fig. 4.2). The absorptions of $l-C_6$ increase only slightly and those of $l-C_6^-$ appear. The electrons that are detached from weakly bound anions by UV photons migrate in the matrix and, on meeting cations, neutralize them. This is the reason the $l-C_6H$ bands become stronger. The neutralization of $l-C_6H^+$ with electrons is an exoenergetic process and some excited $l-C_6H$ molecules undergo a fragmentation, being responsible for the slight growth in intensity of the $l-C_6$ bands upon irradiation. $l-C_6$ does not appear to be

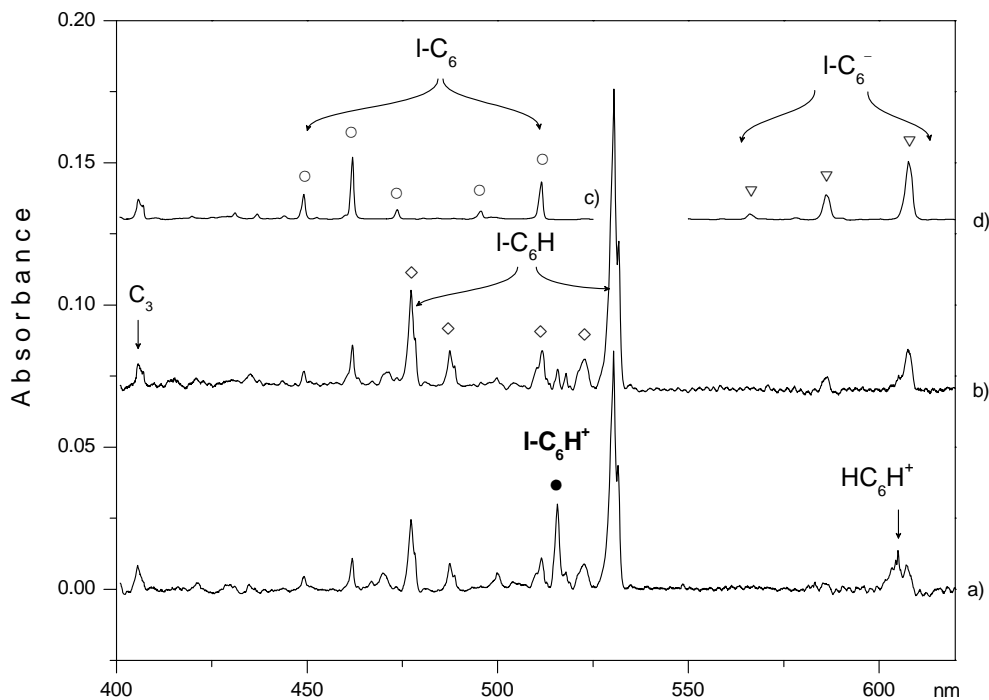


FIGURE 4.2 The electronic transition of $l-C_6H^+$ (●) observed in a 6 K neon matrix after deposition of C_6H^+ produced from C_6Cl_3H (trace (a)) and subsequent UV irradiation (trace (b)). The electronic absorption bands of $l-C_6H$ (◇) are also present as a result of the neutralization and capture of electrons by C_6H^+ . To facilitate the identification of the bands in trace (b), the previously obtained electronic spectra of $l-C_6$ and $l-C_6^-$ are shown in traces (c) and (d).

produced by neutralization of C_6^+ because its absorption was not detected. Some of the liberated electrons are captured by molecules with a high electron affinity, e.g., $l-C_6$. This process leads to the appearance of the C_6^- bands (trace (b)).

A small amount of N_2O (0.25%) was added to neon to improve the trapping efficiency of the C_6H^+ cations during deposition. The resulting spectrum is shown in trace (a) of Figure 4.3. A large difference in the intensity of the bands is evident on comparing traces (a) of Figures 4.2 and 4.3, though the C_6H^+ deposition ion current was comparable. The absorptions of neutral species are nearly absent in trace (a) of Figure 4.3 whereas the 515.8 nm peak and the origin of HC_6H^+ become much stronger. These differences point to a cationic carrier of the 515.8 nm band. The strengthening of the

cationic absorptions and the weakening of the neutrals' ones was previously observed in the study of the electronic absorption spectra of C_n^+ ($n=6-9$) trapped in a neon matrix containing N_2O [26, 27]. The latter is a scavenger for electrons which are released from

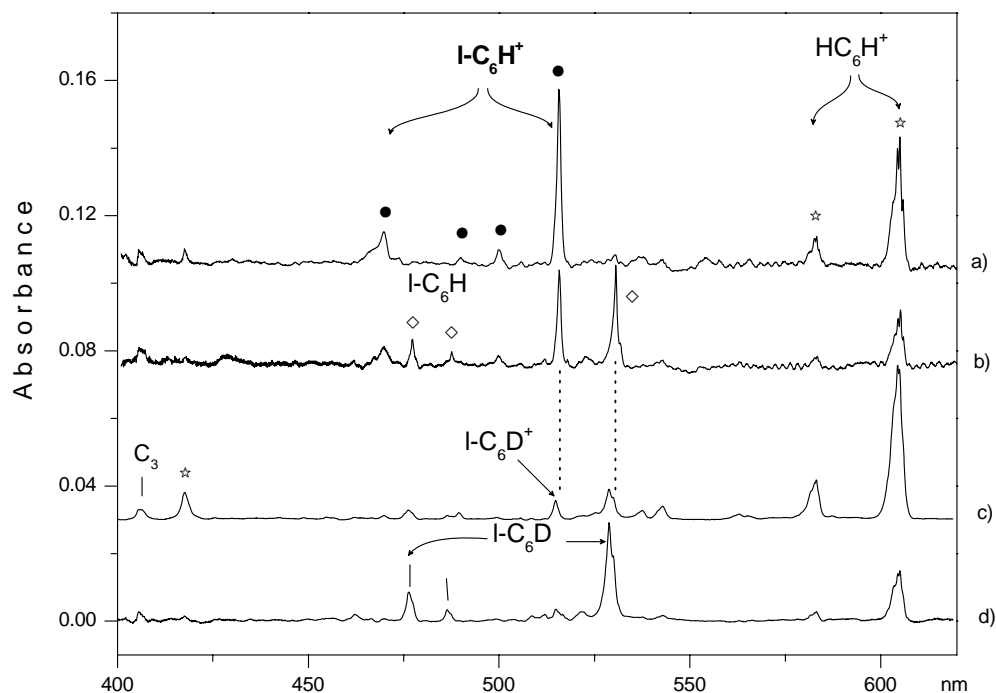


FIGURE 4.3 The electronic transition of $l-C_6H^+$ (●) observed in the visible region after deposition of mass-selected C_6H^+ in a matrix containing 0.25% N_2O (trace (a)). Trace (b) shows the spectrum recorded after UV irradiation; the bands which grow in intensity originate from $l-C_6H$ (◊). Apart from $l-C_6H^+$, the electronic absorption bands of $C_6H_2^+$ (☆) are also present in trace (a) due to the low mass resolution (± 1 amu) used. C_6D^+ was produced from dideuterodiacetylene. The spectrum recorded after deposition is shown in trace (c) and after subsequent UV irradiation in trace (d).

metal surfaces by collisions with cations being deposited. As a result the density of free electrons in the matrix is reduced and the neutralization efficiency of deposited cations suppressed. Therefore neutral species ($l-C_6H$) are nearly absent in the matrix containing N_2O .

The matrix was then irradiated with $\lambda \geq 305$ nm photons leading to trace (b) of Figure 4.3. The bands of HC_6H^+ and the system with the onset at 515.8 nm diminish, while the absorption of neutral $l-C_6H$ appears. One can therefore conclude that the 515.8 nm band system originates from C_6H^+ . The oscillator strength of this electronic transition of C_6H^+ is estimated to be comparable to that of the $2^2\Pi-X^2\Pi$ electronic transition of $l-C_6H$, calculated to be ~ 0.02 [12, 13].

Further experiments have been carried out in which linear and cyclic C_6^+ were generated from perchlorobenzene, mass selected, and trapped in a neon matrix containing 1% of H_2 . The 515.8 nm absorption band was detectable. It is known from gas-phase [28, 29] and matrix experiments [26] that $l-C_6^+$ is more reactive than its cyclic isomer. Therefore one can expect that linear C_6H^+ was formed in the matrix by the reaction of $l-C_6^+$ with H_2 . The above studies on C_6^+ show that the structure of the cations depends on the precursor used for their generation. The linear and cyclic isomers of C_6^+ were formed from perchlorobenzene, whereas solely the cyclic one from perbromobenzene [26].

In the next experiment cations of mass 74 were generated from dideuterodiacetylene precursor. The spectrum recorded after deposition is shown in trace (c) and after subsequent UV irradiation in trace (d) of Figure 4.3. The $A^2\Pi_g-X^2\Pi_u$ system of HC_6H^+ and the band of C_6D^+ around 515 nm are observed, both having the same mass. Trace (c) is scaled by factor of 0.2 to obtain the same intensity of the origin band of HC_6H^+ (\star in traces (a),(c)) for a better visual comparison.

After $\lambda \geq 305$ nm irradiation the bands of the cations diminish and the $l-C_6D$ system grows in intensity (trace (d) of Fig. 4.3). Trace (d) was normalized to the intensity of the origin band of $l-C_6D$ for comparison with plot (b). The origin bands of $l-C_6D$ and C_6D^+ are shifted to the blue by 1.6 and 1 nm with respect to the $l-C_6H$ and C_6H^+ species, respectively. The $l-C_6D/l-C_6H$ gas-phase shift is 1.424 nm [8].

These results indicate that only one isomer of C₆H(D)⁺ with the band origin around 515 nm was observed in a neon matrix irrespective of the precursor (C₆Cl₅H or DC₄D) or of the production method (electron impact ionization or the reaction of *l*-C₆⁺ with H₂). This suggests that it is the linear C₆H(D)⁺. The electronic absorption spectrum of this cation is simple and comprises the 515 nm origin and three weaker vibronic bands. Their assignment in Table 4.1 is made by comparison to the calculated vibrational frequencies of *l*-C₆H [13].

l-C₆H⁺ is isoelectronic with *l*-C₆. The ground-state electronic configuration of *l*-C₆ is ...1π_u⁴ 6σ_u² 7σ_g² 1π_g⁴ 2π_u², which leads to a X ³Σ_g⁻ electronic ground state [30]. *l*-C₆H⁺ has a lower symmetry with configuration ...1π⁴ 12σ² 2π⁴ 13σ² 3π². The hydrogen atom in this cation will mostly affect the energy of the σ orbitals. The main difference in the electronic spectra of *l*-C₆ and *l*-C₆H⁺ will be caused by a promotion of electron from the 12σ² and 13σ² orbital. The strongest (1) ³Σ_u⁻ ← X ³Σ_g⁻ electronic transition of *l*-C₆ with the onset at 511 nm [25] results from the 1π_g → 2π_u excitation. One can also expect that the corresponding 2π → 3π promotion will be responsible for the electronic transition of *l*-C₆H⁺ in the similar spectral range. Indeed, the origin band of the *l*-C₆H⁺ (515.8 nm) absorption system lies close to the (1) ³Σ_u⁻ ← X ³Σ_g⁻ electronic transition of *l*-C₆ (origin at 511 nm).

THEORETICAL PREDICTION FOR C₆H⁺

Previously it was shown that for the linear structures there is a low lying ³Π state close to X ³Σ⁻ in C₆ or ²Σ⁺ (13σ → 3π) in C₆H [13]. This state has been detected experimentally for C₆H 0.18 eV above the X ²Π state [31]. In the present CASSCF calculations on C₆H⁺ the two states lie even closer (Fig. 4.4); at equilibrium geometries the ³Π state is predicted to lie lower than ³Σ⁻ by 0.04 eV. It is calculated that due to strong changes of the π orbital system the transition ²Π ← ¹Π with T_v = 2.36 eV has a large transition moment of 3.2 debye. To obtain a more reliable estimate on the relative positions of the ground state, RCCSD(T)/cc-pVQZ calculations were performed at the optimized geometries of the lowest ³Π, ³Σ⁻, and ¹A₁ states, in which all 24 valence

electrons were correlated. The cyclic X^1A_1 state is found to be 0.51 eV more stable than the linear $X^3\Sigma^-$, and 0.84 eV more stable than the $^3\Pi$ state. The electronic ground state has $^3\Sigma^-$ symmetry in the linear geometry. At higher energies the multidimensional potential energy surfaces of both triplets can exhibit avoided crossings and vibronic couplings.

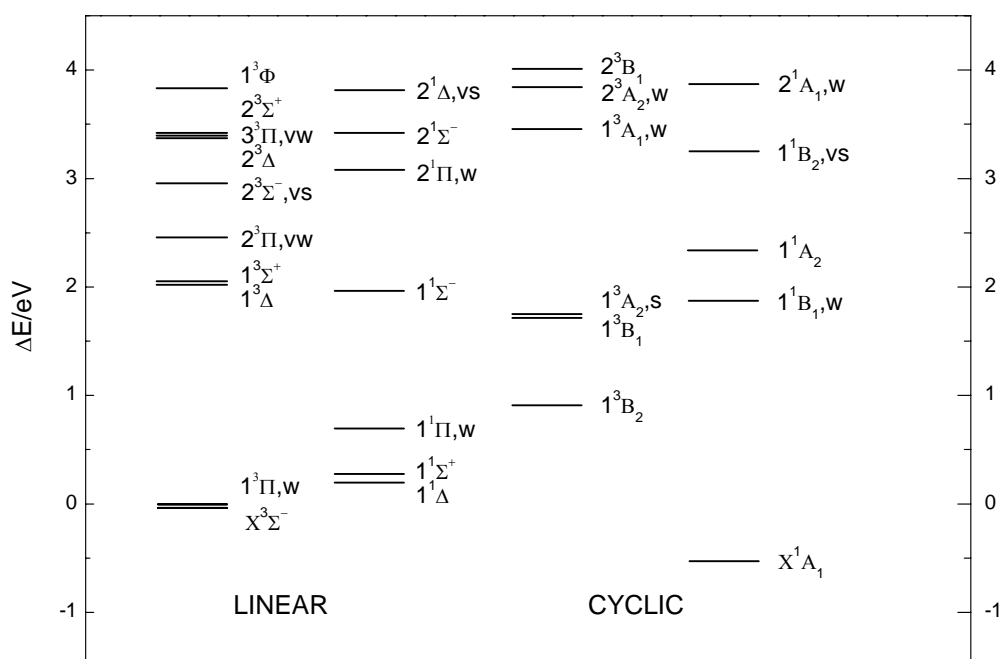


FIGURE 4.4 CASSCF vertical electronic excitation energies for linear and cyclic C_6H^+ relative to the RCCSD(T) energy of the $X^3\Sigma^-$ (linear) state at its equilibrium geometry. The strengths of allowed transition are indicated by vw=very weak, w=weak, s=strong, and vs=very strong.

The pattern of CASSCF vertical excitation energies for the triplets and singlets of the linear and cyclic structure of C_6H^+ is shown in Figure 4.4. These are plotted relative to the RCCSD(T) energies for equilibrium geometries of the $X^3\Sigma^-$ or X^1A_1

states. The strongest transition in the linear triplets is ${}^3\Sigma^- \leftarrow X\ {}^3\Sigma^-$ calculated at 2.92 eV (adiabatic 2.77 eV) with a moment of 1.48 debye. This energy difference is higher than the experimental value of 2.4 eV due to the missing electron correlation contribution in the present ansatz. The ${}^3\Pi \leftarrow X\ {}^3\Sigma^-$ transition at 2.39 eV vertical excitation (adiabatic 2.24 eV) has only a small moment of 0.02 debye and thus cannot be responsible for the rather intense feature detected experimentally. Similarly, the ${}^1B_1 \leftarrow X\ {}^1A_1$ transition at 2.39 eV (adiabatic 1.82 eV) has a smaller moment of 0.43 debye. Hence the pattern of allowed transitions advocates the assignment of the band at 515.8 nm to the linear isomer. The schemes of the electronic states of linear C_6 and its protonated form C_6H^+ are analogous, although the ordering differs for higher energy states. The largest change in the ground states is the strong distortion of the C_6H^+ cyclic form relative to the neutral C_6 ring.

ELECTRONIC SPECTRUM OF C_8H^+

C_8H^+ was produced in the ion source from a mixture of diacetylene with helium (1:3). The known absorptions of linear C_8H with the onset at 631 nm [6] and a weak band system of tetraacetylene cation, HC_8H^+ , with the origin at 714 nm [17] are present in trace (a) (Fig. 4.5). The l - C_8H bands grow in intensity while the peaks of the HC_8H^+ diminish substantially upon UV irradiation (trace (b)).

Apart from l - C_8H and HC_8H^+ , a new band system with the origin at 628.4 nm is discernible in trace (a). This absorption diminishes upon UV irradiation similarly as the ones of HC_8H^+ (trace (b)). The new band system partially overlaps with the absorption of l - C_8H . Trace (c) shows the spectrum obtained after subtraction bands of l - C_8H . Two absorptions with origin at 628.4 nm and one at 564.5 nm (*i.e.*, 1802 cm^{-1} to higher energy) dominate in this spectrum. These bands have a peculiar intensity distribution because they are equally strong but no overtone transition around 512 nm ($2 \times 1802\text{ cm}^{-1}$) could be detected.

To check whether these bands belong to one or two isomers of C_8H^+ , an additional experiment was carried out. C_8H^+ was trapped in a neon matrix containing N_2O (0.25%) as the electron scavenger and reactant of C_8H^+ . Trace (d) (Fig. 4.5) shows

the absorptions after deposition and trace (e) after irradiation. No absorptions of l - C_8H are present in trace (d), which indicate that the neutralization of C_8H^+ was completely suppressed. The bands at 628.4 and 564.5 nm are clearly seen in trace (d) and they diminish upon irradiation (trace (e)). Although these peaks are weaker than in trace (a), their relative intensity remains the same as in the experiment without scavenger. These results suggest that the 628.4 and 564.5 nm bands originate from the same isomer of C_8H^+ . Apart from the bands of C_8H^+ , a strong absorption of HC_8H^+ is also observed in

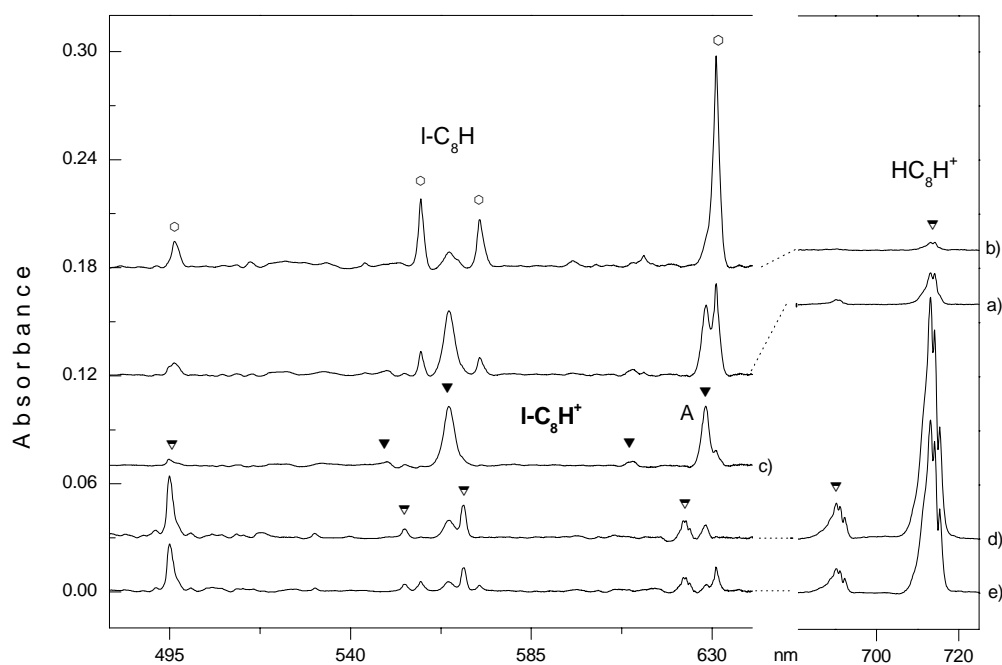


FIGURE 4.5 The electronic transition of l - C_8H^+ (\blacktriangledown) observed after deposition of mass-selected C_8H^+ in a 6 K neon matrix from diacetylene (trace (a)). Trace (b) shows the spectrum recorded after UV irradiation; the bands which grow in intensity originate from l - C_8H (\circ). Trace (c) shows the spectrum obtained after subtracting bands of l - C_8H . Trace (d) shows the absorptions after deposition of C_8H^+ in a neon matrix containing N_2O (0.25%), and trace (e) was obtained after irradiation. \blacktriangledown indicates the bands of l - $C_8H_2^+$.

trace (d). The intensity of the HC_8H^+ absorption is much higher than in trace (a), due to a lower mass resolution used in this experiment and/or consumption of C_8H^+ in the reaction with N_2O in the matrix. The linear isomer of C_8H^+ is expected to be more reactive than the cyclic one.

The origin band of C_8H^+ (at 628.4 nm) lies very close to that of the $(1)^3\Sigma_u^- - X^3\Sigma_g^-$ electronic transition of the isoelectronic $l-C_8$, at 639.8 nm[6]. Because C_8H^+ was produced from the linear precursor (HC_4H) one can expect that the linear geometry will be preserved in the C_8H^+ cation. Thus it is concluded that the new band system with the onset at 628.4 nm is due to the $^3\Sigma^- - X^3\Sigma^-$ electronic transition of $l-C_8H^+$. The oscillator strength of this transition is about two times smaller than for $l-C_8H$ with the onset at 631 nm [6].

The wavelengths of the observed absorption bands in the electronic spectrum of $l-C_8H^+$ are given in Table 4.1. The vibrational assignment is based on the theoretical calculations for $l-C_8$ [32]. The calculated ground state frequencies of $l-C_8$ and those observed in the excited electronic state of $l-C_8H^+$ are in reasonable accord. The numbering of the modes differs: $l-C_8H^+$ has three more vibrations than $l-C_8$ (one of σ symmetry (ν_1) around 3000 cm^{-1} and two doubly degenerate π modes). The band at 564.5 nm corresponds to the ν_5 vibrational excitation in the $^3\Sigma^-$ electronic state of $l-C_8H^+$. Two weaker bands (trace (c)) correspond to the ν_8 vibration and the combination with the ν_5 mode.

Traces (a) of Figures 4.5 and 4.6 were recorded in the same experiment. Trace (b) represents another experiment in which the ion current was lower, and the bands are therefore weaker. They vanish after UV irradiation (trace (c)). Trace (d) was recorded after deposition of C_8H^+ with an admixture of N_2O . The bands seen in trace (d) are very weak similar to those of $l-C_8H^+$ shown in visible part (Fig. 4.5). None of the absorption peaks in trace (d) of Figure 4.6 originate from HC_8H^+ because the visible bands of this cation are much stronger than in trace (a). Thus the rich absorption system seen in trace (a) of Figure 4.6 is due to $l-C_8H^+$.

One can distinguish four electronic transitions of $l-C_8H^+$ in the UV spectral range (trace (a) of Fig. 4.6). The clear origin bands of these are at 379.3, 327.8, 314.1,

and 267.1 nm. and they are marked with capital letters B–E in Figure 4.6. The strongest E–X ${}^3\Sigma^-$ $l-C_8H^+$ lies close to the (2) ${}^3\Sigma_u^-$ –X ${}^3\Sigma_g^-$ transition of the isoelectronic $l-C_8$ molecule (at 277.2 nm) [30]. A weaker ${}^3\Pi_u$ –X ${}^3\Sigma_g^-$ system of $l-C_8$ lies at 303.6 nm. $l-C_8H^+$ has one, or two, partially overlapping electronic transitions (C and D) in this spectral region.

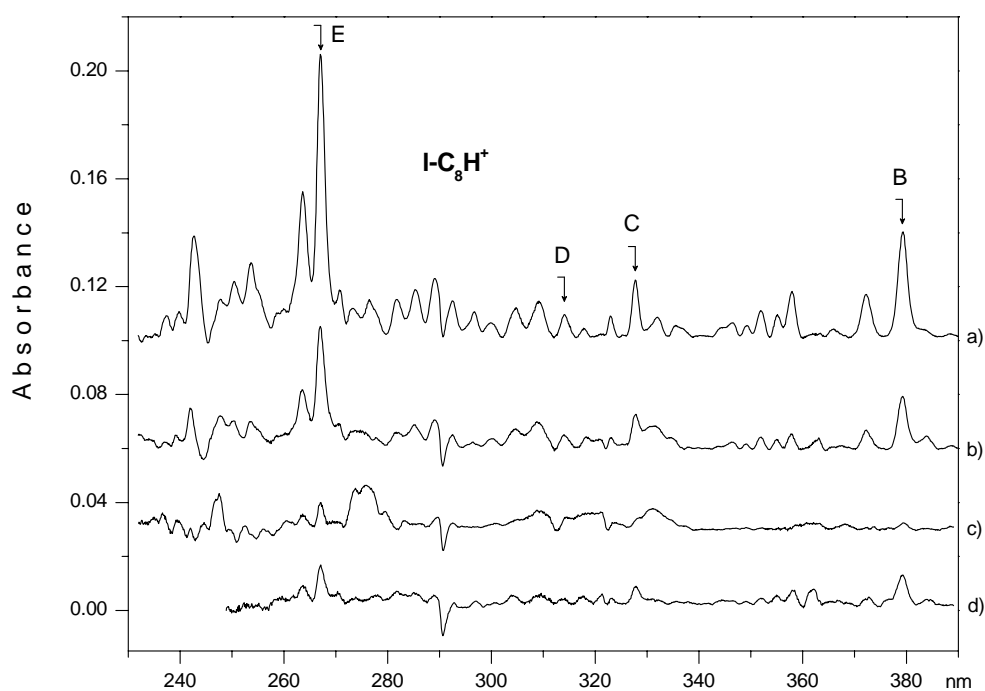


FIGURE 4.6 UV electronic transition of $l-C_8H^+$ observed in 6 K neon matrices generated from diacetylene. Trace (a) was recorded in the same experiment as trace (a) of Figure 4.3. Trace (b) represents another experiment in which the ion current was lower. Trace (c) shows the spectrum recorded after UV irradiation. The spectrum recorded after deposition of C_8H^+ with an admixture of N_2O is shown in trace (d). Letters A, B, D, C, E indicate the positions of the origin band of the respective electronic transition of $l-C_8H^+$.

TABLE 4.1 Observed bands (± 0.2 nm) in the electronic absorption spectra of *l*-C₆H⁺, *l*-C₆D⁺ and *l*-C₈H⁺ in 6 K neon matrices and the suggested assignments^a.

Species	λ [nm]	ν [cm ⁻¹]	Δ [cm ⁻¹]	Assignment
<i>l</i> -C ₆ H ⁺	515.8	19387	0	0_0^0 (1) $^3\Sigma^- - X^3\Sigma^-$
	500.0	20000	613	ν_6
	489.8	20416	1029	ν_5
	469.7	21290	1903	ν_4
<i>l</i> -C ₆ D ⁺	514.8	19425	0	0_0^0 (1) $^3\Sigma^- - X^3\Sigma^-$
	499.4	20024	599	ν_6
	469.7	21290	1865	ν_4
<i>l</i> -C ₈ H ⁺	628.4	15913	0	0_0^0 (1) $^3\Sigma^- - X^3\Sigma^-$
	610.2	16388	475	ν_8
	564.5	17715	1802	ν_5
	549.1	18212	2299	$\nu_5 + \nu_8$
	379.3	26364	0	0_0^0 B-X $^3\Sigma^-$
	372.2	26867	503	ν_8
	357.9	27941	1577	ν_6
	355.1	28161	1797	ν_5
	351.9	28417	2053	ν_4
	349.2	28637	2273	$\nu_5 + \nu_8$
	346.5	28860	2496	$\nu_4 + \nu_8$
	327.8	30506	0	0_0^0 C-X $^3\Sigma^-$
	323.0	30960	454	ν_8
	318.0	31447	941	ν_7
	314.1	31837	0	0_0^0 D* - X $^3\Sigma^-$
	309.2	32342	505	ν_8
	304.7	32819	982	ν_7
	299.9	33344	1507	ν_6
	296.7	33704	1867	ν_5
	292.6	34176	2339	$\nu_5 + \nu_8$
	289.1	34590	2753	$\nu_5 + \nu_7$
	285.3	35051	3214	
	281.7	35499	3662	$2\nu_5$
267.1	37439	0	0_0^0 E-X $^3\Sigma^-$	
263.6	37936	497	ν_8	
253.7	39417	1978	ν_4	
250.4	39936	2497	$\nu_4 + \nu_8$	
242.7	41203	3764	$2\nu_4$	

^a The letters in the last column refer to the excited electronic states indicated in Figures 5 and 6. $l-C_6H$: (σ) $\nu_1=3457$, $\nu_2=2137$, $\nu_3=2105$, $\nu_4=1895$, $\nu_5=1224$, $\nu_6=650$ cm^{-1} ; (π) $\nu_8=567$, $\nu_9=570$, $\nu_{10}=397$, $\nu_{11}=210$, $\nu_{12}=93$ cm^{-1} [13]. $l-C_8H$: (σ) 2168 (u), 2144 (g), 2032 (g), 1770 (u), 1404 (g), 979 (u), 516 (g) cm^{-1} ; (π) 706 (g), 584 (u), 413 (g), 264 (u), 160 (g), 65 (u) [26]. *-tentative.

CONCLUSIONS

The ${}^3\Sigma^- - X {}^3\Sigma^-$ electronic transitions of linear C_6H^+ and C_8H^+ in the visible spectral region are close to those of the isoelectronic C_n , $n=6,8$, carbon chains with oscillator strength similar to ones of $l-C_nH$, $n=6,8$. Several electronic transitions in the UV range of $l-C_8H^+$ are also observed, and the strongest at 267.1 nm has a counterpart in the $l-C_8$ spectrum. The identification of the electronic spectra of these astrophysically important species in neon matrices is a good starting point for gas-phase studies.

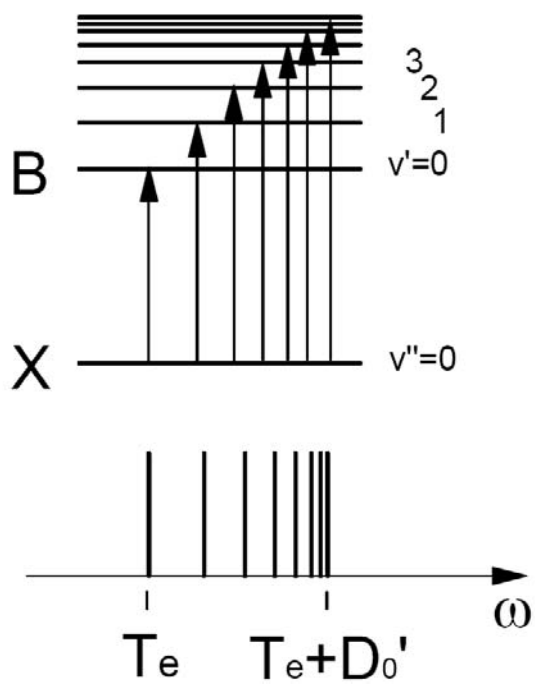
BIBLIOGRAPHY

- [1] M. GUÉLIN, J. CERNICHARO, C. KAHANE, J. GOMEZ-GONZALEZ, and C.M. WALMSLEY. Detection of a heavy radical in IRC + 10216 - The hexatriynyl radical C₆H. *Astronomy and Astrophysics*, 175: L5-L8, 1987
- [2] M. GUÉLIN, J. CERNICHARO, M.J. TRAVERS, M.C. MCCARTHY, C.A. GOTTLIEB, P. THADDEUS, M. OHISHI, S. SAITO, and S. YAMAMOTO. Detection of a new linear carbon chain radical: C₇H. *Astronomy and Astrophysics*, 317: L1-L4, 1997
- [3] J. CERNICHARO and M. GUÉLIN. Discovery of the C₈H radical. *Astronomy and Astrophysics*, 309: L27-L30, 1996
- [4] M.C. MCCARTHY, M.J. TRAVERS, A. KOVÁCS, C.A. GOTTLIEB, and P. THADDEUS. Laboratory detection of the C₈H radical. *Astronomy and Astrophysics*, 309: L31-L33, 1996
- [5] C.A. GOTTLIEB, M.C. MCCARTHY, M.J. TRAVERS, J.-U. GRABOW, and P. THADDEUS. Rotational spectra of the carbon chain free radicals C₁₀H, C₁₂H, C₁₃H, and C₁₄H. *The Journal of Chemical Physics*, 109: 5433-5438, 1998
- [6] P. FREIVOGEL, J. FULARA, M. JAKOBI, D. FORNEY, and J.P. MAIER. Electronic absorption spectra of linear carbon chains in neon matrices. II. C_{2n}⁺, C_{2n}, and C_{2n}H. *The Journal of Chemical Physics*, 103: 54-59, 1995
- [7] M. KOTTERER and J.P. MAIER. Electronic spectrum of C₆H: ²Π-X²Π in the gas-phase detected by cavity ringdown. *Chemical Physics Letters*, 266: 342-346, 1997
- [8] H. LINNARTZ, T. MOTYLEWSKI, O. VAIZERT, J.P. MAIER, A.J. APPONI, M.C. MCCARTHY, C.A. GOTTLIEB, and P. THADDEUS. Electronic ground and excited state spectroscopy of C₆H and C₆D. *Journal of Molecular Spectroscopy*, 197: 1-11, 1999
- [9] H. LINNARTZ, T. MOTYLEWSKI, and J.P. MAIER. The ²Π-X²Π electronic spectra of C₈H and C₁₀H in the gas phase. *The Journal of Chemical Physics*, 109: 3819-3823, 1998
- [10] F. PAUZAT and Y. ELLINGER. The lowest two electronic states of the hexatriynyl radical - C₆H. *Astronomy and Astrophysics*, 216: 305-309, 1989
- [11] D.E. WOON. A correlated ab initio study of linear carbon-chain radicals C_nH (n=2-7). *Chemical Physics Letters*, 244: 45-52, 1995

- [12] A.L. SOBOLEWSKI and L. ADAMOWICZ. Ab initio characterization of electronically excited states in highly unsaturated hydrocarbons. *The Journal of Chemical Physics*, 102: 394-399, 1995
- [13] Z. CAO and S.D. PEYERIMHOFF. Electronic spectra of linear isoelectronic species HC_6H^+ , C_6H , HC_5N^+ . *Physical Chemistry Chemical Physics*, 3: 1403-1406, 2001
- [14] D.K. BOHME, S. WŁODEK, L. WILLIAMS, L. FORTE, and A. FOX. Laboratory measurements of gas-phase reactions of polyatomic carbon ions C_n^+ ($n=1-6$) and C_nH^+ ($n=2-5$) with carbon monoxide. *The Journal of Chemical Physics*, 87: 6934-6938, 1987
- [15] A.E. DOUGLAS and G. HERZBERG. Note on CH^+ in interstellar space and in the laboratory. *The Astrophysical Journal*, 94: 381, 1941
- [16] W.S. ADAMS. Observations of interstellar hydrogen and potassium, molecular lines, and radial velocities in the spectra of 300 O and B stars. *The Astrophysical Journal*, 109: 354-379, 1949
- [17] P. FREIVOGEL, J. FULARA, D. LESSEN, D. FORNEY, and J.P. MAIER. Absorption spectra of conjugated hydrocarbon cation chains in neon matrices. *Chemical Physics*, 189: 335-341, 1994
- [18] R. ROSSETTI and L.E. BRUS. Waveguide propagation in frozen gas matrices. *Review of Scientific Instruments*, 51: 467-470, 1980
- [19] C. GILLERY, P. ROSMUS, H.-J. WERNER, H. STOLL, and J.P. MAIER. A theoretical study of the electronically excited states in linear and cyclic C_6^+ . *Molecular Physics*, 102: 2227-2236, 2004
- [20] T.H. DUNNING JR. Gaussian basis sets for use in correlated molecular calculations. I. The atoms boron through neon and hydrogen. *The Journal of Chemical Physics*, 90: 1007-1023, 1989
- [21] R.A. KENDALL, T.H. DUNNING JR, and R.J. HARRISON. Electron affinities of the first-row atoms revisited. Systematic basis sets and wave functions. *The Journal of Chemical Physics*, 96: 6796-6806, 1992
- [22] M. FEHÉR and J.P. MAIER. The geometric and electronic structures of C_6H and its ions. *Chemical Physics Letters*, 227: 371-376, 1994
- [23] H.-J. WERNER and P.J. KNOWLES. *Molpro program. further information can be obtained from <http://www.molpro.net/>,*
- [24] C. GILLERY, *PhD Thesis*. 2005, University of Marne la Vallée: France.

- [25] D. FORNEY, J. FULARA, P. FREIVOGEL, M. JAKOBI, D. LESSEN, and J.P. MAIER. Electronic absorption spectra of linear carbon chains in neon matrices. I. C_6^- , C_6 , and C_6H . *The Journal of Chemical Physics*, 103: 48-53, 1995
- [26] J. FULARA, E. RIAPLOV, A. BATALOV, I. SHNITKO, and J.P. MAIER. Electronic and infrared absorption spectra of linear and cyclic C_6^+ in a neon matrix. *The Journal of Chemical Physics*, 120: 7520-7525, 2004
- [27] J. FULARA, I. SHNITKO, A. BATALOV, and J.P. MAIER. Electronic absorption spectra of linear and cyclic C_n^+ $n=7-9$ in a neon matrix. *The Journal of Chemical Physics*, 123: 044305(6), 2005
- [28] S.W. MCELVANY, B.I. DUNLAP, and A. O'KEEFE. Ion molecule reactions of carbon cluster ions with D_2 and O_2 . *The Journal of Chemical Physics*, 86: 715-725, 1987
- [29] M.B. SOWA-RESAT, J.N. SMOLANOFF, and I.B. GOLDMAN. N-O versus N-N bond activation in reaction of N_2O with carbon cluster ions: experimental and ab initio studies of the effects of geometric and electronic structure. *The Journal of Chemical Physics*, 100: 8784-8794, 1994
- [30] M. GRUTTER, M. WYSS, E. RIAPLOV, and J.P. MAIER. Electronic absorption spectra of linear C_6 , C_8 and cyclic C_{10} , C_{12} in neon matrices. *The Journal of Chemical Physics*, 111: 7397-7401, 1999
- [31] T.R. TAYLOR, C. XU, and D.M. NEUMARK. Photoelectron spectra of the $C_{2n}H^-$ ($n=1-4$) and $C_{2n}D^-$ ($n=1-3$) anions. *The Journal of Chemical Physics*, 108: 10018-10026, 1998
- [32] J.M.L. MARTIN, J. EL-YAZAL, and J.-P. FRANÇOIS. Structure and vibrational spectra of carbon clusters C_n ($n=2-10, 12, 14, 16, 18$) using density functional theory including exact exchange contributions. *Chemical Physics Letters*, 242: 570-579, 1995

CHAPTER 5. SULFUR SPECIES



This chapter is a slightly modified form of the article published in:
Shnitko et. al., Chemical Physics

ELECTRONIC TRANSITIONS OF S_2^- AND S_3^-

INTRODUCTION

Sulfur and its compounds are of interest from a fundamental point of view as well as in terrestrial and space environments. S and S_2 have been observed by the Hubble Space Telescope in the volcanically driven atmosphere of Jupiter's moon Io [1, 2]. Photochemical models predict that the vapor of the Pele-type volcanoes may contain sulfur clusters up to S_{10} [3]. These are also thought to play a role in the photochemistry of Venus lower atmosphere [4, 5] and in the circumstellar shells of carbon-rich evolved stars [6].

Sulfur has more allotropes than any other element [7, 8]. The smallest S_n $n=2-8$ neutral species were studied by Raman [9-12], infrared [13], microwave [14, 15] and optical spectroscopy [16-21] in the gas-phase and noble gas matrixes. The S_n^- anions have also been the goal of numerous experimental [22-36] and theoretical studies [35-40]; however most of the works concern S_2^- and S_3^- . These species isolated in alkali halide or silicate matrices have been characterized by means of electron spin resonance [22-24], Raman [25-29], and optical spectroscopy [25, 27-32]. In addition to the matrix experiments, photodetachment processes of gaseous S_2^- and S_3^- have been investigated [33, 34]. The photoelectron studies of S_n^- $n=4-11$ have revealed that the most stable isomers are ring-like up to S_5^- , chain-like for S_8^- and S_9^- whereas S_6^- and S_7^- can occur in both forms [35, 36].

The spectroscopic data which are the most relevant to the present work come from the emission and absorption of S_2^- embedded in alkali halide crystals [27, 28, 30, 31] and absorption of S_3^- in such crystals and basic solvents [25, 41]. S_2^- is characterized by a distinct band system with the onset at ~ 500 nm [31]. S_3^- has a strong broad absorption with a maximum around 620 nm [25, 41], and is responsible for the blue colour of the mineral lapis lazuli and synthetic ultramarine [32].

In this chapter the electronic absorption spectra of S_n^- ($n=2,3$) isolated in neon matrixes are reported. Though these spectra agree with the reported ones in crystals,

they reveal a rich vibrational structure and are more suitable for comparison with theoretical calculations due to the less interacting nature of the neon environment.

EXPERIMENTAL

The absorption spectra were recorded following mass-selective deposition in neon matrices using the described instrument [42]. Sulfur anions S_n⁻ n=2,3 were produced from a mixture of CS₂ with argon in a hot cathode discharge source (Fig. 2.9). Ions were then extracted, deflected by 90°, and selected with a quadrupole mass filter. They were codeposited on a 6 K cold surface with an excess of neon over a period of ~3 hours. The substrate was a rhodium coated sapphire plate that was cooled by a closed cycle helium cryostat. The temperature was measured and controlled with a silicon diode sensor and a 25 W heater.

Absorption spectra of the species embedded in solid neon were recorded in the 220–1100 nm range using a single beam spectrometer which consists of a xenon or halogen light source, monochromator, and detector (photomultiplier or silicon diode). The light was passed parallel to the substrate surface in a waveguide mode [43]. The matrix samples were then exposed to filtered radiation ($\lambda > 305$ nm) from a medium pressure mercury lamp and the spectrum was recorded again to distinguish transitions of neutral species and ions.

RESULTS AND DISCUSSION

LINEAR S₂⁻

The electronic absorption spectrum in a neon matrix recorded after mass-selective deposition of S₂⁻ is shown in Figure 5.1. This band system vanishes after irradiation of the matrix with a medium pressure mercury lamp ($\lambda > 305$ nm) which indicates its ionic origin, while a strong band system of the S₂ molecule appears in the

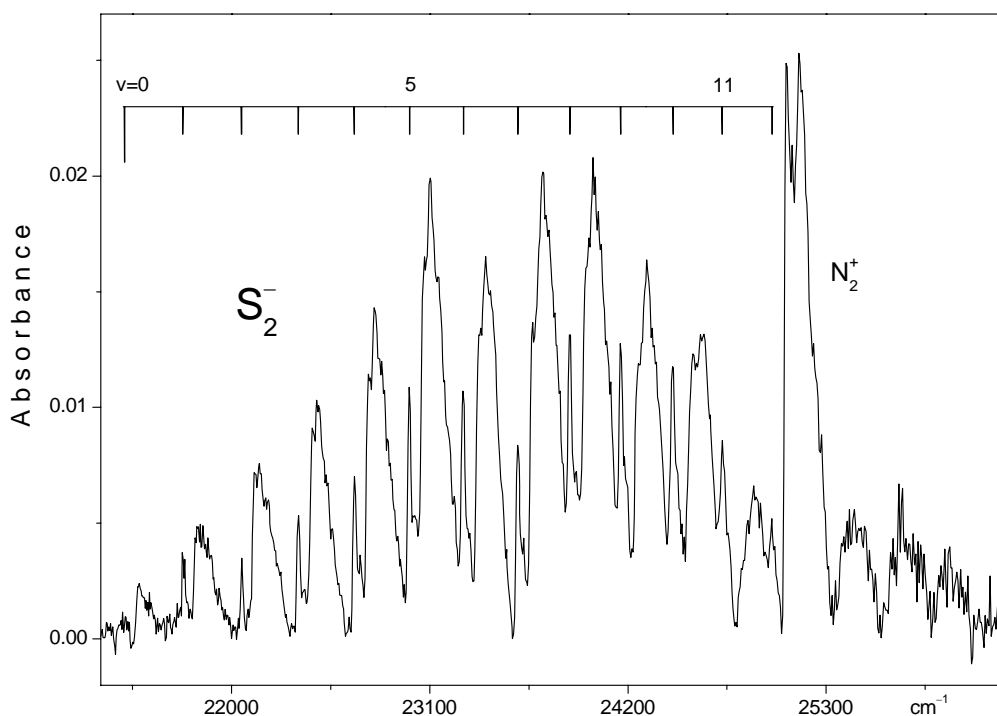


FIGURE 5.1 The $A^2\Pi_u \leftarrow X^2\Pi_g$ electronic absorption spectrum of S_2^- in a 6 K neon matrix. Vertical bars indicate zero phonon lines (discussed in the second chapter of this thesis) of the vibrational mode excited in the upper state.

UV part of the spectrum. Figure 5.2 shows this known [17] $B^3\Sigma_u^- \leftarrow X^3\Sigma_g^-$ transition of S_2 . Thus the new band system seen in Figure 5.1 is ascribed to the S_2^- anion.

The spectrum of S_2^- comprises a number of alternately distributed narrow and broad bands. The narrow ones lying to low energy are the zero-phonon lines (ZPL), as already noted [44]. The broad ones are the phonon side-bands. Each ZPL has a shoulder $\sim 33 \text{ cm}^{-1}$ to higher energy. The first narrow structure in the phonon side-bands lies $\sim 82 \text{ cm}^{-1}$ above ZPL and the following peaks are spaced by $30\text{--}40 \text{ cm}^{-1}$ from each other. This pattern is quite regular and is seen in almost all the vibrational bands of S_2^- except

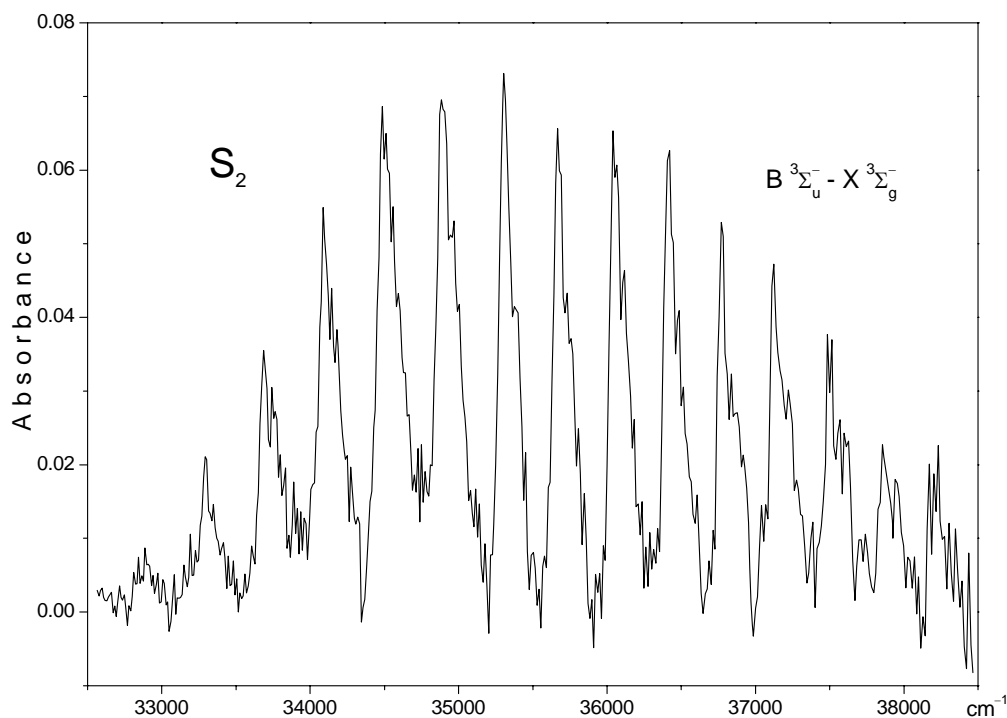


FIGURE 5.2 The $B^3\Sigma_u^- \leftarrow X^3\Sigma_g^-$ electronic absorption spectrum of S_2 in a 6 K neon matrix produced from S_2^- upon UV irradiation.

for the three highest energy ones. The band around 25000 cm^{-1} is due to N_2^+ , formed during the matrix growth by the collision-induced ionization of residual N_2 in the system.

ZPLs and the narrow structures on the phonon side-bands are regularly spaced in the spectrum of S_2^- . The positions of these bands fit well a second order polynomial as a function of the vibrational quantum number ν . The first weak broad band at $21487 \pm 5\text{ cm}^{-1}$ is genuine, though ZPL is not seen in this case, because it lies exactly in the position predicted (21491 cm^{-1}) from the parabolic fit for the phonon side-bands. This weak broad band is the origin of the electronic transition. The ZPL of the origin band of S_2^- is not seen in the spectrum and is likely buried in the noise of the spectrum. The position of ZPL of the origin band at 21407 cm^{-1} is estimated from the fit for all

observed ZPLs. The spectroscopic constants $\omega_0'=328.4\pm 1$ and $\omega_0'x_0'=2.4\pm 0.1$ cm^{-1} in the excited electronic state of S_2^- were also determined from this. Positions of the observed ZPLs with their suggested assignment are given in Table 5.1.

TABLE 5.1 Positions of the zero-phonon lines (ZPL) (± 0.2 nm) observed for the ${}^2\Pi_u \leftarrow X^2\Pi_g$ transition of S_2^- in a 6 K neon matrix.

Species	λ/nm	$\tilde{\nu}/\text{cm}^{-1}$	$\Delta\tilde{\nu}/\text{cm}^{-1}$	Assignment
S_2^-	467.1	21407 ^a	0	0-0
	460.2	21730	323	1-0
	453.4	22056	649	2-0
	447.0	22371	964	3-0
	440.9	22681	1274	4-0
	435.0	22989	1582	5-0
	429.4	23288	1881	6-0
	423.9	23590	2183	7-0
	418.8	23878	2471	8-0
	413.9	24160	2753	9-0
	409.0	24450	3043	10-0
	404.5	24722	3315	11-0
400.0	25000	3593	12-0	

^a $\omega_0'=328.4\pm 1$, $\omega_0'x_0'=2.4\pm 0.1$, $\omega_e'=331\pm 1.2$, $\omega_e'x_e'=2.43\pm 0.08$ cm^{-1} , ν_{0-0} were determined from the parabolic fit ($\tilde{\nu} = \nu_{0-0} + \omega_0' * \nu - \omega_0'x_0' * \nu^2$) of the observed ZPLs.

Disulfur anion was extensively investigated by its emission spectrum in alkali halide crystals held at cryogenic temperatures [27, 28, 30]. The emission is composed of numerous bands in the 500–900 nm region reflecting the vibrational excitation in the ground state. Two series of sharp ZPLs are seen in the spectra of S_2^- and they result from the crystal field splitting [27, 28]. The energy of the 0–0 transition as well as ω_0'' and $\omega_0''x_0''$ spectroscopic constants for both sublevels were determined from the position of these ZPLs. The 0–0 band of the lower energy series lies in the

19455–20468 cm^{-1} range in KI, RbI, NaI, KBr KCl crystals [27, 28]. The ground state vibrational frequency ω_0'' increases from 599 to 623 cm^{-1} among this series. The ω_0'' value (600 cm^{-1}), determined from Raman studies, is close to the one inferred from the emission spectrum (599 cm^{-1}) for KI [28].

S_2^- dissolved in a KI crystal held at 2 K was also studied by absorption spectroscopy [31]. Numerous weak structured bands were observed. The sharp peaks occurred in pairs separated by $\sim 80 \text{ cm}^{-1}$, and by 320–360 cm^{-1} to the next ones. The spacing decreases to higher excitation energy. The pairs of sharp bands were interpreted as two series of ZPLs reflecting the crystal field splitting in the excited state electronic levels of the anion. The derived 0–0 transition is 20027 cm^{-1} and is in a good agreement with the value obtained from the emission studies (20028 cm^{-1}) [27, 28]. The upper ground state sublevel of S_2^- located at 575 cm^{-1} above the lower one in a KI crystal was not populated at 2 K and, therefore, the lower energy 0–0 transition derived from the emission spectrum (19455 cm^{-1}) and associated with this sublevel could not be observed. The ω_0' and $\omega_0'x_0'$ spectroscopic constants in the excited electronic state of S_2^- in the KI crystal were determined as 362 and 2.0 cm^{-1} respectively [31].

The ν_{0-0} , ω_0' and $\omega_0'x_0'$ spectroscopic constants of S_2^- in alkali halide crystals can be compared with the results of the present studies. The 21407 cm^{-1} origin band of S_2^- in a neon matrix is 1380 cm^{-1} blue shifted [31]. In the halide crystals the environments interact more strongly than a neon matrix; it is particularly true for ionic guest species which are more stabilized in the crystal field than neutral molecules. The series of higher energy bands, $\sim 80 \text{ cm}^{-1}$ spaced from ZPLs in the absorption spectrum of S_2^- in KI, is also seen in the spectrum of S_2^- in a neon matrix. These are the phonon sidebands on which the sharp features are imposed. The ionic crystal environment has a smaller effect on the energy of the vibrational levels than for the electronic transitions. The ω_0' frequency in the excited electronic state of S_2^- changes from 362 to 329 cm^{-1} on passing from KI to a neon environment.

The $\omega_0'=362 \text{ cm}^{-1}$ value in the excited electronic state of S_2^- in KI [31] differs considerably from $\omega_0''=599 \text{ cm}^{-1}$ in the ground state. The ω_0'' frequency of S_2^- in a neon matrix is yet unknown. However, it will not differ much from the value in a KI crystal.

A large difference in the frequency of the vibrational mode in the ground and the excited electronic states of S_2^- reflects the change of the SS bond length upon the excitation, becoming longer. This has also an influence on the appearance of the electronic spectrum and explains the weak origin band and a long progression. The electronic spectrum of S_2^- (Fig. 5.1) resembles the spectrum of neutral S_2 (Fig. 5.2), and the vibrational frequency of S_2 in the $X^3\Sigma_g^-$ ground ($\omega_0''=723\text{ cm}^{-1}$) and $B^3\Sigma_u^-$ excited state ($\omega_0'=431\text{ cm}^{-1}$) differs considerably to the anion values [45].

The ground and several lower lying excited electronic states of S_2^- have been investigated by a multireference configuration interaction method [38]. The strongest electronic transition from the $X^2\Pi_g$ ground state was predicted to the $A^2\Pi_u$ state. The potential energy curves of these electronic states are shifted considerably. The calculated equilibrium bond length in the $X^2\Pi_g$ state is 0.2019 nm and it increases to 0.2365 nm in the $A^2\Pi_u$ state. Therefore the weak origin band and a long vibrational progression are expected in the absorption spectrum of S_2^- . The strongest vibrational band will correspond to the vertical transition from the equilibrium geometry of the ground state of this anion. The predicted vertical transition is 3.12 eV (25172 cm^{-1}) [38]. The maximum intensity in the spectrum of S_2^- in a neon matrix is not well defined but lies in the $23100\text{--}24100\text{ cm}^{-1}$ range. Hence the calculations overestimate the energy of the vertical transition of S_2^- by 0.13–0.26 eV. The 0–0 transition of S_2^- in a neon matrix lies at 21407 cm^{-1} . This value is $\sim 0.27\text{ eV}$ smaller than the calculated one (19232 cm^{-1}) [38]. The correction for the zero point energy difference between the ground and excited state is +0.02 eV and the expected shift from a neon matrix to the gas phase is $\sim \pm 0.03\text{ eV}$. The calculations predict well the frequency of the vibration [38] $\omega_e'=340\text{ cm}^{-1}$ in the $A^2\Pi_u$ state of S_2^- compared to the experimental value $\omega_e'=331\text{ cm}^{-1}$.

LINEAR S_3^-

S_3^- was produced from CS_2 in the hot cathode discharge source. The spectrum shown in Figure 5.3 was recorded after a 3 hour deposition of mass-selected S_3^- , resulting in a total current of 60 μC . A medium intensity band system observed in 550–700 nm region consists of many peaks which decrease in intensity after UV

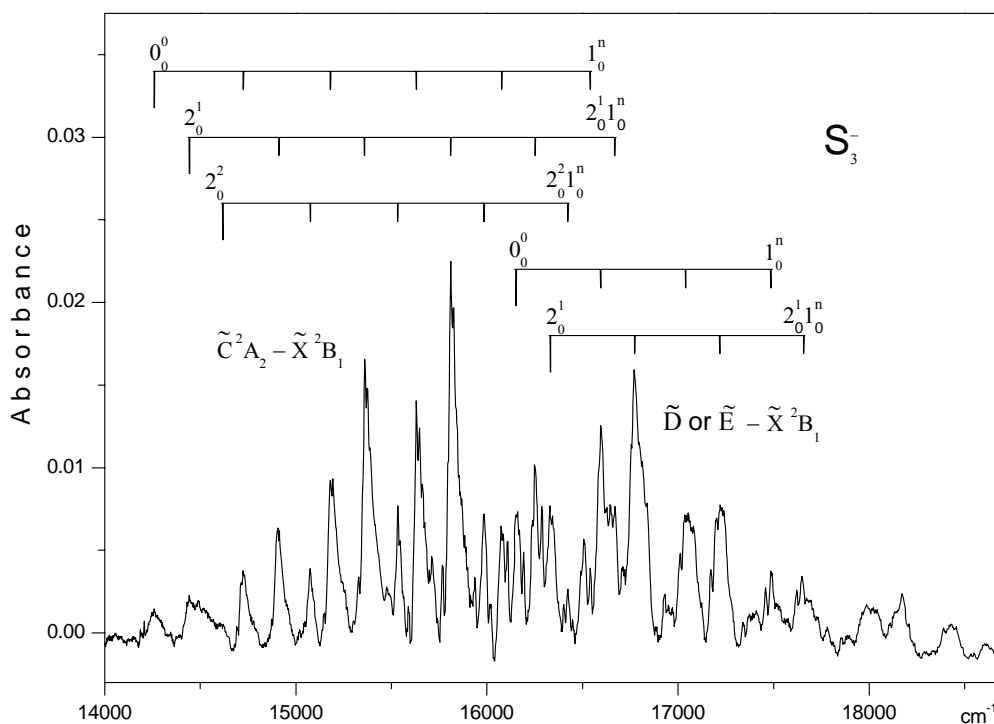


FIGURE 5.3 Electronic absorption spectrum of S_3^- in a 6 K neon matrix recorded after mass-selective co-deposition with neon. A bimodal intensity distribution results from the overlapping $\tilde{C}^2A_2 \leftarrow \tilde{X}^2B_1$ and $(\tilde{D} \text{ or } \tilde{E}) \leftarrow \tilde{X}^2B_1$ systems of S_3^- (see text).

irradiation of the matrix with a medium-pressure Hg lamp with a cut-off filter ($\lambda > 305$ nm). A new band system then appears in the 360–420 nm range (Fig. 5.4). This is similar in appearance to the known electronic transition of neutral S_3 in an argon matrix [18]. The 550–770 nm band system is attributed to the S_3^- anion because neutral S_3 appears after UV irradiation of the matrix.

In the past, S_3^- anion was studied in solutions and melted salts. The blue color which develops after heating sulfur with water and basic salts is due to S_3^- [41]. Blue

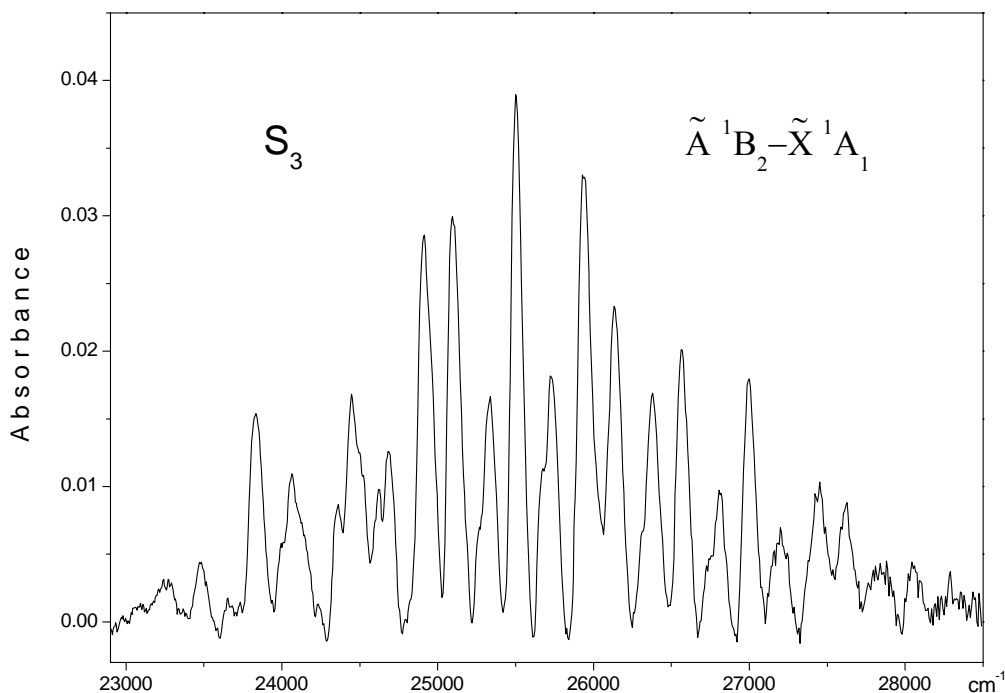


FIGURE 5.4 The $\tilde{A}^1B_2 \leftarrow \tilde{X}^1A_1$ electronic absorption spectrum of S_3 in a 6 K neon matrix produced from S_3^- upon UV irradiation.

solutions are also formed after dissolving sulfur and alkali polysulfides in solvents like dimethylformamide and dimethyl sulfoxide. The color of ultramarine and lapis lazuli minerals also originates from S_3^- [24, 29, 32], and have been investigated by visible, UV, infrared, Raman, and electron spin resonance spectra [41]. The spectrum of such solutions exhibits of relatively strong but structureless band in the 500–750 nm region with a maximum around 610–620 nm [25, 41]. This falls in the spectral region where the new absorption system is observed in this work, but revealing a well resolved vibrational structure (Fig. 5.3) due to the more inert neon environment.

A bimodal intensity distribution of the absorption bands is seen in the spectrum of S_3^- (Fig. 5.3). The maxima of these two distributions are spaced by $\sim 960 \text{ cm}^{-1}$. The 701.3 nm band of the lowest energy in the spectrum of S_3^- (Fig. 5.3) is the origin of this

transition. The bands to higher energy correspond to vibrational excitation in the upper state and are associated with the totally symmetric fundamental modes of S_3^- . Theoretical calculations on S_3^- confirm its C_{2v} nature in the ground electronic state [39], S_3^- ion possesses two fundamentals of a_1 (529 and 216 cm^{-1}) and one of b_1 (557 cm^{-1}) symmetry. Excitation of these modes is responsible for the rich vibronic structure of Figure 5.3.

A long progression with a 460 cm^{-1} spacing is observed. Another progression $\sim 180\text{ cm}^{-1}$ is also seen. These correspond to the two fundamentals ν_1 and ν_2 of S_3^- . The energy of the ν_1 mode in the excited electronic state of S_3^- differs from the calculated one for the ground electronic state (529 cm^{-1}) and from the experimental frequency of S_3^- in alkali halide crystals determined from the Raman studies (531 cm^{-1}) [26]. Nevertheless, the energy of the ν_1 mode (450 cm^{-1}) in the 1B_2 excited electronic state of S_3 in an argon matrix [18] is close to ν_1 of S_3^- .

A congestion of the vibronic bands in Figure 5.3 results from the combinations of the ν_1 and ν_2 modes. However, not all of the bands in this spectrum are due to these, which can explain only the lower energy part. The maxima of the bimodal intensity distribution of the vibrational bands in the spectrum of S_3^- are spaced by 960 cm^{-1} . The higher energy part of the spectrum is associated with the next electronic transition of S_3^- . Analysis of the vibrational pattern in this region reveals two totally symmetric fundamental modes of 177 and 446 cm^{-1} energy, which form overtone and combination bands. The 619.1 nm peak (Fig. 5.3) is the origin of this second electronic transition. The suggested assignment is given in Table 5.2.

Theoretical calculations using coupled-clusters and multireference CI methods have been carried out for the low-lying electronic states of S_3^- in C_{2v} and D_{3h} symmetries [40, 46]. The ground state is predicted to be 2B_1 . The energies of the three low-lying electronic states (\tilde{A}^2B_2 , \tilde{B}^2A_1 , \tilde{C}^2A_2) are calculated to be 1.66 , 1.75 and 2.09 eV above the ground state, respectively. The dipole allowed excitations from the \tilde{X}^2B_1 ground state to the \tilde{B}^2A_1 and \tilde{C}^2A_2 states are characterized by differing

TABLE 5.2 Positions of the Band Maxima (± 0.2 nm) Observed for the $\tilde{C}^2A_2 \leftarrow \tilde{X}^2B_1$ and $(\tilde{D} \text{ or } \tilde{E}) \leftarrow \tilde{X}^2B_1$ Electronic Transitions of S_3^- in a 6 K Neon Matrix.

Species	λ/nm	$\tilde{\nu}/\text{cm}^{-1}$	$\Delta\tilde{\nu}/\text{cm}^{-1}$	Assignment
S_3^-	701.3	14259	0	$0_0^0 \quad \tilde{C}^2A_2 \leftarrow \tilde{X}^2B_1$
	692.4	14443	184	ν_2
	684.1	14618	359	$2\nu_2$
	679.1	14725	466	ν_1
	670.6	14912	653	$\nu_1 + \nu_2$
	663.3	15076	817	$\nu_1 + 2\nu_2$
	660.2	15147	888	$2\nu_3$
	658.7	15181	922	$2\nu_1$
	652.4	15328	1069	$\nu_2 + 2\nu_3$
	651.1	15359	1100	$2\nu_1 + \nu_2$
	643.8	15533	1274	$2\nu_1 + 2\nu_2$
	641.4	15591	1332	$\nu_1 + 2\nu_3$
	639.8	15630	1371	$3\nu_1$
	636.4	15713	1454	$2\nu_1 + 3\nu_2$
	634.2	15768	1509	$\nu_1 + \nu_2 + 2\nu_3$
	632.5	15810	1551	$3\nu_1 + \nu_2$
	627.5	15936	1677	$\nu_1 + 2\nu_2 + 2\nu_3$
	625.6	15985	1726	$3\nu_1 + 2\nu_2$
	624.2	16021	1762	$2\nu_1 + 2\nu_3$
	622.0	16077	1818	$4\nu_1$
	620.8	16108	1849	$\nu_1 + 3\nu_2 + 2\nu_3$
	617.6	16192	1933	$2\nu_1 + \nu_2 + 2\nu_3$
	615.3	16252	1993	$4\nu_1 + \nu_2$

614.0	16287	2028		$\nu_1+4\nu_2+2\nu_3$
608.9	16423	2164		$4\nu_1+2\nu_2$
604.6	16540	2281		$5\nu_1$
598.4	16711	2452		$5\nu_1+\nu_2$
619.1	16152	0	0_0^0	$(\tilde{D} \text{ or } \tilde{E}) \leftarrow \tilde{X}^2B_1$
612.4	16329	177		ν_2
605.7	16510	358		$2\nu_2$
602.5	16598	446		ν_1
599.9	16669	517		$3\nu_2$
596.3	16770	618		$\nu_1+\nu_2$
590.7	16929	777		$\nu_1+2\nu_2$
586.9	17039	887		$2\nu_1$
580.8	17218	1066		$2\nu_1+\nu_2$
571.9	17486	1334		$3\nu_1$
566.3	17658	1506		$3\nu_1+\nu_2$
555.5	18002	1850		$3\nu_1+3\nu_2$
550.2	18175	2023		$3\nu_1+4\nu_2$
542.6	18430	2278		$4\nu_1+3\nu_2$
537.4	18608	2456		$4\nu_1+4\nu_2$

transition moments, the former being by about a factor of 40 smaller than the latter [40, 46].

Therefore, the band system with the energy of the 0_0^0 band (1.77 eV) observed in the present work (Fig. 5.3) is assigned to the $\tilde{C}^2A_2 \leftarrow \tilde{X}^2B_1$ transitions of this anion. The calculations [46] predict also next two 2A_1 and 2B_1 electronic states which are accessible from the \tilde{X}^2B_1 state by an optical excitation and they lie above the \tilde{C}^2A_2

state. Therefore the next band system with the origin band at 619.1 nm could be transition of ones of these (\tilde{D} or \tilde{E}) states. The complexity of the structure above 16000 cm⁻¹ can also be the result of state mixing.

BIBLIOGRAPHY

- [1] L.M. FEAGA, M.A. MCGRATH, and P.D. FELDMAN. The abundance of atomic sulfur in the atmosphere of Io. *The Astrophysical Journal*, 570: 439, 2002
- [2] J.R. SPENCER, K.L. JESSUP, M.A. MCGRATH, G.E. BALLESTER, and R. YELLE. Discovery of gaseous S₂ in Io's Pele plume. *Science*, 288: 1208-1210, 2000
- [3] J.I. MOSES, M.Y. ZOLOTOV, and B.J. FEGLEY. Photochemistry of a volcanically driven atmosphere on Io: sulfur and oxygen species from a Pele-type Eruption. *Icarus*, 156: 76-106, 2002
- [4] J.S. LEWIS and F.A. KREIMENDAHL. Oxidation state of the atmosphere and crust of Venus from pioneer venus results. *Icarus*, 42: 330-337, 1980
- [5] M.Y. ZOLOTOV. *Lunar Planet. Sci.*, 16: 942, 1985
- [6] A.E. GLASSGOLD. Circumstellar photochemistry. *Annual Review of Astronomy and Astrophysics*, 34: 241-277, 1996
- [7] B. ECKERT and R. STEUDEL. Molecular spectra of sulfur molecules and solid sulfur allotropes. *Top. Curr. Chem.*, 231: 31-98, 2003
- [8] I. KROSSING. Homoatomic sulfur cations. *Top. Curr. Chem.*, 230: 135-152, 2003
- [9] M.S. BOUMEDIEN, J. CORSET, and E. PICQUENARD. *Journal of Raman Spectroscopy*, 30: 463-472, 1999
- [10] P. LENAIN, E. PICQUENARD, J. CORSET, D. JENSEN, and R. STEUDEL. *Ber. Bunsen Ges. Phys. Chem.*, 92: 859, 1988
- [11] P. LENAIN, E. PICQUENARD, J.L. LESNE, and J. CORSET. *J. Mol. Struct.*, 142: 355, 1988
- [12] M. SCHMIDT. Elemental sulfur - a challenge to theory and practice. *Angewandte Chemie International Edition in English*, 12: 445-455, 1973
- [13] D.G. BRABSON, Z. MIELKE, and L. ANDREWS. Infrared spectra and structures of isotopically enriched S₃ and S₄ in solid argon. *Journal of Physical Chemistry*, 95: 79-86, 1991

- [14] M.C. MCCARTHY, S. THORWIRTH, C.A. GOTTLIEB, and P. THADDEUS. The rotational spectrum and geometrical structure of thiozone, S₃. *Journal of the American Chemical Society*, 126: 4096-4097, 2004
- [15] S. THORWIRTH, M.C. MCCARTHY, C.A. GOTTLIEB, P. THADDEUS, H. GUPTA, and J.F. STANTON. Rotational spectroscopy and equilibrium structures of S₃ and S₄. *The Journal of Chemical Physics*, 123: 054326-10, 2005
- [16] R.I. BILLMERS and A.L. SMITH. Ultraviolet-visible absorption spectra of equilibrium sulfur vapor: molar absorptivity spectra of S₃ and S₄. *Journal of Physical Chemistry*, 95: 4242-4245, 1991
- [17] V.E. BONDYBEY and J.H. ENGLISH. B ³Σ_u⁻ predissociation and relaxation processes in matrix isolated S₂. *The Journal of Chemical Physics*, 72: 3113-3122, 1980
- [18] P. HASSANZADEH and L. ANDREWS. Vibronic absorption spectra of S₃ and S₄ in solid argon. *Journal of Physical Chemistry*, 96: 6579-6585, 1992
- [19] B. MEYER, T.V. OOMMEN, and D. JENSEN. The color of liquid sulfur. *Journal of Physical Chemistry*, 75: 912-917, 1971
- [20] B. MEYER and T. STROYER-HANSEN. Infrared spectra of S₄. *Journal of Physical Chemistry*, 76: 3968-3969, 1972
- [21] B. MEYER, T. STROYER-HANSEN, and T.V. OOMMEN. The visible spectrum of S₃ and S₄. *Journal of Molecular Spectroscopy*, 42: 335-343, 1972
- [22] J. SCHNEIDER, B. DISCHLER, and A. RAUBER. *Phys. Status Solidi*, 13: 141, 1966
- [23] J.H. LUNSFORD and D.P. JOHNSON. Electron paramagnetic resonance study of S₃⁻ formed on magnesium oxide *The Journal of Chemical Physics*, 58: 2079-2083, 1973
- [24] S. KOWALAK, A. JANKOWSKA, S. ZEIDLER, and A.B. WIECKOWSKI. Sulfur radicals embedded in various cages of ultramarine analogs prepared from zeolites. *Journal of Solid State Chemistry*, 180: 1119-1124, 2007
- [25] W. HOLZER, W.F. MURPHY, and H.J. BERNSTEIN. Raman spectra of negative molecular ions doped in alkali halide crystals. *Journal of Molecular Spectroscopy*, 32: 13-23, 1969
- [26] W. HOLZER, W.F. MURPHY, and H.J. BERNSTEIN. Resonance Raman effect of Si doped in NaCl single crystal. *Chemical Physics Letters*, 4: 641-642, 1970

- [27] M. IKEZAVA and J. ROLFE. Zero-phonon transitions in O_2^- , S_2^- , and SeS^- molecules dissolved in alkali halide crystals. *The Journal of Chemical Physics*, 58: 2024-2038, 1973
- [28] C.A. SAWICKI and D.B. FITCHEN. Laser-excited spectra and reorientation of the S_2^- ion in alkali halides. *The Journal of Chemical Physics*, 65: 4497-4507, 1976
- [29] R.J.H. CLARK and D.G. COBBOLD. Characterization of sulfur radical anions in solutions of alkali polysulfides in dimethylformamide and hexamethylphosphoramide and in the solid state in ultramarine blue, green, and red. *Inorganic Chemistry*, 17: 3169-3174, 1978
- [30] J. ROLFE. Emission spectra of S_2^- , Se_2^- , and SeS^- ions in KI crystals. *The Journal of Chemical Physics*, 49: 4193-4197, 1968
- [31] G.J. VELLA and J. ROLFE. Zero-phonon absorption transitions in S_2^- and Se_2^- molecules dissolved in potassium iodide crystals. *The Journal of Chemical Physics*, 61: 41-47, 1974
- [32] T. CHIVERS. Ubiquitous trisulfur radical ion S_3^- . *Nature*, 252: 32-33, 1974
- [33] S. MORAN and G.B. ELLISON. Photoelectron spectroscopy of sulfur ions. *Journal of Physical Chemistry*, 92: 1794-1803, 1988
- [34] N.R. NIMLOS and G.B. ELLISON. Photoelectron spectroscopy of SO_2^- , S_3^- , and S_2O^- . *Journal of Physical Chemistry*, 90: 2574-2580, 1986
- [35] G. GANTEFÖR, S. HUNSICKER, and R.O. JONES. Prediction and observation of ring and chain isomers in S_n^- ions. *Chemical Physics Letters*, 236: 43-49, 1995
- [36] S. HUNSICKER, R.O. JONES, and G. GANTEFÖR. Rings and chains in sulfur cluster anions S_2 to S_9 2: Theory (simulated annealing) and experiment (photoelectron detachment). *The Journal of Chemical Physics*, 102: 5917-5936, 1995
- [37] F.A. COTTON, J.B. HARMON, and R.M. HEDGES. Calculation of the ground state electronic structures and electronic spectra of di- and trisulfide radical anions by the scattered wave-SCF-X α method. *Journal of the American Chemical Society*, 98: 1417-1424, 1976
- [38] C. HEINEMANN, W. KOCH, G.-G. LINDNER, and D. REINEN. Electronic spectrum of S_2^- , the electronic affinity of S_2 , and the binding energies of neutral and anionic S_3 clusters. *Physical Review A*, 52: 1024-1038, 1995
- [39] M.D. CHEN, M.L. LIU, L.S. ZHENG, Q.E. ZHANG, and C.T. AU. A density functional study for the isomers of anionic sulfur clusters S_n^- ($n=3-20$). *Chemical Physics Letters*, 350: 119-127, 2001

- [40] W. KOCH, J. NATTERER, and C. HEINEMANN. Quantum chemical study on the equilibrium geometries of S_3 and S_3^- , The electron affinity of S_3 and the low lying electronic states of S_3^- . *The Journal of Chemical Physics*, 102: 6159-6167, 1995
- [41] T. CHIVERS and I. DRUMMOND. Characterization of the trisulfur radical anion S_3^- in blue solutions of alkali polysulfides in hexamethylphosphoramide. *Inorganic Chemistry*, 11: 2525-2527, 1972
- [42] P. FREIVOGEL, J. FULARA, D. LESSEN, D. FORNEY, and J.P. MAIER. *Chem. Phys.*, 189: 335, 1994
- [43] R. ROSSETTI and L.E. BRUS. Waveguide propagation in frozen gas matrices. *Review of Scientific Instruments*, 51: 467-470, 1980
- [44] K. REBANE and L. REBANE. *Izv. Akad. Nauk est. S.S.R.*, 14: 309, 1995
- [45] K.P. HUBER and G. HERZBERG. *Constants of Diatomic Molecules*: Van Nostrand, New York, 1979
- [46] R. LINGUERRI, N. KOMIHA, J. FABIAN, P. ROSMUS, *Z. Phys. Chem.* 1: 1, 2008

CHAPTER 6. APPENDIX

C₆H₄

JOURNAL OF CHEMICAL PHYSICS

VOLUME 118, NUMBER 23

15 JUNE 2003

High-resolution electronic spectroscopy of a nonlinear carbon chain radical C₆H₄⁺

Mitsunori Araki,^{a)} Harold Linnartz,^{b)} Pawel Cias, Alexey Denisov, Jan Fulara, Anton Batalov, Ivan Shnitko, and John P. Maier
Department of Chemistry, Klingelbergstrasse 80, CH-4056 Basel, Switzerland

(Received 19 March 2003; accepted 27 March 2003)

A high-resolution gas-phase spectrum of a molecular absorption band around 604 nm is assigned as due to an electronic transition of a nonlinear C₆H₄⁺ planar species starting from its ²A'' electronic ground state. The spectrum is observed in direct absorption by cavity ringdown spectroscopy through a supersonic planar discharge through a mixture of acetylene in helium. The spectrum has a clear rotational and K-type structure. This allows an accurate determination of the B and C rotational constants and an estimate for the A rotational constant in ground and electronically excited states. The resolved spectrum of the fully deuterated species C₆D₄⁺ has been obtained as well. The results are compared both to the outcome of *ab initio* geometry optimizations and low-resolution absorption spectra in 6 K neon matrices obtained after mass-selective deposition. © 2003 American Institute of Physics. [DOI: 10.1063/1.1575736]

I. INTRODUCTION

In recent years many experimental studies have been reported presenting high-resolution spectra of pure and highly unsaturated carbon chain radicals. Microwave,¹ infrared,² and UV-VIS spectra^{3,4} are available both from matrix and gas-phase studies, all of them having in common that the major part of the observed geometries is linear. Even for very long chains, such as HC₂₂H (Ref. 5) and HC₁₇N (Ref. 6), linear structures have been found. Theoretical studies, however, predict for longer chains cyclic structures as well.⁷ In the case of C₁₃, for example, theory⁸ predicts a cyclic ground-state structure, but the experimentally observed IR spectrum is clearly that of a linear chain.⁹ A reason for this discrepancy might be simply that the experimental techniques—supersonic jet expansions or matrix deposition experiments—favor the production of linear species, because large-amplitude bending motions (that are necessary to close the ring) are frozen in the production process. A similar situation might apply to the interstellar medium, where many linear carbon chain species already have been identified and the number of cyclic structures is still rather limited.¹⁰

In this work the electronic spectrum of a member of a so-far-unstudied class of carbon chain radicals is presented: a nonlinear and noncyclic species. The spectrum was observed more or less accidentally around 604 nm when scanning for coincidences with diffuse interstellar band features in a hydrocarbon plasma. The observed spectrum has a clear rotational and K-type structure. Simulation of the spectrum allows an accurate determination of the molecular constants of the carrier. Study of the partially and completely deuterated species gives information on the number of (equivalent) hy-

drogen atoms. Final identification becomes possible following semiempirical and *ab initio* geometry optimizations for a number of species. These indicate that the band at 604 nm is due to the carbon chain cation C₆H₄⁺ with a nonlinear H-C≡C-C≡C-CH=CH₂⁺ planar molecular geometry. This is confirmed by the observation of their transition in the absorption spectrum obtained after mass-selective deposition of C₆H₄⁺ ions generated in a hydrocarbon plasma in a 6 K neon matrix.

Spectroscopic data for species of the form C₆H₄⁽⁺⁾ are so far missing. Only a photodissociation study has been reported in which C₆H₄⁺ was generated following a ring opening reaction in cyanobenzene.¹¹ In the latter study geometry optimizations are reported using MNDO calculations, which result in a series of equilibrium structures for the cation in which the heat formation of the possible acyclic structures is about 150 kJ mol⁻¹ lower than that of benzene-type structures. Among these is a geometry that is confirmed in the present study, a linear noncyclic structure that is very close to the geometry proposed for the neutral species: 1-hexene-3,5-diyne.^{12,13}

II. EXPERIMENT

The experimental method has been described and uses cavity ringdown (CRD) spectrometer sampling a supersonic planar plasma.¹⁴ The plasma is generated by a discharge through a gas pulse (-300 V, 30 Hz repetition rate) of a 0.5% C₂H₂ (and/or C₂D₂) in He mixture with a backing pressure of 10 bars in the throat of a 3 cm × 100 μm multilayer slit nozzle geometry. Rotational temperatures of the order of 20–40 K are routinely achieved. The nozzle is mounted in an optical cavity where the expansion is intersected approximately 2 mm downstream by the pulsed light of a tunable dye laser (resolution 0.15 cm⁻¹). The light leaking out of the cavity is detected with a photodiode, and the resulting ringdown event is used as input for a standard ringdown

^{a)} Author to whom correspondence should be addressed. Fax: +41 61 2673855. Electronic mail: mitsunori.araki@unibas.ch

^{b)} Present address: Department of Physical Chemistry, Vrije Universiteit, De Boelelaan 1083, NL 1081 HV Amsterdam, the Netherlands.

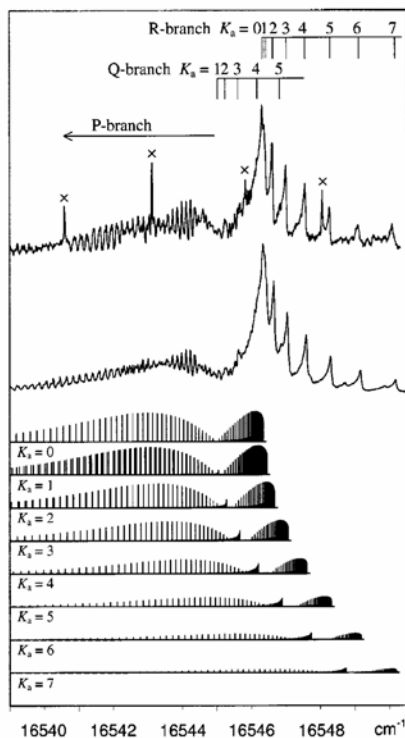


FIG. 1. Band observed at 604 nm using CRD spectroscopy through a supersonic planar plasma expansion. The rotational and K -type structure that is observed experimentally (top trace) can be simulated with a rotational temperature of 40 K, using constants derived from geometry optimizations for the nonlinear planar and noncyclic $C_6H_4^+$ carbon chain cation (second trace). The assignment is indicated in the figure and further illustrated by stick diagrams of each individual K_a . Lines marked with \times are due to another carrier.

analysis.¹⁵ A spectrum is recorded by determining an averaged ringdown time as a function of the laser frequency and calibrated by simultaneously recording an iodine spectrum.

III. RESULTS AND DISCUSSION

The CRD gas-phase spectrum of the band around 604 nm is shown in Fig. 1. A series of overlapping rotational transitions is observed as well as a K -type structure ($K=0-7$), typical for a nonlinear species. Using C_2D_2 instead of C_2H_2 yields a 67 cm^{-1} blueshifted spectrum with nearly identical spectral features, as shown in Fig. 2. This indicates that the carrier is of the form C_nH_m or $C_nH_m^{+/-}$.¹⁶ In order to determine the values for n and m , a C_2H_2/C_2D_2 mixture has been used. A low-resolution scan, in which mainly the strong peaks for $K=0$ and 1 will be visible, gives five broadbands including bands originating from fully H- ($16\,546\text{ cm}^{-1}$) and fully D- ($16\,613\text{ cm}^{-1}$) substituted species. Three remaining bands located at $16\,500\text{ cm}^{-1}$ (a), $16\,560\text{ cm}^{-1}$ (b), and $16\,595\text{ cm}^{-1}$ (c) are due to partially deuterated species. From this it can be concluded that $m=4$: the a, b, and c bands correspond to species with one, two, and three D

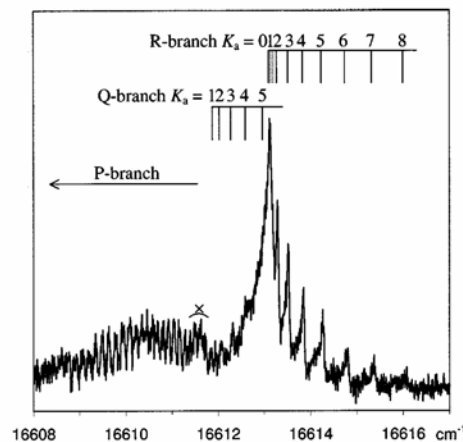


FIG. 2. Spectrum for the fully deuterated $C_6D_4^+$ species, blueshifted by approximately 67 cm^{-1} with respect to the $C_6H_4^+$ cation. Lines marked with \times are due to another carrier.

atoms, respectively. The one-, two-, and threefold-deuterated species should have four, six, and four peaks by statistical arguments, but three, four, and three peaks are observed. This indicates that two of the four hydrogen atoms are rather similar.

The rotational analysis of the spectra with C_2H_2 and C_2D_2 as precursors allows the determination of the number of carbon atoms (n) in the chain. The stick diagrams (Fig. 1) show how the observed spectrum can be dissected into rotational transitions belonging to individual K values. The P branch consists of a series of transitions that are closely overlapping, causing some fluctuations in overall intensity, but which give a good indication for the value of B'' (C''). The change in rotational constants upon electronic excitation is reflected by a change of line distances, particularly for higher J levels on the P branch and gives values for B' (C'). The R -branch region consists of a series of unresolved bands with clear bandheads corresponding to $K=0-7$ as indicated in Fig. 1. The distance between the bandheads is a good indication for the value $\Delta A - \Delta B = (A'' - A') - (B'' - B')$, and the intensity ratio can be used to estimate A'' . The Q -branch bands are rather weak and cannot be assigned directly. The overall pattern indicates a rotational temperature of the order of 40(5) K.

The spectra of $C_nH_4^{(+)}$ ($C_nD_4^{(+)}$) can now be rather well reproduced with rotational B and C constants of the order of 0.045 cm^{-1} (0.040 cm^{-1}) and an A constant of approximately 1.2 cm^{-1} (0.9 cm^{-1}) using WANG.¹⁷ In view of the available constants for different kinds of carbon chain radicals determined in previous studies¹⁸⁻²⁰ this makes it very likely that $n=6$ or 7. Therefore possible equilibrium structures have been calculated for isomers of $C_6H_4^{(+)}$ and $C_7H_4^{(+)}$ (and fully deuterated isotopes) using MOPAC (Ref. 21) (PM3/UHF). The structure that gets closest to the observations is that of the nonlinear chain $H-C\equiv C-C\equiv C-CH=CH_2^+$ (Fig. 3) for which $A''=1.230\text{ cm}^{-1}$, $B''=0.0465\text{ cm}^{-1}$, and $C''=0.0448\text{ cm}^{-1}$. This struc-

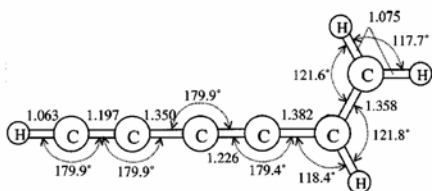


FIG. 3. Optimized molecular structure of C₆H₄⁺ using *ab initio* calculations. The bond lengths are given in Å.

ture corresponds to one of the geometries calculated in Ref. 11 and is close to the previously proposed geometry of the neutral C₆H₄. Other isomeric structures yield sets of substantially different constants, particularly for the fully deuterated species, whereas the corresponding D-C≡C-C≡C-CD=CD₂⁺ gives $A''=0.889$ cm⁻¹, $B''=0.0414$ cm⁻¹, and $C''=0.0395$ cm⁻¹, close to the simulated values for the spectrum observed here.

In order to improve the geometry optimization *ab initio* calculations have been performed using GAMESS.²² In previous work ROHF/6-31G** calculations have been reported on the isomerization of C₄H₄ radical cations.²³ An identical method is applied here to C₆H₄⁺. Rotational constants of C₆H₄⁺ were determined using the *ab initio* optimized structure with bond lengths and angles as indicated in Fig. 3. The resulting constants are summarized in Table I and are close to the MOPAC results, as may be expected. The simulated spectrum, using the *ab initio* results, is plotted in Fig. 1 both as stick diagrams for individual K values and as an overall spectrum with an assumed resolution of 0.05 cm⁻¹. The calculated and observed spectra match very well apart from minor intensity deviations and a few lines that may belong to another carrier.

At this stage, however, two points remain unclear. First, it is not possible to discriminate between the neutral and cationic species from the rotational analysis alone. However, the neutral C₆H₄ is a closed-shell system and as a consequence it is unlikely that a strong electronic band is found at

TABLE I. Observed and calculated molecular constants of C₆H₄⁺ and C₆D₄⁺.

	C ₆ H ₄ ⁺		C ₆ D ₄ ⁺	
	Obs. ^a	<i>Ab initio</i> ^b	Obs. ^a	<i>Ab initio</i> ^b
A''	1.24	1.217	0.89	0.889
B''	0.0467	0.0471	0.0416	0.0420
C''	0.0449	0.0453	0.0400	0.0401
$A'-A''$			0.0767	0.0450
$B'-B''$			0.0452	0.0403
$C'-C''$			0.0434	0.0387
$(A'-A'')-(B'-B'')$ ^c			0.0782	0.0463
T_{00}	16 544.980		16 611.91	

^aExpected errors of the rotational constants are 0.1 cm⁻¹ in A and 0.001 cm⁻¹ in B and C , whereas 0.0006 cm⁻¹ and 0.001 cm⁻¹ for $B-C$ and $(A'-A'')-(B'-B'')$. Expected errors of T_{00} are 0.01 cm⁻¹ for C₆H₄⁺ and 0.1 cm⁻¹ for C₆D₄⁺.

^bEquilibrium values.

^cAssuming $B'-B''=C'-C''$.

a rather low energy of 604 nm. In this case electronic transitions are expected in the UV. Indeed, the experimental conditions are in favor of a charged species. Second, it is not clear whether the band observed here is the origin band or a band that involves excitation of a vibrational mode in the upper electronic state—even though such bands are generally rather weak;³ i.e., the origin band may be redshifted by a few thousands cm⁻¹. The change in rotational constants upon electronic excitation is minor and reflects a small elongation of the molecule in the upper electronic state. It is hard to conclude from these values that no vibrational excitation is involved. However, the present band is close to the well-studied and closely related $A^2\Pi_g-X^2\Pi_u$ electronic origin band transition of the linear triacetylene cation (C₆H₂⁺) that has been located at 600 nm.²⁴ In analogy with the latter system, which is due to a transition from a $\cdots\pi_g^4\pi_u^3$ to a $\cdots\pi_g^3\pi_u^4$ configuration, it is very likely that the upper state of the observed band of the nonlinear C₆H₄⁺ will have $^2A''$ symmetry. In this case the origin band of C₆H₄⁺ is expected to be rather close to that of C₆H₂⁺, as is observed.

Proof comes from a mass-selective matrix study that was performed following the gas phase analysis. This experiment combines mass selection and matrix isolation spectroscopy and has been described.²⁵ The C₆H₄⁺ (C₆D₄⁺) cations were produced from a phenylacetylene–deuterated-2,4-hexadiyne– helium mixture in a hot cathode discharge source. A 90° deflector and a quadrupole mass spectrometer are used to steer the ion beam onto the matrix, where the mass-selected ions are codeposited with excess of neon at 6 K. The absorption spectra are recorded by guiding monochromatized light (0.1 nm bandpass) through the matrix onto a photomultiplier. The resulting spectra for matrices prepared with mass of C₆H₄⁺ or C₆D₄⁺ are shown in Fig. 4. Two strong bands are observed, one around 609 nm and one around 585 nm, for C₆H₄⁺. No strong bands are observed to lower energy; i.e., the band at 609 nm corresponds to the origin band. The main structures to the blue of the dominant peaks (609 nm for C₆H₄⁺ and 606 nm for C₆D₄⁺) are matrix artifacts, site structure. The 114 cm⁻¹ blueshift of the gas-phase spectrum with respect to the matrix band at 609 nm is typical for a chain of this size and in this frequency regime.³ The band at 585 nm is due to another isomer of C₆H₄⁺, since the relative intensity of the two bands varies strongly with different precursors. Upon deuteration the band at 609 nm shifts by 62(3) cm⁻¹ to the blue—i.e., close to the 67 cm⁻¹ shift observed in the gas phase upon deuteration. The band observed at 585 nm in the matrix only shifts 17(3) cm⁻¹ upon deuteration. Subsequent neutralization of the trapped species by irradiation of the matrix with a medium-pressure mercury lamp leads to the disappearance of both bands. This confirms that the carrier of the 609 nm matrix and the 604 nm gas-phase carrier is a C₆H₄⁺ cation, as was concluded from the gas-phase spectrum.

IV. ASTROPHYSICAL RELEVANCE

All the spectroscopic information is in favor of the identification of the band observed at 604 nm as due to the $^2A''-X^2A''$ electronic origin band transition of the nonlinear

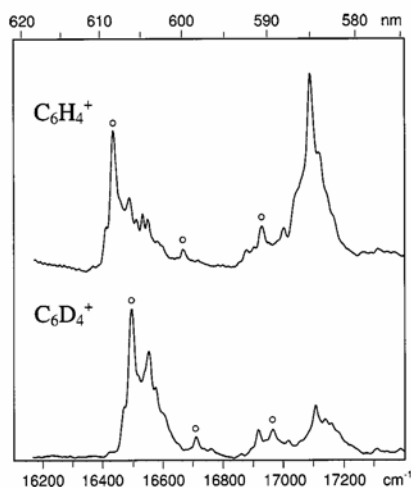


FIG. 4. Electronic absorption spectra of C₆H₄⁺ (upper trace) and C₆D₄⁺ (lower trace) measured in 6 K matrices after codeposition of mass-selected cations with excess of neon. The bands at 609 nm of C₆H₄⁺ and at 606 nm of C₆D₄⁺ correspond to the gas-phase spectra shown in Figs. 1 and 2. The weaker bands at 600 and 591 nm for C₆H₄⁺ and 599 and 590 nm for C₆D₄⁺ (indicated by ○) exhibit an identical chemical behavior as the 609 nm band on C₆H₄⁺ and the 606 nm band on C₆D₄⁺ and are due to transitions to vibrationally excited levels in the upper ²A' state. The bands at 585.3 and 584.7 nm of C₆H₄⁺ and C₆D₄⁺ are due to another isomer.

planar H-C≡C-C≡C-CH=CH₂⁺ carbon chain cation. The inferred rotational constants may guide a search for this species by millimeter-wave spectroscopy to allow a more accurate geometry determination. This is of interest as the number of microwave studies of carbon chain cations is still rather limited.²⁶ It furthermore would make a radio-astronomical search for this species in dense interstellar clouds possible. The optical spectrum obtained here allows a comparison with the available lists of diffuse interstellar

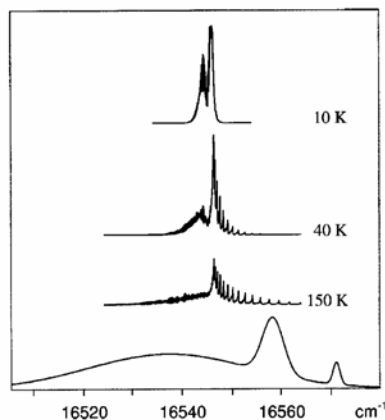


FIG. 5. Artificial DIB spectrum (Ref. 27) in the 604 nm range (lowest trace) and the simulated C₆H₄⁺ spectra for 10, 40, and 150 K (upper three traces).

band (DIB) positions.^{27,28} A comparison with the hitherto reported DIBs shows that there exists an overlap between the band observed around 16 545 cm⁻¹ and a broad DIB [full width at half maximum (FWHM) ~14 cm⁻¹] reported at 16 537.3 cm⁻¹. In order to check whether this discrepancy of 8 cm⁻¹ might be due to a temperature effect, a comparison has been made between an artificial DIB spectrum in the 604 nm range and the C₆H₄⁺ spectrum for low (10 K), intermediate (40 K), and high (150 K) temperatures (Fig. 5). Although it is clear that for higher temperatures the spectrum of the nonlinear C₆H₄⁺ might start filling up the broadband around 16 545 cm⁻¹, it is hard to account for the difference in intensity of the *P* and *R* branches. This is not reflected in the DIB spectrum.

ACKNOWLEDGMENTS

This work has been supported by the Swiss National Science Foundation (Project No. 20-63459.00). M.A. thanks the Foundation for Promotion of Astronomy in Japan, and H.L. thanks FOM (Fundamenteel Onderzoek der Materie).

- ¹M. C. McCarthy and P. Thaddeus, *Chem. Soc. Rev.* **30**, 177 (2001).
- ²A. van Orden and R. J. Saykally, *Chem. Rev.* **98**, 2313 (1998).
- ³J. P. Maier, *J. Phys. Chem. A* **102**, 3462 (1998).
- ⁴H. Linnartz, D. Pfluger, O. Vaizert, P. Cias, P. Birza, D. Khoroshev, and J. P. Maier, *J. Chem. Phys.* **116**, 924 (2002) and references therein.
- ⁵T. Pino, H. B. Ding, F. Guthe, and J. P. Maier, *J. Chem. Phys.* **114**, 2208 (2001).
- ⁶M. C. McCarthy, J. U. Grabow, M. J. Travers, W. Chen, C. A. Gottlieb, and P. Thaddeus, *Astrophys. J. Lett.* **494**, L231 (1998).
- ⁷K. Aoki and S. Ikuta, *J. Mol. Struct.: THEOCHEM* **310**, 229 (1994).
- ⁸J. M. L. Martin, J. P. Francois, R. Gijbels, and J. Almlöf, *Chem. Phys. Lett.* **187**, 367 (1991).
- ⁹T. F. Giesen, A. Vanorden, H. J. Hwang, R. S. Fellers, R. A. Provencal, and R. J. Saykally, *Science* **265**, 756 (1994).
- ¹⁰P. Thaddeus and M. C. McCarthy, *Spectrochim. Acta, Part A* **57**, 757 (2001).
- ¹¹W. J. van der Hart, E. Oosterveld, T. A. Molenaar-Langeveld, and N. M. M. Nibbering, *Org. Mass Spectrom.* **24**, 59 (1989).
- ¹²C. A. Arrington, C. Ramos, A. D. Robinson, and T. S. Zwier, *J. Phys. Chem. A* **103**, 1294 (1999).
- ¹³T. Böhm-Gossel, W. Hunsmann, L. Rohrschneider, W. Schneider, and M. Ziegenbein, *Chem. Ber.* **96**, 2504 (1963).
- ¹⁴T. Motylewski and H. Linnartz, *Rev. Sci. Instrum.* **70**, 1305 (1999).
- ¹⁵A. O'Keefe and D. A. G. Deacon, *Rev. Sci. Instrum.* **59**, 2544 (1998).
- ¹⁶The density of anions in the plasma is generally low, and therefore these are not considered.
- ¹⁷D. Luckhaus and M. Quack, *Mol. Phys.* **63**, 745 (1989).
- ¹⁸P. Cias, O. Vaizert, A. Denisov, J. Mes, H. Linnartz, and J. P. Maier, *J. Phys. Chem. A* **106**, 9890 (2002).
- ¹⁹H. Linnartz, D. Pfluger, O. Vaizert, P. Cias, P. Birza, D. Khoroshev, and J. P. Maier, *J. Chem. Phys.* **116**, 924 (2002).
- ²⁰M. C. McCarthy, M. J. Travers, A. Kovacs, C. A. Gottlieb, and P. Thaddeus, *Astrophys. J.* **113**, 105 (1997).
- ²¹J. P. Stewart, computer code MOPAC, a semiempirical molecular orbital program, QCPE, 455, 1983; version 6.0, 1990.
- ²²M. W. Schmidt, K. K. Baldrige, J. A. Boatz, et al. *J. Comput. Chem.* **14**, 1347 (1993).
- ²³G. Koster and W. J. van der Hart, *Int. J. Mass Spectrom. Ion Processes* **163**, 169 (1997).
- ²⁴M. Allan, E. Kloster-Jensen, and J. P. Maier, *Chem. Phys.* **17**, 11 (1976).

J. Chem. Phys., Vol. 118, No. 23, 15 June 2003

Spectroscopy of a carbon chain 10565

²⁵P. Freivogel, J. Fulara, D. Lessen, D. Forney, and J. P. Maier, Chem. Phys. **189**, 335 (1994).

²⁶C. A. Gottlieb, A. J. Apponi, M. C. McCarthy, P. Thaddeus, and H. Linartz, J. Chem. Phys. **113**, 895 (2000).

²⁷P. Jenniskens and F.-X. Désert, Astron. Astrophys., Suppl. Ser. **106**, 39 (1994).

²⁸S. Ó. Tuairisg, J. Cami, B. H. Foing, P. Sonnentrucker, and P. Ehrenfreund, Astron. Astrophys., Suppl. Ser. **142**, 225 (2000).

B₃

Available online at www.sciencedirect.com

SCIENCE @ DIRECT®

Chemical Physics Letters 404 (2005) 315–317

CHEMICAL
PHYSICS
LETTERS

www.elsevier.com/locate/cplett

The near infrared $1^2A_2'' \leftarrow X^2A_1'$ electronic transition of B₃ in a neon matrix

Anton Batalov, Jan Fulara¹, Ivan Shnitko, John P. Maier**Department of Chemistry, University of Basel, Klingelbergstrasse 80, CH-4056 Basel, Switzerland*

Received 9 January 2005

Abstract

The $1^2A_2'' \leftarrow X^2A_1'$ electronic transition of the B₃ molecule with origin band at 5990 cm^{-1} has been observed in a 6 K neon matrix. A vibrational progression in the spectrum corresponds to the excitation of the $\nu_1(a_1')$ vibrational mode in the $1^2A_2''$ state with a frequency of $\sim 1092\text{ cm}^{-1}$. The band system was detected after laser ablation of a boron rod and the origin band also after mass-selected deposition of B₃⁻ anions with subsequent neutralization.

© 2005 Elsevier B.V. All rights reserved.

1. Introduction

Structure and properties of boron clusters are interesting for fundamental science. Boron is the only element except carbon that can build molecules of any size by covalent bonds, and there are a number of applications [1,2]. Nevertheless, even molecules as small as B₃ are spectroscopically not thoroughly investigated. The first study of B₃ was by ESR [3] followed by IR spectroscopy [4] both in rare gas matrices. A previous publication reported the $1^2E' \leftarrow X^2A_1'$ and $2^2E' \leftarrow X^2A_1'$ electronic transitions of B₃ in a 6 K neon matrix [5]. The rotationally resolved origin band of the $2^2E' \leftarrow X^2A_1'$ transition has been measured since then in absorption in the gas phase and analyzed [6]. Ab initio calculations on the ground and excited electronic states of B₃ are available [5,7]. In the present work the $1^2A_2'' \leftarrow X^2A_1'$ electronic transition of B₃ has been observed for the first time in a 6 K neon matrix.

2. Experimental

The main features of the experimental set up have been described [8]. Two approaches were used to produce boron clusters: one with a cesium sputter ion source and the other by laser ablation. Boron rod (99.6% purity) with a natural isotopic composition was used as a target for the laser vaporization. B₄C, LaB₆ and BN rods were used as well.

A slowly rotating sample rod was installed $\sim 10\text{ cm}$ from the matrix substrate. A 532-nm pulsed Yag laser beam, $\sim 20\text{ mJ}$, 20 Hz, was focused on the rod. A mixture of ionic and neutral ablation products was co-deposited with excess of neon (or argon) onto a sapphire substrate coated with rhodium and cooled to a temperature of 6 K. Spectra in the $1100\text{--}12000\text{ cm}^{-1}$ range were recorded after sampling the neon matrix by a Fourier transform spectrometer applying a double reflection technique. The light beam reflects from the metal surface of the substrate on which the neon matrix sits, then from a mirror into the matrix again and back from the substrate. Absorption spectra in the 220–1100 nm region have been measured by passing monochromatic light through the matrix in a wave-guide manner [9].

* Corresponding author. Fax +41 61 267 38 55.

E-mail address: j.p.maier@unibas.ch (J.P. Maier).

¹ Permanent address: Institute of Physics, Polish Academy of Sciences, Al.Lotnikow 32-46, Pl-02668 Warsaw, Poland.

In order to assign the observed band system, experiments with mass-selected boron anions, produced in a cesium sputter source [10] have been carried out. The anions produced in the source were guided by means of electrostatic lenses into the quadrupole mass filter and were separated from neutral molecules by deflecting the beam through 90°. The B₃⁻ ions were mass selected and co-deposited with excess of neon to form a matrix at ~6 K. A typical current of B₃⁻ impinging on the matrix was ~5 nA. This technique allowed the deposition of B₃⁻ exclusively but it was not possible to obtain a high concentration of neutral B₃ in the matrix.

Neutral B₃ was produced by irradiation of the matrix with a mercury medium pressure lamp during ~30 min. An important procedure was annealing up to 8.5 K making the neon matrix softer and thus allowing relaxation of the trapped molecules to their energetic minima (and even some reactions to proceed).

3. Observations

Several new bands were seen after laser vaporization of the boron rod in the infrared (Fig. 1), in addition to the previously reported 1²E' ← X²A₁' and 2²E' ← X²A₁' absorption systems of the B₃ molecule [5,6] and those of the B and B₂ species [11–13] in the visible and UV. The new system comprises three peaks, separated by ~1092 cm⁻¹, with origin band at 5990 cm⁻¹ (Table 1). This was seen after vaporization of B₄C and LaB₆ rods as well. The intensity of the bands increases after irradiation of the matrix with UV photons indicating a neutralization process. Thus one can conclude that the carrier is a neutral boron molecule. The band system is not likely due to a boron and hydrogen (common

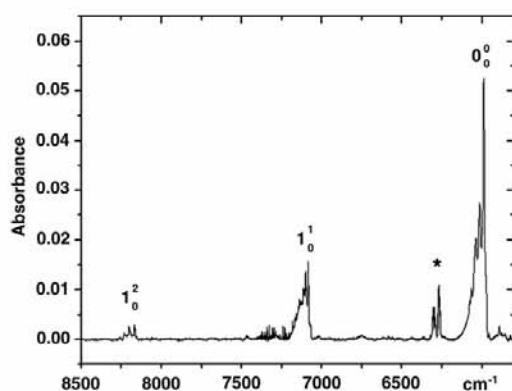


Fig. 1. The 1²A₂' ← X²A₁' electronic absorption spectrum of B₃ in a 6 K neon matrix after laser vaporization of a pure boron rod. The band marked with * is due to an unknown impurity.

Table 1
Positions of the band maxima (±0.2 cm⁻¹) in the 1²A₂' ← X²A₁' electronic transition of B₃ in a 6 K neon matrix

ν (cm ⁻¹)	$\Delta\nu$ (cm ⁻¹)	Vibrational transition
5990	0	0 ₀ ⁰
7085	1095	1 ₀ ¹
8169	2179	2 ₀ ²

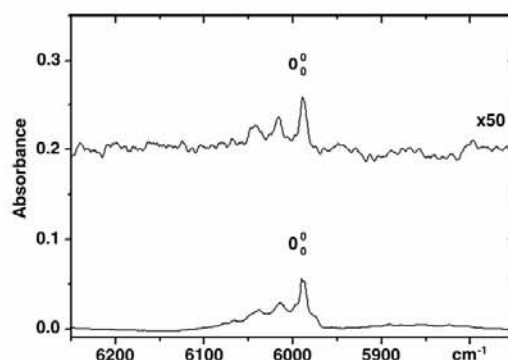


Fig. 2. The origin band of the 1²A₂' ← X²A₁' electronic absorption of B₃ in a 6 K neon matrix after laser vaporization of a pure boron rod (lower trace), and after mass-selected deposition of B₃ with subsequent neutralization by UV irradiation (upper trace multiplied by a factor of 50 and smoothed).

impurity) containing species. When 1% of hydrogen was introduced into the matrix (Ne/H₂ ratio of 100/1) the intensity of bands remained the same. The absorption band at 6268 cm⁻¹ (marked with *) is due to an unknown impurity. Its intensity depended on the rod used.

Fine structure of the bands is due to matrix site effects. The trapped molecules have different orientations in the neon lattice. One can see that the three bands of the new system possess the same structure. After annealing to 8.5 K intensity redistribution is observed. The site-pattern is different when argon is used as the matrix.

Mass selected deposition of B₃⁻ followed by neutralization led also to the appearance of the 5990 cm⁻¹ absorption band (Fig. 2). The wavelength of the band and the site structure are exactly the same as in the laser vaporization spectrum. However, the intensity is about 50 times lower for the mass selected case. The bands at 7085 and 8169 cm⁻¹ corresponding to vibrational excitation in the upper electronic state were not observed in the mass-selected experiment due to a low signal to noise ratio. It is concluded that the observed system with the origin band at 5990 cm⁻¹ is an electronic transition of B₃.

4. Discussion

It is theoretically established that B₃ has an equilateral triangle structure (D_{3h} group) with ²A₁' symmetry in the ground state with electronic configuration (1a₁')²(1e')⁴(1a₂')²(2a₁')¹ [5,7,14]. The only excited states accessible from the ground state by electric dipole transitions are ²A₂' and ²E'. The electronic transitions 1²E' ← X²A₁' and 2²E' ← X²A₁' of B₃ in a neon matrix have been studied earlier [5]. The ab initio calculations predict that the transition to the lowest excited state with ²A₂' symmetry lies at ~6300 cm⁻¹; in an earlier calculation 7000 cm⁻¹ was obtained [7]. These are energetically in good agreement with the observed origin band (Fig. 1). Consequently the new absorption system is assigned to the 1²A₂' ← X²A₁' dipole-allowed electronic transition of B₃.

B₃⁻ has been studied by photoelectron spectroscopy [14] giving the vertical detachment energies of 2.82 and 3.56 eV to the B₃ final states X²A₁' and 1²A₂'. The 0.74 eV (~6000 cm⁻¹) difference between these is also in agreement with the present observations.

Equilateral triangular B₃ molecule has two normal vibrations: a₁' and e'. Only transitions to the totally symmetric vibrational levels of the upper state (1²A₂') are allowed from the X²A₁' ground state, the solely populated level at 6 K. Hence the bands at 7085 and 8169 cm⁻¹ (Table 1) are assigned as the first two members of the progression structure associated with the a₁' normal mode excitation in the upper 1²A₂' state. The ν₁(a₁') frequency is thus inferred to be 1092 ± 3 cm⁻¹, in agree-

ment with the analysis of the photoelectron spectrum [14] of B₃⁻ which yielded the value 1130 ± 30 cm⁻¹.

Acknowledgments

This study was supported by the Office of Aerospace Research and Development and the Swiss National Science Foundation (Project 200020-100019/1).

References

- [1] R.N. Grimes, *J. Chem. Ed.* 81 (2004) 658.
- [2] L.H. Hanley, J.L. Whitten, S.L. Anderson, *J. Am. Chem. Soc.* 92 (1988) 5803.
- [3] Y.M. Hamrick, R.J. Van Zee, W.J. Weltner, *J. Chem. Phys.* 96 (1992) 1767.
- [4] S. Li, R.J. Van Zee, W.J. Weltner, *Chem. Phys. Lett.* 262(1996) 298.
- [5] M. Wyss, E. Riaplov, A. Batalov, J.P. Maier, T. Weber, W. Meyer, P. Rosmus, *J. Chem. Phys.* 119 (2003) 9703.
- [6] P. Cias, M. Araki, A. Denisov, J.P. Maier, *J. Chem. Phys.* 121 (2004) 6776.
- [7] R. Hernandez, J. Simons, *J. Chem. Phys.* 94 (1991) 2961.
- [8] J.P. Maier, *Chem. Soc. Rev.* 26 (1997) 21.
- [9] V.E. Bondybey, T.J. Sears, J.H. English, T.A. Miller, *J. Chem. Phys.* 73 (1980) 2063.
- [10] D. Forney, J. Fulara, P. Freivogel, M. Jakobi, D. Lessen, *J. Chem. Phys.* 103 (1995) 48.
- [11] W.R.M. Graham, W. Weltner, *J. Chem. Phys.* 65 (1976) 1516.
- [12] S. Tam, M. Macler, M.E. DeRose, M.E. Fajardo, *J. Chem. Phys.* 113 (2000) 9067.
- [13] P.J. Bruna, J.S. Wright, *J. Phys. B: At. Mol. Opt. Phys.* 23 (1990) 2197S.
- [14] H.-J. Zhai, L.-S. Wang, A.N. Alexandrova, A.I. Boldyrev, V.G. Zakrzewski, *J. Phys. Chem. A* 107 (2003) 9319.

C_NCl (N=5,6)

J. Phys. Chem. A 2004, 108, 4219–4223

4219

Electronic Absorption Spectra of C_nCl Radicals (n = 5, 6) and Their Cations in Neon MatricesJennifer van Wijngaarden,[‡] Anton Batalov,[‡] Ivan Shnitko,[‡] Jan Fulara,^{‡,§} and John P. Maier^{*,§}

Department of Chemistry, University of Basel, Klingelbergstrasse 80, CH-4056 Basel, Switzerland, and Instytut Fizyki Polskiej Akademii Nauk, Al. Lotników 32-46, 02-668 Warsaw, Poland

Received: January 8, 2004; In Final Form: March 4, 2004

Electronic absorption spectra of C₆Cl, C₆Cl⁺, C₅Cl, and C₅Cl⁺ have been recorded in 6 K neon matrices. The bands observed are assigned to the B ²Π ← X ²Π electronic transition of C₆Cl, ³Σ⁻ ← X ³Σ⁻ of C₆Cl⁺, and ¹Σ⁺ ← X ¹Σ⁺ of C₅Cl⁺ with band origins at 545.8, 527.4, and 226.1 nm, respectively. Two electronic band systems are apparent for C₅Cl and these are tentatively assigned to a ²Π ← X ²Π transition with a band origin at 247.1 nm and to Σ⁺ ← X ²Π at 532.3 nm. For each of the four molecules, several transitions due to the excitation of vibrational modes in the excited electronic states are observed. The spectral assignments in each case are based upon the observation of clear, vibronic progressions with appropriate spacing for C–C and C–Cl stretching modes and by comparison with the absorption spectra of the isoelectronic sulfur-terminated carbon chains.

Introduction

A number of neutral and ionic carbon chain molecules have been studied by experimentalists and theoreticians due to their proposed roles as intermediates in various terrestrial chemical reactions and their established presence in circumstellar and interstellar bodies.¹ Laboratory-based rotational spectra have proved integral to the identification of these molecules and their electronic spectra may finally lead to the assignment of the carriers of the diffuse interstellar bands. In recent years, carbon chains terminated by second row elements, such as Si, P, and S, have received increasing attention since several short chains of this type have been positively identified in space.²

Chlorine-terminated carbon chains are also candidates for astronomical detection, although to date, the only chlorine-containing molecules to be observed are (HCl)³ and a small number of metal chlorides (AlCl, NaCl, and KCl)⁴ in interstellar and circumstellar environments, respectively. The formation of C–Cl bonds under interstellar conditions is thought to be feasible by reaction of HCl with C⁺ or by reaction of H₂Cl⁺ with C to produce CCl⁺ in both cases.^{5,6} It has been proposed, on the basis of an ab initio study,⁷ that the product of the latter reaction is actually HCCl⁺, which is a precursor of the CCl dimer. More recently, ab initio calculations have predicted the formation of the triatomic chain C₂Cl by dissociative recombination of HC₂Cl⁺ formed via the reaction of C₂H⁺ and HCl.⁸ As a result of these studies, it is expected that these molecules, along with longer C_nCl chains and their corresponding ions, are promising candidates for interstellar observation.

To date, the CCl radical is the most extensively studied of these species in the laboratory and spectra have been reported in the microwave,⁹ infrared,^{10–12} and ultraviolet regions.^{13–15} Emission spectra of the CCl⁺ cation have also been reported¹⁶ and rotationally analyzed.¹⁷ The triatomic radical C₂Cl was

recently investigated by using a combination of microwave spectroscopy and ab initio calculations.¹⁸ The results of this study support the presence of strong vibronic coupling between the ground (²Σ⁺) and first excited (²Π) electronic states resulting in a bent molecular geometry. Earlier ab initio calculations similarly predicted a small energy separation for the two lowest states but had their ordering reversed.^{19,20}

Recently, ground-state electronic structures and vibrational frequencies have been estimated for the C_nCl, C_nCl⁺, and C_nCl⁻ (n = 1–7) series, using DFT (B3LYP).^{21,22} For all but C₃Cl, the lowest energy structures are predicted to be linear or quasilinear chains terminated on one end by the chlorine atom. In the case of C₃Cl, geometry optimization calculations suggest that the ground-state structure is a cyclic triatomic carbon ring with an exocyclic chlorine (²B₂) although quasilinear (²A₁) and linear (²Π) structures lie approximately 12 kJ/mol higher in energy.²³ For the larger species, the calculated C–C bond distances suggest that the most important valence structures are cumulenic although the observation of bond length alternation suggests that polyynic ones also contribute. For each of the C_nCl neutral species, the ground state corresponds to a doublet state electronic configuration and the lowest lying quartet state is more than 150 kJ/mol higher in energy. The n-even C_nCl⁺ cations have triplet ground states while the n-odd clusters are singlets. The C_nCl⁻ anions are characterized by singlet ground states for all values of n (with the exception of CCl which is ³Σ) although the n-odd species also possess low-lying triplet states. Furthermore, a pattern of alternating stability of the molecules was reported depending on the parity of n. For the C_nCl⁺ cations, the n-odd chains are predicted to be more stable than the n-even ones, while for the neutral and anionic counterparts, the trend is reversed. These results can be rationalized in terms of the corresponding electronic configurations (orbital occupancies). Spectroscopic investigations of chlorine-terminated carbon molecules thus provide a useful test of these theoretical predictions, and furthermore, a comparison with known spectra of carbon chains with other second row

* Corresponding author. E-mail: j.p.maier@unibas.ch. Phone: +41 61 267 38 26. Fax: +41 61 267 38 55.

[‡] University of Basel.

[§] Instytut Fizyki Polskiej Akademii Nauk.

4220 *J. Phys. Chem. A, Vol. 108, No. 19, 2004*

van Wijngaarden et al.

elements at the end may establish interesting periodic trends in their molecular properties.

In this paper, we report the first spectroscopic study of C₅Cl and C₆Cl and their cations, C₅Cl⁺ and C₆Cl⁺, using mass-selective neon matrix isolation spectroscopy. The band assignments of each molecule are based upon the observation of clear vibronic progressions of C–C and C–Cl excited state stretching modes which are slightly smaller than those predicted for the ground state from ab initio calculations as expected.²¹ The spectral assignments are further verified through comparison with the bands reported earlier for the isoelectronic C_nS and C_nS⁻ species (n = 5, 6).²⁴

Experimental Section

The electronic absorption spectra of the C_nCl and C_nCl⁺ (n = 5, 6) species were recorded following mass-selective deposition in neon matrices.²⁵ A gas mixture containing the appropriate precursor was prepared by passing helium over a heated sample of solid C₆Cl₆ or liquid C₅Cl₆. From these respective mixtures, a series of C₆Cl_m⁺ and C₅Cl_m⁺ cations were produced, along with the corresponding neutral and anionic species, using a hot cathode discharge source, and the cation beam was focused and directed into a quadrupole mass filter by using a series of electrostatic lenses.²⁶ The singly chlorinated carbon cations were mass-selected and ion currents of 25 and 18 nA were obtained for C₆Cl⁺ and C₅Cl⁺, respectively. The cations were deposited simultaneously with neon on a rhodium-coated sapphire substrate over a period of 3 h to produce a 6 K matrix. The sample was irradiated with monochromatic light from halogen and xenon arc lamps with beams running parallel to the substrate surface. The absorption spectra of the trapped species were recorded between 220 and 1100 nm, using photomultiplier and silicon diode detectors. Following exposure to UV light (~5.4 eV) from a medium-pressure mercury lamp, the same spectral region was rescanned to identify the absorptions of the corresponding neutral species, C₆Cl and C₅Cl. During co-deposition of neon and the mass-selected cations, positive charge is quickly built up in the matrix and subsequent cations are repelled. These cations collide with nearby metal surfaces and liberate electrons which are electrostatically attracted toward the positively charged neon matrix and recombine with the cations to form neutral molecules. These electrons also form weakly bound anions with impurity molecules in the matrix. After UV irradiation, the electrons are photodetached from these weakly bound anions and neutralize the remaining cations.

Results and Discussion

(a) **C₆Cl and C₆Cl⁺.** After mass selection, C₆Cl⁺ was co-deposited with an excess of neon to form a 6 K matrix and the electronic absorption spectrum of this sample was subsequently recorded. As shown in Figure 1, two clear vibronic band systems are observed in the visible spectral range between 470 and 570 nm. The higher energy band system disappeared after irradiation with UV light and is consequently attributed to the C₆Cl⁺ cation. The remaining band system is assigned to the C₆Cl neutral.

For linear C₆Cl, the ground-state electronic configuration is doublet X ²Π...5π³ and electronic excitation to the first excited state involves promotion of an electron from a lower energy orbital to the 5π orbital. In the case of the linear C₆Cl⁺ cation, the ground state is described by a triplet X ³Σ⁻...5π² electronic configuration and the first excited state is likewise expected to involve excitation to the 5π orbital. The electronic absorption spectra corresponding to the lowest energy transitions of both C₆Cl and C₆Cl⁺ are therefore expected to arise from electronic

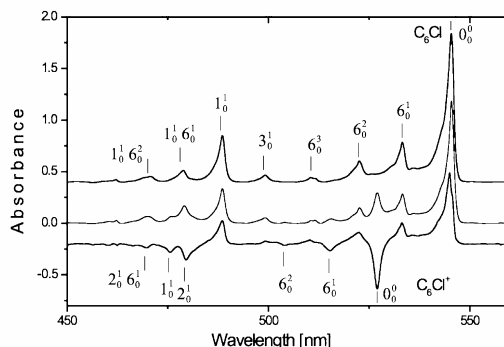


Figure 1. Electronic absorption spectra of the B ²Π ← X ²Π electronic transition of C₆Cl and the ³Σ⁻ ← X ³Σ⁻ electronic transition of C₆Cl⁺ recorded in a 6 K neon matrix. The upper trace shows the bands which remain after UV irradiation of the sample which are assigned to the C₆Cl neutral radical. The middle trace is the spectrum of the same sample before UV irradiation and contains absorptions due to both the neutral and cationic species. The lower trace is the difference between the first two traces multiplied by a factor of 2 for better visualization. The peaks which point downward are those that vanish after UV exposure and are thus attributed to C₆Cl⁺.

TABLE 1: Positions of the Band Maxima (±0.2 cm⁻¹) Observed for the B ²Π ← X ²Π Electronic Transition of C₆Cl in a 6 K Neon Matrix

λ/nm	$\tilde{\nu}/\text{cm}^{-1}$	$\Delta\tilde{\nu}/\text{cm}^{-1}$	assignment
545.8	18322		0 ₀ ⁰
533.7	18737	415	6 ₀ ¹
523.0	19120	798	6 ₀ ²
510.9	19573	1251	6 ₀ ³
499.7	20012	1690	3 ₀ ¹
489.0	20450	2128	1 ₀ ¹
479.3	20864	2542	1 ₀ ¹ 6 ₀ ¹
471.3	21218	2896	1 ₀ ¹ 6 ₀ ²

excitation within the bonding manifold and the band origins of these two species are anticipated to be similar in energy. This is supported by the observation of two band systems in Figure 1 within 18 nm of each other in the visible region, one of which disappears after UV irradiation.

The band centered at 545.8 nm in Figure 1 corresponds to the band origin of the B ²Π ← X ²Π electronic transition of C₆Cl. The position of the observed band maximum of C₆Cl is comparable to that attributed to the analogous transition of the isoelectronic C₆S⁻ anion at 608 nm in a neon matrix.²⁴ This result is reasonable because these electronic transitions predominantly involve electronic excitation within the π-bonding systems of the carbon chains, and thus it is not surprising that the band origins differ by 62 nm. It is also interesting to note that the position of the band origin of C₆Cl is only 16 nm higher than that observed for the B ²Π ← X ²Π transition of C₆H in a neon matrix, which was reported at 530 nm.²⁷

Analysis of the vibrational structure of the B ²Π ← X ²Π electronic transition of C₆Cl reveals the excitation of three vibrational modes as indicated by the list of the observed band positions in Table 1. These modes essentially correspond to stretching motions of the C–C bonds (ν₁, ν₂) and to the C–Cl stretch (ν₆) in the excited electronic state of C₆Cl as well as to several overtone and combination bands. The experimentally

Electronic Absorption Spectra of C_nCl Radicals

J. Phys. Chem. A, Vol. 108, No. 19, 2004 4221

TABLE 2: Positions of the Band Maxima ($\pm 0.2 \text{ cm}^{-1}$) Observed for the ${}^3\Sigma^- \leftarrow X \text{ }^3\Sigma^-$ Electronic Transition of C₆Cl⁺ in a 6 K Neon Matrix

λ/nm	$\tilde{\nu}/\text{cm}^{-1}$	$\Delta\tilde{\nu}/\text{cm}^{-1}$	assignment
527.4	18961		0_0^0
515.7	19391	430	6_0^1
504.3	19829	868	6_0^2
480.0	20833	1872	2_0^1
476.1	21004	2043	1_0^1
470.1	21272	2311	$2_0^1, 6_0^1$

determined vibrational frequencies are lower in energy than the calculated values for the ground electronic state²¹ ($\nu_1 = 2194$, $\nu_3 = 1917$, and $\nu_6 = 441 \text{ cm}^{-1}$) as expected since the electronic transition in question corresponds to promotion of an electron to an orbital with a greater number of nodes.

The peak centered at 527.4 nm in Figure 1 is assigned to the band origin of the ${}^3\Sigma^- \leftarrow X \text{ }^3\Sigma^-$ electronic transition of the linear C₆Cl⁺ cation. For the isoelectronic C₆S molecule, the observed band origin in a neon matrix for the analogous transition lies 47 nm to the red at 574.2 nm.²⁴ The blue shift of the chlorinated species relative to the isoelectronic sulfur-containing species is slightly smaller for the C₆Cl⁺ cation (47 nm) than for the C₆Cl neutral (62 nm), suggesting that the former has more energetically similar electronic states to C₆S than the latter has to C₆S⁻. Ab initio calculations involving population analysis of the C_nCl⁺ cations suggest that the positive charge is mainly carried by the carbon chain in these species but that a certain degree of π donation from chlorine to the chain produces a small positive charge on the terminal chlorine atom.²¹ In effect, the positive charge is, to some extent, spread over the entire molecule resulting in electronic states with energies comparable to those of the neutral C₆S molecule.

The vibrational structure of the C₆Cl⁺ cation is similar to that observed for the neutral molecule and the positions of the band maxima of the assigned modes are listed in Table 2. As with C₆Cl, the experimentally observed frequencies are lower than the calculated ground-state values²¹ ($\nu_1 = 2153$, $\nu_2 = 2139$ and $\nu_6 = 488 \text{ cm}^{-1}$) as expected for such a $\pi-\pi$ transition. A comparison of the observed spectrum with the vibrational modes reported for the isoelectronic C₆S species ($\nu_1 = 2081$, $\nu_2 = 1863$, and $\nu_6 = 452 \text{ cm}^{-1}$)²⁴ shows agreement within tens of wavenumbers for each of the observed modes. Furthermore, the vibrational frequencies of C₆Cl⁺ are similar to those of C₆Cl, which suggests that there is little difference in their excited-state geometries upon electronic excitation to these particular states. Ab initio predictions suggest that for the ground electronic states of these molecules, the ν_6 mode (essentially the C-Cl stretch) is slightly larger for C₆Cl⁺ than for C₆Cl and the optimized geometry of the ground state of the cation predicts a shorter C-Cl bond distance (1.583 Å) compared to that of the neutral (1.626 Å).²¹ The vibrational frequencies extracted from the present experiment seem to support a similar phenomenon in the excited electronic state and the observed larger ν_6 vibrational frequency for C₆Cl⁺ can be attributed to a greater degree of electron donation from chlorine to the carbon π backbone in the cationic species.

(b) C₅Cl and C₅Cl⁺. An analogous experiment was performed by co-depositing mass-selected C₅Cl⁺ with neon to form a 6 K matrix. The electronic absorption spectra of this sample revealed one clear band system in the UV range between 240 and 270 nm and a second system in the visible region between 430 and 550 nm as shown in Figures 2 and 3, respectively. The band system originating at 532.3 nm is assigned to the C₅Cl neutral since the spectral lines became more intense after

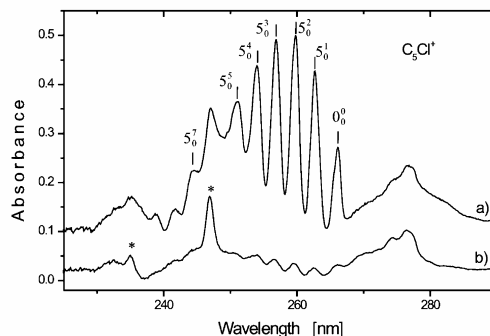


Figure 2. Electronic absorption spectra of the ${}^1\Sigma^+ \leftarrow X \text{ }^1\Sigma^+$ electronic transition of C₅Cl⁺ recorded in a 6 K neon matrix. The traces show the observed absorptions both (a) before and (b) after UV irradiation of the sample. The bands marked by asterisks are tentatively assigned to a higher excited electronic transition of C₅Cl (${}^2\Pi \leftarrow X \text{ }^2\Pi$) as described in the text.

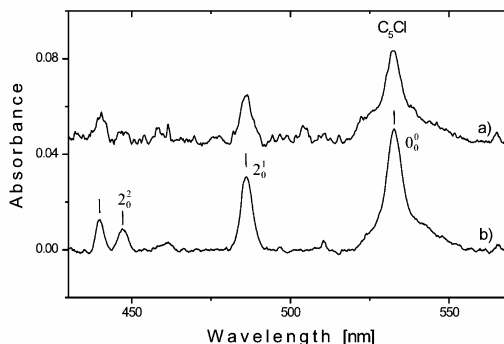


Figure 3. Electronic absorption spectra of the $\Sigma^+ \leftarrow X \text{ }^2\Pi$ electronic transition of C₅Cl recorded after mass selected deposition of C₅Cl⁺ in a 6 K neon matrix. The traces show the observed absorptions in the visible region both (a) before and (b) after UV irradiation of the sample. The intensity increases after irradiation due to an increase in the concentration of C₅Cl in the matrix upon neutralization of some C₅Cl⁺ cations.

UV irradiation. The band system in the UV range has its origin at 266.1 nm and disappeared after irradiation with UV light. These transitions are thus assigned to the C₅Cl⁺ cation.

For the linear C₅Cl⁺ cation, the ground state is described by a singlet X ${}^1\Sigma^+ \dots 4\pi^4$ electronic configuration and the lowest excited electronic state involves promotion of an electron to the $5\pi^*$ antibonding orbital. The vibronic band system originating at 266.1 nm in Figure 2 is assigned to the ${}^1\Sigma^+ \leftarrow X \text{ }^1\Sigma^+$ electronic transition of C₅Cl⁺ and it is not surprising that this is found at UV wavelengths because the ground state of the cation is energetically stabilized as a consequence of its closed shell electronic configuration. The band origin reported for the ${}^1\Sigma^+ \leftarrow X \text{ }^1\Sigma^+$ transition of the isoelectronic C₅S molecule in a neon matrix lies only 18 nm to the red at 284.3 nm.²⁴

The rich vibrational structure observed for C₅Cl⁺ consists of several bands which are approximately evenly spaced. These are assigned to the ν_5 vibrational mode (essentially the C-Cl stretch) and to overtones of this mode and the positions of the band maxima are listed in Table 3. The experimentally determined vibrational frequency, 486 cm^{-1} , is in good agreement with the calculated value for the ${}^1\Sigma^+$ ground electronic state, $\nu_5 = 514 \text{ cm}^{-1}$, and is greater than the C-Cl stretching

4222 *J. Phys. Chem. A, Vol. 108, No. 19, 2004*

van Wijngaarden et al.

TABLE 3: Positions of the Band Maxima (± 0.2 cm⁻¹) Observed for the ${}^1\Sigma^+ \leftarrow X {}^2\Sigma^+$ Electronic Transition of C₅Cl⁺ in a 6 K Neon Matrix

λ/nm	$\tilde{\nu}/\text{cm}^{-1}$	$\Delta\tilde{\nu}/\text{cm}^{-1}$	assignment
266.1	37580		0 ₀ ⁰
262.7	38066	486	5 ₀ ¹
259.8	38491	911	5 ₀ ²
257.0	38911	1331	5 ₀ ³
254.0	39370	1790	5 ₀ ⁴
251.2	39809	2229	5 ₀ ⁵
244.5	40900	3320	5 ₀ ⁶

TABLE 4: Positions of the Band Maxima (± 0.2 cm⁻¹) Observed for Two Electronic Transitions of C₅Cl in a 6 K Neon Matrix

λ/nm	$\tilde{\nu}/\text{cm}^{-1}$	$\Delta\tilde{\nu}/\text{cm}^{-1}$	assignment
532.3	18786		$\Sigma^+ \leftarrow X {}^2\Pi$ 0 ₀ ⁰
485.9	20580	1794	2 ₀ ¹
447.0	22331	3545	2 ₀ ²
439.9	22732	3946	2 ₀ ² 5 ₀ ¹ B ${}^2\Pi \leftarrow X {}^2\Pi$
247.1	40469		0 ₀ ⁰
235.3	42499	2030	1 ₀ ¹

frequencies of C₆Cl and C₆Cl⁺ as predicted for a shorter chain.²¹ On the basis of the assignment given in Table 3, the higher order overtones corresponding to the excitation of two or three quanta of the ν_5 mode in the excited state of C₅Cl⁺ are the most intense. This is anomalous in comparison to the vibronic progressions observed for C₆Cl and C₆Cl⁺ in which the predominant bands correspond to single excitation of the ν_6 mode. This difference may be attributed to a comparatively larger geometry change upon promotion of an electron to the $5\pi^*$ antibonding orbital in C₅Cl⁺.

The ground-state electronic configuration of linear C₅Cl corresponds to a doublet X ${}^2\Pi..5\pi^1$, and like C₅Cl⁺, one possible electronic excitation involves electron promotion to a π^* antibonding orbital as was suggested for the isoelectronic C₅S⁻ anion. This transition was predicted to lie in the UV region for C₅S⁻ but could not be observed due to lack of an accessible bound state.²⁴ For C₅Cl, this transition is also expected to fall in the UV range and its origin should be similar to that of the ${}^1\Sigma^+ \leftarrow X {}^1\Sigma^+$ electronic transition of C₅Cl⁺. In Figure 2, the weak bands marked by asterisks were observed to remain after UV irradiation and are therefore attributed to some neutral species in the matrix sample. If the sharp band observed at 247.1 nm is the band origin of this $\pi-\pi^*$ transition, then the next observed band is blue shifted by 2030 cm⁻¹. This is a reasonable value for excitation of the ν_1 mode in the excited electronic state of C₅Cl as it is smaller than the value predicted for the ground electronic state, 2108 cm⁻¹.²¹ Furthermore, the magnitude of the ν_1 mode is comparable to that observed for C₆Cl (2128 cm⁻¹) in this work, which was also slightly smaller than the predicted ground-state vibrational frequency (2194 cm⁻¹). The assignment of this electronic transition, as shown in Table 4, is offered only tentatively and would be more convincing if these bands increased in intensity after exposure to UV light.

Figure 3 shows the electronic absorption spectra recorded for this same matrix sample in the visible range. Four bands are observed and each increases in intensity after UV irradiation, which suggests that these bands arise from electronic excitation of the C₅Cl neutral. Since the promotion of an electron to a π^* orbital is expected to lie in the UV region, the band centered at 532.3 nm must therefore correspond to the band origin of a

lower energy transition involving electron promotion from a fully occupied molecular orbital to the 5π partially occupied valence orbital. Strong transitions of this type have been reported for other carbon chain molecules with X ${}^2\Pi$ ground electronic states. In the case of the C_nH ($n = \text{even}$) species, $\pi-\pi$ transitions have been observed in the visible region²⁸ whereas for the C_nH ($n = \text{odd}$) chains, $\sigma-\pi$ transitions have been recorded in this range.²⁷ As there are no calculations available for the excited-state configurations of C₅Cl, it is not possible to definitively assign the upper state involved in the transition with origin at 532.3 nm. The low intensity of the band system suggests that the transition is likely of the type $\Sigma^+ \leftarrow X {}^2\Pi$ because its absorbance is an order of magnitude less than for other $\pi-\pi$ transitions (see Figures 1 and 3). In the case of C₄O⁻, for example, the A ${}^2\Sigma^+ \leftarrow X {}^2\Pi$ transition was also observed to have considerably lower intensity than the B ${}^2\Pi \leftarrow X {}^2\Pi$ band in a neon matrix.²⁹

The vibrational assignment of the bands observed for C₅Cl in Figure 3 is given in Table 4. The transition closest to the origin band is blue shifted by 1794 cm⁻¹, which is consistent with the excitation of the ν_2 vibrational mode in the excited electronic state based on the ab initio calculations of the ground electronic state which predict $\nu_2 = 1959$ cm⁻¹.²¹ A comparable difference has been observed for the ν_2 modes of related molecules when the experimental excited-state vibrational frequencies and the ground-state theoretical values are considered. For example, in the case of C₆Cl⁺, C₆S, and C₅S, the experimentally determined excited state ν_2 stretching frequencies are 1872, 1863, and 1734 cm⁻¹, while the predicted ground-state values of these modes are 2139, 2025, and 2013 cm⁻¹, respectively.³⁰ The transition appearing at 439.9 nm in Figure 3 is blue shifted from the nearest band by only 401 cm⁻¹. This value is considerably smaller than the ν_3 vibrational frequency predicted for the ground electronic state, 501 cm⁻¹,²¹ and that determined for the ${}^1\Sigma^+$ excited state of C₅Cl⁺, 486 cm⁻¹, in this work. The observed blue shift of this band in the spectrum of C₅Cl is, however, comparable to the experimentally determined ν_6 frequencies for the excited states of C₆Cl and C₆Cl⁺, 415 and 430 cm⁻¹, respectively. Consequently, the band centered at 439.9 nm in Figure 3 may be tentatively assigned to the excitation of a vibronic transition involving the coupling of the $2\nu_2$ and ν_3 vibrational modes in the excited electronic state of C₅Cl as listed in Table 4 although the band in question may alternatively be due to excitation of a higher energy electronic state.

Conclusion

In this work, electronic absorption spectra of the chlorine-terminated carbon chains C₆Cl, C₆Cl⁺, C₅Cl, and C₅Cl⁺ have been recorded in 6 K neon matrices. The transitions observed are B ${}^2\Pi \leftarrow X {}^2\Pi$ for C₆Cl, ${}^3\Sigma^- \leftarrow X {}^3\Sigma^-$ for C₆Cl⁺, ${}^2\Pi \leftarrow X {}^2\Pi$ and $\Sigma^+ \leftarrow X {}^2\Pi$ for C₅Cl, and ${}^1\Sigma^+ \leftarrow X {}^1\Sigma^+$ for C₅Cl⁺. These studies provide the basis for gas-phase spectroscopic measurements which are necessary for determining whether these or related species play a role in the chemistry of the interstellar medium via electronic spectroscopy.

Acknowledgment. This research was supported by the Swiss National Science Foundation (project 200020-100019). J.v.W. thanks the Natural Science and Engineering Research Council of Canada for postdoctoral support.

References and Notes

- (1) Thaddeus, P.; McCarthy, M. C. *Spectrochim. Acta A* **2001**, *57*, 757.

Electronic Absorption Spectra of C_nCl Radicals*J. Phys. Chem. A, Vol. 108, No. 19, 2004* **4223**

- (2) McCarthy, M. C.; Gottlieb, C. A.; Thaddeus, P. *Mol. Phys.* **2003**, *101*, 697.
- (3) Blake, G. A.; Keene, J.; Phillips, T. J. *Astrophys. J.* **1985**, *295*, 501.
- (4) Cernicharo, J.; Guelin, M. *Astron. Astrophys.* **1987**, *183*, L10.
- (5) Barrientos, C.; Largo, A.; Redondo, P.; Pauzat, F.; Ellinger, Y. *J. Phys. Chem.* **1993**, *97*, 173.
- (6) Blake, G. A.; Anicich, V. G.; Huntress, W. T. *Astrophys. J.* **1986**, *300*, 415.
- (7) Rayon, V. M.; Barrientos, C.; Largo, A. *J. Mol. Struct. (THEOCHEM)* **1996**, *363*, 319.
- (8) Rayon, V. M.; Barrientos, C.; Largo, A. *J. Mol. Struct. (THEOCHEM)* **1998**, *432*, 75.
- (9) Endo, Y.; Saito, S.; Hirota, E. *J. Mol. Spectrosc.* **1982**, *94*, 199.
- (10) Yamada, C.; Nagai, K.; Hirota, E. *J. Mol. Spectrosc.* **1981**, *85*, 416.
- (11) Burkholder, J. B.; Sinha, A.; Hammer, P. D.; Howard, C. J. *J. Mol. Spectrosc.* **1988**, *127*, 61.
- (12) Jin, P.; Chang, B. C.; Fei, R.; Sears, T. J. *J. Mol. Spectrosc.* **1997**, *182*, 189.
- (13) Venkateswarlu, P. *Phys. Rev.* **1950**, *77*, 79.
- (14) Verma, R. D.; Mulliken, R. S. *J. Mol. Spectrosc.* **1961**, *6*, 419.
- (15) Gordon, R. D.; King, G. W. *Can. J. Phys.* **1961**, *39*, 252.
- (16) Barrow, R. F.; Drummond, G.; Walker, S. *Proc. Phys. Soc. A* **1954**, *67*, 186.
- (17) Bredohl, H.; Dubois, I.; Melen, F. *J. Mol. Spectrosc.* **1983**, *98*, 495.
- (18) Sumiyoshi, Y.; Ueno, T.; Endo, Y. *J. Chem. Phys.* **2003**, *119*, 1426.
- (19) Largo, A.; Barrientos, C. *Chem. Phys.* **1989**, *138*, 291.
- (20) Largo-Cabrerizo, A.; Barrientos, C. *Chem. Phys. Lett.* **1989**, *155*, 550.
- (21) Largo, A.; Cimas, A.; Redondo, P.; Barrientos, C. *Int. J. Quantum Chem.* **2001**, *84*, 127.
- (22) Li, G.; Tang, Z. *J. Phys. Chem. A* **2003**, *107*, 5317.
- (23) Redondo, P.; Redondo, J.; Barrientos, C.; Largo, A. *Chem. Phys. Lett.* **1999**, *315*, 224.
- (24) Riaplov, E.; Maier, J. P. *J. Phys. Chem. A* **2003**, *107*, 8856.
- (25) Maier, J. P. *Chem. Soc. Rev.* **1997**, *1997*, 21.
- (26) Freivogel, P.; Fulara, J.; Lessen, D.; Fomey, D.; Maier, J. P. *Chem. Phys.* **1994**, *189*, 335.
- (27) Ding, H.; Pino, T.; Gütthe, F.; Maier, J. P. *J. Chem. Phys.* **2002**, *117*, 8362.
- (28) Maier, J. P. *J. Phys. Chem. A* **1998**, *102*, 3462.
- (29) Riaplov, E.; Wyss, M.; Lakin, N.; Maier, J. P. *J. Phys. Chem. A* **2001**, *105*, 4894.
- (30) Lee, S. *Chem. Phys. Lett.* **1997**, *268*, 69.

C₃CL AND C₄CL

J. Phys. Chem. A 2005, 109, 5553–5559

5553

Electronic Absorption Spectra of C₃Cl, C₄Cl, and Their Ions in Neon MatricesJennifer van Wijngaarden,[†] Ivan Shnitko, Anton Batalov, Przemyslaw Kolek, Jan Fulara,[‡] and John P. Maier*

Department of Chemistry, University of Basel, Klingelbergstrasse 80, CH-4056 Basel, Switzerland

Received: March 23, 2005; In Final Form: April 25, 2005

Electronic absorption spectra of C₃Cl, C₃Cl⁺, C₃Cl⁻, C₄Cl, and C₄Cl⁺ have been recorded in 6 K neon matrices following mass selection. Ab initio calculations were performed (CCSD(T) and CASSCF) to identify the ground and accessible excited states of each molecule. The estimated excitation energies and transition moments aid the assignment. The absorptions observed for C₃Cl are the 5²A' ← X²A' and 3²A'' ← X²A' transitions of the bent isomer and the 2¹A₁ ← X²B₂ transition of the cyclic form in the UV (336.1 nm), visible (428.7 nm), and near-IR (1047 nm) regions, respectively. The band systems for bent C₃Cl⁻ (435.2 nm) and linear C₃Cl⁺ (413.2 nm) are both in the visible region and correspond to 2¹A'' ← X¹A' and 1¹Π ← X¹Σ⁺ type transitions. The C₄Cl and C₄Cl⁺ chains are linear, and the band origins of the 2²Π ← X²Π and 2³Π ← X³Π electronic transitions are at 427.0 and 405.7 nm. The spectral assignments are supported by analysis of the vibrational structure associated with each electronic transition.

Introduction

A number of carbon chains terminated by the second row elements—Si, P, and S—have been experimentally and theoretically investigated in recent years due to the detection of the shorter chains in astrophysical environments.¹ The chlorine containing analogues are likewise gaining interest and are thought to be good candidates for astronomical detection, as it is predicted that C–Cl bonds can be formed under interstellar conditions.² Furthermore, spectroscopic studies of heteroatom-terminated carbon chain molecules serve as tests of current theoretical models through the identification of periodic trends in molecular properties as a function of the end atom and chain length.

The ground state electronic structures and vibrational frequencies have been determined for the C_nCl, C_nCl⁻, and C_nCl⁺ (*n* = 1–7) molecules using DFT (B3LYP).^{3,4} For all but C₃Cl, the lowest energy structures are thought to be linear or quasilinear chains terminated on one end by the chlorine atom. In the case of C₃Cl, geometry optimization calculations suggest that the ground state structure is a cyclic triatomic carbon ring with an exocyclic chlorine (²B₂) C_{2_v}; however, quasilinear (²A') C₂ and linear (²Π) structures are estimated to lie only 12 kJ/mol higher in energy.⁵ For the larger species, the calculated C–C bond distances suggest that the most important valence structures are cumulenic, although the observation of bond length alternation suggests that polyynic ones also contribute, particularly for the *n* = even chains. The ab initio results further predict that the C_nCl and C_nCl⁺ chains exhibit alternating stability depending on whether *n* is even or odd. For the neutral species, the *n* = even chains are predicted to be more stable than the *n* = odd ones, but the trend is reversed for the corresponding cations.

Experimentally, the CCl radical is the most extensively studied of the C_nCl species and spectra have been reported in the microwave,⁶ infrared,^{7–9} and ultraviolet regions.^{10–12} High resolution gas phase spectroscopic studies have been conducted for other small molecules of this type such as the CCl⁺ cation¹³ and the C₂Cl radical,¹⁴ and recently, the absorption spectra of the longer chains—C₅Cl, C₅Cl⁺, C₆Cl, and C₆Cl⁺—were reported in neon matrices.¹⁵ Spectroscopic investigations of the intermediate chlorine-terminated carbon chain molecules will bridge the gap in the existing experimental data and will further provide a test of the current theoretical results for this series of molecules.³

In this paper, the first spectroscopic study of C₃Cl and C₄Cl and their ions, C₃Cl⁻, C₃Cl⁺, and C₄Cl⁺, using mass-selective neon matrix isolation spectroscopy is reported. The band assignments of each molecule are based upon ab initio predictions of the expected electronic transitions and ground state vibrational frequencies. The spectral assignments are further supported by comparisons with the previously reported spectra of the longer C_nCl and C_nCl⁺ (*n* = 5, 6) chains and with the isoelectronic species C_nS and C_nS⁻, as appropriate.¹⁶

Experimental Method

The electronic absorption spectra of the C_nCl (*n* = 3, 4) species and their ions were recorded following mass-selective deposition in neon matrices using the described instrument.¹⁷ A gas mixture containing the appropriate precursor was prepared by passing helium over a liquid sample of *c*-C₃Cl₄ or C₄Cl₆. From these respective mixtures, a number of C₃Cl_{*m*}⁺ and C₄Cl_{*m*}⁺ cations were produced, along with the corresponding neutral and anionic species, using a hot cathode discharge source. The cation beam was focused and directed into a quadrupole mass filter using a series of electrostatic optics.¹⁸ The C₃Cl⁺ or C₄Cl⁺ cations were selected with a mass resolution of ±2 amu for each experiment, and the typical ion currents achieved were 44 and 75 nA for the two species, respectively.

The mass-selected cations were deposited simultaneously with neon on a rhodium-coated sapphire substrate over a period of

* Corresponding author. E-mail: J.P.Maier@unibas.ch. Phone: +41 61 267 38 26. Fax: +41 61 267 38 55.

[†] Current address: Department of Chemistry, Mount Holyoke College, 50 College St., South Hadley, MA, 01075.

[‡] Permanent address: Instytut Fizyki Polskiej Akademii Nauk, Al. Lotników 32-46, 02-668 Warsaw, Poland.

5554 *J. Phys. Chem. A, Vol. 109, No. 25, 2005*

van Wijngaarden et al.

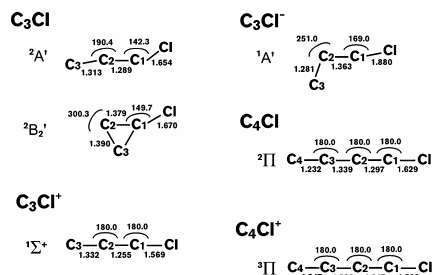


Figure 1. Calculated structural parameters for the observed electronic states of the C_nCl species at the CCSD(T)/cc-pVTZ level. Bond lengths are given in angstroms and bond angles in degrees.

3 h to produce a 6 K matrix. Due to a high incidence of electron recombination and molecular dissociation events in the matrix, additional measures were necessary to suppress these processes so that the desired species could be spectroscopically probed. During the deposition of C₃Cl⁺ ions, a positive potential of 25 V was applied to the matrix to slow the approaching ions and reduce fragmentation. To suppress the neutralization of C₃Cl⁺ and C₄Cl⁺, small concentrations of N₂O or CCl₄ were added to the neon gas in ratios of approximately 1:250. These impurities served as scavengers by removing free electrons that were attracted to the positively charged matrix after liberation from surrounding metal surfaces.

The samples were irradiated with monochromatic light from halogen and xenon arc lamps with beams running parallel to the substrate surface. Absorption spectra of the trapped species were recorded between 220 and 1100 nm using photomultiplier and silicon diode detectors. Spectra in the 12 000–1100 cm⁻¹ range were recorded after sampling the neon matrix by a Fourier transform spectrometer, whereby the light was passed twice through the ~150 μm thickness of the matrix being reflected off the rhodium substrate. The matrix samples were then exposed to filtered radiation (λ > 305 nm) from a medium pressure mercury lamp and later to the full radiation (including λ < 305 nm) of this lamp as a next step. After each irradiation step, a spectrum was recorded to distinguish transitions of stable species from those of ions and photounstable molecules.

Computational Method

An ab initio study of C₃Cl, C₃Cl⁺, C₃Cl⁻, C₄Cl, and C₄Cl⁺ was performed using the MOLPRO software package¹⁹ with cc-pVTZ basis sets described in more detail elsewhere.²⁰ To start, the ground state geometries were optimized using the CASSCF and CCSD(T) methods for comparison. Once the geometries were determined, vertical excitation energies and transition moments were computed for several excited states simultaneously using CASSCF with state-averaged orbitals. Both quasilinear and cyclic structures were considered, as previous theoretical work predicted that their ground state energies were similar for C₃Cl.⁵

Results and Discussion

(a) C₃Cl. After mass selection, C₃Cl⁺ was co-deposited with an excess of neon to form a 6 K matrix and the absorption spectrum was recorded. This reveals three clear systems in the UV, visible, and near-IR regions with band origins at 336.1, 428.7, and 1047 nm, respectively. These are attributed to the C₃Cl molecules formed by neutralization of the cationic precursor in the matrix. The assignment is supported by the

TABLE 1: Electronic Excitation Energies of C₃Cl and C₄Cl and Their Ions Computed with CASSCF/cc PVTZ

excited state	excitation energy		transition moment/D		
	experimental (adiabatic)	CASSCF (vertical)	a	b	c
<i>b</i> -C ₃ Cl					
X ² A'					
1 ² A'		2.60	0.051	0.631	
2 ² A'		3.34	0.158	0.198	
3 ² A'		4.02	-0.002	0.248	
4 ² A'		4.30	-0.409	0.099	
5 ² A'	3.70	4.55	0.961	0.121	
6 ² A'		5.73	0.529	0.050	
1 ² A''		0.64			-0.230
2 ² A''		2.69			-0.219
3 ² A''	2.89	3.06			-0.809
4 ² A''		3.79			0.003
5 ² A''		4.03			0.180
6 ² A''		5.04			0.086
7 ² A''		5.42			-0.185
8 ² A''		5.67			-0.156
<i>c</i> -C ₃ Cl					
X ² B ₂					
1 ² A ₁	1.18	1.48		-1.789	
1 ² B ₁		3.64		forbidden	
1 ² A ₂		4.00			0.362
2 ² B ₁		4.29		forbidden	
2 ² A ₂		5.29			-0.857
2 ² A ₁		5.59		0.85	
1 ² B ₂		5.76	-1.22		
<i>b</i> -C ₃ Cl ⁻					
X ¹ A'					
1 ¹ A'		4.11	-0.276	0.533	
2 ¹ A'		4.35	0.075	-0.455	
3 ¹ A'		4.72	0.007	0.147	
1 ¹ A''		2.03			-0.589
2 ¹ A''	2.85	3.23			1.203
3 ¹ A''		3.96			-0.078
<i>l</i> -C ₃ Cl ⁺					
X ¹ Σ ⁺					
1 ¹ Π	3.00	3.29		-0.775	-0.775
1 ¹ Δ		3.78	forbidden		
<i>l</i> -C ₄ Cl					
³ Π	2.90	3.34	1.670		
2 ² Σ ⁺		5.27		0.660	0.660
<i>l</i> -C ₄ Cl ⁺					
³ Π					
1 ³ Δ		2.54		0.136	0.136
2 ² Σ ⁺		2.60		0.129	0.129
2 ³ Π	(2.87), 3.06	2.92	2.553		

observation that the bands increased in intensity after UV irradiation, as positively charged molecules are known to be neutralized under these conditions.

The lowest energy C₃Cl isomer is cyclic C_{2v}, in the X²B₂ electronic state, although a bent isomer lies only 17.4 kJ/mol higher in energy at the CCSD(T) level (present work) and 12 kJ/mol higher according to DFT calculations.⁵ The nonlinear structure is similar to that reported earlier (DFT/B3LYP and QCISD) but with a greater deviation from linearity in the C–C–Cl angle (142.3°/144.0° from CCSD(T) and CASSCF). Because the species in the matrix are produced via neutralization of the linear C₃Cl⁺ precursor, it was expected that the chain isomer of C₃Cl would be the primary neutral constituent of the sample even though the cyclic form is lower in energy. The excitation energies and transition moments of the allowed electronic transitions less than 6 eV are listed in Table 1 for both isomers, and the calculated ground state structures are shown in Figure 1.

A rich vibrational structure is observed for the UV band of C₃Cl in Figure 2 and is attributed to the 5²A' ← X²A' transition of the bent isomer; the vibrational assignments are listed in Table 2. This is predicted to have a large transition moment, and the observed band origin at 336.1 nm falls 0.86 eV below the ab initio prediction. The discrepancy is partially explained by the fact that the comparison is between vertical and adiabatic

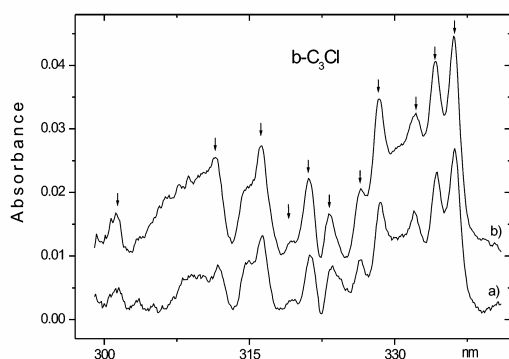
Electronic Absorption Spectra of C₃Cl and C₄Cl

Figure 2. Electronic absorption spectra of the $5^2A' \leftarrow X^2A'$ transition of bent C₃Cl in the UV region. The spectra were recorded in a 6 K neon matrix both (a) before and (b) after UV irradiation ($\lambda > 305$ nm).

TABLE 2: Positions of the Band Maxima (± 0.2 nm) Observed for Electronic Transitions of C₃Cl, C₃Cl⁻, and C₃Cl⁺ in 6 K Neon Matrixes

species	λ/nm	ν/cm^{-1}	$\Delta\nu/\text{cm}^{-1}$	assignment	
<i>b</i> -C ₃ Cl	$5^2A' \leftarrow X^2A'$	336.1	29 753	0	0_0^0
		334.2	29 922	169	ν_6
		332.2	30 102	349	$2\nu_6$
		328.4	30 451	698	ν_3
		326.5	30 628	875	$\nu_3 + \nu_6$
		323.3	30 931	1178	ν_2
		321.1	31 143	1390	$2\nu_3$
		319.2	31 328	1575	$2\nu_3 + \nu_6$
		316.2	31 626	1873	ν_1
		314.7	31 776	2023	$\nu_1 + \nu_6$
		311.5	32 103	2350	$2\nu_2$
		301.3	33 190	3437	$3\nu_2$
	$3^2A'' \leftarrow X^2A'$	428.7	23 326	0	0_0^0
	423.9	23 590	264	ν_5	
<i>c</i> -C ₃ Cl	$1^2A_1 \leftarrow X^2B_2$	1047	9552	0	0_0^0
		987.5	10 127	576	ν_4
		958.5	10 433	882	$2\nu_6$
		951.5	10 510	959	$2\nu_5$
		937.2	10 670	1119	ν_2
		910.2	10 987	1436	$2\nu_3$
		896.2	11 158	1607	ν_1
		883.5	11 319	1768	$4\nu_6$
		878.2	11 387	1836	$4\nu_5$
		865.7	11 551	2000	$2\nu_3 + \nu_4$
	<i>b</i> -C ₃ Cl ⁻	$2^1A'' \leftarrow X^1A'$	435.2	22 978	0
		418.0	23 923	945	ν_2
<i>t</i> -C ₃ Cl ⁺	$1^1\Pi \leftarrow X^1\Sigma$	413.2	24 201	0	0_0^0
	IR: <i>t</i> -C ₃ Cl ⁺		$\nu_1 = 2142.6 \text{ cm}^{-1}$	<i>b</i> -C ₃ Cl $\nu_1 = 1859.1 \text{ cm}^{-1}$	

excitation energies which typically differ by ~ 0.2 – 0.3 eV. The remaining error may be attributed to the limitations of the CASSCF method which often produces unusually large correlation energies for higher excited states.

The observed vibrational bands in Figure 2 correspond to the excitation of four vibrational modes of C₃Cl as well as to their combinations and overtones. At 6 K, the molecules are primarily in the lowest vibrational level of the ground state, and thus, the observed progression is due to excitation of carbon chain stretching and bending modes ($\nu_1 = 1873$, $\nu_2 = 1178$, $\nu_3 = 698$, $\nu_6 = 169 \text{ cm}^{-1}$) in the excited electronic state of C₃Cl. The values compare favorably with the frequencies computed via ab initio methods for the ground electronic state (B3LYP/6-311G+(d): $\nu_1 = 1932$, $\nu_2 = 1338$, $\nu_3 = 672$, $\nu_6 = 176 \text{ cm}^{-1}$).³ The IR spectrum of C₃Cl was also measured in its ground

J. Phys. Chem. A, Vol. 109, No. 25, 2005 5555

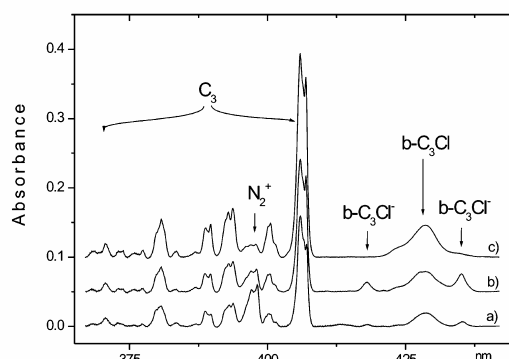


Figure 3. Electronic absorption spectra in the visible region of the $3^2A'' \leftarrow X^2A'$ transition of bent C₃Cl and the $2^1A'' \leftarrow X^1A'$ transition of bent C₃Cl⁻ in 6 K neon matrixes. The traces show the observed spectra (a) after deposition, (b) after exposure to UV wavelengths ($\lambda > 305$ nm), and (c) after irradiation with a broader spectrum (including $\lambda < 305$ nm). Both C₃ and N₂⁺ present in the matrix absorb in this spectral region.

electronic state revealing only the ν_1 band (1859.1 cm^{-1}) which differs by 14 cm^{-1} from the excited state vibrational frequency extracted from the electronic spectrum (Figure 2).

A second band of the bent C₃Cl radical is observed in the visible region at 428.7 nm (Figure 3) and is assigned to the origin of the $3^2A'' \leftarrow X^2A'$ system in Table 2. This is predicted to be the second strongest transition of this isomer and lies within 0.17 eV of the theoretical prediction. A smaller band, blue-shifted by 264 cm^{-1} , is assigned to the ν_5 vibrational mode in the excited electronic state based on the ab initio estimate of ground state fundamental frequency ($\nu_5 = 227 \text{ cm}^{-1}$). Additional vibrational bands may be present, but their assignment is precluded by the strong C₃ and N₂⁺ absorptions in this spectral region. The excitation of one quantum of ν_1 stretch, for example, would result in a band at 397 nm in Figure 3 which overlaps with the N₂⁺ absorption.

The third electronic transition of the C₃Cl radical is considerably weaker than the others and appears in the near-IR (NIR) region. This absorption is attributed to a cyclic C₂ isomer where the chlorine atom is bonded to a triatomic carbon ring. The band origin at 1047 nm in Figure 4 is assigned to the $2^1A_1 \leftarrow X^2B_2$ transition of *c*-C₃Cl and is 0.28 eV lower in energy than the theoretical estimate. The observed vibrational pattern supports the assignment of this band to the cyclic isomer, as the progression involves all six vibrational modes of *c*-C₃Cl (Table 2). The experimentally observed frequencies for the 2^1A_1 state ($\nu_1 = 1607$, $\nu_2 = 1119$, $\nu_3 = 718$, $\nu_4 = 576$, $\nu_5 = 480$, $\nu_6 = 441 \text{ cm}^{-1}$) correlate well with the ab initio values determined in this work at the DFT B3LYP level for the 2^1B_2 ground state ($\nu_1 = 1650$, $\nu_2 = 1222$, $\nu_3 = 772$, $\nu_4 = 595$, $\nu_5 = 412$, $\nu_6 = 350 \text{ cm}^{-1}$). The largest discrepancies are for the low frequency modes which correspond to the C–C–Cl bending (ν_5 , ν_6) and C–Cl stretching modes (ν_4). The modes relating to ring deformation (ν_2 , ν_3) and stretching (ν_1) are in close agreement with the experimental values which lends strong support for the assignment of these bands to the cyclic isomer, *c*-C₃Cl.

An additional experiment was performed in which a matrix sample containing both structural isomers of C₃Cl was exposed to a broad spectrum of UV wavelengths and subsequently exposed to filtered light containing only longer wavelengths ($\lambda > 305 \text{ nm}$). The UV and visible bands of bent C₃Cl were

5556 *J. Phys. Chem. A, Vol. 109, No. 25, 2005*

van Wijngaarden et al.

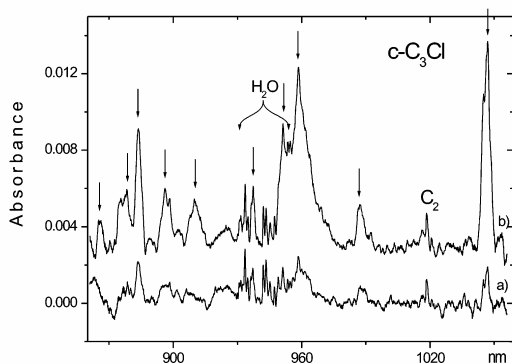


Figure 4. Near-IR band origin of the ${}^2A_1 \leftarrow X^2B_2$ electronic transition of *c*-C₃Cl recorded in a 6 K matrix. The bands marked by arrows are assigned to this structural isomer. Trace a was recorded after the initial deposition of C₃Cl⁺ and shows little *c*-C₃Cl. Trace b demonstrates that the spectrum becomes enriched in the cyclic isomer after stepwise UV irradiation ($\lambda > 305$ nm), as described in the text. The spectra also reveal the presence of H₂O vapor in the chamber and C₂ fragments.

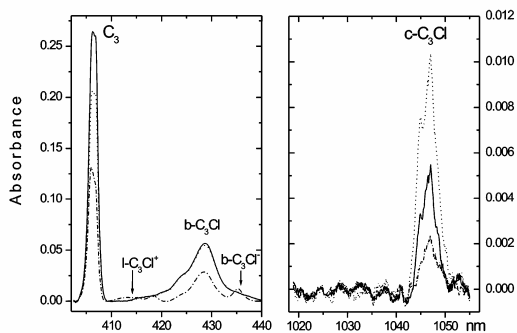


Figure 5. Comparison of the behavior of the origin bands of C₃ and *c*-C₃Cl upon UV irradiation. The traces drawn with dashed–dotted lines show the bands immediately after the matrix is formed. After irradiation including high energy photons ($\lambda < 305$ nm), the bands assigned to C₃ and *c*-C₃Cl increase in intensity (solid trace). Following a second irradiation involving only lower energy photons ($\lambda > 305$ nm), the C₃ band decreases and that due to *c*-C₃Cl increases (dotted trace) in intensity, suggesting that the cyclic isomer of *c*-C₃Cl is formed from C₃.

only affected by the first irradiation, while the NIR band of *c*-C₃Cl grew in intensity after both exposures, as seen in Figure 5. This increase in intensity of the cyclic isomer was accompanied by a simultaneous decrease in the intensity of the C₃ band at 407 nm. The *c*-C₃Cl isomer therefore appears to be formed from C₃, and the additional UV exposure must provide the energy for the transformation in the matrix.

(b) C₃Cl⁻. During the assignment of the neutral C₃Cl species in Figure 3, two additional bands were observed at 435.2 and 418.0 nm which could not be attributed to neutral or cationic species. The transitions increased in intensity upon UV irradiation with longer wavelengths ($\lambda > 305$ nm) and then decreased when exposed to higher energy photons ($\lambda < 305$ nm). Absorption bands related to neutral molecules usually grow or remain constant in intensity as a result of each irradiation step, while those attributable to cations decrease. Exposure to UV light, however, can increase the number of sample anions by liberating electrons from weakly bound anions (e.g., OH⁻) present in the matrix. When subsequently exposed to higher

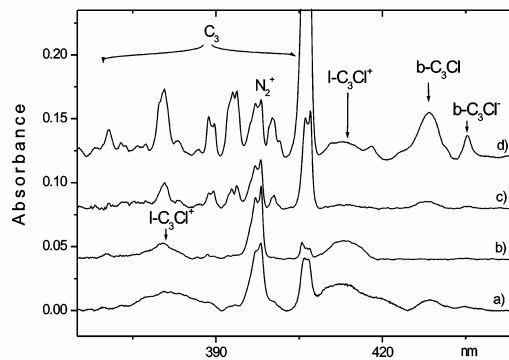


Figure 6. Band origin of the $1^1\Pi \leftarrow X^1\Sigma^+$ electronic transition of C₃Cl⁺ recorded in a 6 K matrix. Traces a and b show the spectrum recorded after deposition of C₃Cl⁺ in a neon matrix containing 0.25% CCl₄ and N₂O, respectively. Trace c is the resulting spectrum after UV irradiation of the matrix sample containing the N₂O electron scavenger. Trace d was observed after deposition of low kinetic energy (~ 15 eV) cations (C₃Cl⁺).

energy, the observed signal will decrease if the photons are of sufficient energy to detach electrons from the newly formed anions (e.g., C₃Cl⁻) in the sample. This is precisely the behavior that was observed for the two additional bands in Figure 3. Evidence for the presence of anions in the matrix sample is the observation that the bands at 435.2 and 418.0 nm were suppressed when electron scavengers (CCl₄ or N₂O) were introduced into the matrix. These molecules have high electron affinities and restrict the formation of other molecular anions.

The lowest energy structure of C₃Cl⁻ is predicted to be bent (Figure 1), and the ground state electronic configuration corresponds to a singlet ${}^1A'$ state. The strongest electronic transition is estimated to be of the type $2^1A'' \leftarrow X^1A'$, with an energy of 3.23 eV (Table 1). This correlates well with the observed band at 435.2 nm (2.85 eV). The second band is blue-shifted by 945 cm⁻¹ and is assigned to the excitation of the ν_2 vibrational mode in the $2^1A''$ state of C₃Cl⁻ in Table 2. The ground state vibrational frequency is predicted to be considerably higher (DFT, 1157 cm⁻¹), but the corresponding mode was similarly overestimated by ab initio calculations for the neutral C₃Cl counterpart (experiment, 1178 cm⁻¹; DFT, 1338 cm⁻¹). The electron affinity of C₃Cl is estimated to be around 2.68 eV (CCSD(T)/aug-cc-pVTZ), but the anion appears to be stabilized in the matrix, as electron detachment is not observed until photons with energies greater than 4 eV are used.

(c) C₃Cl⁺. The first spectra recorded after mass-selected deposition of C₃Cl⁺ ions with neon revealed no evidence of the cation in the matrix. This is a consequence of an efficient neutralization process whereby electrons liberated from nearby metal surfaces are attracted to the positively charged matrix. To observe the spectrum of C₃Cl⁺, it was necessary to mix the neon gas with a small amount of N₂O (250:1 ratio). Since N₂O is a good scavenger, the number of free electrons in the matrix was reduced and the concentration of C₃Cl⁺ was sufficient for a spectroscopic study. Subsequently, a broad transition was observed at 413.2 nm (Figure 6) which disappeared upon UV exposure. The same band was observed when the kinetic energy of C₃Cl⁺ being deposited was decreased through the application of a positive voltage to the matrix. The 413.2 nm band is consequently attributed to the C₃Cl⁺ cation.

The ground state of linear C₃Cl⁺ (Figure 1) is described by a singlet $X^1\Sigma^+$ electronic configuration, and the lowest energy

Electronic Absorption Spectra of C₃Cl and C₄Cl

J. Phys. Chem. A, Vol. 109, No. 25, 2005 5557

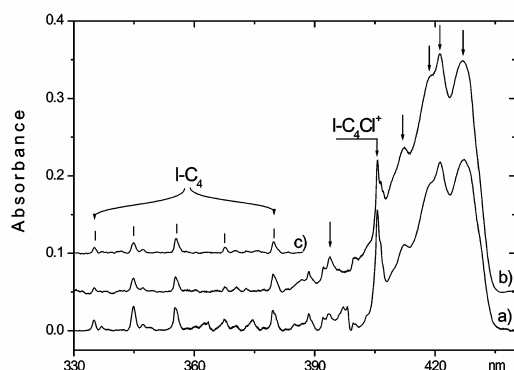


Figure 7. Electronic absorption spectra of the $2^2\Pi \leftarrow X^2\Pi$ electronic transition of C_4Cl recorded in a 6 K neon matrix both (a) before and (b) after UV irradiation. The transitions marked by arrows increased in intensity after exposure to UV light and are assigned to linear C_4Cl . Additional bands are due to C_4Cl^+ and C_4 . Trace c shows the linear C_4 absorptions after C_4^+ mass-selected deposition and subsequent matrix neutralization.

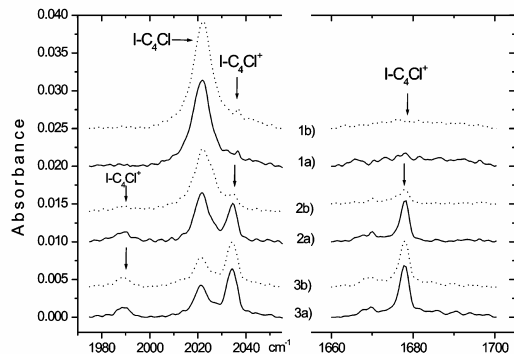


Figure 8. Infrared absorption spectra of C_4Cl and C_4Cl^+ in neon matrices. The solid traces (1a, 2a, and 3a) are the spectra recorded in a pure neon matrix and in matrices containing 0.25% of the electron scavengers N_2O and CCl_4 , respectively. The dotted traces (1b, 2b, and 3b) show the same bands after UV irradiation ($\lambda > 305$ nm).

transition involves electronic excitation to an antibonding orbital. For the analogous $\pi-\pi^*$ type excitations in linear C_5Cl and C_5Cl^+ , the band origins were observed in the UV region at 247.1 and 266.1 nm, respectively, in neon matrices.¹⁵ The $1^1\Pi \leftarrow X^1\Sigma^+$ transition of C_3Cl^+ is predicted to be of lower energy, however, and the band at 413.2 nm is within 0.3 eV of the calculated transition (3.29 eV).

On the basis of DFT calculations of the ground electronic state of linear C_3Cl^+ , the most intense transition in the IR spectrum is predicted to be the ν_1 mode (2224 cm^{-1}),³ and this is consistent with the IR absorption spectrum of this matrix sample. A band is observed at 2142.6 cm^{-1} which decreases in intensity when irradiated with wavelengths longer than 305 nm and disappears completely when exposed to shorter wavelengths, as expected for a cationic species. The electronic absorption spectrum of the related odd chain C_3Cl^+ molecule was dominated by a vibronic progression arising from the excitation of the C–Cl stretch (486 cm^{-1}) in the excited electronic state.¹⁵ For C_3Cl^+ , this mode is predicted to have a higher frequency (690 cm^{-1}) and this vibronic band is expected to nearly coincide with a known transition of C_3 .

TABLE 3: Positions of the Band Maxima (± 0.2 nm) Observed for Electronic Transitions of C_4Cl and C_4Cl^+ in 6 K Neon Matrixes

species	λ/nm	ν/cm^{-1}	$\Delta\nu/\text{cm}^{-1}$	assignment
$l\text{-}C_4Cl$	$2^2\Pi-X^2\Pi$	427.0	23 419	0_0^0
		421.3	23 736	ν_5
		418.8	23 878	ν_4
		412.3	24 254	$\nu_4 + \nu_5$
		393.8	25 394	ν_1
$l\text{-}C_4Cl^+$	$2^2\Pi-X^2\Pi$	405.7	24 649	0_0^0
		397.1	25 183	ν_4
		388.4	25 747	$2\nu_4$
		378.1	26 448	ν_2
		374.4	26 709	ν_1
		366.8	27 263	$\nu_1 + \nu_4$
		359.2	27 840	$\nu_1 + 2\nu_4$
		355.0	28 169	$2\nu_2$
		431.7	23 164	0_0^0
		420.6	23 776	ν_4

IR: $l\text{-}C_4Cl$ $\nu_1 = 2022.1\text{ cm}^{-1}$; $l\text{-}C_4Cl^+$ $\nu_1 = 2034.4\text{ cm}^{-1}$, $\nu_4 = 1678.0\text{ cm}^{-1}$

(d) C_4Cl . An analogous experiment was carried out by co-depositing mass-selected C_4Cl^+ with neon to form a 6 K matrix, and the resulting electronic absorption spectrum is shown in Figure 7. The strong vibronic band system between 390 and 430 nm was observed to increase in intensity after UV irradiation and is thus assigned to the neutral C_4Cl molecule.

The 3π and 6σ orbitals are close in energy, resulting in two nearly degenerate states, $2^2\Pi$ and $2^2\Sigma^+$, for the linear form of C_4Cl . The $2^2\Pi$ state is lower in energy by only 7.5 kJ/mol at the CCSD(T) level of theory. The ground state of C_4Cl is predicted to be quasilinear ($2^2A'$) (correlating with the $2^2\Pi$ state), and the barrier to linearity is extremely small (0.7 kJ/mol). The $2^2\Pi$ state has a permanent dipole moment of 4.5 D (CASSCF) which is significantly larger than that of the $2^2\Sigma^+$ state (0.75 D), making it the primary candidate for observation in the neon matrix. The vertical excitation energies below 6 eV and transition moments are listed in Table 1 for transitions originating in the $2^2\Pi$ state of C_4Cl , and the corresponding structure is shown in Figure 1. The appearance of alternating C–C bond lengths suggests that the bonds have polyacetylenic character, as expected for a linear carbon chain.

The band origin in Figure 7 appears at 427.0 nm and is attributed to the $2^2\Pi \leftarrow X^2\Pi$ electronic transition of linear C_4Cl . The assignment is based upon the observation that the band falls within 0.42 eV of the predicted excitation energy and that this transition is expected to be strong. The associated vibrational structure is given in Table 3 and reveals the excitation of three vibrational modes. These modes correspond to the excitation of stretching ($\nu_1 = 1975\text{ cm}^{-1}$) and bending ($\nu_4 = 459\text{ cm}^{-1}$) modes of the carbon chain and to the C–Cl stretch ($\nu_5 = 317\text{ cm}^{-1}$) in the upper electronic state of C_4Cl . The C–Cl stretching frequency of C_4Cl is lower than that measured for C_6Cl (415 cm^{-1}),¹⁵ suggesting that the C–Cl bond is longer in the excited state of the former. This is consistent with ground state calculations which predict a slight shortening of the C–Cl bond with increasing n among the $n = \text{even}$ neutral chains.³ The experimentally determined vibrational frequencies for the excited state of C_4Cl are lower than the calculated values for the ground electronic state (DFT: $\nu_1 = 2175$, $\nu_4 = 555$, and $\nu_5 = 324\text{ cm}^{-1}$),³ as observed earlier for other C_nCl chains and as expected for electronic promotion to an orbital with a greater number of nodes. Only one mode was observed in the IR spectrum (Figure 8) for the ground electronic state of C_4Cl . This transition is assigned to the C–C stretching mode ($\nu_1 = 2022.1$

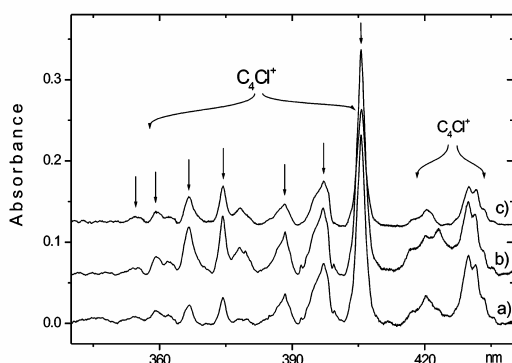


Figure 9. Electronic absorption spectra of the $2^3\Pi \leftarrow X^3\Pi$ electronic transition of C_4Cl^+ recorded after deposition of the cation with neon and CCl_4 to form a 6 K matrix. Traces a and b show the spectra obtained both before and after UV exposure, respectively. Trace c is a difference spectrum of the other two traces scaled to remove the C_4Cl band origin at 427.0 nm.

cm^{-1}), as it compares favorably with the theoretically determined frequency (2175 cm^{-1}) and is slightly larger than the value in the first excited electronic state (1975 cm^{-1}).

The irregular line widths for the transitions in the vibrational progression in Figure 7 are unusual in comparison to the spectra recorded for other members of the C_nCl family.¹⁵ The observed broadening may be a consequence of the interaction of the $2^3\Pi$ ground state with the nearby $2^1\Sigma^+$ state, although the strength of the observed transition certainly suggests that the states involved are predominantly of Π character. The irregular line shapes may also be a result of Fermi resonance contributions.

(e) C_4Cl^+ . As observed for C_3Cl^+ , the spectrum recorded after the deposition of mass-selected C_4Cl^+ ions was dominated by absorptions of neutral species. To observe a clear spectrum of C_4Cl^+ , both N_2O and CCl_4 were added to the neon gas in separate experiments to act as electron scavengers and suppress the neutralization of deposited cations. The spectra of both matrix samples revealed a strong band system between 360 and 410 nm. Figure 9 shows the absorption with CCl_4 present, and the bands assigned to the C_4Cl^+ cation are those that disappear or decrease in intensity after exposure to UV light. A similar spectrum was seen when N_2O was used, confirming that the transitions were not dependent on the added impurity.

In the case of the linear C_4Cl^+ cation, the ground state is $3^3\Sigma^-$ and the nearest state, $3^3\Pi$, is predicted to be approximately 25 kJ/mol (CCSD(T)) and 19 kJ/mol (CCSD) higher in energy. As in the neutral analogue, the Π state has a considerably larger dipole moment and is expected to be stabilized relative to the $3^3\Sigma^-$ ground state in the matrix. Transition moments from the $3^3\Sigma^-$ state of C_4Cl^+ are predicted to be an order of magnitude smaller than those originating in the $3^3\Pi$ state, and thus, only the latter are included in Table 1. The calculated structure of C_4Cl^+ in the $3^3\Pi$ state is shown in Figure 1, and as observed for the neutral counterpart, the carbon backbone of C_4Cl^+ appears to have some polyacetylenic character.

The main band system in Figure 9 is assigned to the $2^3\Pi \leftarrow X^3\Pi$ transition of linear C_4Cl^+ . The origin at 405.7 nm falls within 0.14 eV of the strongest system predicted theoretically. The analogous transition of the isoelectronic C_4S molecule in a neon matrix falls 41 nm to the red of this.¹⁶ A similar red shift (47 nm) was observed upon comparison of the absorption spectra of the longer chains: C_6S and C_6Cl^+ .¹⁵ A second, weaker system, which overlaps with the $2^2\Pi \leftarrow X^2\Pi$ transition of the

neutral C_4Cl chain, is apparent in Figure 9, with the origin band at 431.7 nm. The similar energies observed for the band origins of the neutral and cationic species in Figure 7 are not surprising, given that both observed transitions involve electronic excitations between their 6σ and 3π orbitals. The assignment of the 431.7 nm system is not clear, but it could involve the $3^3\Sigma^+$ or $3^3\Delta$ states calculated to lie nearby (Table 1), the transition gaining intensity from the strong closely located $2^3\Pi \leftarrow X^3\Pi$ system at 405.7 nm.

The vibrational structure observed for the 405.7 nm system of C_4Cl^+ is comparable to that of C_6Cl^+ in a neon matrix,¹⁵ and the positions of the band maxima are listed in Table 3. The bands correspond to the excitation of stretching and bending vibrations involving the carbon chain in the excited electronic state of C_4Cl^+ ($\nu_1 = 2060$, $\nu_2 = 1799$, and $\nu_4 = 534$ cm^{-1}) and are in good agreement with the calculated ground state values (DFT: $\nu_1 = 2147$, $\nu_2 = 1769$, and $\nu_4 = 583$ cm^{-1}).³ The C–C stretching frequencies are similar to those reported for the analogous excited state of C_6Cl^+ ($\nu_1 = 2043$, $\nu_2 = 1872$ cm^{-1})¹⁵ which suggests that the excited states of these two chains are characterized by similar carbon backbones. The IR absorption spectrum of C_4Cl^+ (Figure 8) reveals two strong vibrational bands at 2034.4 and 1678.0 cm^{-1} which are assigned to the ν_1 and ν_2 modes in the ground electronic state of C_4Cl^+ and are similar to the values reported for the excited state in Table 3.

Conclusion

In this work, electronic absorption spectra of the chlorine-terminated carbon chains C_3Cl , C_3Cl^+ , C_3Cl^- , C_4Cl , and C_4Cl^+ in 6 K neon matrices are reported for the first time. The transitions observed reveal that the neutral C_3Cl radical exists in both bent and cyclic forms in the matrix environment with absorptions in the UV, visible, and NIR regions. The ions of C_3Cl have either bent (C_3Cl^-) or linear (C_3Cl^+) structures and absorb near the visible transition of their neutral analogue. The longer chains, C_4Cl and C_4Cl^+ , appear linear. The spectra presented here provide a more complete set of data to complement existing spectroscopic and theoretical studies of the C_nCl family and serve as a basis for future gas phase spectroscopic measurements which may be used to establish trends in the structures and spectra of heteroatom-terminated carbon chains.

Acknowledgment. This research was supported by the Swiss National Science Foundation (project 200020-100019) as well as the EU project “Molecular Universe” (MRTN-CT-2004-51302). J.v.W. thanks the Natural Science and Engineering Research Council of Canada for postdoctoral support.

References and Notes

- (1) McCarthy, M. C.; Gottlieb, C. A.; Thaddeus, P. *Mol. Phys.* **2003**, *101*, 697.
- (2) Rayon, V. M.; Barrientos, C.; Largo, A. *THEOCHEM* **1998**, *432*, 75.
- (3) Largo, A.; Cimas, A.; Redondo, P.; Barrientos, C. *Int. J. Quantum Chem.* **2001**, *84*, 127.
- (4) Li, G.; Tang, Z. *J. Phys. Chem. A* **2003**, *107*, 5317.
- (5) Redondo, P.; Redondo, J.; Barrientos, C.; Largo, A. *Chem. Phys. Lett.* **1999**, *315*, 224.
- (6) Endo, Y.; Saito, S.; Hirota, E. *J. Mol. Spectrosc.* **1982**, *94*, 199.
- (7) Yamada, C.; Nagai, K.; Hirota, E. *J. Mol. Spectrosc.* **1981**, *85*, 416.
- (8) Burkholder, J. B.; Sinha, A.; Hammer, P. D.; Howard, C. J. *J. Mol. Spectrosc.* **1988**, *127*, 61.
- (9) Jin, P.; Chang, B. C.; Fei, R.; Sears, T. J. *J. Mol. Spectrosc.* **1997**, *182*, 189.
- (10) Venkateswarlu, P. *Phys. Rev.* **1950**, *77*, 79.
- (11) Verma, R. D.; Mulliken, R. S. *J. Mol. Spectrosc.* **1961**, *6*, 419.
- (12) Gordon, R. D.; King, G. W. *Can. J. Phys.* **1961**, *39*, 252.

Electronic Absorption Spectra of C₃Cl and C₄Cl*J. Phys. Chem. A*, Vol. 109, No. 25, 2005 **5559**

- (13) Bredohl, H.; Dubois, I.; Melen, F. *J. Mol. Spectrosc.* **1983**, *98*, 495.
(14) Sumiyoshi, Y.; Ueno, T.; Endo, Y. *J. Chem. Phys.* **2003**, *119*, 1426.
(15) van Wijngaarden, J.; Batalov, A.; Shnilko, I.; Fulara, J.; Maier, J. P. *J. Chem. Phys. A* **2004**, *108*, 4219.
(16) Riplov, E.; Wyss, M.; Lakin, N. M.; Maier, J. P. *J. Phys. Chem. A* **2001**, *105*, 4894.

- (17) Maier, J. P. *Chem. Soc. Rev.* **1997**, *26*, 21.
(18) Freivogel, P.; Fulara, J.; Lessen, D.; Forney, D.; Maier, J. P. *Chem. Phys.* **1994**, *189*, 335.
(19) MOLPRO, version 2002.1, a package of ab initio programs designed by H.-J. Werner and P. J. Knowles, with contributions from others; www.molpro.net.
(20) Kolek, P. Manuscript in preparation.

$H_2C_nH^+$ ($N=4,6,8$)

10404

J. Phys. Chem. A 2006, 110, 10404–10408Electronic Absorption Spectra of the Protonated Polyacetylenes $H_2C_nH^+$ ($n = 4, 6, 8$) in Neon MatrixesAnton Batalov, Jan Fulara,[†] Ivan Shnitko, and John P. Maier*

Department of Chemistry, University of Basel, Klingelbergstrasse 80, CH-4056 Basel, Switzerland

Received: May 1, 2006; In Final Form: June 28, 2006

Electronic absorption spectra of the protonated polyacetylenic chains $H_2C_nH^+$ ($n = 4, 6, 8$) and the neutral H_2C_8H have been observed in 6 K neon matrixes after mass selection. The wavelength of the $H_2C_nH^+$ electronic transitions depends quasi-linearly on n , typical of carbon chains. The origin band is at 286.0, 378.6, and 467.6 nm for $n = 4, 6$, and 8, respectively. Two ground-state vibrations of $H_2C_4H^+$ in the IR absorption spectrum were also detected. On the basis of the spectroscopic trends and the assignment of the vibrational frequencies in the ground and excited electronic states, it is concluded that the $H_2C_nH^+$ species are C_{2n} linear carbon chains with one H atom on one end and two on the other.

Introduction

Unsaturated hydrocarbons with a linear carbon backbone are important constituents of the interstellar medium (ISM).¹ Highly polar carbon chain radicals^{2–4} C_nH ($n = 2–8$) and cumulenes^{5,6} H_2C_n ($n = 3, 4, 6$) have been detected in dark molecular clouds, and circumstellar shells of carbon reach stars by means of radio astronomy. One can expect that the nonpolar isomers of cumulenes—polyacetylenes ($HC_{2n}H$) should also be abundant in such environments, although they cannot be observed via microwave spectroscopy.

Acetylene and diacetylene were detected a long time ago in hydrocarbon-rich planetary atmospheres in the solar system.⁷ Diacetylene is formed from simple hydrocarbons in the upper atmosphere as a result of chemical reactions driven by the solar UV photons. It plays a similar role as ozone on Earth shielding the lower atmospheric layers against UV photons. Larger polyacetylenes were predicted to be present in this environment;⁸ however, they have not yet been observed. Recently, diacetylene and triacetylene were detected with the Infrared Space Observatory in the circumstellar medium.⁹

According to current models, most chemical reactions in the ISM are between ions and molecules. Important intermediates in the hydrocarbon reaction network leading to production of linear carbon chain radicals C_nH and cumulenes H_2C_n are polyacetylene cations and protonated polyacetylenes $H_2C_{2n}H^+$.¹⁰ Therefore, the spectroscopic study of these species is also of interest related to astrochemistry. Among them, only the polyacetylene cations have been extensively studied so far in noble gas matrixes^{11,12} and the gas phase^{13,14} by means of electronic and vibrational spectroscopy. The protonated counterparts are still elusive with the exception of $H_2C_3H^+$, the electronic absorption spectrum of which has been measured in a neon matrix.¹⁵ The next member, $H_2C_4H^+$, of this homologous series has been studied only by mass spectrometry^{16–18} and quantum mechanical methods.^{18–21} In this paper, the electronic absorption spectra of protonated diacetylene ($H_2C_4H^+$), triacetylene ($H_2C_6H^+$), and tetraacetylene ($H_2C_8H^+$) cations isolated in neon matrixes are reported.

* To whom correspondence should be addressed. Fax +41-61-267-38-55. Electronic mail: j.p.maier@unibas.ch

[†] Also at Institute of Physics, Polish Academy of Sciences, Al.Lotnikow 32-46, Pl-02668 Warsaw, Poland.

Experimental Section

The experimental setup has been described.²² The $C_nH_3^+$ ($n = 4, 6, 8$) cations were produced in an electron impact ion source from diacetylene; $C_4H_3^+$ also from benzene and dimethylacetylene. The precursor molecules were mixed with helium in an 1:3 ratio. The exit aperture of the ion source was reduced in order to increase the inner pressure and enhance production of larger $C_nH_3^+$ ($n > 4$) cations. Experimental conditions (e.g., pressure in the source, temperature of filament, extraction potential) were optimized for the ion of interest. After extraction from the source, ions were guided by means of electrostatic lenses to a 90° bender to get rid of neutral molecules, and then to a quadrupole mass filter. Mass-selected ions with near-unity resolution were co-deposited with neon during 1–2 h onto a rhodium-coated sapphire matrix substrate held at 6 K. The energy of the ions arriving at the surface was ~50 eV, which led to their partial fragmentation. The newly detected electronic transition of $C_4H_3^+$ has a low oscillator strength, and its absorption bands were weak (low signal-to-noise ratio). Because of this, an electron scavenger (N_2O) was occasionally mixed with neon in concentrations of 1:300 to suppress ion neutralization during deposition. N_2O molecules readily accept electrons, preventing their recombination with cations. Thus, using a scavenger, one can significantly increase the intensity of cationic absorptions. Typical integrated ion currents on the substrate for the $C_4H_3^+$, $C_6H_3^+$, and $C_8H_3^+$ ions were 50, 10, and 8 μC , respectively. Irradiation of the matrix (30 min) with a medium pressure mercury lamp was used to neutralize the trapped cations. UV photons release electrons from weakly bonded anions, which in turn recombine with the cations. Thus, photobleaching helps to distinguish charged and neutral species. Electronic absorption spectra have been measured in the 220–1100 nm spectral range by using a waveguide technique.²³ Infrared spectra have been measured in the 1100–12000 cm^{-1} region by a Fourier transform spectrometer applying a double reflection method.²⁴

Observations

$C_4H_3^+$. Mass-selected deposition of $C_4H_3^+$ ($m/z = 51$) revealed two electronic absorption band systems. The first one with origin at 507.4 nm is known and belongs to the

Electronic Absorption Spectra of Protonated Polyacetylenes

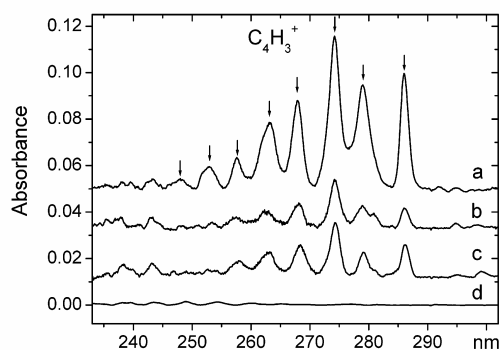


Figure 1. Electronic absorption spectra of the $C_4H_3^+$ cation in 6 K neon matrices obtained after mass-selected deposition with a mixture of neon and electron scavenger (N_2O) in a proportion of 300:1 (trace a), after UV irradiation of the same matrix (trace b), after $C_4H_3^+$ deposition without electronic scavenger (trace c), and after deposition of $C_4H_2^+$ (trace d).

$A^2\Pi_u \leftarrow X^2\Pi_g$ transition of the HC_4H^+ cation,²⁵ which is produced by detachment of a hydrogen atom from $C_4H_3^+$ (fragmentation during deposition). A new system with origin at 286.0 nm is also detected (Figure 1). Its absorption pattern was independent of the selected precursor. The intensity of this system decreases after UV irradiation of the matrix (compare traces a and b), which indicates its ionic origin. In the presence of the electron scavenger N_2O (trace a), the intensity of the new bands was stronger than in a pure neon matrix (trace c), although the deposited charges (integral currents) of $C_4H_3^+$ ions were practically the same in both cases. This leads to the conclusion that the carrier of the new absorption is positively charged. Mass-selected deposition of $C_4H_2^+$ ($m/z = 50$) (trace d) did not show a similar pattern; neither did C_4H^+ deposition. Therefore, the new system of bands with the onset at 286.0 nm can be assigned to the $C_4H_3^+$ cation and not to one of its fragments such as $C_4H_2^+$ or smaller. Positions of the origin band and vibronic components of the new transition are given in Table 1. Absorptions of smaller fragments (C_4H , C_4 , C_3) of the deposited ion were also detected, but only very weakly. This shows that the fragmentation, except for one H-atom loss, is quite negligible, supporting the proposed assignment.

The infrared vibrational spectrum of $C_4H_3^+$ reveals two new absorptions located at 2086 and 2949 cm^{-1} (Figure 2, Table 1) which are not present in the case of $C_4H_2^+$ deposition and behave in a manner similar to that of the UV bands of $C_4H_3^+$. Hence, they can be assigned to the latter cation. Matrix site effect is responsible for the doublet structure of both peaks. Molecules or ions of interest can occupy different positions in a neon cage having slightly different stabilization energies, which leads to a complex structure of the spectral lines.

$C_6H_3^+$. After $C_6H_3^+$ ($m/z = 75$) deposition, one known and one new electronic absorption were observed. The system with origin band at 604.6 nm is the $A^2\Pi_g \leftarrow X^2\Pi_u$ transition of the HC_6H^+ ion,¹¹ produced by H-atom loss during the impact on the matrix substrate. The new system with the onset at 378.6 nm together with the absorption band of N_2^+ , a common matrix impurity, is seen in Figure 3. UV irradiation of the matrix (compare traces a and b) led nearly to the extinction of the new absorptions indicating their ionic origin. Mass-selected deposition of $C_6H_2^+$ ($m/z = 74$) (traces c and d) did not reveal the same system of bands. Traces c and d were normalized to have

TABLE 1: Observed Electronic and Vibrational Absorption Bands for $C_nH_3^+$ ($n = 4, 6, 8$) and C_8H_3 in 6 K Neon Matrixes

species	λ/nm	$\tilde{\nu}/cm^{-1}$	$\Delta\tilde{\nu}/cm^{-1}$	assignment
$C_4H_3^+$	286.0	34965	0	0_0^0
	279.0	35842	877	CC str
	274.2	36470	1505	CC str
	267.9	37327	2362	1505 + 877
	263.1	38008	3043	CH str
	257.6	38820	3855	$2 \times 1505 + 877$
	253.0	39526	4561	1505 + 3043
	248.0	40323	5358	877 + 1505 + 3043
$C_6H_3^+$	378.6	26413	0	0_0^0
	369.9	27034	621	CC str
	357.3	27988	1575	CC str
	353.0	28329	1916	CC str
	349.7	28596	2183	621 + 1575
	338.7	29525	3112	CH str
	334.6	29886	3473	1575 + 1916
	467.6	21386	0	0_0^0
$C_8H_3^+$	457.5	21858	472	CC str
	442.6	22594	1208	
	436.7	22899	1513	CC str
	433.4	23073	1687	
	427.9	23370	1984	CC str
	419.4	23844	2458	1984 + 472
	410.3	24372	2986	CH str
	402.3	24857	3471	2986 + 472
C_8H_3	358.5	27894	0	0_0^0
	334.4	29904	2010	CC str
	318.4	31407	3513	

IR

	$\tilde{\nu}/cm^{-1}$	assignment
$C_4H_3^+$	2086	} CC str
	2093	
	2949	} CH str
	2953	

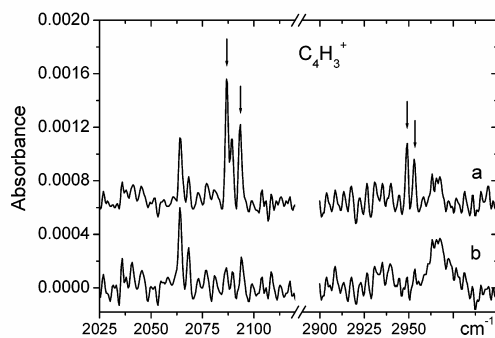


Figure 2. IR absorption spectra of the $C_4H_3^+$ cation in a 6 K neon matrix after mass-selected deposition (trace a) and after UV irradiation of the same matrix (trace b).

the same intensity of the HC_6H^+ $A^2\Pi_g \leftarrow X^2\Pi_u$ absorption system, as in the case of $C_6H_3^+$ deposition (traces a and b). C_6H^+ has recently been studied in a neon matrix, but its absorptions fall in the visible spectral range.²⁶ Therefore, the new system of bands with origin at 378.6 nm has been assigned to the $C_6H_3^+$ cation. Positions of vibronic components are given in Table 1. Very weak known bands of the smaller fragments (C_6H^+ , C_6H , C_5) were also detected.

$C_8H_3^+$ and C_8H_3 . Deposition of $C_8H_3^+$ ($m/z = 99$) revealed the known $A^2\Pi_u \leftarrow X^2\Pi_g$ band system of HC_8H^+ with origin

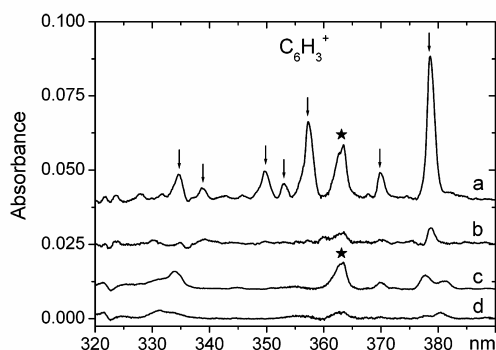


Figure 3. Electronic absorption spectra of the $C_6H_3^+$ cation in a 6 K neon matrix obtained after mass-selected deposition (trace a), after UV irradiation of the same matrix (trace b), after deposition of $C_6H_2^+$ (trace c), and after UV irradiation of that matrix (trace d). Spectra in traces c and d are normalized to have equal intensity of the $C_6H_2^+ A^2\Pi_g \leftarrow X^2\Pi_u$ absorption (origin at 604.6 nm, not shown on figure) after $C_6H_3^+$ and $C_6H_2^+$ depositions (traces a and c) and also after irradiation (traces b and d). The bands marked with a star correspond to the absorption of the N_2^+ ion.

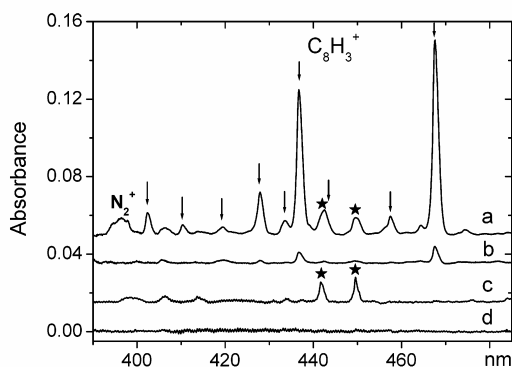


Figure 4. Electronic absorption spectra of the $C_8H_3^+$ cation in a 6 K neon matrix after mass-selected deposition (trace a), after UV irradiation of the same matrix (trace b), after deposition of $C_8H_2^+$ (trace c), and after UV irradiation of that matrix (trace d). Spectra in traces c and d are normalized to have the same intensity as the $HC_8H^+ A^2\Pi_u \leftarrow X^2\Pi_g$ transition, as in the case of $C_8H_3^+$ deposition. Two medium-intensity bands marked with stars can be assigned to other absorptions of HC_8H^+ . Their intensity was proportional to that of the HC_8H^+ transition at 713.2 nm, before and after UV irradiation of the matrix, independent of the experiment or exact mass selection. Somewhat better spectral resolution was used to obtain traces c and d. The new system of bands (marked with arrows) with the onset at 467.6 nm (Table 1) disappears after UV irradiation and is not present in the case of $C_8H_2^+$ and C_8H^+ deposition and, hence, can be assigned to the $C_8H_3^+$

at 713.2 nm,¹¹ a result of fragmentation. A new electronic absorption with onset at 467.6 nm was observed (Figure 4 traces a and b). Spectra after deposition of $C_8H_2^+$ (traces c and d) were normalized to have the same intensity as the $HC_8H^+ A^2\Pi_u \leftarrow X^2\Pi_g$ transition, as in the case of $C_8H_3^+$ deposition. Two medium-intensity bands marked with stars can be assigned to other absorptions of HC_8H^+ . Their intensity was proportional to that of the HC_8H^+ transition at 713.2 nm, before and after UV irradiation of the matrix, independent of the experiment or exact mass selection. Somewhat better spectral resolution was used to obtain traces c and d. The new system of bands (marked with arrows) with the onset at 467.6 nm (Table 1) disappears after UV irradiation and is not present in the case of $C_8H_2^+$ and C_8H^+ deposition and, hence, can be assigned to the $C_8H_3^+$

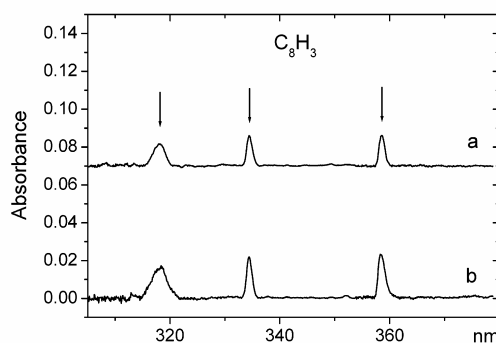


Figure 5. Electronic absorption spectra of the C_8H_3 molecule in a 6 K neon matrix after mass-selected deposition (trace a) and after UV irradiation of the same matrix (trace b).

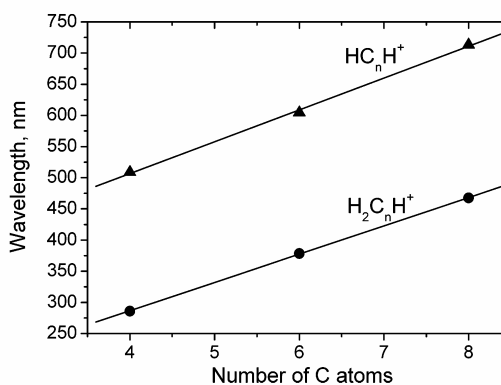


Figure 6. Wavelengths of the origin bands observed for the protonated polyacetylenic chains $H_2C_nH^+$ (circles) and for the known $A^2\Pi \leftarrow X^2\Pi$ transitions of the HC_nH^+ chains¹¹ (triangles) in neon matrixes versus number of C atoms. Solid lines are linear fits.

cation. The peak at 442.6 nm (trace a) appears to be a superposition of the HC_8H^+ band (trace c) and the $C_8H_3^+$ vibronic component, as can be seen from the relative intensities of the lines marked with a star. Very weak absorptions of C_8H were also detected.

Other new absorptions in the UV spectral range were also observed after $C_8H_3^+$ mass-selected deposition (Figure 5). These bands increase in intensity after UV exposure (compare traces a and b), and thus, they must originate from a neutral molecule. They were not detected after $C_8H_2^+$ or C_8H^+ depositions and are assigned to the absorption of neutral C_8H_3 (Table 1).

Discussion

The wavelengths of the origin bands in the electronic transitions of the $C_nH_3^+$ ($n = 4, 6, 8$) ions are plotted versus n in Figure 6. A near-linear behavior typical for carbon chains is evident.²² The corresponding data for the HC_nH^+ linear chains¹¹ ($A^2\Pi \leftarrow X^2\Pi$ transitions) are shown for comparison. The slopes of the linear fits for the $C_nH_3^+$ and HC_nH^+ chains are almost equal, suggesting similar structures. Absorption bands are more intense for larger $C_nH_3^+$ ions despite their smaller concentrations in the matrix. Hence, the oscillator strength of the newly detected $C_nH_3^+$ transitions grows with n , as for other carbon chains.²²

Electronic Absorption Spectra of Protonated Polyacetylenes

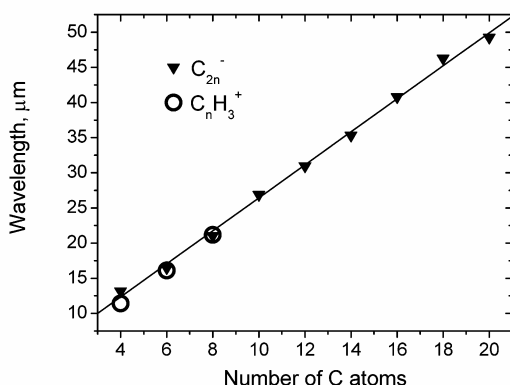


Figure 7. Wavelengths of the lowest-energy totally symmetric vibrations of the C_{2n}^- ($n = 2-10$) carbon chains (filled triangles) and the $H_2C_nH^+$ ($n = 4, 6, 8$) chains (open circles) in neon matrixes versus number of C atoms.

Ground-state geometry optimizations of $C_4H_3^+$ by different ab initio methods have been carried out;^{19-21,27,28} the most extensive work took six different structural isomers into consideration.¹⁸ Although there are some contradictions between the reported relative total energies of $C_4H_3^+$ isomers, the linear C_{2v} $H_2C_4H^+$ structure is invariably considered to be the most stable one, with a second-lowest structure lying $\sim 0.7-1.5$ eV higher. Thus, the isomer $H_2C_4H^+$ and the longer ones $H_2C_6H^+$ and $H_2C_8H^+$ with C_{2v} symmetry are considered the most plausible structures for the observed electronic absorptions in Figures 1, 3, and 4. Presumably, the structure of C_8H_3 is the same as that of $C_8H_3^+$, because it is formed during neutralization of the cation in the matrix (C_8H_3 absorptions increase after UV irradiation).

Electronic absorption spectra in 6 K neon matrixes reveal only the excited-state vibrational energy levels of the investigated molecule. This is because at 6 K only the zero vibrational level in the ground state is populated. In contrast, IR absorption spectra probe the ground state. The vibrational frequencies inferred from the spectra in the ground and excited states are listed in Table 1.

The C-H stretching vibration in the CH_2 group was detected for all the $C_nH_3^+$ ($n = 4, 6, 8$) ions. The frequencies of this mode in the excited electronic state of the cations are 3043, 3112, and 2986 cm^{-1} for $n = 4, 6$, and 8, respectively. In the IR spectra of $C_4H_3^+$, this vibration is observed at 2949 cm^{-1} . These values are close to the frequencies of this mode at 3026 and 3015 cm^{-1} for the structurally relevant neutral molecules ethylene and allene.²⁹ The band that corresponds to the stretching of the C-C bonds is also seen in the electronic spectra of $C_nH_3^+$ (i.e., in the excited states) at 1916 and 1984 cm^{-1} for $n = 6$ and 8. The C-C stretch in the ground state of $C_4H_3^+$ is observed at 2086 cm^{-1} . The frequency of this mode was predicted by CEPA-I calculations at 2010 ± 10 cm^{-1} .²¹

A strong vibronic band in the $C_nH_3^+$ electronic absorption spectra lies 1505, 1575, and 1513 cm^{-1} to higher energy of the origin band for $n = 4, 6$, and 8. Its intensity indicates considerable excited-state geometry change along this mode. Such a vibrational frequency is seldom observed in the electronic spectra of carbon chains. The frequency of this mode is higher than that of the CH_2 scissoring vibration in the ground state of many structurally relevant molecules (e.g., in ethylene, it is at 1342 cm^{-1} ; in allene, at 1443 cm^{-1}).²⁹ Ground-state normal-

mode analysis (B3LYP/6-311G* ab initio calculations)³⁰ shows that the closest totally symmetric vibrations are the CH_2 scissoring at 1321 cm^{-1} and the carbon chain stretch at 1855 cm^{-1} . Excited-state vibrations are usually lower in frequency than in the ground state, and thus, the strong vibronic lines at ~ 1500 cm^{-1} presumably correspond not to the scissoring mode but to the carbon chain stretching.

The lowest-frequency totally symmetric vibration of a linear carbon skeleton is inversely proportional to the size of a considered molecule. This vibration is detected in the excited state of $C_nH_3^+$ at 877, 621, and 472 cm^{-1} for $n = 4, 6$, and 8 (Table 1). This regularity can be seen if one plots the wavelengths of the C_{2n}^- ($n = 2-10$) carbon chains lowest-energy vibrations³¹ versus the number of C atoms (Figure 7). Other carbon chains (e.g., $C_{2n}H$, $C_{2n}HC_{2n}H^+$)^{11,31} behave in the same way. The wavelengths of the $C_nH_3^+$ vibrations (open circles in Figure 7) lie on the same line as the ones of the C_{2n}^- chains.

Therefore, the vibrational frequencies obtained from the $C_nH_3^+$ spectra confirm the presence of the CH_2 group and the linear carbon skeleton supporting the assignment to the protonated polyacetylene structure $H_2C_nH^+$ with C_{2v} symmetry. The observation of the electronic transitions of this class of ions, $C_nH_3^+$, opens the way to gas-phase studies and direct comparisons with astronomical data.

Acknowledgment. This work has been supported by the Swiss National Science Foundation (project 200020-100019).

References and Notes

- (1) McCarthy, M. C.; Travers, M. J.; Kovács, A.; Gottlieb, C. A.; Thaddeus, P. *Astrophys. J. Suppl. Ser.* **1997**, *113*, 105.
- (2) Cernicharo, J.; Guélin, M. *Astron. Astrophys.* **1996**, *309*, L27.
- (3) Guélin, M.; Cernicharo, J.; Travers, M. J.; McCarthy, M. C.; Gottlieb, C. A.; Thaddeus, P.; Ohishi, M.; Saito, S.; Yamamoto, S. *Astron. Astrophys.* **1997**, *317*, L1.
- (4) Bell, M. B.; Feldman, P. A.; Watson, K. G.; McCarthy, M. C.; Travers, M. J.; Gottlieb, C. A.; Thaddeus, P. *Astrophys. J.* **1999**, *518*, 740.
- (5) Langer, W. D.; Velusamy, T.; Kuiper, T. B. H.; Peng, R.; McCarthy, M. C.; Travers, M. J.; Kovács, A.; Gottlieb, C. A.; Thaddeus, P. *Astrophys. J.* **1997**, *480*, L63.
- (6) Kawaguchi, K.; Kaifu, N.; Ohishi, M.; Ishikawa, S.-I.; Hirahara, Y.; Yamamoto, S.; Saito, S.; Takano, S.; Murakami, A.; Vrtilek, J. M.; Gottlieb, C. A.; Thaddeus, P.; Irvine, W. M. *Publ. Astron. Soc. Jpn.* **1991**, *43*, 607.
- (7) Kunde, V. G.; Aikin, A. C.; Hanel, R. A.; Jennings, D. E.; Maguire, W. C.; Samuelson, R. E. *Nature (London)* **1981**, *292*, 686.
- (8) Shindo, F.; Benilan, Y.; Guillemin, J.-C.; Chaquin, P.; Jolly, A.; Raulin, F. *Planet. Space Sci.* **2003**, *51*, 9.
- (9) Cernicharo, J.; Heras, A. M.; Tielens, A. G. G. M.; Pardo, J. R.; Herpin, F.; Guélin, M.; Waters, L. B. F. M. *Astrophys. J.* **2001**, *546*, L123.
- (10) Turner, B. E.; Herbst, E.; Terzieva, R. *Astrophys. J. Suppl. Ser.* **2000**, *126*, 427.
- (11) Freivogel, P.; Fulara, J.; Lessen, D.; Forney, D.; Maier, J. P. *Chem. Phys.* **1994**, *189*, 335.
- (12) Szczepanski, J.; Wang, H.; Jones, B.; Arrington, C. A.; Vala, M. T. *Phys. Chem. Chem. Phys.* **2005**, *7*, 738.
- (13) Pfluger, D.; Motylewski, T.; Linnartz, H.; Sinclair, W. E.; Maier, J. P. *Chem. Phys. Lett.* **2000**, *329*, 29.
- (14) Pfluger, D.; Sinclair, W. E.; Linnartz, H.; Maier, J. P. *Chem. Phys. Lett.* **1999**, *313*, 171.
- (15) Wyss, M.; Riaplov, E.; Maier, J. P. *J. Chem. Phys.* **2001**, *114*, 10355.
- (16) Deakne, C. A.; Meot-Ner, M.; Buckley, T. J.; Metz, R. J. *Chem. Phys.* **2001**, *86*, 2334.
- (17) Scott, G. B. I.; Fairley, D. A.; Freeman, C. G.; McEwan, M. J.; Adams, N. G.; Babcock, L. M. *J. Phys. Chem. A* **1997**, *101*, 4973.
- (18) Schröder, D.; Loos, J.; Schwarz, H.; Thissen, R.; Rothova, J.; Herman, Z. *Int. J. Mass Spectrom.* **2003**, *230*, 113.
- (19) Anand, S.; Schlegel, H. B. *J. Phys. Chem. A* **2005**, *109*, 11551.
- (20) Petrie, S.; Knight, J. S.; Freeman, C. G.; MacLagan, R. G. A. R.; McEwan, M. J.; Sudkeaw, P. *Int. J. Mass Spectrom. Ion Processes* **1991**, *105*, 43.

10408 *J. Phys. Chem. A*, Vol. 110, No. 35, 2006

Batalov et al.

- (21) Botschwina, P.; Schramm, H.; Sebald, P. *Chem. Phys. Lett.* **1990**, *169*, 121.
- (22) Maier, J. P. *Chem. Soc. Rev.* **1997**, *26*, 21.
- (23) Bondybey, V. E.; Sears, T. J.; English, J. H.; Miller, T. A. *J. Chem. Phys.* **1980**, *73*, 2063.
- (24) Batalov, A.; Fulara, J.; Shnitko, I.; Maier, J. P. *Chem. Phys. Lett.* **2005**, *404*, 315.
- (25) Bondybey, V. E.; English, J. H. *J. Chem. Phys.* **1979**, *71*, 777.
- (26) Shnitko, I.; Fulara, J.; Batalov, A.; Gillery, C.; Masso, H.; Rosmus, P.; Maier, J. P. *J. Phys. Chem. A* **2006**, *110*, 2885.

- (27) Hori, K.; Yamabe, T.; Tachibana, A.; Asai, Y.; Fukui, K.; Kobayashi, S.; Taniguchi, H. *THEOCHEM* **1987**, *153*, 295.
- (28) Milburn, R. K.; Bohme, D. K.; Hopkinson, A. C. *Int. J. Mass Spectrom.* **2000**, *195/196*, 393.
- (29) Shimanouchi, T. *Tables of Molecular Vibrational Frequencies Consolidated*, National Bureau of Standards: U.S. Government Printing Office: Washington, DC, 1972; Vol. 1, p 1.
- (30) Dr. P. Kolek, private communication.
- (31) Freivogel, P.; Fulara, J.; Jakobi, M.; Fomey, D.; Maier, J. P. *J. Chem. Phys.* **1995**, *103*, 54.

OUTLOOK

Matrix isolation is challenged by a variety of laser-based techniques, which, in the gas phase, have demonstrated their ability to obtain high-resolution vibrational and electronic spectra of transient molecules, free of possible perturbation by the matrix environment. Despite this challenge, there are important reasons why matrix studies of transient molecules are, in fact, complementary to laser studies and should continue to yield valuable contributions to the study of chemically reactive intermediates. While lasers are tuneable over limited spectral ranges, observations in rare-gas matrices provide a broad spectral survey, extending from the FIR to the VUV. Thus, all of the products can be detected. Matrix-shifts from the gas-phase band center are typically small enough to provide a guide for the choice and tuning of lasers for more detailed gas-phase studies. Also, while isotopic substitution is crucial to positively identify a particular system, these studies are more readily conducted in matrices. Matrix absorption observations are also helpful in spectral assignments, due to the fact that spectral contributions from hot bands are eliminated; at cryogenic temperatures all absorptions originate from the molecular ground state.

Unfortunately, a direct comparison of the spectra obtained from matrix isolation measurements can not be conclusive; however, the localized electronic transitions and vibrational patterns provide crucial information for gas phase investigations. Therefore, matrix absorption observations, if complemented by appropriate gas phase studies, will serve as a guide for investigation of astrophysically relevant molecules in the interstellar medium.

The results of the spectroscopic studies on C_n^+ $n=6-9$, obtained during the present PhD work, locate the wavelength range and the relative intensities of their electronic absorptions. Additionally the photobleaching experiments permit a comparison with the transition intensities of their neutral counterparts. Neutral *I*-C₆ and *I*-C₈ have an electronic transition with origin at 511 and 640 nm in a neon matrix but the oscillator strength is an order of magnitude smaller than for the 646 nm band system of

$l\text{-C}_6^+$ or 890 nm of $l\text{-C}_8^+$. In view of this and the UV radiation field in the interstellar medium, these linear cations may be more readily detected than their neutral chains in the optical region where the diffuse absorption bands are observed. On the other hand, in the UV both $l\text{-C}_8$ (around 277 nm) and $l\text{-C}_8^+$ (308 nm) have strong electronic transitions of comparable intensity. The neutral chains $l\text{-C}_7$ and $l\text{-C}_9$ have much stronger electronic transitions than $l\text{-C}_7^+$ and $l\text{-C}_9^+$ both in the UV and visible, and should therefore be the easier ones to detect. Based on this work, one should search for the strong absorption near 250 and 295 nm for $l\text{-C}_7$ and $l\text{-C}_9$, respectively; their calculated oscillator strengths are very large. Thus gas phase spectra of these neutral and cation carbon chains are now required.

Matrix isolation is not powerful in structure determination of the produced species. For example, it is difficult to conclude exclusively from the matrix spectroscopic data which isomer, linear or cyclic, is produced while using a cyclic precursor, but, as experience shows, linear species are more readily generated when linear precursors are used. A helpful technique includes introducing a Ne/N₂O mixture for deposition. N₂O plays a dual role in the matrix: as a reactant and as an electron scavenger. Gas-phase ion mobility and bimolecular reactivity studies indicate that the linear isomers are more reactive. Comparing spectra obtained using pure Ne for deposition with those using the Ne/N₂O mixture, as was in the case of C_{*n*}⁺ cations, allows reasonable confidence as to which of the species (cyclic or linear) were collected.

One of the beauties of the cesium sputter source is its use of pure rods, specifically, rods which do not contain any hydrogen atoms. The absence of hydrogen in a precursor simplifies the mass selection process. Thus, it was possible to obtain B₃ molecule after mass-selected deposition of B₃⁻ anion with subsequent irradiation. The main problem which occurs with anions' deposition is the ability to keep a stable current. After a couple of minutes of deposition the latter drops. Irradiating the matrix while depositing is help, but in this way only neutral species are obtained. The solution comes with introducing a new source, which could eliminate the current dropping. This

new source (for example Xe^+ source) has to be put in the matrix chamber and directed onto the matrix substrate. In this way Xe cations are also collected in the matrix and further arriving of anions should not be suppressed.

The electron impact ion sources are straightforward to operate. A stable discharge, obtained with gaseous precursors, makes the deposition process easier. The disadvantage here is in choosing a different precursor for each new species of interest (preferentially without a hydrogen atom). That is why one should think about introducing some new additional sources for ions production. One of the possible candidates is a magnetron sputtering source, which gives not high but sufficient current. A symbiosis of a stable current and mass selection is the heart of the matrix isolation. The magnetron sputtering source has at least two electrically mutually isolated stationary bar-shaped target arrangements mounted one alongside the other and separated by respective slits. Each of the target arrangements includes a respective electric pad so that each target arrangement may be operated electrically independently from the other target arrangement. Each target arrangement also has a controlled magnet arrangement for generating a time-varying magnetron field upon the respective target arrangement. The magnet arrangements may be controlled independently from each others. The source further has an anode arrangement with anodes alongside and between the target arrangements and/or along smaller sides of the target arrangements. This will allow studying of new species in the matrix, such as: C_n^\pm , C_nO^\pm , C_nN^\pm , MeC_n^\pm , S_n^\pm , B_n^\pm as well as their neutral analogues.

CURRICULUM VITAE

PERSONAL INFORMATION

Name Ivan G. Shnitko
Born on 26th January 1981, [Magadan, Russia](#)
Nationality Russian
Marital status single
E-mail Ivan.Shnitko@gmail.com



EDUCATION

University of Basel – Institute of Physical Chemistry <i>Ph.D. in physical chemistry</i> <i>Thesis title:</i> Absorption Spectroscopy of Carbon and Sulfur Chains in Neon Matrices <i>Supervisor:</i> Prof. Dr. John P. Maier	Basel, Switzerland <i>Sep. 2003 – Feb. 2008</i>
University of Basel – Institute of Physical Chemistry <i>M. Sc. in chemistry</i> (specialization in physical chemistry) <i>Thesis title:</i> Electronic and IR spectra of C ₆ Radicals and Ions <i>Supervisor:</i> Prof. Dr. John P. Maier	Basel, Switzerland <i>Nov. 2002 – Sep. 2003</i>
Novosibirsk State University – Natural Science Department <i>Mgr. Sc. in chemistry (with honours)</i> <i>Supervisor:</i> Prof. Dr. Nikolai M. Bazhin	Novosibirsk, Russia <i>Jul. 2002 – Jun. 2004</i>
Novosibirsk State University – Natural Science Department <i>B.Sc. in environmental chemistry</i>	Novosibirsk, Russia <i>Sep. 1998 – Jun. 2002</i>
<i>Physico-Mathematical school funded by</i> Novosibirsk State University	Novosibirsk, Russia <i>Aug. 1997 – Jun. 1998</i>
Lyceum № 1 <i>Primary and Secondary school A-Level</i>	Magadan, Russia <i>Sep. 1988 – Jun. 1997</i>

LIST OF PUBLICATIONS

- [1] M. ARAKI, H. LINNARTZ, P. CIAS, A. DENISOV, J. FULARA, A. BATALOV, I. SHNITKO, and J. MAIER. High-resolution electronic spectroscopy of a nonlinear carbon chain radical $C_6H_4^+$. *The Journal of Chemical Physics*, 118: 10561–10565, 2003
- [2] J. FULARA, E. RIAPLOV, A. BATALOV, I. SHNITKO, and J. MAIER. Electronic and infrared absorption spectra of linear and cyclic C_6^+ in a neon matrix. *The Journal of Chemical Physics*, 120: 7520–7525, 2004
- [3] A. BATALOV, J. FULARA, I. SHNITKO, and J. MAIER. The near infrared $1^2A_2'' \leftarrow X^2A_1'$ electronic transition of B_3 in a neon matrix. *Chemical Physics Letters*, 404: 315–317, 2005
- [4] J. VAN WIJNGAARDEN, A. BATALOV, I. SHNITKO, J. FULARA, and J. MAIER. Electronic absorption spectra of C_nCl radicals ($n = 5, 6$) and their cations in neon matrices. *Journal of Physical Chemistry A*, 108: 4219–4223, 2004
- [5] J. VAN WIJNGAARDEN, I. SHNITKO, A. BATALOV, P. KOLEK, J. FULARA, and J. MAIER. Electronic absorption spectra of C_3Cl , C_4Cl , and their ions in neon matrices. *Journal of Physical Chemistry A*, 109: 5553–5559, 2005
- [6] J. FULARA, I. SHNITKO, A. BATALOV, and J. MAIER. Electronic absorption spectra of linear and cyclic C_n^+ $n = 7-9$ in a neon matrix. *The Journal of Chemical Physics*, 123: 044305–6, 2005
- [7] I. SHNITKO, J. FULARA, A. BATALOV, C. GILLERY, H. MASSO, P. ROSMUS, and J. MAIER. $^3\Sigma^- - X^3\Sigma^-$ Electronic transition of linear C_6H^+ and C_8H^+ in neon matrixes. *Journal of Physical Chemistry A*, 110: 2885–2889, 2006
- [8] A. BATALOV, J. FULARA, I. SHNITKO, and J. MAIER. Electronic absorption spectra of the protonated polyacetylenes $H_2C_nH^+$ ($n = 4, 6, 8$) in neon matrixes. *Journal of Physical Chemistry A*, 110: 10404–10408, 2006
- [9] I. SHNITKO, J. FULARA, I. GARKUSHA, A. NAGY, and J. MAIER. Electronic transitions of S_2^- and S_3^- in neon matrixes. *In press in Chemical Physics*